



HAL
open science

A very efficient approach for the analysis of delamination in infinitely long multilayered plates

Navid Saeedi

► **To cite this version:**

Navid Saeedi. A very efficient approach for the analysis of delamination in infinitely long multilayered plates. Other. Université Paris-Est, 2012. English. NNT : 2012PEST1160 . pastel-00806390

HAL Id: pastel-00806390

<https://pastel.hal.science/pastel-00806390>

Submitted on 30 Mar 2013

HAL is a multi-disciplinary open access archive for the deposit and dissemination of scientific research documents, whether they are published or not. The documents may come from teaching and research institutions in France or abroad, or from public or private research centers.

L'archive ouverte pluridisciplinaire **HAL**, est destinée au dépôt et à la diffusion de documents scientifiques de niveau recherche, publiés ou non, émanant des établissements d'enseignement et de recherche français ou étrangers, des laboratoires publics ou privés.

UNIVERSITÉ PARIS-EST
ÉCOLE DOCTORALE SCIENCES, INGÉNIERIE ET ENVIRONNEMENT

THÈSE

présentée pour obtenir le grade de
DOCTEUR DE L'UNIVERSITÉ PARIS-EST
Spécialité: Structures et Matériaux

par

Navid Saeedi

UNE APPROCHE TRÈS EFFICACE POUR
L'ANALYSE DU DÉLAMINAGE DES PLAQUES
STRATIFIÉES INFINIMENT LONGUES

A VERY EFFICIENT APPROACH FOR THE ANALYSIS OF
DELAMINATION IN INFINITELY LONG MULTILAYERED PLATES

Thèse soutenue le 18 décembre 2012 devant le jury composé de :

M. DOMINIQUE LEGUILLON	Directeur de Recherche, UPMC	<i>Rapporteur</i>
M. CHRISTOPHE BOUVET	Professeur, ISAE	<i>Rapporteur</i>
M. NICOLAS CARRÈRE	Professeur, ENSTA-Bretagne	<i>Examineur</i>
M. JEAN-FRANÇOIS CARON	Professeur, ENPC	<i>Examineur</i>
M. KARAM SAB	Professeur, ENPC	<i>Directeur de thèse</i>



Remerciements

Tout d'abord, je tiens à remercier mon directeur de thèse KARAM SAB pour son encadrement scientifique très riche et le suivi efficace et dynamique de mon travail. Je le remercie également pour son soutien moral et ses encouragements dans les moments difficiles durant toutes ces années. Je lui suis sincèrement reconnaissant pour sa disponibilité et le temps qu'il m'a consacré malgré ses nombreuses occupations notamment la direction du laboratoire Navier.

Je souhaite remercier également JEAN-FRANÇOIS CARON, le directeur de l'équipe Matériaux et Structures Architecturés (MSA), avec qui j'ai eu des échanges scientifiques enrichissantes. Ainsi, je le remercie pour m'avoir donné l'opportunité d'enseigner à l'Ecole Nationale des Ponts et Chaussées et ailleurs.

Je tiens à remercier l'ensemble des membres du jury pour l'honneur qu'ils m'ont fait. Je remercie DOMINIQUE LEGUILLON pour avoir été rapporteur de ma thèse et aussi présidé le jury. De même, je remercie CHRISTOPHE BOUVET pour avoir accepté d'être rapporteur de ma thèse. Je remercie également NICOLAS CARRÈRE et JEAN-FRANÇOIS CARON qui ont participé à mon jury de thèse en tant qu'examineurs. Je remercie tous les membres du jury pour leur écoute attentive et leurs remarques intéressantes et profondes.

Ensuite, j'adresse mes plus chaleureux remerciements à tout le personnel du laboratoire Navier et spécialement à l'équipe MSA. Je remercie tous les chercheurs, secrétaires, techniciens et doctorants avec qui j'ai passé plus de trois ans de ma vie. Je les remercie du fond de mon cœur pour leur bonne humeur, sympathie, générosité, solidarité,... Merci à tous pour les bons moments inoubliables que j'ai passés avec vous et grâce à vous.

J'aimerais également remercier ma famille pour m'avoir permis de faire des études, plus particulièrement ma chère mère qui m'a consacré sa vie. Enfin, je remercie ma chère femme SAHAR qui m'a supporté non seulement dans ma vie privée mais aussi quotidiennement dans le laboratoire comme un collègue pendant trois ans. Je lui adresse toute ma gratitude et mon amour pour son soutien moral durant toute ma vie.

Résumé

L'analyse des phénomènes locaux comme les effets de bord libre et le délaminage dans les structures multicouches nécessite des théories fines qui donnent une bonne description de la réponse locale. Étant donné que les approches tridimensionnelles sont, en général, très coûteuses en temps de calcul et en mémoire, des approches bidimensionnelles de type “*layerwise*” sont souvent utilisées. Dans ce travail de doctorat, un modèle *layerwise* en contrainte, appelé LS1, est appliqué au problème du multi-délaminage dans les plaques stratifiées invariantes dans le sens longitudinal. L'invariance dans la direction de la longueur nous permet d'aborder le problème analytiquement. Dans un premier temps, nous proposons une méthode analytique pour l'analyse des plaques multicouches multi-délaminiées soumises à la traction uniaxiale. La singularité des contraintes interlaminaires aux bords libres et l'initiation du délaminage en mode III sont étudiées. Un modèle raffiné, nommé LS1 raffiné, est proposé pour améliorer les approximations dans les zones de singularités telles que les bords libres et les pointes de fissure. Les résultats du modèle raffiné sont validés en les comparant avec ceux obtenus par éléments finis tridimensionnels. Dans un deuxième temps, l'approche analytique proposée est étendue à la flexion cylindrique des plaques multicouches. La propagation du délaminage en modes I et II est étudiée et les approximations du modèle LS1 sont validées. À la fin, nous généralisons la méthode analytique proposée afin de prendre en considération tous les chargements invariants dans le sens longitudinal. L'approche finale permet d'analyser les plaques multicouches rectangulaires soumises à des charges invariantes sur les faces supérieure et inférieure, les forces ou les déplacements imposés sur les bords latéraux ainsi que quatre types de chargement sur les extrémités longitudinales: traction uniaxiale, flexion hors plan, torsion et flexion dans le plan. La solution analytique du modèle LS1 est obtenue pour une plaque stratifiée soumise à tous les chargements mentionnés ci-dessus. L'approche est validée en comparant avec la méthode des éléments finis tridimensionnels pour plusieurs types de chargement.

Mots-clés: Matériaux multicouches, Plaques stratifiées, Effets de bord libre, Multi-délaminage, Amorçage et propagation du délaminage, Contraintes interlaminaires, Taux de restitution d'énergie, Critères de délaminage



Abstract

The analysis of local phenomena such as free-edge effects and delamination in multilayered structures requires the accurate theories which can provide a good description of the local response. Since the three-dimensional approaches are generally very expensive in computational time and memory, the “*layerwise*” two-dimensional approaches are widely used. In this Ph.D. thesis, a stress layerwise model, called LS1, is applied to the multi-delamination problem in longitudinally invariant multilayered plates. The invariance in the longitudinal direction allows us to solve the problem analytically. At first, we propose an analytical method for the analysis of multi-delaminated multilayered plates subjected to the uniaxial traction. The free-edge interlaminare stress singularities and the mode III delamination onset are investigated. A refined model, called Refined LS1, is proposed in order to improve the approximations in singularity zones such as free edges and crack tips. The results of the refined model are validated by comparing them with those obtained by a three-dimensional finite element model. Afterwards, the proposed analytical approach is extended to the cylindrical bending of the multilayered plates. The propagation of delamination in modes I and II is studied and the approximations of the LS1 model are validated. At last, we generalize the proposed analytical method to take into account all invariant loads in the longitudinal direction. The final approach allows us to analyze the rectangular multilayered plates subjected to invariant loads on the top and bottom surfaces, imposed displacements or forces at the lateral edges, and also four types of loading at the longitudinal ends: uniaxial traction, out-of-plane bending, torsion and in-plane bending. The analytical solution of the LS1 model is obtained for a laminated plate subjected to all the loads mentioned above. The approach is validated by comparison with the three-dimensional finite element method for various types of loading.

Keywords: Multilayered materials, Laminated plates, Free-edge effects, Multi-delamination, Onset and propagation of delamination, Interlaminar stresses, Energy release rate, Delamination criteria

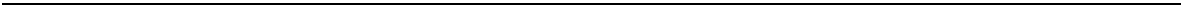


Table des matières

Tables des matières	9
Table des figures	13
Liste des tableaux	17
Introduction générale	19
1 Étude bibliographique	23
1.1 Modèles de plaques multicouches	26
1.1.1 Approche monocouche équivalente	28
1.1.1.1 Modèle de Kirchhoff-Love	28
1.1.1.2 Modèle de Reissner-Mindlin	29
1.1.1.3 Modèles d'ordre supérieur	31
1.1.2 Approche par couche	35
1.1.2.1 Le modèle layerwise de Reddy	37
1.1.3 Les modèles zig-zag	40
1.1.4 Modèles Multiparticulaires	43
1.2 Problématique du délaminage des matériaux multicouches	46
1.2.1 Mécanique de la rupture - Mécanique de l'endommagement	46
1.2.2 Mécanismes de rupture - Cadre de l'étude	47
1.2.3 Modes de rupture	49
1.2.4 Essais de délaminage	49
1.2.5 Critères de délaminage	49
1.2.5.1 Critères en contrainte	50
1.2.5.2 Critères en facteur d'intensité de contrainte	53
1.2.5.3 Critères énergétiques	54
1.2.5.4 Critère en déplacement d'ouverture de fissure	57
1.2.5.5 Double critère en résistance/ténacité	58
Annexe 1.A Formulation du model LS1	60
1.A.1 Méthode d'approximation de Hellinger-Reissner pour un problème d'élasticité 3D	60
1.A.2 Position du problème - Notation	62
1.A.3 Efforts généralisés	63
1.A.4 Déplacements généralisés	65

TABLE DES MATIÈRES

1.A.5	Déformations généralisées	66
1.A.6	Équations d'équilibre	67
1.A.7	Conditions aux limites	67
1.A.7.1	Conditions aux limites en contrainte	67
1.A.7.2	Conditions aux limites en déplacement	69
1.A.8	Relations de comportement	70
2	Delaminated multilayered plates under uniaxial extension. Part I: Analytical analysis using a layerwise stress approach	75
2.1	Introduction	77
2.2	The LS1 model	79
2.2.1	Generalized stresses and 3D stress field	80
2.2.2	Generalized displacements and generalized strains	80
2.2.3	Constitutive and equilibrium equations	81
2.2.4	Boundary conditions	82
2.3	Analysis of non-delaminated multilayered plate	83
2.3.1	Problem description	83
2.3.2	LS1 problem formulation	83
2.4	Analysis of delaminated multilayered plate	86
2.4.1	Laminate with one interfacial crack	86
2.4.2	Laminate with several interfacial cracks	88
2.5	Finite element validation	89
2.5.1	Interlaminar stress distributions	91
2.5.2	3D-stress distributions at layers	91
2.5.2.1	Stress distributions at the middle plane of the layers	91
2.5.2.2	Stress distributions through the thickness	92
2.6	Conclusion	93
Appendix 2.A	Expression of the 3D stress field	100
Appendix 2.B	Analytical solution of non-delaminated multilayered plate	101
Appendix 2.C	Analytical solution of delaminated multilayered plate - a single interfacial crack	104
Appendix 2.D	Analytical solution of delaminated multilayered plate - several interfacial cracks	105
3	Delaminated multilayered plates under uniaxial extension. Part II: Efficient layerwise mesh strategy for the prediction of delamination onset	107
3.1	Introduction	109
3.1.1	Analytical methods	110
3.1.2	Numerical methods	111
3.1.3	Present study	112
3.2	Problem description and LS1 Solution	114
3.3	An efficient layerwise mesh strategy	116
3.4	Numerical validation and discussion	118
3.4.1	Layerwise mesh influence	118

TABLE DES MATIÈRES

3.4.1.1	Free edge singularity	119
3.4.1.2	Crack tip singularity	119
3.4.1.3	Energy release rate	121
3.4.2	Finite element comparison	121
3.4.2.1	Non-delaminated state	124
3.4.2.2	Delaminated state	125
3.4.2.3	Delamination initiation criterion - Experimental comparison	127
3.4.3	Discussion	129
3.5	Conclusion	130
Appendix 3.A	Crack tip stress singularity curves for $a = e$ and $a = 10e$. . .	132
4	Cylindrical bending of multilayered plates with multi-delamination via a layerwise stress approach	135
4.1	Introduction	137
4.2	Cylindrical bending problem	140
4.2.1	Problem description	140
4.2.2	Formulation of the LS1 model	140
4.2.3	x -invariance hypothesis	142
4.3	Analytical LS1 solution	143
4.3.1	Non-delaminated zone	143
4.3.2	Delaminated zone	145
4.3.3	Solution	147
4.4	Numerical examples	148
4.4.1	Mode I delamination - DCB like test	149
4.4.2	Mode II delamination - ENF like test	153
4.5	Conclusion	155
Appendix 4.A	Definition of matrices	157
Appendix 4.B	Solution of homogeneous system of second-order differential equations	158
4.B.1	Simple eigenvalues	158
4.B.2	Repeated and zero eigenvalues	158
5	Stress analysis of long multilayered plates subjected to invariant loading: Analytical solutions by a layerwise stress model	161
5.1	Introduction	163
5.2	x -invariance condition	165
5.2.1	Problem description	165
5.2.2	3D formulation	166
5.2.3	LS1 model formulation	169
5.3	LS1 solution	171
5.3.1	System of equations	172
5.3.2	Solution	172
5.4	Numerical examples	173
5.4.1	Overall stiffness matrix	174

TABLE DES MATIÈRES

5.4.2	Interfacial stresses	176
5.4.3	Effects of end constraint	179
5.5	Conclusion	181
Appendix 5.A	Reduced form of 3D displacement field	183
Appendix 5.B	General formulation of the LS1 model	185
Appendix 5.C	Definition of scalars, vectors and matrices	187
Appendix 5.D	LS1 system of equations	190
Appendix 5.E	Kirchhoff-Love solution	194
Conclusion générale et perspectives		197
Références bibliographiques		201

Table des figures

1.1	Structures multicouches: panneau sandwich (à gauche) - plaque composite (à droite)	25
1.2	Cinématique du modèle de Kirchhoff-Love	29
1.3	Cinématique du modèle de Reissner-Mindlin	30
1.4	Cinématique d'un modèle d'ordre supérieur	31
1.5	Approche par couche	35
1.6	Modèle layerwise de Reddy: interpolation linéaire des déplacements	39
1.7	Champ de déplacement dans le modèle zig-zag du premier ordre	42
1.8	Modes de rupture d'une fissure	49
1.9	Différents essais de délaminage existant dans la littérature	51
1.10	Critère en déplacement d'ouverture de fissure	57
1.11	Multicouche dans le repère Cartésien - Notation du modèle LS1	62
2.1	Laminate geometry, imposed displacements and coordinate system	83
2.2	Laminate with an interfacial crack of length a at the interface $k, k + 1$	86
2.3	Laminate section with several cracks at different interfaces	88
2.4	Solving method for the laminate with several cracks	89
2.5	$(30^\circ, 60^\circ)_s$ laminate under uniaxial extension with delamination at the interfaces $30^\circ/60^\circ$	90
2.6	Finite element model of the laminate in delaminated state - 3D model (top); mesh in the yz plane (bottom)	90
2.7	Distribution of the interlaminar stresses σ_{xz} , σ_{yz} and σ_{zz} at the $30^\circ/60^\circ$ interface of $(30^\circ, 60^\circ)_s$ laminate	92
2.8	Distribution of the normal stress σ_{xx} at the middle of the layers in $(30^\circ, 60^\circ)_s$ laminate	94
2.9	Distribution of the normal stress σ_{yy} at the middle of the layers in $(30^\circ, 60^\circ)_s$ laminate	94
2.10	Distribution of the shear stress σ_{xy} at the middle of the layers in $(30^\circ, 60^\circ)_s$ laminate	94
2.11	Distribution of the shear stress σ_{xz} at the middle of the layers in $(30^\circ, 60^\circ)_s$ laminate	95
2.12	Distribution of the shear stress σ_{yz} at the middle of the layers in $(30^\circ, 60^\circ)_s$ laminate	95
2.13	Distribution of the normal stress σ_{zz} at the middle of the layers in $(30^\circ, 60^\circ)_s$ laminate	95

TABLE DES FIGURES

2.14	Distribution of the normal stress σ_{xx} through the thickness of $(30^\circ, 60^\circ)_s$ laminate	96
2.15	Distribution of the normal stress σ_{yy} through the thickness of $(30^\circ, 60^\circ)_s$ laminate	96
2.16	Distribution of the shear stress σ_{xy} through the thickness of $(30^\circ, 60^\circ)_s$ laminate	97
2.17	Distribution of the shear stress σ_{xz} through the thickness of $(30^\circ, 60^\circ)_s$ laminate	97
2.18	Distribution of the shear stress σ_{yz} through the thickness of $(30^\circ, 60^\circ)_s$ laminate	98
2.19	Distribution of the normal stress σ_{zz} through the thickness of $(30^\circ, 60^\circ)_s$ laminate	98
3.1	Laminate geometry; imposed displacements and coordinate system . . .	114
3.2	Laminate section with several cracks at different interfaces - Subdivision in the section	116
3.3	Laminate under uniaxial extension; irregular and regular layerwise mesh through the thickness	117
3.4	Progressive layerwise mesh through the physical layer thickness	118
3.5	Laminate section with four interfacial cracks at the interfaces $\theta/ - \theta$. .	119
3.6	Distribution of the interlaminar shear stress σ_{xz} at the interface $10^\circ/ - 10^\circ$ - Free edge singularity ($a = 0$); (P is the number of mathematical layers per physical layer and k_{xz} denotes the normalized interlaminar stress) .	120
3.7	Convergence of the interlaminar shear stress σ_{xz} at different distances from the free edge	120
3.8	Distribution of the interlaminar shear stress σ_{xz} at the interface $10^\circ/ - 10^\circ$ - Crack tip singularity ($a=0.1e$); (P is the number of mathematical layers per physical layer and k_{xz} denotes the normalized interlaminar stress) .	122
3.9	Convergence of the interlaminar shear stress σ_{xz} at different distances from the crack tip ($a = 0.1e$)	122
3.10	Convergence of the energy release rate for different interlaminar crack lengths a	123
3.11	Finite element model of the laminate in non-delaminated state - 3D model (top); mesh in the yz plane (bottom)	124
3.12	Distribution of the interlaminar stresses at the interface $\theta/ - \theta$ of $(\pm\theta)_s$ laminates	125
3.13	Distribution of the interlaminar shear stress σ_{xz} at the interface $\theta/ - \theta$ of $(\pm\theta)_s$ laminates	126
3.14	3D-FE model: mesh in the yz plane in delaminated state	126
3.15	The normalized incremental energy release rate $\bar{A}(a)$ versus the normalized crack length a/e at the interface $\theta/ - \theta$ of $(\pm\theta)_s$ laminates	128
3.16	Distribution of the interlaminar shear stress σ_{xz} at the interface $\theta/ - \theta$ of $(\pm\theta)_s$ laminates in delaminated state	128

TABLE DES FIGURES

3.17	Comparison of the predicted critical longitudinal stress at delamination onset (continuous lines) with the experimental values (points) for $(\pm\theta)_s$ laminates	129
3.18	Distribution of the interlaminar shear stress σ_{xz} at the interface $10^\circ/-10^\circ$ - Crack tip singularity ($a=e$); (P is the number of mathematical layers per physical layer and k_{xz} denotes the normalized interlaminar stress)	132
3.19	Distribution of the interlaminar shear stress σ_{xz} at the interface $10^\circ/-10^\circ$ - Crack tip singularity ($a = e$)	132
3.20	Distribution of the interlaminar shear stress σ_{xz} at the interface $10^\circ/-10^\circ$ - Crack tip singularity ($a=10e$); (P is the number of mathematical layers per physical layer and k_{xz} denotes the normalized interlaminar stress)	133
3.21	Distribution of the interlaminar shear stress σ_{xz} at the interface $10^\circ/-10^\circ$ - Crack tip singularity ($a = 10e$)	133
4.1	Laminate geometry, bending load and coordinate system (top); Laminate section in the yz plane	139
4.2	Solving method for laminate with several interfacial cracks	143
4.3	R-Curves (Resistance versus crack extension) used for mode I and mode II delamination	149
4.4	Mode I delamination : Undeformed State (Top); Deformed state (Bottom)	150
4.5	Mode I delamination - Finite element model	151
4.6	Compliance (Left) and energy release rate (right) versus crack length - Mode I delamination	151
4.7	Crack opening displacement versus crack length - Mode I delamination	152
4.8	Applied load versus crack length - Mode I delamination	152
4.9	Applied load versus crack opening displacement - Mode I delamination	152
4.10	Mode II delamination : Undeformed State (Top); Deformed state (Bottom)	153
4.11	Mode II delamination - Finite element model	153
4.12	Compliance (Left) and energy release rate (right) versus crack length - Mode II delamination	154
4.13	Midspan deflection versus crack length - Mode II delamination	155
4.14	Applied load versus crack length - Mode II delamination	155
4.15	Applied load versus midspan deflection - Mode II delamination	155
5.1	(a) Loading on the top/bottom surfaces of the laminate ($z = \pm h$) - (b) Arbitrary boundary conditions at the lateral edges ($y = \pm b$)	166
5.2	A long plate under different types of loading at its longitudinal ends	167
5.3	Laminate under different types of loading at the ends $x = \pm l$	169
5.4	Finite element model of the laminate: undeformed state (top); deformed state in torsion (bottom)	174
5.5	Layerwise mesh used in the LS1 model	177
5.6	Free-edge stresses in the 3D-FEM for the load condition 6	177
5.7	Distribution of interfacial stresses for the load condition 4	177
5.8	Distribution of interfacial stresses for the load condition 6	178
5.9	Distribution of interfacial stresses for the load condition 8	179

TABLE DES FIGURES

5.10 Distribution of interfacial stresses: comparison between the load conditions 1 and 2 180

5.11 Distribution of interfacial stresses: comparison between the load conditions 5 and 6 181

Liste des tableaux

- 1.1 Les différents modèles $M4$ en comparant avec les modèles classiques de plaques 44
- 1.2 Essais de délaminage 50

- 3.1 Generalized stresses and generalized strains of layer i 115
- 3.2 Generalized stresses and generalized strains of interface $i, i + 1$ 115
- 3.3 Mechanical material properties of the ply for G947/M18 and CTE1/T700 carbon-epoxy 123

- 5.1 Overall stiffness matrix of $(0^\circ, -60^\circ, 45^\circ, -30^\circ)$ laminate: comparison between the Kirchhoff-Love, LS1 and 3D-FE models 175

LISTE DES TABLEAUX

Introduction générale

Au cours des dernières décennies, l'utilisation des matériaux multicouches dans différentes applications d'ingénierie a largement augmenté. Malgré les avantages que présentent ces matériaux (grande rigidité, résistance mécanique élevée, légèreté,...), ils apportent aussi des problèmes spécifiques liés principalement à leur hétérogénéité. Il est bien connu dans la littérature que la différence des propriétés mécaniques entre des couches adjacentes peut entraîner des contraintes très élevées aux interfaces près des bords libres. Ces contraintes interfaciales élevées peuvent engendrer des fissurations au niveau des interfaces qu'on appelle délaminage. Ce problème a attiré beaucoup d'attention en raison de son influence significative sur la résistance et la rigidité des structures multicouches.

Le délaminage est en réalité un phénomène local tridimensionnel (3D). Vu la complexité du problème, des approches numériques 3D sont souvent utilisées. L'avantage de ces approches est qu'elles sont précises et peuvent fournir une bonne description des phénomènes. Cependant, elles sont souvent très coûteuses en temps de calcul et en mémoire. C'est la raison pour laquelle des approches alternatives à la fois précises et efficaces sont toujours recherchées.

L'épaisseur relativement faible des structures multicouches permet d'utiliser des approches bidimensionnelles (2D) pour leur analyse. Différentes théories de plaques de type "*monocouche équivalente*" ou "*layerwise*" ont été proposées dans la littérature pour l'analyse des plaques multicouches. Les approches *monocouche équivalente* considèrent la plaque multicouche comme une plaque homogène. Bien que ces approches fournissent des résultats relativement acceptables pour la réponse globale du multicouche, leurs approximations au niveau local sont très imprécises. Elles ne sont pas pertinentes pour étudier des phénomènes locaux comme les effets de bord libre, le délaminage, etc. En revanche, les modèles *layerwise* considèrent chaque couche comme une plaque 2D. Ces approches permettent d'étudier des réponses locales dans des structures multicouches et assurent un bon compromis entre la précision et l'efficacité. C'est pourquoi des modèles *layerwise* sont d'excellentes alternatives aux modèles 3D.

Dans le cadre de cette thèse de doctorat, nous utilisons un modèle *layerwise*, appelé *LS1*, pour l'analyse des stratifiés multicouches soumis à des chargements invariants dans le sens de la longueur. Inspiré du modèle de Pagano [1978a], le modèle LS1 a été développé au Laboratoire Navier en considérant les couches comme des plaques de Reissner-Mindlin qui sont reliées au niveau des interfaces. Le modèle LS1 a été utilisé et validé dans plusieurs travaux de recherche menés au sein du Laboratoire Navier. La plupart de ces travaux ont été effectués en utilisant des approches numériques et

un code de calcul aux éléments finis spécifique, appelé MPFEAP, qui a été développé dans le laboratoire. Dans ce travail, nous nous intéressons aux plaques multicouches soumises à des chargements invariants dans le sens de la longueur. Nous montrons que l'utilisation du modèle LS1 permet de résoudre le problème d'une manière analytique même en présence d'un multi-délaminage.

Le premier chapitre est consacré à une étude bibliographique sur modèles de plaques et sur le délaminage. Nous faisons tout d'abord une présentation des modèles de type monocouche équivalente: les théories classiques du premier ordre de Kirchhoff-Love et de Reissner-Mindlin et puis différents modèles d'ordre supérieur. Ensuite, des approches par couche (layerwise) et des modèles de type zig-zag sont présentés. Une synthèse est effectuée sur les modèles multiparticulaires similaires au modèle LS1. Le chapitre se termine par une bibliographie sur la problématique du délaminage: approches mécaniques de la fissuration, modes de rupture, essais classiques et critères d'initiation et de propagation seront décrits. Les étapes de construction du modèle LS1 dans le cadre de l'élasticité linéaire et sa formulation complète sont détaillées dans l'annexe.

Au chapitre 2, on utilise le modèle LS1 pour étudier des plaques multicouches soumises à la traction uniaxiale. D'abord, la solution analytique du modèle dans le cas des plaques non-délaminées est obtenue. Ensuite, le modèle est étendu au cas des plaques multicouches avec une configuration quelconque de multi-délaminage dans la section. Une méthode systématique est proposée pour traiter le problème et la solution analytique du modèle LS1 est obtenue en utilisant la méthode de décomposition en vecteurs propres. On remarque que le multi-délaminage fait qu'il y a, en général, des valeurs propres nulles, répétitives, et complexes. Afin de vérifier la précision du modèle LS1, ses résultats sont comparés avec ceux obtenus par la méthode des éléments finis 3D.

Pour améliorer la précision du modèle LS1 dans les zones où il y a des singularités de contraintes, on propose au chapitre 3 une sorte de maillage dans l'épaisseur de chaque couche physique qu'on appelle le maillage layerwise. Cela consiste à modéliser chaque couche physique par plusieurs couches dans le modèle. Au lieu d'une discrétisation régulière dans l'épaisseur de chaque couche (qu'on trouve dans la littérature), on propose un maillage layerwise irrégulier. La stratégie est de diminuer progressivement les épaisseurs des couches fictives au voisinage des interfaces physiques (comme un raffinement du maillage près des interfaces dans des simulations numériques). Le modèle raffiné, appelé le modèle LS1 raffiné, est appliqué au problème de l'initiation de délaminage en traction uniaxiale (mode III) dans des plaques composites. Les singularités de contraintes aux bords libres et aux pointes de fissures sont étudiées et les résultats du modèle LS1 raffiné sont comparés avec ceux des éléments finis 3D.

Après l'étude de l'amorçage du délaminage au chapitre 3, on applique au chapitre 4 le modèle LS1 au problème de la propagation du délaminage. On propose d'étudier la propagation du délaminage en modes I et II. Pour ce faire, on traite la flexion cylindrique d'une longue plaque multicouche soumise à un chargement quelconque sur sa face supérieure. Le délaminage peut consister en une ou plusieurs interfaces fissurées avec des longueurs différentes dans la section de la plaque. La formulation du modèle LS1 est effectuée pour ce problème et la solution est obtenue analytiquement. Deux

essais classiques de la propagation de délaminage en mode I (DCB) et en mode II (ENF) sont traités. Les résultats du modèle LS1 en termes de force, déplacement, taux de restitution d'énergie, complaisance,... sont validés en comparaison avec des éléments finis 3D.

Les chapitres 2 à 4 portent sur deux types de chargement: traction uniaxiale et flexion cylindrique. On propose au chapitre 5 d'aborder le problème dans le cas le plus général en considérant tous les chargements possibles. On reste toujours dans le cadre des plaques multicouches pour lesquelles on peut supposer que les déformations sont invariantes dans la direction longitudinale. Pour une telle plaque rectangulaire, on peut distinguer trois types de chargement: le premier est le chargement sur les faces supérieure et inférieure de la plaque. Le deuxième consiste à imposer des forces ou des déplacements sur les bords latéraux de la plaque, se traduisant par des conditions aux limites dans notre approche. Ces deux types de chargement sont supposés invariants dans la direction longitudinale. Le troisième concerne le chargement aux extrémités longitudinales de la plaque. Afin d'identifier tous les chargements possibles à ces extrémités, on écrit la formulation 3D du problème. En se basant sur l'invariance du champ de déformations dans le sens longitudinal et en intégrant les relations déformation-déplacement, la forme réduite des déplacements 3D est obtenue. Il en résulte qu'il y a seulement quatre types de chargement qui peuvent être appliqués aux extrémités: traction uniaxiale, flexion hors plan, torsion et flexion dans le plan. Le modèle LS1 est ainsi étendu à l'analyse des plaques multicouches rectangulaires soumises à tous les chargements invariants mentionnés. La formulation du problème est écrite sous la forme matricielle et la solution analytique du problème est présentée. Afin d'illustrer la précision et l'efficacité de la méthode proposée, on traite plusieurs exemples correspondant à différents types de chargement. Des comparaisons entre les résultats du modèles LS1 et des éléments finis 3D sont faites en termes de la matrice de rigidité, des contraintes d'interfaces près des bords libres, etc.

Chapitre 1

Étude bibliographique

Ce chapitre a pour objectif de faire une synthèse bibliographique sur la modélisation des matériaux multicouches. D'abord, nous présentons différents modèles de plaques multicouches existants dans la littérature. Ensuite, la formulation complète du modèle LS1 qui va être utilisé dans le cadre de cette thèse sera présentée en détail. A la fin, nous abordons le problème du délaminage ou fissuration interlaminaire dans des plaques multicouches en présentant différents mécanismes et modes de rupture, approches de modélisations, critères, etc.

Sommaire

1.1 Modèles de plaques multicouches	26
1.1.1 Approche monocouche équivalente	28
1.1.1.1 Modèle de Kirchhoff-Love	28
1.1.1.2 Modèle de Reissner-Mindlin	29
1.1.1.3 Modèles d'ordre supérieur	31
1.1.2 Approche par couche	35
1.1.2.1 Le modèle layerwise de Reddy	37
1.1.3 Les modèles zig-zag	40
1.1.4 Modèles Multiparticulaires	43
1.2 Problématique du délaminage des matériaux multicouches	46
1.2.1 Mécanique de la rupture - Mécanique de l'endommagement	46
1.2.2 Mécanismes de rupture - Cadre de l'étude	47
1.2.3 Modes de rupture	49
1.2.4 Essais de délaminage	49
1.2.5 Critères de délaminage	49
1.2.5.1 Critères en contrainte	50
1.2.5.2 Critères en facteur d'intensité de contrainte	53
1.2.5.3 Critères énergétiques	54
1.2.5.4 Critère en déplacement d'ouverture de fissure	57
1.2.5.5 Double critère en résistance/ténacité	58
Annexe 1.A Formulation du model LS1	60
1.A.1 Méthode d'approximation de Hellinger-Reissner pour un problème d'élasticité 3D	60
1.A.2 Position du problème - Notation	62
1.A.3 Efforts généralisés	63
1.A.4 Déplacements généralisés	65
1.A.5 Déformations généralisées	66
1.A.6 Équations d'équilibre	67
1.A.7 Conditions aux limites	67
1.A.7.1 Conditions aux limites en contrainte	67
1.A.7.2 Conditions aux limites en déplacement	69
1.A.8 Relations de comportement	70

Les structures multicouches sont de plus en plus utilisées dans le cadre de différents projets d'ingénierie, notamment dans les secteurs industriels de l'aéronautique, de l'automobile, du génie civil, de la marine et du sport et loisirs. Par exemple, un panneau sandwich (Fig. 1.1) est une structure à trois couches constituée d'une couche centrale souple (l'âme) et deux couches externes rigides (les peaux). Les matériaux composites sont aussi des stratifiés multicouches constitués de plusieurs couches collées entre elles. Chaque couche (pli) est composée des fibres de renfort qui sont incorporées dans un matériau appelé la matrice. Les fibres ont, en général, de très hautes caractéristiques mécaniques dans la direction longitudinale pour assurer la tenue mécanique. Le rôle de la matrice est la cohésion de la structure, la répartition des contraintes dans les fibres et la protection des fibres vis-à-vis des conditions environnementales. Les fibres sont généralement en carbone, métal, verre, polymère, etc. Les matrices peuvent être en diverses résines rigides (très souvent en époxy). Comme d'autres exemples de structures multicouches, nous pouvons citer des panneaux lamellés-collés, des isolants thermiques multicouches, des plaques multicouches piézoélectriques, etc.

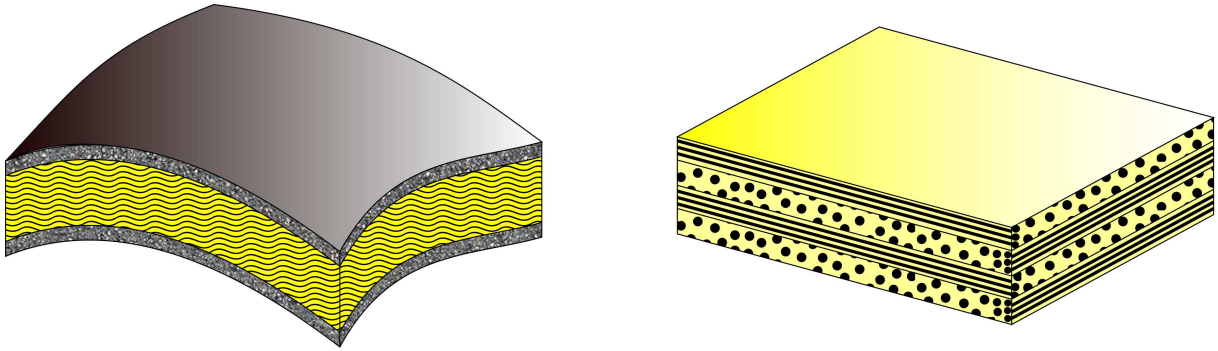


Figure 1.1: Structures multicouches: panneau sandwich (à gauche) - plaque composite (à droite)

L'analyse des structures multicouches est toujours une problématique importante nécessitant des théories raffinées qui prennent en compte différents phénomènes. Par exemple, l'anisotropie très forte dans les structures sandwichs, c'est-à-dire le faible rapport du module de cisaillement transverse de l'âme par rapport au module d'élasticité longitudinal des peaux, exige un modèle qui rende compte des effets de cisaillement transverse. À cause de la complexité du problème, les approches tridimensionnelles sont souvent utilisées dans la littérature. Ces approches donnent une bonne description des phénomènes tridimensionnels comme des effets de bord libre, délaminage, fissuration transverse, etc. et permettent d'obtenir des résultats très précis. Toutefois, elles aboutissent à des équations différentielles qui ne peuvent pas être résolues facilement. La résolution analytique de ces équations différentielles est limitée à quelques cas de géométrie, empilement et chargement simple, bord libre droit, etc. [Pagano 1969, 1970b, Srinivas and Rao 1970]. C'est pourquoi différentes méthodes numériques (éléments finis, éléments de frontières, éléments discrets,...) sont développées pour la résolution des équations tridimensionnelles. Ces méthodes sont en général très coûteuses en temps de calcul et en mémoire. En conséquence, beaucoup d'approches bidimensionnelles sim-

plifiées sont proposées dans la littérature pour l'analyse des structures multicouches.

Une structure multicouche peut être considérée comme un solide hétérogène constituée d'un nombre fini de couches homogènes anisotropes. En général, les structures multicouches ont une épaisseur faible par rapport aux autres dimensions, ce qui permet de ramener le problème tridimensionnel (3D) à un problème bidimensionnel (2D) et d'utiliser des théories bidimensionnelles de type plaque qui sont plus pratiques pour l'analyse. Le passage de 3D à 2D se fait en éliminant la variable d'épaisseur. En général, cette élimination est effectuée via une intégration dans la direction de l'épaisseur et peut être réalisée selon différentes méthodes. Dans ce qui suit, nous effectuons, dans un premier temps, une synthèse bibliographique de la plupart des modèles de plaques multicouches qui existent dans la littérature. Nous essayons de décrire les hypothèses de base des modèles présentés afin de pouvoir comparer les avantages et les inconvénients de chaque modèle. Ensuite, nous nous concentrons sur le modèle LS1 qui sera utilisé dans le cadre de ce travail. La formulation complète et les travaux déjà effectués sur ce modèle seront décrits. À la fin, nous effectuerons une analyse bibliographique sur la fissuration interlaminaire ou le délaminage dans des plaques multicouches, et différents approches et critères concernant ce mode de rupture seront présentés.

1.1 Modèles de plaques multicouches

Durant ces dernières années, plusieurs modèles bidimensionnels (2D) ont été développés pour l'analyse des structures multicouches. Ces modèles peuvent être regroupés selon différents points de vue:

- Élimination de la variable d'épaisseur:
 - approche axiomatique
 - approche asymptotique

- Choix des champs inconnus:
 - approche en déplacement
 - approche en contrainte
 - approche mixte

- Description des champs dans l'épaisseur:
 - approche monocouche équivalente
 - approche par couche

Les approches axiomatiques, qui sont très classiques, supposent explicitement la forme des champs inconnus dans l'épaisseur du multicouche, par exemple des fonctions

polynomiales. Puisque dans ce type d'approches on postule la forme des champs, il n'y a pas, a priori, de convergence vers la solution 3D quand le rapport entre l'épaisseur et la longueur de plaque tend vers zéro. Dans les approches asymptotiques, les équations 3D sont développées en termes d'une variable de perturbation δ (en général $\delta = h/L$ où h et L sont, respectivement, l'épaisseur et la longueur de la structure). Ce développement intervient au niveau des équations de l'élasticité et les termes avec le même ordre en δ sont identifiés. L'avantage des approches asymptotiques est qu'elles donnent des approximations cohérentes dans le sens où tous les termes ayant le même ordre sont retenus. En outre, il est évident que quand δ tend vers zéro, la solution du développement asymptotique tend vers la solution 3D. En revanche, la précision de ce type d'approches diminue avec l'augmentation de l'épaisseur. Par ailleurs, la prise en compte de l'anisotropie dans des structures multicouches hétérogènes nécessite un travail supplémentaire. Certaines études dans ce domaine peuvent être trouvées dans les travaux de [Friedrichs and Dressler \[1961\]](#), [Gol'denveizer \[1961, 1962\]](#), [Gol'denveizer and Kolos \[1965\]](#), [Cicala \[1965\]](#), [Widera \[1970\]](#), [Johnson and Widera \[1971\]](#), [Ciarlet and Destuynder \[1979\]](#), [Ciarlet and Paumier \[1986\]](#), [Ciarlet and Lods \[1996a,b,c\]](#), [Ciarlet et al. \[1996\]](#), [Ciarlet \[1998\]](#), [Caillerie and Nedelec Communicater \[1984\]](#), [Caillerie and Sanchez-Palencia \[1995\]](#), [Mittelstedta and Becker \[2005\]](#), [Dallot and Sab \[2008a\]](#). Dans ce qui suit, on ne détaille pas les approches asymptotiques étant donné que la plupart des modèles existants dans la littérature sont basés sur des approches axiomatiques.

La résolution des équations du problème (équilibre, compatibilité et loi de comportement) se fait en faisant un choix sur les champs inconnus. Dans les approches en déplacement, les déplacements de la structure sont considérés comme les champs inconnus alors que dans les approches en contrainte, ce sont les contraintes qui sont utilisées comme des variables inconnues. Dans le cas d'une approche mixte, à la fois les déplacements et les contraintes sont introduits comme des champs inconnus. En fonction du choix des variables inconnues, beaucoup de méthodes variationnelles, théorèmes et principes ont été présentés dans la littérature pour la construction de solutions approchées. À titre d'exemple, nous pouvons citer les principes des déplacements virtuels, des forces virtuelles, des puissances virtuelles, le principe de Hellinger-Reissner, le principe de Hu-Washizu, etc.

Une fois choisis des champs inconnus, leur description dans l'épaisseur peut être de type monocouche ou par couche. Dans une approche monocouche, les champs sont introduits sur toute la plaque dans la direction transverse. De cette manière, le champ inconnu $f(x, y, z)$ est considéré:

$$f(x, y, z) = f_1(x, y) F_1(z) + \dots + f_N(x, y) F_N(z) \quad (1.1)$$

où x et y sont les directions dans le plan et z signifie la direction de l'épaisseur. En revanche, dans une approche par couche, chaque couche i est considérée comme une plaque indépendante. Dans ce cas, le champ f est écrit comme suit:

$$f^i(x, y, z) = f_1^i(x, y) F_1^i(z) + \dots + f_N^i(x, y) F_N^i(z) \quad , \quad h_-^i \leq z \leq h_+^i \quad (1.2)$$

où h_-^i et h_+^i sont les cotes inférieure et supérieure de la couche i .

1.1.1 Approche monocouche équivalente

Dans ce type d'approche, le multicouche hétérogène est considéré comme une seule couche homogène équivalente. Par conséquent, le nombre d'équations du modèle ne dépend pas du nombre de couches. La plupart de ces modèles sont des approches en déplacement et se distinguent par la forme choisie pour la section transverse. Les modèles de Kirchhoff-Love et de Reissner-Mindlin sont les modèles classiques les plus connus.

1.1.1.1 Modèle de Kirchhoff-Love

Le modèle classique de Kirchhoff-Love se base sur l'hypothèse que la section transverse de la plaque reste plane et perpendiculaire au plan moyen après déformation [Kirchhoff 1850, Love 1927, Stavsky and Loewy 1971] (Fig. 1.2) Cela revient à dire que le cisaillement hors plan est supposé négligeable dans ce. De plus, il est supposé que la variation de l'épaisseur de la plaque est négligeable. Ces hypothèses imposent la cinématique suivante ($\alpha, \beta \in \{x, y\}$):

$$\begin{aligned} U_\alpha(x, y, z) &= u_\alpha(x, y) - z u_{z,\alpha}(x, y) \\ U_z(x, y, z) &= u_z(x, y) \end{aligned} \quad (1.3)$$

où u_α est le déplacement membranaire du plan moyen dans la direction α et u_z est la flèche du plan moyen de la plaque.

A partir du champ de déplacement ci-dessus, les déformations s'obtiennent comme suit:

$$\begin{aligned} \varepsilon_{\alpha\beta}(x, y, z) &= E_{\alpha\beta}(x, y) + z \chi_{\alpha\beta}(x, y) \\ \varepsilon_{\alpha z}(x, y, z) &= \varepsilon_{z\alpha}(x, y, z) = 0 \end{aligned} \quad (1.4)$$

avec

$$\begin{aligned} E_{\alpha\beta}(x, y) &= \frac{1}{2} [u_{\alpha,\beta}(x, y) + u_{\beta,\alpha}(x, y)] \\ \chi_{\alpha\beta}(x, y) &= -u_{z,\alpha\beta}(x, y) \end{aligned} \quad (1.5)$$

où $E_{\alpha\beta}$ représente les déformations membranaires et $\chi_{\alpha\beta}$ les courbures.

Remarque: Les efforts généralisés du modèle de Kirchhoff-Love sont:

$$N_{\alpha\beta}(x, y) = \int_h \sigma_{\alpha\beta}(x, y, z) dz \quad , \quad M_{\alpha\beta}(x, y) = \int_h z \sigma_{\alpha\beta}(x, y, z) dz \quad (1.6)$$

où $N_{\alpha\beta}$ et $M_{\alpha\beta}$ sont, respectivement, des efforts membranaires et des moments. En effet, à part $\sigma_{\alpha\beta}$ les autres contraintes sont supposées négligeables. Cela veut dire que le modèle de Kirchhoff-Love est en réalité un modèle en contraintes planes, ce qui semble contredire la cinématique précédente en déformations planes.

L'application du modèle de Kirchhoff-Love aux structures multicouches est souvent désigné comme "*Classical Lamination Theory (CLT)*".

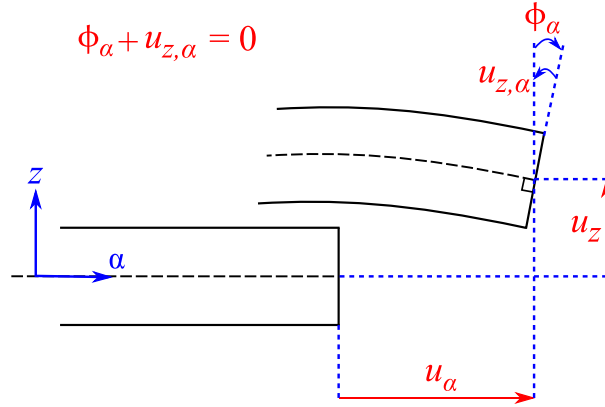


Figure 1.2: Cinématique du modèle de Kirchhoff-Love

1.1.1.2 Modèle de Reissner-Mindlin

Dans le modèle de Reissner-Mindlin, afin de prendre en considération l'effet du cisaillement transverse, il est supposé que la section transverse reste plane mais pas forcément normale au plan moyen de la plaque [Reissner 1945, Mindlin 1951, Whitney 1969] (Fig. 1.3). D'après cette hypothèse, les déplacements s'écrivent ($\alpha, \beta \in \{x, y\}$):

$$\begin{aligned} U_\alpha(x, y, z) &= u_\alpha(x, y) + z \phi_\alpha(x, y) \\ U_z(x, y, z) &= u_z(x, y) \end{aligned} \quad (1.7)$$

où u_α est le déplacement membranaire du plan moyen dans la direction α , u_z est la flèche du plan moyen et ϕ_α est la rotation du plan moyen.

Ces déplacements génèrent les déformations suivantes:

$$\begin{aligned} \varepsilon_{\alpha\beta}(x, y, z) &= E_{\alpha\beta}(x, y) + z \chi_{\alpha\beta}(x, y) \\ \varepsilon_{\alpha z}(x, y, z) &= \frac{1}{2} [\phi_\alpha(x, y) + u_{z,\alpha}(x, y)] \\ \varepsilon_{zz}(x, y, z) &= 0 \end{aligned} \quad (1.8)$$

avec

$$\begin{aligned} E_{\alpha\beta}(x, y) &= \frac{1}{2} [u_{\alpha,\beta}(x, y) + u_{\beta,\alpha}(x, y)] \\ \chi_{\alpha\beta}(x, y) &= \frac{1}{2} [\phi_{\alpha,\beta}(x, y) + \phi_{\beta,\alpha}(x, y)] \end{aligned} \quad (1.9)$$

où $E_{\alpha\beta}$ représente les déformations membranaires et $\chi_{\alpha\beta}$ les courbures.

Puisque $\varepsilon_{\alpha\beta}$ est affine en z , les contraintes dans le plan $\sigma_{\alpha\beta}$ sont affines par couches. Au niveau du cisaillement transverse les déformations $\varepsilon_{\alpha z}$ sont constantes en z . Par conséquent, les contraintes de cisaillement transverse $\sigma_{\alpha z}$ sont constantes par couche. Ceci est une mauvaise approximation même dans le cas des plaques homogènes car si

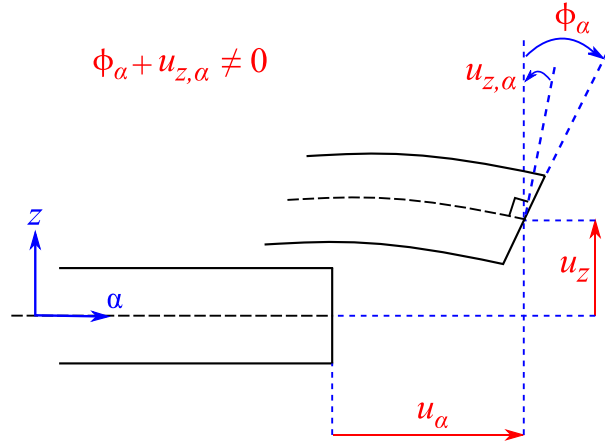


Figure 1.3: Cinématique du modèle de Reissner-Mindlin

$\sigma_{\alpha\beta}$ est affine en z par couche, d'après les équations d'équilibre $\sigma_{\alpha z}$ doit être quadratique en z). De plus, $\varepsilon_{zz} = 0$ est en contradiction avec l'hypothèse classique des contraintes planes ($\sigma_{zz} = 0$). Tout ceci fait que le modèle prédit très mal le comportement en cisaillement transverse et qu'il faut introduire la notion de coefficient correcteur pour améliorer la prise en compte des effets de cisaillement hors plan [Whitney 1973, Levinson 1980]. Dans le cas des plaques multicouches, le fait que les contraintes de cisaillement transverse sont constantes par couche entraîne des discontinuités de contrainte aux interfaces.

Remarque: En imposant $\varepsilon_{xz} = \varepsilon_{yz} = 0$ dans la formulation du modèle de Reissner-Mindlin, on arrive au modèle de Kirchhoff-Love:

$$\varepsilon_{\alpha z}(x, y, z) = 0 \quad \implies \quad \phi_\alpha(x, y) = -u_{z,\alpha}(x, y) \quad (1.10)$$

L'application du modèle de Reissner-Mindlin aux structures multicouches est souvent désigné comme "*First-order Shear Déformation Theory (FSDT)*" car les déformations de cisaillement transverse $\varepsilon_{\alpha z}$ sont considérées uniformes dans l'épaisseur.

Afin de résoudre la contradiction apparente mentionnée (contraintes planes/déformations planes) dans les modèles de Kirchhoff-Love et de Reissner-Mindlin, Lebée [2010], Lebée and Sab [2011a] ont récemment présenté un modèle monocouche équivalente en contrainte, appelé le modèle Bending-Gradient. Contrairement au modèle classique du premier ordre, ce modèle est conforme à la théorie de développement asymptotique. Ce modèle, destiné aux plaques épaisses, utilise les six inconnues statiques de la théorie de Kirchhoff-Love ($N_{\alpha\beta}, M_{\alpha\beta}$) auxquelles sont ajoutées six nouvelles inconnues représentant le gradient du moment de flexion ($R_{\alpha\beta\gamma} = M_{\alpha\beta,\gamma}$). Ce nouveau modèle peut être considéré comme une extension aux plaques hétérogènes du modèle de Reissner-Mindlin qui apparaît comme un cas particulier lorsque la plaque est homogène. Lebée and Sab [2011b] ont appliqué la théorie Bending-Gradient aux plaques stratifiées sous flexion cylindrique et comparé les résultats de ce modèle avec

la solution exacte de Pagano [1969] ainsi qu'avec d'autres approches. Ils ont montré que leur modèle donne de bonnes prédictions pour la flèche, pour la distribution des contraintes de cisaillement transverse ainsi que pour les déplacements plans dans de nombreuses configurations matérielles. Lebée and Sab [2012] ont aussi appliqué la théorie du Bending-Gradient à l'homogénéisation des panneaux sandwichs épais à âme pliable en chevrons.

1.1.1.3 Modèles d'ordre supérieur

Pour améliorer la mauvaise approximation du cisaillement transverse dans des modèles classiques du premier ordre, plusieurs théories d'ordre supérieur ont été proposées dans la littérature. La plupart de ces théories sont des approches en déplacement et utilisent un développement en série de Taylor du champ de déplacement sous la forme suivante:

$$\underline{U}(x, y, z) = \underline{u}(x, y) + z \underline{\phi}^1(x, y) + z^2 \underline{\phi}^2(x, y) + \dots + z^n \underline{\phi}^n(x, y) \quad (1.11)$$

où n détermine l'ordre utilisé dans le modèle. Dans la théorie de Kirchhoff-Love $n = 0$. La théorie de Reissner-Mindlin est une théorie du premier ordre avec $n = 1$ pour les déplacements dans le plan et $n = 0$ pour le déplacement normal. La figure 1.4 montre une cinématique schématique d'un modèle d'ordre supérieur.

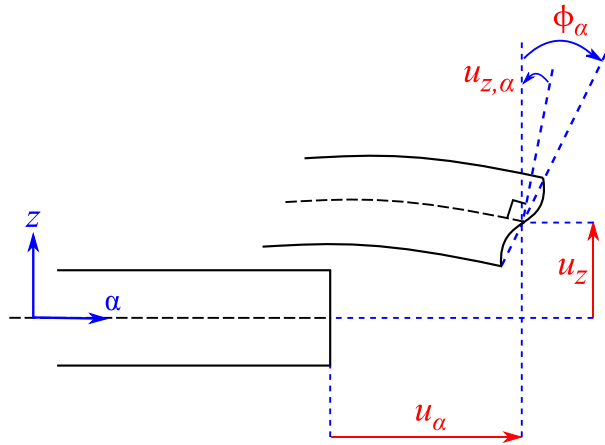


Figure 1.4: Cinématique d'un modèle d'ordre supérieur

Modèle proposé par Hildebrand et al. [1949] peut être considéré comme la première tentative d'amélioration de la théorie classique des plaques par une théorie d'ordre supérieur. Ce modèle considère la forme suivante pour les déplacements:

$$\begin{aligned} U_\alpha(x, y, z) &= u_\alpha(x, y) + z \phi_\alpha(x, y) \\ U_z(x, y, z) &= u_z(x, y) + z \phi_z(x, y) + z^2 \varphi_z(x, y) \end{aligned} \quad (1.12)$$

Nelson and Lorch [1974] ont proposé un modèle avec neuf champs inconnus pour l'analyse des plaques multicouches. Librescu [1975] a utilisé une théorie d'ordre

supérieure basée sur la moyenne des déplacements transversaux pour l'analyse des plaques multicouches. [Lo et al. \[1977a,b\]](#) ont étudié l'effet de la déformation normale transverse en utilisant une théorie à onze champs inconnus.

[Vlasov \[1957\]](#), [Reddy \[1984a,b\]](#) ont utilisé un modèle de plaques avec des déplacements d'ordre trois dans le plan:

$$\begin{aligned} U_\alpha(x, y, z) &= u_\alpha(x, y) + z \phi_\alpha(x, y) + z^2 \theta_\alpha(x, y) + z^3 \lambda_\alpha(x, y) \\ U_z(x, y, z) &= u_z(x, y) \end{aligned} \quad (1.13)$$

Cette cinématique présente neuf champs inconnus. En imposant $\sigma_{\alpha z} = 0$ sur les faces supérieure et inférieure de la plaque ($\sigma_{\alpha z}(x, y, \pm h/2) = 0$), le nombre des champs inconnus est réduit à cinq et la cinématique devient:

$$\begin{aligned} U_\alpha(x, y, z) &= u_\alpha(x, y) + z \phi_\alpha(x, y) - \frac{4z^3}{3h^2} \left(\phi_\alpha(x, y) + u_{z,\alpha}(x, y) \right) \\ U_z(x, y, z) &= u_z(x, y) \end{aligned} \quad (1.14)$$

Il y a d'autres travaux dans la littérature dans lesquels le champ de déplacement est approché de la même manière dans l'épaisseur. Ce type de théories est connu sous le nom de *Third-order Shear Deformation Theory (TSDT)* dans la littérature. Dans le cas général, ces théories considèrent le champ de déplacement sous la forme suivante:

$$\begin{aligned} U_\alpha(x, y, z) &= u_\alpha(x, y) - z u_{z,\alpha}(x, y) + f(z) \left[\phi_\alpha(x, y) + u_{z,\alpha}(x, y) \right] \\ U_z(x, y, z) &= u_z(x, y) \end{aligned} \quad (1.15)$$

On constate que les champs inconnus sont les mêmes que ceux considérés dans la théorie de Reissner-Mindlin ($u_\alpha, \phi_\alpha, u_z$). On remarque que $\phi_\alpha + u_{z,\alpha} = \gamma_\alpha^{RM} = \frac{1}{2} \varepsilon_{\alpha z}^{RM}$ est la déformation de cisaillement du modèle de Reissner-Mindlin qui est en réalité la déformation de cisaillement sur le plan moyen de la plaque. Les déplacements ainsi définis génèrent la déformation de cisaillement $\gamma_\alpha(x, y, z) = f'(z) \gamma_\alpha^{RM}(x, y)$. On constate que la dérivée de la fonction $f(z)$ donne la distribution de la déformation de cisaillement transverse dans l'épaisseur. Cette fonction est souvent appelée la *fonction de cisaillement*. Les expressions les plus importantes considérées dans la littérature pour cette fonction sont les suivantes:

- [Ambartsumian \[1958a\]](#)

$$f(z) = \frac{zh^2}{8} \left(1 - \frac{4z^2}{3h^2} \right)$$

- [Kaczkowski \[1968\]](#), [Panc \[1975\]](#), [Reissner \[1975\]](#)

$$f(z) = \frac{5z}{4} \left(1 - \frac{4z^2}{3h^2} \right)$$

- Vlasov [1957], Levinson [1980], Murthy [1981], Reddy [1984a,b], Bhimaraddi and Stevens [1984] (Modèle de Reddy)

$$f(z) = z \left(1 - \frac{4z^2}{3h^2} \right)$$

- Touratier [1991]

$$f(z) = \frac{h}{\pi} \sin \left(\frac{\pi z}{h} \right)$$

- Soldatos and Timarci [1993]

$$f(z) = h \sinh \left(\frac{z}{h} \right) - z \sinh \left(\frac{1}{2} \right)$$

- Karama et al. [2003]

$$f(z) = z e^{-2(z/h)^2}$$

- Aydogdu [2009]

$$f(z) = z \alpha^{\frac{-2(z/h)^2}{\ln(\alpha)}}, \quad \alpha > 0$$

- Mantari et al. [2012a]

$$f(z) = \sin \left(\frac{\pi z}{h} \right) e^{m \cos \left(\frac{\pi z}{h} \right)} + m \frac{\pi z}{h}$$

Dans toutes ces expressions, la fonction $f(z)$ est définie de telle sorte que $f'(\pm \frac{h}{2}) = 0$ et donc $\gamma_\alpha(x, y, \pm h/2) = 0$. Par conséquent, les conditions aux limites de bord libre sur les surfaces supérieure et inférieure de la plaque sont satisfaites ($\sigma_{\alpha z}(z = \pm h/2) = 0$). Ces modèles aboutissent à une expression parabolique des contraintes de cisaillement transverse dans l'épaisseur qui est beaucoup plus proche de la réalité dans des plaques homogènes. Reddy and Liu [1985] ont aussi développé cette théorie d'ordre supérieur pour l'analyse des coques multicouches. Touratier [1991], Soldatos and Timarci [1993], Karama et al. [2003], Aydogdu [2009] ont proposé des formes sinusoïdale, exponentielle,... pour la fonction de cisaillement. Ces modèles se rapprochent beaucoup des modèles d'ordre supérieur de type de série de Taylor. Par rapport à la solution exacte, ces modèles donnent, en général, de meilleurs résultats que le modèle de Reddy. Un élément finit triangulaire à six nœuds, basé sur les travaux de Touratier, est présenté dans [Polita and Touratier 1997, Dau et al. 2006] pour l'analyse des structures multicouches avec non-linéarités géométriques.

Remarque: En considérant l'équation 1.15, les modèles de Kirchhoff-Love et de Reissner-Mindlin correspondent à $f(z) = 0$ et à $f(z) = z$ respectivement.

Kant et al. [1982], Kant [1982] sont les premiers à avoir proposé une formulation aux éléments finis d'ordre supérieur. Ils ont présenté une théorie qui prend en compte les effets de la déformation de cisaillement transverse en considérant la cinématique suivante [Pandya and Kant 1988a,b,c,d]:

$$\begin{aligned} U_\alpha(x, y, z) &= u_\alpha(x, y) + z \theta_\alpha(x, y) + z^2 u_\alpha^*(x, y) + z^3 \theta_\alpha^*(x, y) \\ U_z(x, y, z) &= u_z(x, y) \end{aligned} \quad (1.16)$$

où u_α est le déplacement dans le plan du plan moyen dans la direction α , u_z est le déplacement transverse du plan moyen de la plaque et θ_α est la rotation du plan moyen de la plaque. u_α^* et θ_α^* sont les termes d'ordre supérieur dans les séries de Taylor et sont définis sur le plan moyen. Cette théorie est un modèle de plaques avec neuf variables inconnues. Dans ce modèle, le déplacement transverse u_z dans l'épaisseur de la plaque est supposé constant ($\varepsilon_{zz} = 0$). Sur les travaux de Kant, un autre modèle de plaques a été proposé dans lequel le développement de série de Taylor est considéré jusqu'à l'ordre trois pour les trois déplacements [Kant and Manjunatha 1988, Kant and Mallikarjuna 1989]:

$$U_k(x, y, z) = u_k(x, y) + z \theta_k(x, y) + z^2 u_k^*(x, y) + z^3 \theta_k^*(x, y) \quad , \quad k \in \{x, y, z\} \quad (1.17)$$

La cinématique de ce modèle est basée sur douze champs inconnus. A partir de ce modèle, Kant and Manjunatha [1988] ont développé un élément fini avec douze degrés de liberté par nœud pour l'analyse des plaques multicouches non-symétriques.

Gaudenzi [1992] a proposé une approche en déplacement et développé une théorie générale d'ordre supérieur basée sur le champ de déplacement polynomial dans l'épaisseur. Cho and Parmerter [1993] a utilisé une variation cubique du champ de déplacement dans l'épaisseur pour étudier la flexion cylindrique des plaques multicouches. Whitney [1997] a utilisé une théorie d'ordre supérieur pour l'analyse des contraintes d'interface dans des plaques multicouches. En montrant que l'hypothèse de $\varepsilon_{zz} = 0$ ne peut pas fournir de résultats précis, il a proposé deux théories d'ordre supérieur qui donnent des déformations normales transverses constantes et linéaires dans l'épaisseur. Kant and Khare [1997] ont présenté un modèle de coque en déplacement avec une cinématique à neuf champs inconnus et développé une formulation éléments finis à partir de ce modèle. Zenkour and Fares [1999] ont proposé une approche basée sur la déformation de cisaillement d'ordre trois pour l'analyse des plaques composites rectangulaires en flexion. Sheikh and Chakrabarti [2003] ont développé un élément de plaque basé sur la théorie d'ordre supérieur de Reddy pour analyser des plaques multicouches sous la flexion. Kant and Swaminathan [2001, 2002], Swaminathan and Ragounadin [2004] ont utilisé le modèle de Kant pour l'analyse statique et vibratoire des plaques composites et panneaux sandwich. En utilisant une nouvelle méthode sans maillage (meshless), Ferreira et al. [2003] ont discrétisé la théorie d'ordre trois de Reddy pour l'analyse des plaques stratifiées sous la traction uniforme. Comme les publications plus récentes sur les modèles d'ordre supérieur, nous pouvons mentionner les travaux de Pradyumna and Bandyopadhyay [2008], Sudha Ramesh et al. [2009], Aydogdu [2009],

Demasi [2009], Panda and Singh [2009], Sinan Oktem and Guedes Soares [2011], Mantari et al. [2011, 2012b].

1.1.2 Approche par couche

Les modèles de type monocouche équivalente donnent, relativement, une bonne approximation du comportement global de la structure multicouche. Ils sont efficaces car le nombre des champs inconnus ne dépend pas du nombre des couches. En revanche, en ce qui concerne le comportement local, ces modèles ne sont pas capables de fournir de résultats satisfaisants. Des hypothèses fortes et simplifiées considérées dans ces modèles entraînent une perte importante d'information et une imprécision notable au niveau local (discontinuité des contraintes transversales aux interfaces, non-satisfaction des conditions aux limites,...). Pour les multicouches minces, l'erreur due à la discontinuité des contraintes interlaminaires peut être négligeable. En revanche, pour les structures multicouches épaisses, les modèles de type monocouche équivalente peuvent aboutir à des résultats inacceptables. Pour franchir les limites des modèles de type monocouche équivalente, les approches par couche (layerwise) ont été proposées. Dans ces approches, la forme des champs inconnus est écrite pour chaque couche séparément (l'équation 1.2).

En effet, dans ces approches chaque couche est considérée comme une plaque indépendante (Fig. 1.5) et les équations sont écrites pour chaque couche de la structure multicouche. Par conséquent, le nombre d'équations du modèle dépend du nombre des couches. Il faut noter que les champs inconnus sont indépendants dans chaque couche mais les continuités des déplacements et des contraintes transversales doivent être satisfaites aux interfaces. Des modèles layerwise peuvent être basés sur des approches en déplacement, en contrainte ou des approches mixtes.

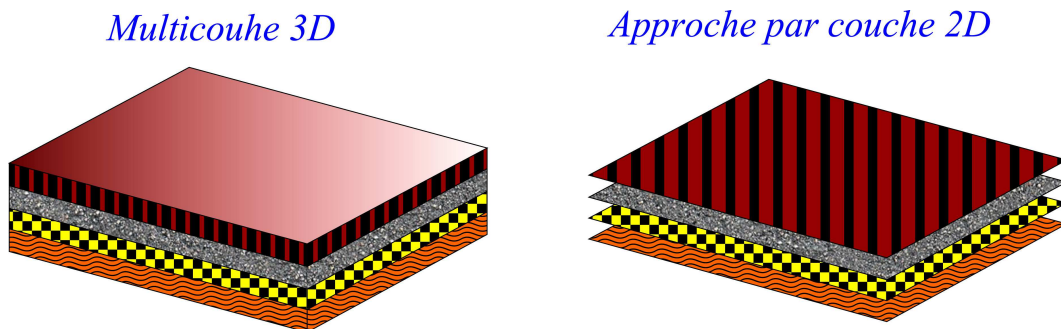


Figure 1.5: Approche par couche

Dans des structures multicouches, le changement brutal des caractéristiques mécaniques entre deux couches adjacentes provoquent la discontinuité des contraintes dans le plan au niveau des interfaces. Les solutions exactes 3D obtenues par Pagano [1969, 1970b], Srinivas and Rao [1970], Srinivas et al. [1970], Noor [1973a,b], Savoia and Reddy [1992] pour des plaques multicouches rectangulaires et par Ren [1987], Varadan and Bhaskar [1991] pour des coques multicouches montrent que ces effets de type zigzag

deviennent importants lorsque le multicouche est relativement épais. Pour améliorer les estimations grossières des théories de plaques, [Whitney \[1969\]](#) a utilisé une approche basée sur la variation quadratique des contraintes de cisaillement transverse par couche. Cela aboutit à une variation cubique des déplacements dans le plan par couche. En imposant des conditions de continuité de déplacements, il a trouvé le même nombre de variables que dans la théorie d'ordre un en cisaillement. En revanche, les équations d'équilibre considérées étaient celles de la théorie classique des stratifiés, ce qui n'est pas justifié du point de vue énergétique. Cependant, les résultats obtenus concernant les fréquences propres, la charge de flambement,... étaient acceptables par rapport aux solutions exactes existantes. En supposant que les déformations de cisaillement sont constantes par couche et les déplacements transversaux sont continus dans l'épaisseur, [Swift and Heller \[1974\]](#) ont étudié des poutres multicouches. Une approche similaire a été utilisée par [Durocher and Solechi \[1975\]](#) pour l'analyse des plaques isotropes avec deux ou trois couches. [Srinivas \[1973\]](#), [Seide \[1980\]](#), [Seide and Chaudhuri \[1987\]](#), [Green and Naghdi \[1982\]](#) ont développé les modèles similaires pour l'analyse des plaques multicouches. Dans ces approches, les équations d'équilibre s'écrivent pour chaque couche i de la manière suivante:

$$\begin{aligned} N_{\alpha\beta,\beta}^i + [\sigma_{\alpha z}^i]^+ - [\sigma_{\alpha z}^i]^- &= 0 \\ M_{\alpha\beta,\beta}^i - Q_{\alpha}^i + [z^i \sigma_{\alpha z}^i]^+ - [z^i \sigma_{\alpha z}^i]^- &= 0 \\ Q_{\alpha,\alpha}^i + [\sigma_{zz}^i]^+ - [\sigma_{zz}^i]^- &= 0 \end{aligned} \tag{1.18}$$

où $N_{\alpha\beta}^i$, $M_{\alpha\beta}^i$ et Q_{α}^i sont les efforts membranaires, les moments et les efforts tranchants de la couche i respectivement ($\alpha \in \{x, y\}$). Les exposants $+$ et $-$ correspondent aux cotes supérieure et inférieure de la couche i . Pour un multicouche à n couches, le modèle est constitué de $2(n+1)$ déplacements dans le plan u_x^i et u_y^i (avec $1 \leq i \leq n+1$) et un déplacement normal u_z qui est considéré constant dans toute l'épaisseur de la plaque (u_x^i et u_y^i sont les déplacements au niveau de l'interface i). En imposant les conditions de continuité des déplacements et des contraintes transversales aux interfaces, ainsi que les conditions aux limites en contrainte sur les faces supérieure et inférieure de la plaque, $2n+3$ équations s'obtiennent en fonction de $2n+3$ déplacements du modèle.

Plusieurs autres types de modèles ont été proposés par différents auteurs. En utilisant une approximation explicite pour les contraintes de cisaillement transverse dans chaque couche, [Hsu and Wang \[1970\]](#) ont proposé un modèle pour des coques multicouches cylindriques avec des couches orthotropes. Les contraintes de cisaillement transverse ont été choisies de telle manière que la continuité des contraintes aux interfaces et les conditions aux limites en contrainte sur les faces supérieure et inférieure soient satisfaites. [Rath and Das \[1973\]](#) ont développé ce modèle pour l'analyse des coques symétriques constituées des couches orthotropes. [\[Mau 1973\]](#) a présenté un modèle layerwise en contraintes. Il a supposé la forme des contraintes dans les couches et considéré les contraintes interlaminaires aussi comme des variables inconnues du modèle. [Wu and Hsu \[1993\]](#) ont proposé un modèle layerwise dans lequel les déplacements dans l'épaisseur de chaque couche sont approchés par des fonctions polynomiales. Ils ont

imposé les conditions de continuité de déplacements et de contraintes aux interfaces et présenté une approche variationnelle générale pour leur modèle.

1.1.2.1 Le modèle layerwise de Reddy

L'un des modèles les plus connus est le modèle de Reddy [1987] qui est basé sur une approche en déplacement. Dans ce modèle, l'interpolation lagrangienne unidimensionnelle est utilisée pour la variation transversale des déplacements. La cinématique proposée est de telle sorte que les déformations dans le plan sont continues suivant l'épaisseur alors que les déformations transversales sont discontinues au niveau des interfaces qui permet d'assurer la continuité des contraintes transversales aux interfaces. Le modèle de Reddy est très général et n'importe quel degré d'interpolation peut être utilisé pour les déplacements. Dans cette théorie, les déplacements de la couche k sont considérés comme suit [Reddy 1997]:

$$\begin{aligned} u^k(x, y, z) &= \sum_{j=1}^{m+1} u_j^k(x, y) \phi_j^k(z) \\ v^k(x, y, z) &= \sum_{j=1}^{m+1} v_j^k(x, y) \phi_j^k(z) \\ w^k(x, y, z) &= \sum_{j=1}^{n+1} w_j^k(x, y) \psi_j^k(z) \end{aligned} \tag{1.19}$$

où u^k , v^k et w^k sont les déplacements de la couche k respectivement dans les directions x , y et z . ϕ_j^k et ψ_j^k sont les fonctions continues de z (en général $\phi_j^k \neq \psi_j^k$ et $m \neq n$). Ces fonctions sont très souvent les polynômes d'interpolation de Lagrange. Le degré d'interpolation dans l'épaisseur de chaque couche est m pour les déplacements dans le plan et n pour le déplacement transverse. Le choix du degré d'interpolation est complètement libre et chaque couche peut avoir une variation polynomiale linéaire, quadratique ou d'ordre supérieur des déplacements. Pour les interpolations linéaire ($n = 1$) et quadratique ($n = 2$) les fonctions d'interpolation sont les suivantes:

- Interpolation linéaire

$$\begin{cases} \psi_1^k(z) = -\frac{1}{h^k} \left(\bar{z}^k - \frac{h^k}{2} \right) \\ \psi_2^k(z) = \frac{1}{h^k} \left(\bar{z}^k + \frac{h^k}{2} \right) \end{cases} \tag{1.20}$$

- Interpolation quadratique

$$\begin{cases} \psi_1^k(z) = \frac{2}{(h^k)^2} \bar{z}^k \left(\bar{z}^k - \frac{h^k}{2} \right) \\ \psi_2^k(z) = -\frac{4}{(h^k)^2} \left(\bar{z}^k - \frac{h^k}{2} \right) \left(\bar{z}^k + \frac{h^k}{2} \right) \\ \psi_3^k(z) = \frac{2}{(h^k)^2} \bar{z}^k \left(\bar{z}^k + \frac{h^k}{2} \right) \end{cases} \quad (1.21)$$

où h^k est l'épaisseur de la couche k et \bar{z}^k correspond à la cote moyenne de la couche k dans la direction de l'épaisseur $\left(-\frac{h^k}{2} \leq \bar{z}^k \leq \frac{h^k}{2}\right)$.

De cette façon, pour $n = m$ on aura n plans avec les cotes z_1^k, \dots, z_{n+1}^k suivant l'épaisseur de chaque couche. Du fait que $\psi_j^k(z_i^k) = \delta_{ij}$ (où δ_{ij} est le symbole de Kronecker), u_j^k , v_j^k et w_j^k sont les valeurs de u^k , v^k et w^k sur $z = z_j^k$ (le j ème plan). Pour $n = 1$, u_1^k , v_1^k et w_1^k sont les déplacements au niveau de la cote inférieure et u_2^k , v_2^k et w_2^k sont les déplacements au niveau de la cote supérieure de la couche k .

Le champ de déplacement global peut s'écrire (Fig. 1.6):

$$\begin{aligned} U(x, y, z) &= \sum_{I=1}^N U_I(x, y) \Phi^I(z) \\ V(x, y, z) &= \sum_{I=1}^N V_I(x, y) \Phi^I(z) \\ W(x, y, z) &= \sum_{I=1}^M W_I(x, y) \Psi^I(z) \end{aligned} \quad (1.22)$$

où N et $\Phi_I(z)$ sont, respectivement, le nombre des nœuds et les fonctions d'interpolation globales pour la discrétisation des déplacements U et V suivant l'épaisseur. M et $\Psi_I(z)$ sont, respectivement, le nombre des nœuds et les fonctions d'interpolation globales pour la discrétisation du déplacement transversal W suivant l'épaisseur. Dans le cas où $n = m$ et le degré d'interpolation est identique pour toutes les couches $N = M = n_p \times n + 1$ où n_p est le nombre des couches et n est le degré d'interpolation dans l'épaisseur.

Remarque: Des approximations indépendantes pour les déplacements dans le plan et le déplacement transversal permettent d'utiliser différentes hypothèses. Par exemple, l'hypothèse de l'épaisseur constante ($\varepsilon_{zz} = 0$) est applicable en choisissant $M = 1$ et $\Psi^I(z) = 1$.

Le modèle de Reddy a été utilisé largement dans la littérature pour l'analyse des structures multicouches. A titre d'exemple nous pouvons citer les travaux de [Owen and](#)

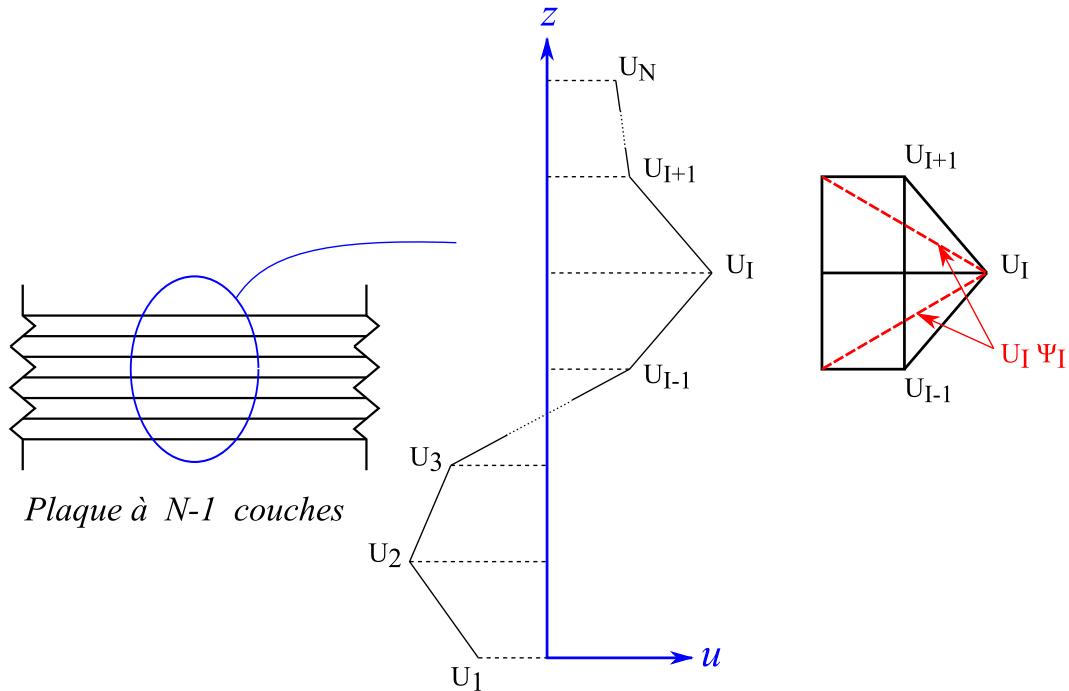


Figure 1.6: Modèle layerwise de Reddy: interpolation linéaire des déplacements

Li [1987a,b], Epstein and Glockner [1977], Epstein and Huttelmaier [1983], Barbero et al. [1990], Robbins and Reddy [1993], Nosier and Bahrami [2006], Mittelstedt and Becker [2008], Sudha Ramesh et al. [2009], Torres et al. [2011].

Les approches par couche en déplacement dans lesquelles le déplacement transversal est considéré constant dans l'épaisseur de la plaque (c'est-à-dire la déformation normale transverse est négligée) donnent les résultats plus précis par rapport aux approches de type monocouche équivalente. Dans ces approches, les déplacements dans le plan sont approchés par couche, ce qui permet de prendre en compte les effets de cisaillement transverse. Cependant, ces approches ne sont pas très précises pour déterminer les contraintes interlaminaires près des discontinuités telles que des bords libres, des trous, des pointes de fissure, etc. Dans la modélisation de ces effets locaux, la prise en compte de la déformation normale transverse est importante pour deux raisons principales. Premièrement, la contrainte normale transverse est considérable et parfois dominante dans ces zones. Deuxièmement, si la déformation normale transverse est négligée, les contraintes de cisaillement transverse ne satisfont pas complètement les conditions aux limites en contrainte. Dans ces approches, les conditions aux limites en contrainte sont satisfaites dans le sens intégral mais pas local. Ce problème n'apparaît pas dans les théories qui considèrent une approche par couche pour tous les déplacements et par conséquent, ces théories tiennent compte des effets de contraintes de cisaillement transverse et de contrainte normale transverse.

1.1.3 Les modèles zig-zag

L'idée principale dans des modèles zig-zag consiste à supposer la forme des déplacements ou des contraintes dans chaque couche et puis écrire la continuité des déplacements et des contraintes transversales au niveau des interfaces afin de réduire le nombre des champs inconnus. Ainsi, les déplacements restent continus suivant l'épaisseur mais les déformations ne sont pas continues car la pente de la fonction de déplacement est différente entre deux couches adjacentes. Le nom de ces modèles provient de la forme zig-zag du déplacement dans l'épaisseur des structures multicouches. Le développement de type zig-zag est effectué pour les approches de monocouche équivalente et également pour les approches layerwise.

Des théories zig-zag appliquées dans les approches de type monocouche équivalente peuvent être regroupées dans trois groupes:

- Approche de *Lekhnitskii-Ren*
- Approche de *Ambartsumian-Whitney-Rath-Das*
- Approche de *Reissner-Murakami-Carrera*

La première théorie zig-zag a été proposée par [Lekhnitskii \[1935\]](#) pour l'analyse des poutres composites. [Ren \[1986a,b\]](#) a développé cette théorie pour les plaques multicouches. La théorie est basée sur une approche en contrainte dans laquelle les contraintes de cisaillement transverse sont supposées sous la forme suivante:

$$\begin{aligned}\sigma_{xz}^k(x, y) &= \xi_x(x, y) a^k(z) + \eta_x(x, y) c^k(z) \\ \sigma_{yz}^k(x, y) &= \xi_y(x, y) b^k(z) + \eta_y(x, y) d^k(z)\end{aligned}\tag{1.23}$$

Quatre fonctions indépendantes ξ_x , ξ_y , η_x et η_y sont utilisées pour la description des contraintes de cisaillement transverse. $a^k(z)$, $b^k(z)$, $c^k(z)$, et $d^k(z)$ sont les fonctions paraboliques en z et assurent la continuité des contraintes σ_{xz} et σ_{yz} aux interfaces. En intégrant les déformations et imposant la continuité aux interfaces, les déplacements s'obtiennent ($\varepsilon_{zz} = 0$):

$$\begin{aligned}u_x^k(x, y, z) &= u_x^0(x, y) - z u_{z,x}(x, y) + \xi_x(x, y) A^k(z) + \eta_x(x, y) C^k(z) \\ u_y^k(x, y, z) &= u_y^0(x, y) - z u_{z,y}(x, y) + \xi_y(x, y) B^k(z) + \eta_y(x, y) D^k(z) \\ u_z(x, y, z) &= u_z^0(x, y)\end{aligned}\tag{1.24}$$

où $A^k(z)$, $B^k(z)$, $C^k(z)$, et $D^k(z)$ s'obtiennent en intégrant $a^k(z)$, $b^k(z)$, $c^k(z)$, et $d^k(z)$ respectivement. Ainsi, les déplacements dans le plan sont cubiques en z dans chaque couche et continus aux interfaces. On constate que le modèle est constitué de sept champs inconnus.

À part les travaux de [Ren \[1986a,b\]](#), il n'y a presque aucun autre travail sur cette théorie dans la littérature. C'est la raison pour laquelle cette théorie a quasiment été oubliée dans les publications récentes.

Ambartsumian [1958b, 1961, 1962] a développé une théorie zig-zag pour la géométrie de plaque et coque. Cette théorie a été utilisée et développée par Whitney [1969], Rath. and Das [1973]. La forme supposée dans cette théorie pour les contraintes de cisaillement transverse est la suivante:

$$\begin{aligned}\sigma_{xz}^k(x, y) &= \left[Q_{55}^k f(z) + a_{55}^k \right] \phi_x(x, y) + \left[Q_{45}^k f(z) + a_{45}^k \right] \phi_y(x, y) \\ \sigma_{yz}^k(x, y) &= \left[Q_{45}^k f(z) + a_{45}^k \right] \phi_x(x, y) + \left[Q_{44}^k f(z) + a_{44}^k \right] \phi_y(x, y)\end{aligned}\tag{1.25}$$

La variation dans le plan des contraintes de cisaillement transverse est liée à deux fonctions indépendantes ϕ_x et ϕ_y . Les paramètres a_{44}^k , a_{45}^k et a_{55}^k sont déterminés en imposant la continuité des contraintes de cisaillement transverse aux interfaces. La fonction $f(z)$ assure la continuité des déplacements aux interfaces. En supposant $\varepsilon_{zz} = 0$ le champ de déplacement s'obtient par intégration comme suit:

$$\begin{aligned}u_x^k(x, y, z) &= u_x^0(x, y) - z u_{z,x}(x, y) + G_1^k(z) \phi_x(x, y) + G_2^k(z) \phi_y(x, y) \\ u_y^k(x, y, z) &= u_y^0(x, y) - z u_{z,y}(x, y) + G_3^k(z) \phi_x(x, y) + G_4^k(z) \phi_y(x, y) \\ u_z(x, y, z) &= u_z^0(x, y)\end{aligned}\tag{1.26}$$

On constate que le nombre des champs inconnus dans ce modèle est le même que dans le modèle de Reissner-Mindlin.

Ce type d'approche zig-zag a été utilisé dans plusieurs études de recherche notamment dans les travaux de Chou and Carleone [1973], Di Sciuva [1984], Di Sciuva et al. [1984], Di Sciuva [1987], Bhaskar and Varadan [1989], Lee et al. [1990], Di Sciuva and Carrera [1992], Touratier [1992a,b], Beakou and Touratier [1993], Cho and Parmerter [1993], Ossadzow et al. [1998].

Une autre manière de formuler des théories zig-zag a été présentée par Reissner [1984, 1986]. Murakami [1986] a utilisé la théorie variationnelle de Reissner pour développer un modèle de plaque. Il a raffiné le modèle de plaque de Reissner-Mindlin en ajoutant un terme zig-zag dans l'expression des déplacements dans le plan:

$$\begin{aligned}u_\alpha(x, y, z) &= u_\alpha^0(x, y) + z \phi_\alpha + M(z) u_\alpha^{ZZ}(x, y) \\ u_z(x, y, z) &= u_z^0(x, y)\end{aligned}\tag{1.27}$$

On constate que par rapport à la théorie classique d'ordre un de Reissner-Mindlin, un déplacement u_α^{ZZ} a été ajouté. La fonction $M(z)$ est une fonction de z qui génère l'effet zig-zag suivant l'épaisseur:

$$M(z) = (-1)^k \times \frac{2(z - \bar{z}^k)}{h^k}, \quad -\frac{h^k}{2} \leq z - \bar{z}^k \leq \frac{h^k}{2}\tag{1.28}$$

où h^k et \bar{z}^k sont l'épaisseur et la cote moyenne de la couche k respectivement. En effet, dans ce modèle, les déplacements dans le plan, sont les résultats de la superposition du champ de déplacement global de la plaque de Reissner-Mindlin et d'un déplacement de type zig-zag dans l'épaisseur (1.7). Ce déplacement est continu dans l'épaisseur mais sa

pente est discontinue aux interfaces. Par conséquent, les déformations de cisaillement transverse sont discontinues aux interfaces, ce qui permet d'assurer la continuité des contraintes de cisaillement transverse aux interfaces. Les contraintes de cisaillement transverse sont supposées paraboliques par couche.

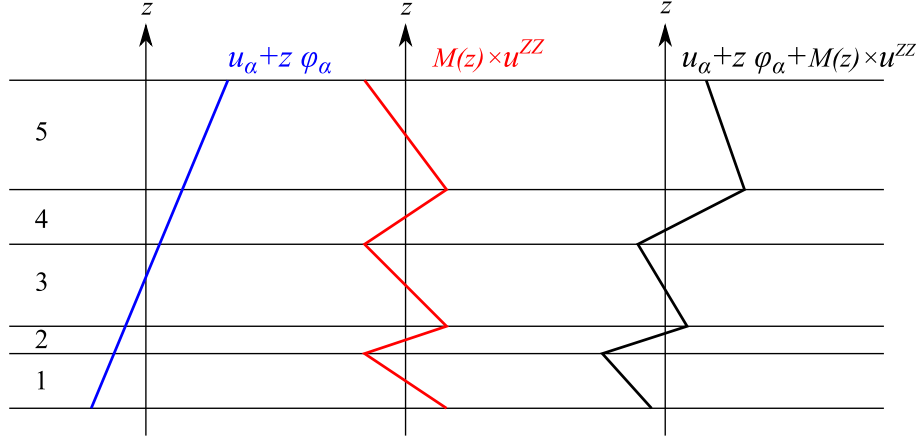


Figure 1.7: Champ de déplacement dans le modèle zig-zag du premier ordre

Toledano and Murakami [1987a] ont développé cette théorie en considérant une cinématique jusqu'au troisième ordre:

$$u_i(x, y, z) = u_i^0(x, y) + z \phi_i(x, y) + z^2 \psi_i(x, y) + z^3 \varphi_i(x, y) + M(z) u_\alpha^{ZZ}(x, y) \quad , \quad i \in \{x, y, z\} \quad (1.29)$$

En considérant les équations d'équilibre 3D, les contraintes de cisaillement transverse et la contrainte normale transverse sont supposées, respectivement, du quatrième et cinquième ordre par couche. Dans une publication ultérieure, Toledano and Murakami [1987b] ont appliqué la méthode variationnelle de Reissner en combinaison avec une approche mixte à la fois en déplacement et en contrainte. Il a été supposé que la variation des déplacements membranaires est linéaire dans l'épaisseur de chaque couche alors que le déplacement transverse reste constant sur toute l'épaisseur de la plaque. Au niveau des contraintes, ils ont supposé que les contraintes de cisaillement transverse sont paraboliques par couche tandis que la contrainte normale transverse est négligeable.

Une généralisation de théorie zig-zag de Murakami a été proposée par Carrera [1995]. Il a présenté une approche systématique basée sur la méthode variationnelle de Reissner pour établir une classe des modèles bidimensionnels multicouches de type zig-zag. Dans cette approche, le champ de déplacement est considéré de la manière suivante:

$$u_i(x, y, z) = u_i^0 + z \phi_i^{(1)} + z^2 \phi_i^{(2)} + \dots + z^N \phi_i^{(N)} + M(z) u_\alpha^{ZZ} \quad , \quad i \in \{x, y, z\} \quad (1.30)$$

Cette théorie zig-zag est une approche monocouche équivalente d'ordre N .

Carrera a développé cette théorie dans des publications suivantes. Des analyses mixtes en déplacement/contrainte ont été effectuées dans [Carrera 1998a] pour le cas statique. Les équations du cas dynamique ont été présentées dans Carrera [1998b]. L'application de l'approche variationnelle mixte de Reissner à la géométrie de coque

fait l'objet des articles [Carrera \[1999c,d\]](#). Des effets de la contrainte normale transverse en statique et en dynamique ont été étudiés dans [Carrera \[1999a,b\]](#). Des théories d'ordre supérieur, de linéaire jusqu'à l'ordre quatre, ont été considérées dans [[Carrera 2000](#)].

L'avantage principal des modèles de type zig-zag est la satisfaction de la continuité des contraintes aux interfaces sans augmenter le nombre des champs inconnus. Le recours à des coefficients de correction pour le cisaillement transverse est évité. En général, les modèles zig-zag assurent relativement un bon compromis entre la précision des solutions et le coût de calcul. Cependant, ces modèles ont des limites importantes. Pour le calcul des contraintes de cisaillement transverse dans des plaques relativement épaisses, la précision des modèles zig-zag est moins satisfaisante. De plus, ces modèles ont des difficultés dans la modélisation du délaminage. Un autre inconvénient des théories zig-zag est la continuité de classe C^0 des déplacements qui complique leur implémentation numérique.

1.1.4 Modèles Multiparticulaires

Des modèles multiparticulaires sont des modèles de type couche discrète (layerwise) dans lesquels le multicouche est représenté par un ensemble de plaques 2D qui sont couplées par des contraintes d'interface. Ainsi, le multicouche devient un objet 2D dont chaque point géométrique est constitué des particules matérielles correspondant aux différentes couches. La superposition des particules en chaque point géométrique justifie la dénomination "modèle multiparticulaire". Ces modèles servent surtout à évaluer les contraintes transversales aux interfaces.

L'une des premières approches qu'on peut considérer comme une approche multiparticulaire est celle de [Puppo and Evensen \[1970\]](#) pour analyser des multicouches soumis à des chargements dans le plan. L'approche est basée sur des champs moyens dans chaque couche et prend en compte des effets de cisaillement d'interface. Le comportement du modèle relie les contraintes de cisaillement transverse interlaminaires aux différences de déplacements moyens des couches adjacentes.

Sur la base de la formulation variationnelle mixte de Hellinger-Reissner, [Pagano \[1978a\]](#) a proposé un modèle layerwise local. Il a utilisé une approche en contrainte en supposant des variations polynomiales des contraintes par couche. Il a considéré une variation linéaire pour les contraintes membranaires dans l'épaisseur de chaque couche. Cela conduit, d'après les équations d'équilibre 3D, à une variation quadratique des contraintes de cisaillement transverse et une variation cubique de la contrainte normale transverse dans l'épaisseur de chaque couche. Le modèle est construit en injectant les contraintes approchées dans la fonctionnelle de Hellinger-Reissner. Les équations du modèle sont obtenues par le théorème variationnel de [Reissner \[1950\]](#). Pagano a fait apparaître des contraintes d'interface dans son modèle et souligné l'absence de singularités pour ces champs. Il a déduit une cinématique à $7n$ champs pour des plaques multicouches constituées de n couches. Ce modèle pose quelques difficultés au niveau des conditions aux limites et reste assez lourd compte tenu du nombre élevé des champs cinématiques intervenants. [Pagano and Soni \[1983\]](#) ont développé un modèle élastique global-local plus opérationnel. Dans ce modèle, on privilégie certaines interfaces et les

Table 1.1: Les différents modèles $M4$ en comparant avec les modèles classiques de plaques

Modèle	Efforts généralisés de la couche i	Efforts généralisés de l'interface $i, i + 1$	Déplacements généralisés
$M4 - 7n$	$N_{\alpha\beta}^i, M_{\alpha\beta}^i, Q_\alpha^i, N_{zz}^i, M_{zz}^i$	$\tau_\alpha^{i,i+1}, \nu^{i,i+1}$	$U_\alpha^i, U_z^i, \phi_\alpha^i, \bar{U}_z^i, \hat{U}_z^i$
$M4 - 5n$	$N_{\alpha\beta}^i, M_{\alpha\beta}^i, Q_\alpha^i$	$\tau_\alpha^{i,i+1}, \nu^{i,i+1}$	$U_\alpha^i, U_z^i, \phi_\alpha^i$
$M4 - 3nP$	$N_{\alpha\beta}^i, M_{\alpha\beta}^i$	$\tau_\alpha^{i,i+1}, \nu^{i,i+1}$	U_α^i, U_z^i
$M4 - 3nM$	$N_{\alpha\beta}^i$	$\tau_\alpha^{i,i+1}, \nu^{i,i+1}$	U_α^i, U_z^i
$M4 - (2n + 1)P$	$N_{\alpha\beta}^i, M_{\alpha\beta}^i$	$\tau_\alpha^{i,i+1}$	U_α^i, U_z
$M4 - (2n + 1)M$	$N_{\alpha\beta}^i$	$\tau_\alpha^{i,i+1}$	U_α^i, U_z
Reissner-Mindlin	$N_{\alpha\beta}, M_{\alpha\beta}, Q_\alpha$	—————	$U_\alpha, U_z, \phi_\alpha$
Kirchhoff-Love	$N_{\alpha\beta}, M_{\alpha\beta}$	—————	U_α, U_z

couches adjacentes à ces interfaces sont modélisées par le modèle local. Les couches restantes sont regroupées et sont approchées par une plaque homogène. L'avantage de ce modèle global-local par rapport au modèle local est la diminution significative du nombre d'inconnues. En revanche, la précision du modèle dépend du choix des interfaces privilégiées.

Le modèle local de Pagano a été le point de départ pour un ensemble de travaux menés au laboratoire Navier par [Ehrlacher et al. \[1994\]](#), [Naciri et al. \[1998\]](#). [Chabot \[1997\]](#) a formalisé ces travaux et construit, à partir de la méthode d'approximation de Hellinger-Reissner, une famille de modèles multiparticulaires élastiques dits $M4$ (*Modèle Multiparticulaire des Matériaux Multicouches*). Le modèle le plus complet, appelé $M4 - 7n$, est identique au modèle local de Pagano. Les autres modèles s'obtiennent moyennant des hypothèses simplificatrices.

Le Tableau 1.1 présente les efforts généralisés et les déplacements généralisés des différents modèles $M4$ en comparant avec les modèles classiques de plaques. Dans ce tableau, $N_{\alpha\beta}$, $M_{\alpha\beta}$ et Q_α sont, respectivement, les efforts membranaires, les moments et les efforts tranchants. $\tau_\alpha^{i,i+1}$ et $\nu^{i,i+1}$ sont les contraintes de cisaillement et la contrainte normale à l'interface $i, i + 1$. N_{zz}^i et M_{zz}^i sont les premier et deuxième moments de la contrainte σ_{zz} par rapport au plan moyen de la couche i . U_α et U_z sont, respectivement, les déplacements dans le plan et transverse et ϕ_α sont les rotations. \bar{U}_z et \hat{U}_z représentent les termes d'ordre supérieur du déplacement transverse. Dans la section suivante, nous présenterons les expressions de tous ces variables généralisées.

Dans les efforts généralisés du modèle $M4 - 7n$, il y a des moments du premier ordre (N_{zz}^i) et du deuxième ordre (M_{zz}^i) de la contrainte normale σ_{zz} par rapport au plan moyen de chaque couche. Ces efforts généralisés n'ont pas de sens physique et compliquent la formulation du modèle. En utilisant les équations d'équilibre du modèle $M4 - 7n$, on peut éliminer ces efforts de la formulation du problème. Ainsi, on arrive au modèle $M4 - 5n$ qui ne fait pas apparaître, explicitement, ces efforts généralisés. Dans ce modèle, chaque couche est considérée comme une plaque de Reissner-Mindlin qui est liée aux couches adjacentes par les contraintes d'interface. De la même façon, en éliminant les efforts tranchants de chaque couche (Q_α^i), on obtient le modèle $M4 - 3nP$. Dans ce modèle, chaque couche est modélisée par une plaque de Kirchhoff-Love (P pour *Plaque*). Si on néglige les moments de flexion et de torsion dans les couches ($M_{\alpha\beta}^i$), on trouve le modèle $M4 - 3nM$ dans lequel chaque couche est considérée comme une membrane (M pour *Membrane*). Les modèles $M4 - (2n + 1)P$ et $M4 - (2n + 1)M$ sont, respectivement, issus des modèles $M4 - 3nP$ et $M4 - 3nM$ en négligeant les contraintes normales aux interfaces ($\nu^{i,i+1}$).

Carreira [1998], Carreira et al. [2002] ont modélisé des quadricouches avec des bords libres en traction par les modèles $M4 - 5n$ et $M4 - 2n + 1$. Ils ont validé les résultats de ces modèles en comparant avec les résultats obtenus par la méthode des éléments finis. Hadj-Ahmed and Ehlacher [2001] ont utilisé le modèle $M4 - 2n + 1$ pour l'analyse des contraintes dans un joint de colle. En effectuant des comparaisons avec des éléments finis, ils ont confirmé la bonne description des contraintes par le modèle $M4 - 2n + 1$. Limam and Ehlacher [2003] ont utilisé le même modèle pour analyser des poutres en béton armé renforcé par des plaques composites. Ils ont utilisé la théorie du calcul à la rupture pour déterminer la capacité portante des poutres renforcées.

Diaz Diaz [2001] a adopté les modèles $M4 - 5n$ et $M4 - 2n + 1$ en prenant en compte des variations de température et des champs inélastiques constants dans chaque couche ainsi que des discontinuités d'interface dans des plaques multicouches soumises à la traction uniaxiale. Un logiciel appelé DEILAM (Détermination des Efforts d'Interface dans un LAMiné) a été développé pour l'analyse des multicouches avec des bords libres en traction [Diaz Diaz et al. 2002]. Dans [Diaz Diaz and Caron 2006b], le modèle $M4 - 2n + 1$ a été utilisé pour analyser le glissement d'interface dans des plaques composites en traction. Caron et al. [2006], Diaz Diaz and Caron [2006a], Diaz Diaz et al. [2007a] ont faits des études expérimentales et numériques avec le modèle $M4 - 5n$ pour la prédiction du délaminage dans des plaques multicouches avec des bords libres en traction uniaxiale. Ils ont proposé un critère d'initiation du délaminage basé sur la valeur de contrainte interlaminaire de cisaillement obtenue par le modèle $M4 - 5n$ aux bords libres ou en pointe de fissure. Bien que les contraintes soient théoriquement singulières, le critère proposé porte sur les valeurs obtenues par le modèle. En comparant avec des résultats expérimentaux, ils identifient des contraintes critiques d'interface qui ne sont pas intrinsèques au matériau mais dépendent du modèle choisi. Leur approche aboutit à un taux de restitution non-nul pour une fissure de longueur nulle, ce qui n'est pas justifié selon la théorie 3D.

Tran [2004] a modélisé des chaussées à l'aide du modèle $M4 - 5n$. Il a modélisé les chaussées par le modèle $M4 - 5n$ et le sol par un massif semi-infini élastique. Le

modèle obtenu, appelé $M4$ -Boussinesq, donne un système des équations différentielles couplées qui a été résolu par la méthode des différences finies. Il a montré l'efficacité de ce modèle en comparant ces résultats à ceux obtenus par éléments finis 3D.

Nguyen [2004], Nguyen and Caron [2006] ont présenté un élément fini de plaque isoparamétrique à huit nœuds basé sur le modèle $M4-5n$. Un code de calcul éléments finis, appelé MPFEAP (MultiParticle Finit Element Analysis Program), a été développé. En utilisant ce code de calcul, Nguyen and Caron [2009] ont étudié des effets de bord libre dans des multicouches symétriques à trois et à quatre couches.

Dallot and Sab [2008b] ont utilisé le modèle $M4 - 5n$ pour étudier des effets de cisaillement dans un panneau sandwich. Ils ont utilisé des méthodes statique et cinématique pour déterminer la charge ultime et comparé les résultats des modèles Kirchhoff-Love, $M4 - 5n$ et éléments finis 3D.

Duong [2008] a enrichi la première version du code MPFEAP par un module dynamique qui permet de calculer des modes propres et un problème d'impact. Duong [2008], Duong et al. [2011] ont aussi développé le modèle $M4 - 5n$ pour la prise en compte des interfaces non-linéaires ou imparfaites.

Nguyen [2012] a implémenté le modèle $M4 - 5n$ dans le code commercial Abaqus et validé des résultats du modèle en effectuant un nombre important de benchmarks en flexion de composites et des panneaux sandwich.

Dans le cadre de cette thèse, on travaille sur le modèle $M4 - 5n$ qui est le modèle le plus utilisé parmi la famille des modèles $M4$. Afin de bien positionner ce modèle dans la littérature, on essaye d'utiliser le classement proposé par Carrera [2004], Ballhause et al. [2005]. Premièrement, le modèle $M4 - 5n$ est un modèle layerwise. Donc, on considère, d'après le classement proposé, un L pour "*Layerwise*". Deuxièmement, le modèle est basé sur une approche en contrainte, non mixte, bien qu'utilisant la formulation variationnelle de Hellinger-Reissner mais sans hypothèses sur les champs de déplacement. Sachant qu'il n'est pas recensé de modèles en contrainte pure dans le classement proposé, on se propose donc de rajouter dans la nomenclature cette distinction et donc un S pour "*Stress*". Étant donné que le modèle est basé sur des approximations linéaires des contraintes membranaires par couche, on y rajoute un chiffre 1 . La dénomination $LS1$ est ainsi justifiée et sera utilisée dans la suite. Les étapes de construction et la formulation complète du modèle LS1 peuvent être trouvées en détail dans l'annexe 1.A. Pour la simplicité de lecture, les équations principales du modèle seront aussi présentées dans chaque chapitre.

1.2 Problématique du délaminage des matériaux multicouches

1.2.1 Mécanique de la rupture - Mécanique de l'endommagement

Pour étudier le phénomène de fissuration dans un matériau, deux approches peuvent être utilisées:

- La mécanique de la rupture
- La mécanique de l'endommagement

La mécanique de la rupture étudie le comportement mécanique d'un matériau en présence de fissures macroscopiques. [Griffith \[1921\]](#) est le premier qui a étudié le problème de la rupture dans un milieu élastique fissuré d'un point de vue énergétique. Il a introduit une variable caractérisant la rupture qui a été appelée plus tard le taux de restitution d'énergie. Depuis, la mécanique de la rupture a été reprise et développée par plusieurs auteurs. On peut citer notamment les travaux de [Irwin \[1958\]](#) qui a introduit les facteurs d'intensité de contrainte ou bien les travaux de [Rice \[1968\]](#) basés sur la mécanique non-linéaire de la rupture introduisant la notion d'intégrale indépendante du contour (l'intégrale J). Tous ces développements théoriques ont pour objectif d'étudier des champs ou des paramètres mécaniques (contraintes, déformations, taux de restitution d'énergie,...) dans les zones de singularités afin de pouvoir juger de la stabilité de fissures préexistantes ou de l'apparition de nouvelles fissures. Selon le comportement du matériau durant la propagation d'une fissure, on peut distinguer deux types de rupture:

Rupture fragile: La déformation plastique est négligeable (mécanique linéaire de la rupture)

Rupture ductile: La déformation plastique est non négligeable (mécanique non linéaire de la rupture).

La mécanique de l'endommagement décrit la dégradation progressive du matériau due à l'apparition, à la croissance, puis à la coalescence de micro-fissures. Cette approche a initialement été introduite par [Kachanov \[1958\]](#) et a été développée par de nombreux auteurs. Lorsque les fissures sont de taille assez grande, cette approche n'est plus pertinente. En effet, en mécanique de l'endommagement, on ne modélise pas réellement les étapes d'amorçage et de propagation de fissures. Ces étapes se produisent naturellement lors de l'adoucissement du matériau et se traduisent par la chute des contraintes dans la zone endommagée. Dans ce cas, la fissure correspond aux zones qui ne transmettent plus d'efforts normaux.

Le choix entre les deux approches dépend de l'étude nécessaire qu'il faut faire. Par exemple, dans certains procédés de mise en forme des matériaux, l'endommagement est souvent critique, et il n'est donc pas nécessaire d'étudier la propagation de fissures. Par contre, dans d'autres procédés (usinage, découpage) ou dans des problématiques de génie civil, l'étude de la propagation de fissures est nécessaire et donc la mécanique de la rupture doit être utilisée.

1.2.2 Mécanismes de rupture - Cadre de l'étude

La rupture des matériaux multicouches peut se produire de plusieurs façons complexes. D'une manière générale, on peut distinguer trois types de rupture:

- Rupture interlaminaire ou délaminage
- Rupture intralaminaire ou fissuration transverse
- Rupture translaminaire ou fissuration longitudinale

La rupture intralaminaire, située à l'intérieur d'une couche, consiste en la rupture de matrice entre les fibres dans les plis désorientés par rapport à la direction sollicitation prédominante [Lafarie-Frenot et al. 2001, Lafarie-Frenot and Ho 2006, Lafarie-Frenot 2006]. C'est pourquoi la rupture est couramment appelée la *fissuration transverse*. Ce type de rupture est principalement dû à la faible résistance de la matrice et de l'adhérence entre la matrice et les fibres. La rupture s'initie, en général, dans la couche la plus faible au plan résistant. Par exemple, dans une plaque multicouche qui subit une traction uniaxiale dans la direction longitudinale, la fissuration transverse se présente, en générale, dans la couche ayant le module de Young transversal le moins élevé. L'apparition de la fissuration transverse peut provoquer le délaminage ou/et la fissuration longitudinale.

La rupture translaminaire concerne la rupture de fibres dans des stratifiés composites à renforts de fibres longues. Comme la fissuration transverse, ce type de rupture se produit au niveau des couches mais dans des couches parallèles à la direction de sollicitation. C'est la raison pour laquelle ce type de rupture est appelé très souvent la *fissuration longitudinale*. Puisque la contrainte à rupture des fibres est beaucoup plus importante que celle des autres constituants, ce mécanisme de rupture entraîne souvent la rupture totale du stratifié. La rupture translaminaire peut être en mode traction ou en mode compression (micro-flambement).

La rupture interlaminaire se traduit par un décollement à l'interface de deux couches adjacentes. Ce type de rupture est couramment appelé le *délaminage*. En terme général, le délaminage se produit à l'issue des contraintes interlaminaires importantes. Ces contraintes d'interface peuvent avoir des origines différentes. Des défauts de fabrication comme des micro-vides ou des impuretés sont des discontinuités locales qui peuvent provoquer des contraintes interlaminaires importantes lors du chargement. Le délaminage peut être à cause des impacts. Un choc à basse vitesse tel qu'une chute d'objet sur un stratifié peut entraîner des ruptures importantes de la matrice à l'intérieur sans laisser de traces apparentes sur la surface [Chai et al. 1981, Geubelle and Baylor 1998, Choi and Chang 1992, Bouvet et al. 2009, Abdallah et al. 2009, Bouvet et al. 2012]. Outre des zones de défauts et d'impacts, des bords libres sont des zones très susceptibles au délaminage. La discontinuité de comportement mécanique entre deux couches adjacentes occasionne des contraintes interlaminaires très élevées près des bords libres. Ce phénomène, appelé *l'effet de bord libre*, est l'un des sujets majeurs d'analyse des structures multicouches.

Dans le cadre de ce travail, on étudie le délaminage dans des plaques multicouches orthotropes sous différents types de chargement. Pour ce faire, on utilise la mécanique linéaire de la rupture. Ainsi, le délaminage est modélisé comme une discontinuité de déplacement à l'interface fissurée. Dans ce qui suit, on fait une brève synthèse sur le délaminage (modes de ruptures, essais classiques, critères,...).

1.2.3 Modes de rupture

De manière générale, on peut distinguer trois modes purs de rupture qui se caractérisent selon les déplacements relatifs des lèvres de fissure (1.8):

- Mode I (ouverture): déplacement relatif des lèvres perpendiculaire au plan de fissure (déplacement opposé des lèvres)
- Mode II (glissement droit): déplacement relatif des lèvres parallèle au plan de fissure et perpendiculaire au front de fissure
- Mode III (glissement vis): déplacement relatif des lèvres parallèle au plan de fissure et parallèle au front de fissure

Le mode I correspond à la contrainte normale au plan de fissure. Dans les modes II et III, les contraintes de cisaillement dans le plan de fissure sont agissantes. En réalité, une fissure se propage dans un matériau sous une combinaison de ces trois modes de rupture.

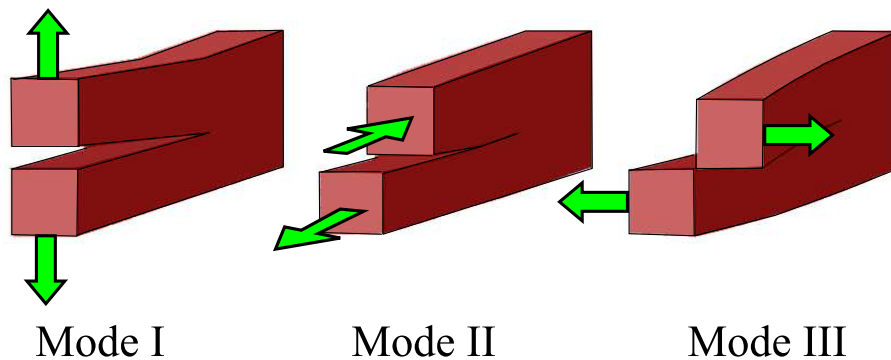


Figure 1.8: Modes de rupture d'une fissure

1.2.4 Essais de délaminage

Ici, on présente des essais de délaminage les plus courants dans la littérature qui sont adoptés par la plupart des normes internationales (ASTM, ESIS, JIS,...). Le Tableau 1.2 énumère les différents essais en modes purs I, II et III et mode mixte I+II. A notre connaissance, les modes mixtes I+III et II+III ne sont pas envisagés pour la normalisation dans un proche avenir. La figure 1.9 montre schématiquement le mécanisme des essais mentionnés.

1.2.5 Critères de délaminage

Les critères utilisés dans la littérature pour la prédiction de délaminage sont très variés. Ces critères peuvent être regroupés dans les catégories suivantes:

Table 1.2: Essais de délaminage

Essai	Nom complet	Mode principal
DCB	Double Cantilever Beam	Mode I
ELS	End Loaded Split	Mode II
ENF	End Notched Flexure	Mode II
4ENF	Four-point End Notched Flexure	Mode II
ECT	Edge Crack Torsion	Mode III
EDT	Edge Delamination Test	Mode III
SCB	Split Cantilever Beam	Mode III
MMF	Mixed Mode Flexure	Mode I+II
MMB	Mixed Mode Bending	Mode I+II
CLS	Cracked Lap Shear	Mode I+II
ADCB	Asymmetric Double Cantilever Beam	Mode I+II
AMMF	Asymmetric Mixed Mode Flexure	Mode I+II

- Critères en contrainte
- Critères en facteur d'intensité de contrainte
- Critères énergétiques
- Critères en déplacement d'ouverture de fissure
- Double critère en contrainte/énergie

1.2.5.1 Critères en contrainte

Il est bien connu que les contraintes interlaminaires 3D sont souvent singulières aux bords libres et aux pointes de fissure [Ting and Chou 1981, Zwiers et al. 1982, Wang and Choi 1982a, Wang 1983, Leguillon and Sanchez-Palencia 1987, Iarve and Pagano 2001, Leguillon et al. 2001, Mittelstedt and Becker 2004, 2005, Chue and Liu 2002]. Par conséquent, il est impossible de définir un critère portant sur la valeur maximale de contrainte. Pour surmonter cette difficulté, Whitney and Nuismer [1974] ont introduit la notion d'une longueur caractéristique pour définir des critères de délaminage en contrainte. Cette longueur est la distance du bord libre ou de la pointe de fissure à laquelle les contraintes sont mesurées, ou bien sur laquelle les contraintes sont moyennées. Ainsi, les critères en contrainte peuvent être définis sur les valeurs ponctuelles ou moyennes

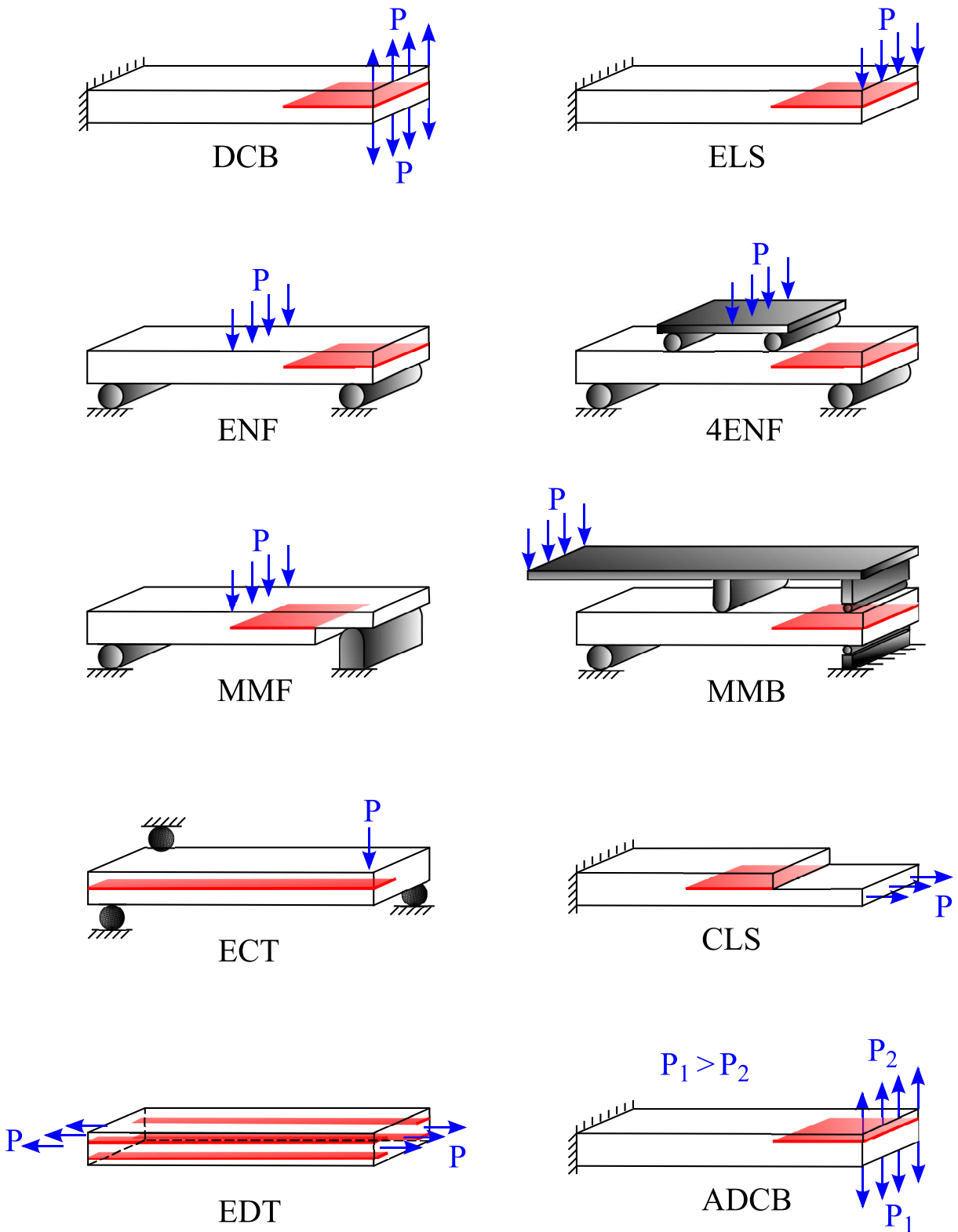


Figure 1.9: Différents essais de délaminage existant dans la littérature

de contraintes. Le critère le plus simple est sous la forme suivante:

$$\left(\frac{\sigma_{xz}}{\sigma_{xz}^D}\right)^2 + \left(\frac{\sigma_{yz}}{\sigma_{yz}^D}\right)^2 + \left(\frac{[\sigma_{zz}]^+}{\sigma_{zz}^D}\right)^2 = 1 \quad (1.31)$$

où σ_{xz} et σ_{yz} sont les contraintes interlaminaires de cisaillement et $[\sigma_{zz}]^+$ est la partie positive de la contrainte normale. En fonction du critère, les valeurs de ces contraintes sont des valeurs ponctuelles (à une distance) ou des valeurs moyennes (sur une longueur caractéristique). σ_{xz}^D , σ_{yz}^D et σ_{zz}^D sont les résistances interlaminaires (en modes III, II et I respectivement).

Kim and Soni [1984] ont proposé un critère d'initiation de délaminage en mode I portant sur la valeur moyenne de la contrainte interlaminaire normale $\bar{\sigma}_{zz}$ sur une distance caractéristique du bord libre. Ils ont utilisé la méthode local-global de Pagano and Soni [1983] pour calculer les contraintes d'interface. En reliant la longueur caractéristique à l'épaisseur des couches, ils ont pris en considération les effets d'échelles des multicouches en traction. Kim and Soni [1986] ont proposé ensuite un critère plus général sur les contraintes interlaminaires moyennes de la forme:

$$\left(\frac{\bar{\sigma}_{xz}}{\sigma_{xz}^D}\right)^2 + \left(\frac{\bar{\sigma}_{yz}}{\sigma_{yz}^D}\right)^2 + \left(\frac{\bar{\sigma}_{zz}^2}{\sigma_{zz}^{DT} \sigma_{zz}^{DC}}\right) + \bar{\sigma}_{zz} \left(\frac{1}{\sigma_{zz}^{DT}} - \frac{1}{\sigma_{zz}^{DC}}\right) = 1 \quad (1.32)$$

où σ_{zz}^{DT} et σ_{zz}^{DC} sont les résistances interlaminaires en traction et en compression respectivement. Le dernier terme dans le critère est basé sur le fait que la contrainte normale négative retarde l'initiation du délaminage.

Brewer and Lagace [1988] ont proposé un critère quadratique pour l'initiation du délaminage qui porte sur les valeurs moyennes de contraintes interlaminaires:

$$\left(\frac{\bar{\sigma}_{xz}}{\sigma_{xz}^D}\right)^2 + \left(\frac{\bar{\sigma}_{yz}}{\sigma_{yz}^D}\right)^2 + \left(\frac{\bar{\sigma}_{zz}}{\sigma_{zz}^{DT}}\right)^2 + \left(\frac{\bar{\sigma}_{zz}}{\sigma_{zz}^{DC}}\right)^2 = 1 \quad (1.33)$$

Ce critère suppose que la longueur caractéristique est indépendante de l'épaisseur des couches.

Dans le critère proposé par Sun and Zhou [1988], le signe de la contrainte interlaminaire normale n'est pas pris en compte:

$$\left(\frac{\sigma_{xz}}{\sigma_{xz}^D}\right)^2 + \left(\frac{\sigma_{yz}}{\sigma_{yz}^D}\right)^2 + \left(\frac{\sigma_{zz}}{\sigma_{zz}^D}\right)^2 = 1 \quad (1.34)$$

Leguillon et al. [2001] ont proposé un critère d'initiation en contrainte moyenne du type $\sigma_{xz} = \sigma_{xz}^D$ pour les plaques multicouches en traction. Ils se servent du développement asymptotique et des travaux de Lécuyer [1991], Lécuyer and Engrand [1992] pour évaluer les contraintes d'interface. Les effets d'épaisseur sont pris en compte dans le calcul de la longueur caractéristique. Basé sur les mêmes travaux, Marion [2000], Lorriot et al. [2003] ont proposé un critère d'initiation sous la forme suivante:

$$\left(\frac{\bar{\sigma}_{xz}}{\sigma_{xz}^D}\right)^2 + \left(\frac{\bar{\sigma}_{yz}}{\sigma_{yz}^D}\right)^2 + \frac{\bar{\sigma}_{zz}}{\sigma_{zz}^{DT}} = 1 \quad (1.35)$$

Ce critère considère des longueurs caractéristiques différentes pour les contraintes de cisaillement et la contrainte normale.

1.2.5.2 Critères en facteur d'intensité de contrainte

D'une manière générale, dans le cas de singularité, la contrainte peut s'écrire:

$$\sigma \approx K r^{-\lambda} f(g) \quad (1.36)$$

où K est le facteur d'intensité de contrainte, r est la distance de la pointe de fissure ou du bord libre, $0 \leq \lambda < 1$ est l'exposant de singularité et $f(g)$ est une fonction de géométrie.

Irwin [1958] est le premier qui a reformulé l'approche énergétique de Griffith en termes de facteur d'intensité de contrainte. Pour les matériaux multicouches, les critères de délaminage s'écrivent, en général, sous la forme suivante:

$$\left(\frac{K_I}{K_I^c}\right)^\alpha + \left(\frac{K_{II}}{K_{II}^c}\right)^\beta + \left(\frac{K_{III}}{K_{III}^c}\right)^\gamma = 1 \quad (1.37)$$

où K_I , K_{II} et K_{III} sont les facteurs d'intensité de contrainte respectivement en modes I, II et III. K_I^c , K_{II}^c et K_{III}^c sont les facteurs d'intensité de contrainte critiques supposés intrinsèques au matériau. Les exposants α , β et γ sont positifs et aussi supposés intrinsèques au matériau. On remarque que les modes I, II et III correspondent à σ_{zz} , σ_{yz} et σ_{xz} respectivement.

Chyanbin et al. [1995] ont proposé un critère en facteur d'intensité de contrainte du type 1.37 en identifiant les exposants α , β et γ pour différents matériaux. Ils ont effectué des essais expérimentaux classiques sur des plaques composites pour mesurer les facteurs d'intensités critiques. En utilisant la méthode des éléments finis, ils ont validé leur critère pour différents types de chargement.

Yuuki et al. [1994] ont proposé un critère quadratique en facteur d'intensité de contrainte en mode mixte I+II:

$$\left(\frac{K_I}{K_I^c}\right)^2 + \left(\frac{K_{II}}{K_{II}^c}\right)^2 = const \quad (1.38)$$

Chow and Atluri [1996, 1997] ont développé ce critère en prenant en compte le mode III. Ils ont proposé un critère sous la forme:

$$\left(\frac{K_I}{0.85 K_I^c}\right)^2 + \left(\frac{K_{II}}{K_{II}^c}\right)^2 + \left(\frac{K_{III}}{K_{III}^c}\right)^2 = (\theta_f K_0)^2 \quad (1.39)$$

où K_0 est le facteur d'intensité de contrainte normalisé (adimensionnel). θ_f est un coefficient adimensionnel qui dépend de l'angle entre le front de fissure et la direction de fibres.

Sachant que les facteurs d'intensité de contrainte peuvent être reliés au taux de restitution d'énergie, certains auteurs ont proposé des critères portant sur le taux de restitution d'énergie et l'angle de phase $\psi = \tan^{-1}(K_{II}/K_I)$.

1.2.5.3 Critères énergétiques

Considérons l'état initial statique d'une structure élastique caractérisé par l'énergie potentielle W_p et l'énergie cinétique $W_k = 0$. Le bilan d'énergie entre l'état initial et l'état de la structure après l'initiation d'une fissure ou la propagation d'une fissure préexistante s'écrit:

$$\delta W_p + \delta W_k + G^c \delta S = 0 \quad (1.40)$$

où δW_p et δW_k sont les variations des énergies potentielle et cinétique respectivement. δS est la nouvelle surface de fissure et G^c représente l'énergie de rupture par l'unité de surface qu'on appelle la ténacité (taux de restitution d'énergie critique). Puisque l'état initial est statique $\delta W_k \geq 0$ et donc:

$$\delta W_p + G^c \delta S \leq 0 \implies -\frac{\delta W_p}{\delta S} \geq G^c \quad (1.41)$$

L'équation ci-dessus représente un critère énergétique pour lequel il faut connaître la surface incrémentale δS . Si la fissure se propage en continu, la condition est valable pour tout changement infinitésimal de la surface de fissure. En considérant $\delta S \rightarrow 0$ on trouve la forme différentielle du critère énergétique:

$$G = -\frac{\partial W_p}{\partial S} \geq G^c \quad (1.42)$$

où G est appelé le taux de restitution d'énergie. Ce critère est connu dans la littérature sous le nom de critère de Griffith [Griffith 1921].

Les différents critères énergétiques sont en général basés sur le critère de Griffith. Plusieurs tentatives effectuées ont montré qu'un seul taux de restitution d'énergie n'est pas suffisant pour décrire la rupture [Wang 1989]. Sachant qu'une réelle rupture est très souvent en mode mixte, il faut établir un critère de rupture qui permet de distinguer différents modes de rupture. Par conséquent, la plupart des critères énergétiques portent sur la contribution des taux de restitution d'énergie G_I , G_{II} et G_{III} qui sont associés respectivement aux modes I, II et III ($G = G_I + G_{II} + G_{III}$). Cela nécessite d'introduire trois taux de restitution d'énergie critiques G_I^c , G_{II}^c et G_{III}^c . Dans tous les critères énergétiques, G_I^c , G_{II}^c et G_{III}^c sont supposés être des grandeurs intrinsèques au matériau. Différentes méthodes expérimentales ont été proposées pour l'identification de ces ténacités [Whitney 1989, Benzeggagh and Kenane 1996].

Plusieurs types de critère énergétique ont été proposés dans la littérature pour le délaminage en mode mixte. Pour le mode mixte I+II, les critères les plus simples sont $G_I = G_I^c$ [Whitcomb 1984] considérant seulement le premier mode, et $G_{II} = G_{II}^c$ [Gillespie et al. 1985] qui ne prend en compte que le deuxième mode. Dans [Wu and Reuter Jr. 1965], le critère proposé $G_I + G_{II} = G_{eq}^c$ considère les deux modes. Dans ce critère il est supposé que la ténacité G_{eq}^c ne dépend pas de la contribution des modes; c'est-à-dire $G_{eq}^c = G_I^c = G_{II}^c$. Puisque G_I^c et G_{II}^c sont différents pour la plupart des matériaux, les auteurs ont proposé aussi un critère linéaire en mode mixte I+II du type:

$$\frac{G_I}{G_I^c} + \frac{G_{II}}{G_{II}^c} = 1 \quad (1.43)$$

Ce critère linéaire est éventuellement le critère le plus utilisé dans la littérature [Spencer and Barnby 1976, Jurf and Pipes 1982, Donaldson 1985, Mall and Kochhar 1986]. En généralisant ce critère, un critère en loi puissance a été proposé sous la forme suivante:

$$\left(\frac{G_I}{G_I^c}\right)^\alpha + \left(\frac{G_{II}}{G_{II}^c}\right)^\beta = 1 \quad (1.44)$$

Plusieurs combinaisons pour (α, β) ont été utilisé comme $(\alpha = 0.5, \beta = 1)$ [Wu and Reuter Jr. 1965], $(\alpha = 1, \beta = 1.5)$ [Donaldson 1987] et $(\alpha = 0.64, \beta = 0.8)$ [Hashemi et al. 1990]. Les valeurs optimales de α et β pour un matériau s'obtiennent en minimisant des erreurs par rapport aux données expérimentales.

Yan et al. [1991] ont supposé que la ténacité totale à la rupture est une fonction polynomiale du rapport entre G_{II} et G_I :

$$G_I + G_{II} = G_I^c + \rho \left(\frac{G_{II}}{G_I}\right) + \tau \left(\frac{G_{II}}{G_I}\right)^2 \quad (1.45)$$

En ajustant les paramètres ρ et τ , ce critère peut être utilisé pour une grande variété de matériaux. Parmi les critères mentionnés, ce critère est le seul qui permet à la fois l'augmentation des modes I et II. En revanche, le critère est un peu instable pour un rapport petit entre les modes G_I et G_{II} . C'est pourquoi ce critère n'est pas un bon choix pour un critère général en mode mixte.

[Donaldson 1985] a proposé un critère exponentiel avec un seul paramètre γ à ajuster:

$$G_I + G_{II} = G_{II}^c + (G_I^c - G_{II}^c) e^{\gamma(1-N)} \quad \text{avec} \quad N = \sqrt{1 + \frac{G_{II}}{G_I} \sqrt{\frac{E_{11}}{E_{22}}}} \quad (1.46)$$

Ce critère est basé sur l'angle de hackle $\sqrt{1 + \left(\frac{K_{II}}{K_I}\right)^2}$ où K_I et K_{II} sont les facteurs d'intensité de contrainte en mode I et II respectivement.

Williams [1989] a proposé un critère basé sur l'interaction linéaire des modes I et II:

$$\left(\frac{G_I}{G_I^c} - 1\right) \left(\frac{G_{II}}{G_{II}^c} - 1\right) - \kappa \left(\frac{G_I}{G_I^c}\right) \left(\frac{G_{II}}{G_{II}^c}\right) = 0 \quad (1.47)$$

Le paramètre κ détermine l'interaction entre les modes I et II. Pour $\kappa = 0$ les modes de rupture I et II sont complètement indépendants. Pour $\kappa = 1$ le critère est ramené au critère linéaire. Dans [Hashemi et al. 1990], différentes values de κ de 0,26 à 3,12 ont été identifiées pour différents matériaux. Ce critère donne à peu près les mêmes résultats que le critère en loi puissance avec $\alpha = \beta$. Hashemi et al. [1991] ont enrichi ce critère en considérant une fonction linéaire de $G_I/(G_I + G_{II})$ pour le terme d'interaction:

$$\left(\frac{G_I}{G_I^c} - 1\right) \left(\frac{G_{II}}{G_{II}^c} - 1\right) - \left[\kappa + \varphi \left(\frac{G_I}{G_I + G_{II}}\right)\right] \left(\frac{G_I}{G_I^c}\right) \left(\frac{G_{II}}{G_{II}^c}\right) = 0 \quad (1.48)$$

En ajustant les paramètres κ et φ ce critère est capable de modéliser plusieurs types de matériaux. Néanmoins, sa forme implicite en G_I et G_{II} le rend un peu compliqué à appliquer.

En étudiant le délaminage des composites avec la matrice époxy en mode mixte, [Reeder \[2002\]](#) a observé qu'un changement de mécanisme de rupture peut avoir lieu quand le rapport entre G_I et G_{II} est proche de 1. En se basant sur ce phénomène, il a proposé un critère bilinéaire de la forme:

$$\begin{aligned} \text{Phase 1 : } & G_I = \xi G_{II} + G_I^c \\ \text{Phase 2 : } & G_I = \zeta G_{II} - \zeta G_{II}^c \end{aligned} \quad (1.49)$$

Si on trace G_I en fonction de G_{II} , ξ est la pente de la première ligne qui peut être positive ou négative et ζ est la pente de la deuxième ligne qui est négative. Pour $\xi > 0$ la phase 1 se traduit par une augmentation de G_I avec l'introduction de G_{II} jusqu'à un pic. Ensuite, dans la phase 2, G_I diminue avec l'augmentation de G_{II} jusqu'à $G_I = 0; G_{II} = G_{II}^c$. Il faut remarquer que dans le cas où $\xi < 0$ dans la première phase aussi il y a une diminution de G_I avec l'augmentation de G_{II} . En choisissant $\xi = \zeta = -G_I^c/G_{II}^c$ ce critère se ramène au critère linéaire.

Parmi les critères qui prennent en considération aussi le mode III, les plus utilisés sont les suivants:

- Critère en loi de puissance

$$\left(\frac{G_I}{G_I^c}\right)^\alpha + \left(\frac{G_{II}}{G_{II}^c}\right)^\beta + \left(\frac{G_{III}}{G_{III}^c}\right)^\gamma = 1 \quad (1.50)$$

Ce critère nécessite six données G_I^c , G_{II}^c , G_{III}^c , α , β et γ . En choisissant $\alpha = \beta = \gamma = 1$ ce critère devient le critère linéaire classique.

- Critère de [Benzeggagh and Kenane \[1996\]](#)

$$G = G_{eq}^c \quad \text{avec} \quad G_{eq}^c = G_I^c + (G_{II}^c - G_I^c) \left(\frac{G_{II} + G_{III}}{G_I + G_{II} + G_{III}}\right)^\eta \quad (1.51)$$

Dans ce critère il faut définir G_I^c , G_{II}^c et η .

- Critère de [Reeder et al. \[2002\]](#)

$$G = G_{eq}^c \quad \text{avec} \quad G_{eq}^c = G_I^c + \left[(G_{II}^c - G_I^c) + (G_{III}^c - G_{II}^c) \left(\frac{G_{III}}{G_{II} + G_{III}}\right) \right] \left(\frac{G_{II} + G_{III}}{G_I + G_{II} + G_{III}}\right)^\eta \quad (1.52)$$

Dans ce critère il faut définir G_I^c , G_{II}^c , G_{III}^c et η .

Remarque:

- En mode I ($G_{II} = G_{III} = 0$) le critère se ramène à $G_I = G_I^c$.
- En mode II ($G_I = G_{III} = 0$) le critère se ramène à $G_{II} = G_{II}^c$.
- En mode III ($G_I = G_{II} = 0$) le critère se ramène à $G_{III} = G_{III}^c$.
- Si $G_{II}^c = G_{III}^c$ ou $G_{III} = 0$ le critère se ramène au critère de Benzeggagh et Kenane.

Pour utiliser les critères énergétiques, il faut calculer le taux de restitution d'énergie. Beaucoup de méthodes analytiques (dans les cas simples) et numériques ont été proposées dans la littérature. Parmi les méthodes numériques la méthode d'avancée virtuelle de fissure (Virtual Crack Extension), la méthode de fermeture virtuelle de fissure (Virtual Crack Closure Technic), la méthode de l'intégrale de contour J (J-integral) et calcul par avancée réelle de fissure sont les méthodes couramment utilisées.

1.2.5.4 Critère en déplacement d'ouverture de fissure

Wells [1961], Cottrell [1961] ont introduit pour la première fois le concept d'un déplacement d'ouverture critique derrière la pointe de fissure comme un critère de rupture. La forme la plus courante de ce type de critère est:

$$\delta(r^c) = \delta^c \tag{1.53}$$

où δ est le déplacement d'ouverture de la fissure à une distance caractéristique r^c derrière la pointe de fissure (Fig. 1.10). δ^c est un déplacement d'ouverture critique. La fissure se propage quand le déplacement d'ouverture à une distance r^c de la pointe de fissure atteint la valeur critique δ^c . Il est supposé que δ^c est une caractéristique du matériau et ne dépend pas de la structure ni de la longueur de fissure.

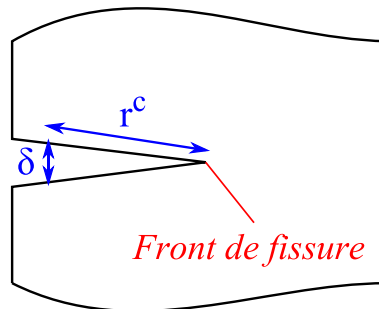


Figure 1.10: Critère en déplacement d'ouverture de fissure

Ce critère s'utilise en général pour la propagation de fissure dans les matériaux ductiles. Le déplacement d'ouverture peut être relié aux facteurs d'intensité de contrainte ou au taux de restitution d'énergie. Par conséquent, ce type de critère peut être transformé en critère énergétique ou en facteur d'intensité de contrainte.

Comme les travaux plus récents utilisant ce type de critère, nous citons les travaux de Xia et al. [1996], Sutton et al. [2000], Fang et al. [2004], Zuo et al. [2008], Werner [2012].

1.2.5.5 Double critère en résistance/ténacité

Il est connu que la limite du taux de restitution d'énergie tend vers zéro quand la longueur de fissure tend vers zéro (voir [Leguillon 1999]). Par conséquent, pour une structure non-fissurée la condition $G = G^c$ n'est jamais satisfaite quelque soit le niveau de chargement extérieur; or les résultats expérimentaux montre qu'à un certain niveau ($\sigma = \sigma^c$) de chargement l'amorçage de fissure se produit. Cela revient à ce que le critère de Griffith ne permet pas de prédire l'amorçage de fissure et ceci est souvent interprété comme un défaut de ce critère dans les matériaux fragiles.

Leguillon [1999, 2002] a cherché une explication à ce problème. En se basant sur le fait que les équations 1.40 et 1.41 (l'équilibre de l'énergie) sont incontestables, il a expliqué que le problème provient de l'hypothèse que l'amorçage et la propagation ont lieu progressivement. Leguillon a expliqué que l'amorçage de fissure est un phénomène brutal qui se produit avec une longueur minimale d'initiation. Pour l'initiation du délaminage, δW_p dans l'équation 1.41 est la différence de l'énergie potentielle entre l'état fissuré et non-fissuré et $\delta S = b \times a$ est la surface de fissure (a est la longueur de fissure et b est la largeur de fissure supposée constante). Ainsi, la forme incrémentale du critère énergétique s'écrit:

$$G^{inc}(a, F) = -\frac{\delta W}{\delta S} = \frac{W(a=0) - W(a)}{b \times a} \geq G^c \quad (1.54)$$

où G^{inc} est le taux de restitution incrémental (vis-à-vis du taux de restitution d'énergie infinitésimal) et $W(a)$ est l'énergie potentielle de la structure fissurée avec une longueur de fissure a . F représente le chargement extérieur. Ce critère est une condition nécessaire mais pas suffisante pour l'initiation du délaminage. Pour l'amorçage de fissure, la contrainte aussi doit atteindre une valeur critique, ce qui est confirmé par les résultats expérimentaux. Donc, la deuxième condition nécessaire s'écrit:

$$\sigma(y, F) \geq \sigma^c \quad \text{pour} \quad y \leq a \quad (1.55)$$

où $\sigma(y)$ est la contrainte dans le cas non-fissuré à une distance y à partir du point de singularité (bord libre) et σ^c est la résistance (la contrainte critique). D'après le critère de Leguillon, à l'instant de l'amorçage de fissure, les deux critères sont satisfaits simultanément:

$$\begin{cases} G^{inc}(a^c, F^c) = G^c \\ \sigma(y = a^c, F^c) = \sigma^c \end{cases} \quad (1.56)$$

Ce double critère s'appuie sur deux conditions une en énergie et une en contrainte. La première condition fait référence à la ténacité du matériau (ou de l'interface) G^c alors que l'autre fait appel à la résistance σ^c . En appliquant les deux conditions simultanément, la longueur critique d'amorçage a^c et la charge au moment de l'amorçage F^c

sont calculées. Il faut remarquer que a^c est la longueur minimale de fissure; c'est-à-dire au moment de l'amorçage, il y a un saut brutal de $a = 0$ à $a = a^c$.

Ce double critère a été mis en œuvre par Leguillon en utilisant une approche asymptotique mais il peut être utilisé facilement avec d'autres approches. [Martin and Leguillon \[2004\]](#), [Martin et al. \[2008, 2010, 2012\]](#) ont exploité ce double critère directement de façon numérique avec la méthode des éléments finis. Dans le chapitre 3, nous utiliserons ce double critère avec une approche analytique par le modèle LS1 ainsi qu'avec une approche numérique aux éléments finis 3D.

Annexe 1.A Formulation du model LS1

Cette section présente la formulation générale du modèle LS1. Ce modèle, appelé anciennement le modèle M4-5n, a été développé au Laboratoire Navier par [Ehrlacher et al.](#) en utilisant la méthode d'approximation de Hellinger-Reissner.

1.A.1 Méthode d'approximation de Hellinger-Reissner pour un problème d'élasticité 3D

Nous considérons un solide Ω de frontière $\partial\Omega$. Le problème d'élasticité 3D à résoudre consiste à déterminer les champs de déplacement \underline{U} et de contrainte $\underline{\underline{\sigma}}$ dans ce domaine satisfaisant les équations suivantes:

- équations de compatibilité:

$$\underline{\underline{\varepsilon}}(\underline{x}) = \frac{1}{2} \left(\underline{\underline{grad}} \underline{U} + \underline{\underline{grad}}^T \underline{U} \right) \quad (1.57)$$

- équations de comportement (supposé élastique):

$$\underline{\underline{\varepsilon}}(\underline{x}) = \underline{\underline{S}}(\underline{x}) : \underline{\underline{\sigma}}(\underline{x}) \quad (1.58)$$

- équations d'équilibre:

$$\underline{\underline{div}} \underline{\underline{\sigma}}(\underline{x}) + \underline{f}(\underline{x}) = \underline{0} \quad (1.59)$$

- conditions aux limites:

$$\underline{U}(\underline{x}) = \underline{U}^d(\underline{x}) \quad \text{sur} \quad \partial\Omega_U \quad (1.60)$$

$$\underline{\underline{\sigma}}(\underline{x}) \cdot \underline{n}(\underline{x}) = \underline{T}^d(\underline{x}) \quad \text{sur} \quad \partial\Omega_T \quad (1.61)$$

avec

$$\partial\Omega_U \cap \partial\Omega_T = \emptyset, \quad \partial\Omega_U \cup \partial\Omega_T = \partial\Omega$$

où:

- \underline{x} est la variable d'espace
- \underline{U} est le vecteur des déplacements 3D en \underline{x}
- $\underline{\underline{\varepsilon}}$ est le tenseur des déformations 3D en \underline{x}
- $\underline{\underline{\sigma}}$ est le tenseur des contraintes 3D en \underline{x}
- $\underline{\underline{S}}$ est le tenseur d'ordre quatre des souplesses en \underline{x}
- \underline{f} est le vecteur des forces de volume en \underline{x}
- $\partial\Omega_U$ est la partie de la frontière sur laquelle il y a des déplacements imposés

- $\partial\Omega_T$ est la partie de la frontière sur laquelle il y a des contraintes imposées
- \underline{U}^d est le vecteur des déplacements imposés sur $\partial\Omega_U$
- \underline{T}^d est le vecteur contrainte imposé sur $\partial\Omega_U$
- \underline{n} est le vecteur normal à la frontière

La fonctionnelle de Hellinger-Reissner sur le couple des champs $(\underline{U}^*, \underline{\sigma}^*)$ est définie comme suit:

$$\begin{aligned} H.R.(\underline{U}^*, \underline{\sigma}^*) &= \int_{\Omega} \left[\underline{\sigma}^*(\underline{x}) : \underline{\varepsilon}(\underline{U}^*(\underline{x})) - \underline{f}(\underline{x}) \cdot \underline{U}^*(\underline{x}) - \frac{1}{2} \underline{\sigma}^*(\underline{x}) : \underline{\underline{S}}(\underline{x}) : \underline{\sigma}^*(\underline{x}) \right] d\Omega \\ &\quad - \int_{\partial\Omega_U} (\underline{\sigma}^*(\underline{x}) \cdot \underline{n}) \cdot (\underline{U}^*(\underline{x}) - \underline{U}^d(\underline{x})) dS - \int_{\partial\Omega_T} \underline{T}^d(\underline{x}) \cdot \underline{U}^*(\underline{x}) dS \end{aligned} \quad (1.62)$$

où \underline{U}^* est un champ de vecteur 3D continu sur Ω (de classe C^1 par morceau) et $\underline{\sigma}^*$ est un champ de tenseur d'ordre deux symétrique (de classe C^1 par morceau).

Étant donné que le tenseur $\underline{\sigma}^*$ est symétrique, en intégrant par parties la fonctionnelle H.R. peut s'écrire sous la forme suivante:

$$\begin{aligned} H.R.(\underline{U}^*, \underline{\sigma}^*) &= - \int_{\Omega} \left[\text{div} \underline{\sigma}^*(\underline{x}) \cdot \underline{U}^*(\underline{x}) + \underline{f}(\underline{x}) \cdot \underline{U}^*(\underline{x}) + \frac{1}{2} \underline{\sigma}^*(\underline{x}) : \underline{\underline{S}}(\underline{x}) : \underline{\sigma}^*(\underline{x}) \right] d\Omega \\ &\quad + \int_{\partial\Omega_U} (\underline{\sigma}^*(\underline{x}) \cdot \underline{n}) \cdot \underline{U}^d(\underline{x}) dS + \int_{\partial\Omega_T} (\underline{\sigma}^*(\underline{x}) \cdot \underline{n} - \underline{T}^d(\underline{x})) \cdot \underline{U}^*(\underline{x}) dS \end{aligned} \quad (1.63)$$

D'après le théorème de Reissner, la solution du problème d'élasticité est le couple $(\underline{U}^*, \underline{\sigma}^*)$ qui rend stationnaire la fonctionnelle définie ci-dessus. La stationnarité par rapport à une variation quelconque du champ de déplacement tridimensionnel \underline{U}^* donne les équations d'équilibre 1.59 et les conditions aux limites en contrainte 1.61. La stationnarité par rapport à une variation quelconque du champ de contrainte tridimensionnel $\underline{\sigma}^*$ donne le comportement élastique linéaire 1.58 et les conditions aux limites en déplacement 1.60. Nous définissons les fonctionnelles $T_1(\underline{U}^*, \underline{\sigma}^*)$ et $T_2(\underline{U}^*, \underline{\sigma}^*)$ déduites de la fonctionnelle de Hellinger-Reissner:

$$T_1(\underline{U}^*, \underline{\sigma}^*) = - \int_{\Omega} [\text{div} \underline{\sigma}^*(\underline{x}) \cdot \underline{U}^*(\underline{x}) + \underline{f}(\underline{x}) \cdot \underline{U}^*(\underline{x})] d\Omega + \int_{\partial\Omega_T} (\underline{\sigma}^*(\underline{x}) \cdot \underline{n} - \underline{T}^d(\underline{x})) \cdot \underline{U}^*(\underline{x}) dS \quad (1.64)$$

$$\begin{aligned} T_2(\underline{U}^*, \underline{\sigma}^*) &= - \int_{\Omega} \left[\text{div} \underline{\sigma}^*(\underline{x}) \cdot \underline{U}^*(\underline{x}) + \frac{1}{2} \underline{\sigma}^*(\underline{x}) : \underline{\underline{S}}(\underline{x}) : \underline{\sigma}^*(\underline{x}) \right] d\Omega \\ &\quad + \int_{\partial\Omega_U} (\underline{\sigma}^*(\underline{x}) \cdot \underline{n}) \cdot \underline{U}^d(\underline{x}) dS + \int_{\partial\Omega_T} (\underline{\sigma}^*(\underline{x}) \cdot \underline{n}) \cdot \underline{U}^*(\underline{x}) dS \end{aligned} \quad (1.65)$$

Dans la fonctionnelle $T_1(\underline{U}^*, \underline{\underline{\sigma}}^*)$ on ne considère que les termes qui font apparaître le champ de déplacement \underline{U}^* . De cette manière, les stationnarités des fonctionnelles $H.R.(\underline{U}^*, \underline{\underline{\sigma}}^*)$ et $T_1(\underline{U}^*, \underline{\underline{\sigma}}^*)$ par rapport à une variation de \underline{U}^* sont identiques. De la même façon, la fonctionnelle $T_2(\underline{U}^*, \underline{\underline{\sigma}}^*)$ ne prend en compte que les termes faisant intervenir le champ de contrainte $\underline{\underline{\sigma}}^*$. Cela nous permet d'utiliser la fonctionnelle $T_2(\underline{U}^*, \underline{\underline{\sigma}}^*)$ à la place de $H.R.(\underline{U}^*, \underline{\underline{\sigma}}^*)$ pour la stationnarité par rapport à une variation de $\underline{\underline{\sigma}}^*$.

1.A.2 Position du problème - Notation

Considérons un multicouche constitué de n couches dans le repère Cartésien (x, y, z) . x et y sont les coordonnées dans le plan alors que z indique la direction normale. Le multicouche occupe le volume $\Omega = \omega \times [h_-^1; h_+^n]$ avec la frontière $\partial\Omega = S_{lat} \cup \omega^+ \cup \omega^-$ où:

- $S_{lat} = \partial\omega \times \{h_-^1; h_+^n\}$ est le bord latéral
- $\omega^+ = \omega \times \{h_+^n\}$ est la surface supérieure
- $\omega^- = \omega \times \{h_-^1\}$ est la surface inférieure

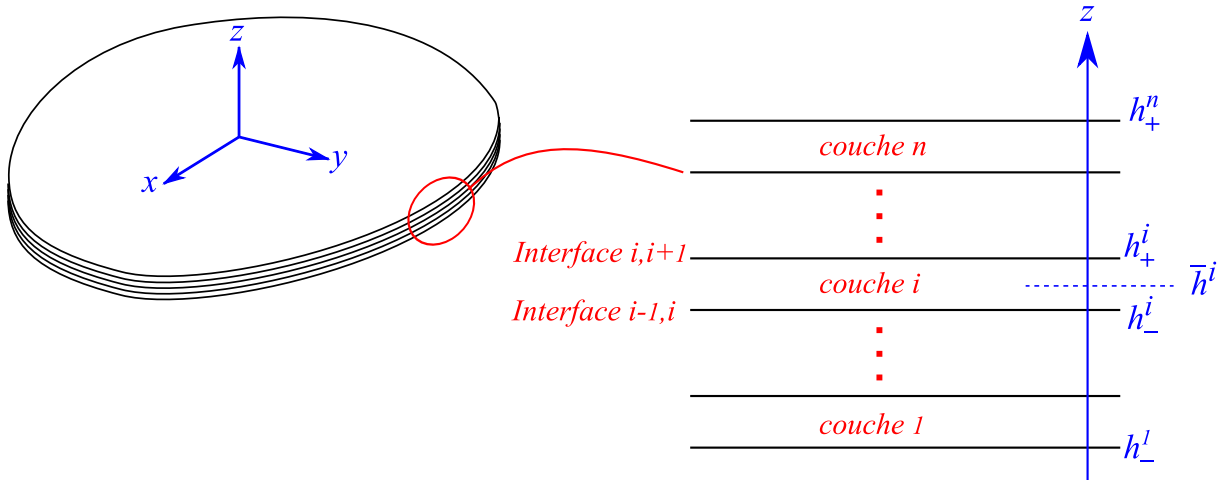


Figure 1.11: Multicouche dans le repère Cartésien - Notation du modèle LS1

Dans ce qui suit, h_-^i , h_+^i et \bar{h}^i représentent, respectivement, la cote inférieure, la cote supérieure et la cote moyenne de la couche i et $e^i = h_+^i - h_-^i$ indique l'épaisseur de cette couche. Les indices grecs $(\alpha, \beta, \gamma, \delta)$ correspondent à $\{x, y\}$ où $\{1, 2\}$ et la convention de sommation d'Einstein est en vigueur sur les indices répétés. L'exposant i avec $1 \leq i \leq n$ désigne la couche i et l'exposant $i, i + 1$ avec $1 \leq i \leq n - 1$ désigne l'interface entre les couches i et $i + 1$. Afin de faciliter la formulation du problème, nous notons les exposants $0, 1$ et $n, n + 1$, respectivement, pour la surface inférieure et la surface supérieur du multicouche .

1.A.3 Efforts généralisés

Dans le modèle LS1, chaque couche est modélisée comme une plaque de Reissner-Mindlin. Ces plaques sont couplées entre elle par des contraintes interlaminaires. En effet, le modèle LS1 est une superposition de plaques de Reissner-Mindlin connectées par des efforts d'interface. Ainsi, les contraintes 3D dans le plan $\sigma_{\alpha\beta}$ sont approchées par des fonctions polynomiales affines en z . D'après les équations d'équilibre 3D, les contraintes de cisaillement transverse $\sigma_{\alpha z}$ et la contrainte normale transverse σ_{zz} doivent être des fonctions polynomiales quadratique et cubique en z . Les coefficients de ces polynômes sont des champs en x et y . Les efforts généralisés du modèle sont choisis de façon à ce qu'ils apparaissent dans l'écriture des contraintes approchées tout en ayant une signification physique. Ils sont choisis de la manière suivante:

Pour la couche i :

- Les efforts membranaires de la couche i

$$N_{\alpha\beta}^i(x, y) = \int_{h_-^i}^{h_+^i} \sigma_{\alpha\beta}(x, y, z) dz \quad (1.66)$$

- Les moments de flexion par rapport au plan moyen de la couche i

$$M_{\alpha\beta}^i(x, y) = \int_{h_-^i}^{h_+^i} (z - \bar{h}^i) \sigma_{\alpha\beta}(x, y, z) dz \quad (1.67)$$

- Les efforts tranchants (ou efforts de cisaillement hors plan) de la couche i

$$Q_{\alpha}^i(x, y) = \int_{h_-^i}^{h_+^i} \sigma_{\alpha z}(x, y, z) dz \quad (1.68)$$

Pour l'interface $i, i + 1$:

- Les contraintes de cisaillement à l'interface $i, i + 1$

$$\tau_{\alpha}^{i,i+1}(x, y) = \sigma_{\alpha z}^i(x, y, h_+^i) = \sigma_{\alpha z}^{i+1}(x, y, h_-^{i+1}) \quad (1.69)$$

- La contrainte normale à l'interface $i, i + 1$

$$\nu^{i,i+1}(x, y) = \sigma_{zz}^i(x, y, h_+^i) = \sigma_{zz}^{i+1}(x, y, h_-^{i+1}) \quad (1.70)$$

Donc, le modèle est constitué de huit efforts généralisés $N_{xx}^i, N_{xy}^i, N_{yy}^i, M_{xx}^i, M_{xy}^i, M_{yy}^i, Q_x^i, Q_y^i$ par couche i et trois efforts d'interface $\tau_x^{i,i+1}, \tau_y^{i,i+1}, \nu^{i,i+1}$ par interface $i, i + 1$.

Pour l'expression des contraintes 3D approchées, on définit les polynômes $P_k^i(z)$ ($0 \leq k \leq 3$):

$$\begin{aligned} P_0^i(z) &= 1 \\ P_1^i(z) &= \frac{z - \bar{h}^i}{e^i} \\ P_2^i(z) &= -6 \left(\frac{z - \bar{h}^i}{e^i} \right)^2 + \frac{1}{2} \\ P_3^i(z) &= -2 \left(\frac{z - \bar{h}^i}{e^i} \right)^3 + \frac{3}{10} \left(\frac{z - \bar{h}^i}{e^i} \right) \end{aligned}$$

Ces polynômes sont reliés aux polynômes de Legendre et donc forment une base orthogonale. C'est-à-dire:

$$\int_{h_-^i}^{h_+^i} P_m^i(z) P_n^i(z) dz = 0 \quad \text{si } m \neq n$$

Cette orthogonalité simplifie l'écriture du problème. Les contraintes approchées dans la couche i s'écrivent sur la base polynomiale définie comme suit:

$$\sigma_{\alpha\beta}^i(x, y, z) = \left[\frac{1}{e^i} N_{\alpha\beta}^i(x, y) \right] P_0^i(z) + \left[\frac{12}{(e^i)^2} M_{\alpha\beta}^i(x, y) \right] P_1^i(z) \quad (1.71)$$

$$\begin{aligned} \sigma_{\alpha z}^i(x, y, z) &= \left[\frac{1}{e^i} Q_{\alpha}^i(x, y) \right] P_0^i(z) + \left[\tau_{\alpha}^{i,i+1}(x, y) - \tau_{\alpha}^{i-1,i}(x, y) \right] P_1^i(z) \\ &+ \left[\frac{1}{e^i} Q_{\alpha}^i(x, y) - \frac{1}{2} \left(\tau_{\alpha}^{i,i+1}(x, y) + \tau_{\alpha}^{i-1,i}(x, y) \right) \right] P_2^i(z) \end{aligned} \quad (1.72)$$

$$\begin{aligned} \sigma_{zz}^i(x, y, z) &= \left[\frac{\nu^{i,i+1}(x, y) + \nu^{i-1,i}(x, y)}{2} + \frac{e^i}{12} \left(\tau_{\alpha,\alpha}^{i,i+1}(x, y) - \tau_{\alpha,\alpha}^{i-1,i}(x, y) \right) \right] P_0^i(z) \\ &+ \left[-\frac{Q_{\alpha,\alpha}^i}{5} + \frac{e^i}{10} \left(\tau_{\alpha,\alpha}^{i,i+1}(x, y) + \tau_{\alpha,\alpha}^{i-1,i}(x, y) \right) + \left(\nu^{i,i+1}(x, y) - \nu^{i-1,i}(x, y) \right) \right] P_1^i(z) \\ &+ \left[\frac{e^i}{12} \left(\tau_{\alpha,\alpha}^{i,i+1}(x, y) - \tau_{\alpha,\alpha}^{i-1,i}(x, y) \right) \right] P_2^i(z) \\ &+ \left[-Q_{\alpha,\alpha}^i + \frac{e^i}{2} \left(\tau_{\alpha,\alpha}^{i,i+1}(x, y) + \tau_{\alpha,\alpha}^{i-1,i}(x, y) \right) \right] P_3^i(z) \end{aligned} \quad (1.73)$$

1.A.4 Déplacements généralisés

Afin d'éviter la complication des notations, nous n'utiliserons plus l'exposant $*$ dans la suite. En outre, nous supposons que les forces de volume \underline{f} sont négligeables. En injectant les expressions des contraintes approchées dans la fonctionnelle T_1 on obtient: ($d\Omega = d\omega dz$):

$$\begin{aligned}
 T_1 = & - \sum_{i=1}^n \int_{\omega} \left[\begin{aligned} & \left(N_{\alpha\beta,\beta}^i + \tau_{\alpha}^{i,i+1} - \tau_{\alpha}^{i-1,i} \right) \cdot U_{\alpha}^i \\ & + \left(M_{\alpha\beta,\beta}^i + \frac{e^i}{2} \left(\tau_{\alpha}^{i,i+1} + \tau_{\alpha}^{i-1,i} \right) - Q_{\alpha}^i \right) \cdot \Phi_{\alpha}^i \\ & + \left(Q_{\alpha,\alpha}^i + \nu^{i,i+1} - \nu^{i-1,i} \right) \cdot U_z^i \end{aligned} \right] d\omega \\
 & + \int_{\omega_T^+} \left[\left(\tau_{\alpha}^{n,n+1} - T_{\alpha}^+ \right) U_{\alpha}^+ + \left(\nu^{n,n+1} - T_z^+ \right) U_z^+ \right] d\omega - \int_{\omega_T^-} \left[\left(\tau_{\alpha}^{0,1} + T_{\alpha}^- \right) U_{\alpha}^- + \left(\nu^{0,1} + T_z^- \right) U_z^- \right] d\omega \\
 & + \sum_{i=1}^n \int_{\partial\omega_T} \left[\begin{aligned} & \left(N_{\alpha\beta}^i n_{\beta} \right) U_{\alpha}^i + \left(M_{\alpha\beta}^i n_{\beta} \right) \Phi_{\alpha}^i + \left(Q_{\alpha}^i n_{\alpha} \right) U_z^i + \\ & e^i \left(\tau_{\alpha}^{i,i+1} - \tau_{\alpha}^{i-1,i} \right) n_{\alpha} \bar{U}_z^i + \left(Q_{\alpha}^i - \frac{e^i}{2} \left(\tau_{\alpha}^{i,i+1} + \tau_{\alpha}^{i-1,i} \right) \right) n_{\alpha} \hat{U}_z^i - \int_{h_-^i}^{h_+^i} \underline{T}^d \cdot \underline{U} dz \end{aligned} \right] ds
 \end{aligned} \tag{1.74}$$

où U_k^+ et U_k^- avec $k \in \{x, y, z\}$ sont les déplacements tridimensionnels respectivement aux surfaces supérieure et inférieure du multicouche. Ainsi, T_k^+ et T_k^- sont les composantes des vecteurs contrainte imposés respectivement sur les surfaces supérieure et inférieure du multicouche. Dans l'équation 1.74 on a introduit les notations suivantes ($\alpha \in \{x, y\}$):

- Les déplacements membranaires de la couche i :

$$U_{\alpha}^i(x, y) = \frac{1}{e^i} \int_{h_-^i}^{h_+^i} F_0^i(z) U_{\alpha}(x, y, z) dz \tag{1.75}$$

- Les rotations de la couche i :

$$\Phi_{\alpha}^i(x, y) = \frac{12}{(e^i)^2} \int_{h_-^i}^{h_+^i} F_1^i(z) U_{\alpha}(x, y, z) dz \tag{1.76}$$

- Le déplacement normal de la couche i :

$$U_z^i(x, y) = \frac{1}{e^i} \int_{h_-^i}^{h_+^i} F_0^i(z) U_z(x, y, z) dz \tag{1.77}$$

- Premier moment du déplacement normal de la couche i :

$$\bar{U}_z^i(x, y) = \frac{1}{e^i} \int_{h_-^i}^{h_+^i} F_1^i(z) U_z(x, y, z) dz \tag{1.78}$$

- Deuxième moment du déplacement normal de la couche i :

$$\widehat{U}_z^i(x, y) = \frac{1}{e^i} \int_{h_-^i}^{h_+^i} P_2^i(z) U_z(x, y, z) dz \quad (1.79)$$

La contribution des déplacements tridimensionnels sur ω est contenue dans les champs suivants:

$$U_x^i(x, y), U_y^i(x, y), \Phi_x^i(x, y), \Phi_y^i(x, y), U_z^i(x, y) \quad (1.80)$$

Ces cinq champs sont considérés comme les déplacements généralisés du modèle LS1.

1.A.5 Déformations généralisées

Afin de trouver les expressions des déformations généralisées du modèle, nous essayons de trouver les variables conjuguées des efforts généralisés du modèle dans l'expression de l'énergie de déformation dans le cœur du multicouche. En faisant une intégration par parties sur les termes de divergence dans l'équation 1.74, on trouve:

$$\begin{aligned} T_1 = & \sum_{i=1}^n \int_{\omega} \left[N_{\alpha\beta}^i \varepsilon_{\alpha\beta}^i + M_{\alpha\beta}^i \chi_{\alpha\beta}^i + Q_{\alpha}^i d_{\Phi_{\alpha}}^i \right] d\omega + \sum_{i=1}^{n-1} \int_{\omega} \left[\tau_{\alpha}^{i,i+1} D_{\alpha}^{i,i+1} + \nu^{i,i+1} D_z^{i,i+1} \right] d\omega \\ & + \int_{\partial\omega} \dots ds + \int_{\omega^+} \dots d\omega + \int_{\omega^-} \dots d\omega \end{aligned} \quad (1.81)$$

avec les notations suivantes:

- Les déformations membranaires de la couches i :

$$\varepsilon_{\alpha\beta}^i(x, y) = \frac{1}{2} \left(U_{\alpha,\beta}^i(x, y) + U_{\beta,\alpha}^i(x, y) \right) \quad (1.82)$$

- Les courbures de la couches i :

$$\chi_{\alpha\beta}^i(x, y) = \frac{1}{2} \left(\Phi_{\alpha,\beta}^i(x, y) + \Phi_{\beta,\alpha}^i(x, y) \right) \quad (1.83)$$

- Les déformations de cisaillement hors plan de la couches i :

$$d_{\Phi_{\alpha}}^i(x, y) = \Phi_{\alpha}^i(x, y) + U_{z,\alpha}^i(x, y) \quad (1.84)$$

- Les déplacements relatifs de cisaillement à l'interface $i, i + 1$:

$$D_{\alpha}^{i,i+1}(x, y) = U_{\alpha}^{i+1}(x, y) - U_{\alpha}^i(x, y) - \frac{1}{2} \left(e^i \Phi_{\alpha}^i(x, y) + e^{i+1} \Phi_{\alpha}^{i+1}(x, y) \right) \quad (1.85)$$

- Le déplacement relatif normal à l'interface $i, i + 1$:

$$D_z^{i,i+1}(x, y) = U_z^{i+1}(x, y) - U_z^i(x, y) \quad (1.86)$$

Ces champs sont considérés comme déformations généralisées du modèle LS1. Ainsi, la dualité énergétique entre les efforts généralisés et les déformations généralisées du modèle est déduite comme suit:

- Pour la couche i ($1 \leq i \leq n$)

$$\varepsilon_{\alpha\beta}^i(x, y) \longleftrightarrow N_{\alpha\beta}^i(x, y) \quad , \quad \chi_{\alpha\beta}^i(x, y) \longleftrightarrow M_{\alpha\beta}^i(x, y) \quad , \quad d_{\Phi_\alpha}^i(x, y) \longleftrightarrow Q_\alpha^i(x, y) \quad (1.87)$$

- Pour l'interface $i, i+1$ ($1 \leq i \leq n-1$)

$$D_\alpha^{i,i+1}(x, y) \longleftrightarrow \tau_\alpha^{i,i+1}(x, y) \quad , \quad D_z^{i,i+1}(x, y) \longleftrightarrow \nu^{i,i+1}(x, y) \quad (1.88)$$

1.A.6 Équations d'équilibre

Pour trouver les équations d'équilibre du modèle, on applique le théorème de Reissner. La stationnarité de la fonctionnelle T_1 (l'équation 1.74) par rapport à une variation quelconque des déplacements généralisés sur ω donne les $5n$ équations d'équilibre suivantes:

$$N_{\alpha\beta,\beta}^i(x, y) + \tau_\alpha^{i,i+1}(x, y) - \tau_\alpha^{i-1,i}(x, y) = 0 \quad (1.89)$$

$$M_{\alpha\beta,\beta}^i(x, y) + \frac{e^i}{2} \left(\tau_\alpha^{i,i+1}(x, y) + \tau_\alpha^{i-1,i}(x, y) \right) - Q_\alpha^i(x, y) = 0 \quad (1.90)$$

$$Q_{\alpha,\alpha}^i(x, y) + \nu^{i,i+1}(x, y) - \nu^{i-1,i}(x, y) = 0 \quad (1.91)$$

On constate que les équations d'équilibre du modèle sont celles de la plaque de Reissner-Mindlin par couche. Il faut remarquer que ces équations sont cohérentes avec les équations d'équilibre tridimensionnelles. En effet, les équations d'équilibre 1.89 à 1.91 sont satisfaites si et seulement si $\underline{\text{div}} \underline{\sigma}^i(x, y, z) = \underline{0}$ où $\underline{\sigma}^i(x, y, z)$ est le tenseur des contraintes 3D approchées définies dans les équations 1.71 to 1.73.

1.A.7 Conditions aux limites

1.A.7.1 Conditions aux limites en contrainte

La stationnarité de la fonctionnelle T_1 (l'équation 1.74) par rapport à une variation quelconque du champ de déplacement sur ω_T^+ et ω_T^- donne les conditions aux limites en contrainte sur la face supérieure et la face inférieure du multicouche:

$$\tau_\alpha^{0,1}(x, y) = -T_\alpha^-(x, y) \quad , \quad \nu^{0,1}(x, y) = -T_z^-(x, y) \quad (1.92)$$

$$\tau_\alpha^{n,n+1}(x, y) = T_\alpha^+(x, y) \quad , \quad \nu^{n,n+1}(x, y) = T_z^+(x, y) \quad (1.93)$$

Pour pouvoir développer le terme de bord $\partial\omega$ dans l'équation 1.74, on écrit le champ \underline{U} sous la forme suivante ($h_-^i \leq z \leq h_+^i$):

$$U_\alpha(x, y, z) = P_0^i(z) U_\alpha^i(x, y) + e^i P_1^i(z) \Phi_\alpha^i(x, y) + \Delta U_\alpha^i(x, y, z) \quad (1.94)$$

$$U_z(x, y, z) = P_0^i(z) U_\alpha^i(x, y) + \Delta U_z^i(x, y, z) \quad (1.95)$$

D'après les expressions des déplacements généralisés du modèle (équations 1.75 à 1.77), $\Delta U_\alpha^i(x, y, z)$ est orthogonal à $P_0^i(z)$ et $P_1^i(z)$ ainsi que $\Delta U_z^i(x, y, z)$ est orthogonal à $P_0^i(z)$. Les champs \bar{U}_z^i et \widehat{U}_z^i selon les équations 1.78 et 1.79 s'écrivent comme suit:

$$\bar{U}_z^i(x, y) = \frac{1}{e^i} \int_{h_-^i}^{h_+^i} P_1^i(z) \Delta U_z(x, y, z) dz \quad (1.96)$$

$$\widehat{U}_z^i(x, y) = \frac{1}{e^i} \int_{h_-^i}^{h_+^i} P_2^i(z) \Delta U_z(x, y, z) dz \quad (1.97)$$

On constate que les champs \bar{U}_z^i et \widehat{U}_z^i sont liés à la perturbation $\Delta U_z(x, y, z)$. Maintenant, en injectant les équations ci-dessus dans l'équation 1.74, la fonctionnelle T_1 s'écrit:

$$T_1 = \int_\omega \dots + \int_{\omega_T^+} \dots + \int_{\omega_T^-} \dots + \sum_{i=1}^n \int_{\partial\omega_T} \left[\begin{aligned} & \left(N_{\alpha\beta}^i n_\beta - [N_\alpha^i]^d \right) U_\alpha^i + \left(M_{\alpha\beta}^i n_\beta - [M_\alpha^i]^d \right) \Phi_\alpha^i + \left(Q_\alpha^i n_\alpha - [Q^i]^d \right) U_z^i \\ & - \int_{h_-^i}^{h_+^i} \left(T_\alpha^d \Delta U_\alpha + T_z^d \Delta U_z \right) dz + \left(\tau_\alpha^{i,i+1} - \tau_\alpha^{i-1,i} \right) n_\alpha \int_{h_-^i}^{h_+^i} P_1^i(z) \Delta U_z dz \\ & + \left(Q_\alpha^i - \frac{e^i}{2} \left(\tau_\alpha^{i,i+1} + \tau_\alpha^{i-1,i} \right) \right) n_\alpha \frac{1}{e^i} \int_{h_-^i}^{h_+^i} P_2^i(z) \Delta U_z dz \end{aligned} \right] ds \quad (1.98)$$

avec:

$$[N_\alpha^i(x_0, y_0)]^d = \int_{h_-^i}^{h_+^i} P_0^i(z) T_\alpha^i(x_0, y_0, z) dz$$

$$[M_\alpha^i(x_0, y_0)]^d = \int_{h_-^i}^{h_+^i} e^i P_1^i(z) T_\alpha^i(x_0, y_0, z) dz$$

$$[Q^i(x_0, y_0)]^d = \int_{h_-^i}^{h_+^i} P_0^i(z) T_z^i(x_0, y_0, z) dz$$

où (x_0, y_0) est un point sur le bord latéral $\partial\omega_T$ du multicouche et T_k^i pour $k \in \{x, y, z\}$ signifie le vecteur contrainte imposé au bord au niveau la couche i ($h_-^i \leq z \leq h_+^i$).

Hypothèse 1: On suppose que la contribution des termes de perturbation $\Delta U_\alpha^i(x, y, z)$ et $\Delta U_z^i(x, y, z)$ dans les termes de bord est négligeable devant celle des déplacements généralisés.

Les conditions aux limites en contrainte sur $\partial\omega$ s'obtiennent grâce à la stationnarité de la fonctionnelle T_1 (l'équation 1.98) par rapport à une variation quelconque des déplacements généralisés ($1 \leq i \leq n$):

$$\begin{aligned} N_{\alpha\beta}^i(x_0, y_0) n_\beta &= [N_\alpha^i(x_0, y_0)]^d \\ M_{\alpha\beta}^i(x_0, y_0) n_\beta &= [M_\alpha^i(x_0, y_0)]^d \\ Q_\alpha^i(x_0, y_0) n_\alpha &= [Q^i(x_0, y_0)]^d \end{aligned} \tag{1.99}$$

1.A.7.2 Conditions aux limites en déplacement

Les conditions aux limites en déplacement sont déduites de la stationnarité de la fonctionnelle H.R (et donc T_2) par rapport à une variation du champ de contrainte. En injectant les expressions des contraintes 3D approchées (1.71 à 1.73) dans l'équation 1.65 et en adoptant l'hypothèse 1 on arrive à:

$$\begin{aligned} T_2 = & - \int_{\Omega} \frac{1}{2} \underline{\underline{\sigma}}(\underline{x}) : \underline{\underline{S}}(\underline{x}) : \underline{\underline{\sigma}}(\underline{x}) d\Omega - \sum_{i=1}^n \int_{\omega} \left[\begin{aligned} & \left(N_{\alpha\beta,\beta}^i + \tau_\alpha^{i,i+1} - \tau_\alpha^{i-1,i} \right) \cdot U_\alpha^i \\ & + \left(M_{\alpha\beta,\beta}^i + \frac{e^i}{2} (\tau_\alpha^{i,i+1} + \tau_\alpha^{i-1,i}) - Q_\alpha^i \right) \cdot \Phi_\alpha^i \\ & + \left(Q_{\alpha,\alpha}^i + \nu^{i,i+1} - \nu^{i-1,i} \right) \cdot U_z^i \end{aligned} \right] d\omega \\ & + \int_{\omega_T^+} \left[\tau_\alpha^{n,n+1} \left(U_\alpha^n + \frac{e^n}{2} \Phi_\alpha^n \right) + \nu^{n,n+1} U_z^n \right] d\omega - \int_{\omega_T^-} \left[\tau_\alpha^{0,1} \left(U_\alpha^1 - \frac{e^1}{2} \Phi_\alpha^1 \right) + \nu^{0,1} U_z^1 \right] d\omega \\ & + \sum_{i=1}^n \int_{\partial\omega_T} \left[\left(N_{\alpha\beta}^i n_\beta \right) U_\alpha^i + \left(M_{\alpha\beta}^i n_\beta \right) \Phi_\alpha^i + \left(Q_\alpha^i n_\alpha \right) U_z^i \right] ds \\ & + \int_{\omega_U^+} \left[\tau_\alpha^{n,n+1} [U_\alpha^+]^d + \nu^{n,n+1} [U_z^+]^d \right] d\omega - \int_{\omega_U^-} \left[\tau_\alpha^{0,1} [U_\alpha^-]^d + \nu^{0,1} [U_z^-]^d \right] d\omega \\ & + \sum_{i=1}^n \int_{\partial\omega_U} \left[\left(N_{\alpha\beta}^i n_\beta \right) [U_\alpha^i]^d + \left(M_{\alpha\beta}^i n_\beta \right) [\Phi_\alpha^i]^d + \left(Q_\alpha^i n_\alpha \right) [U_z^i]^d \right] ds \end{aligned} \tag{1.100}$$

En faisant une intégration par parties sur les divergences, cette équation devient:

$$\begin{aligned}
T_2 = & - \int_{\Omega} \frac{1}{2} \underline{\underline{\underline{\sigma}}}(\underline{x}) : \underline{\underline{\underline{S}}}(\underline{x}) : \underline{\underline{\underline{\sigma}}}(\underline{x}) d\Omega \\
& + \sum_{i=1}^n \int_{\omega} \left[N_{\alpha\beta}^i \varepsilon_{\alpha\beta}^i + M_{\alpha\beta}^i \chi_{\alpha\beta}^i + Q_{\alpha}^i d_{\Phi_{\alpha}}^i \right] d\omega + \sum_{i=1}^{n-1} \int_{\omega} \left[\tau_{\alpha}^{i,i+1} D_{\alpha}^{i,i+1} + \nu^{i,i+1} D_z^{i,i+1} \right] d\omega \\
& + \int_{\omega_U^+} \left[\tau_{\alpha}^{n,n+1} \left([U_{\alpha}^+]^d - U_{\alpha}^n - \frac{e^n}{2} \Phi_{\alpha}^n \right) + \nu^{n,n+1} \left([U_z^+]^d - U_z^n \right) \right] d\omega \\
& - \int_{\omega_U^-} \left[\tau_{\alpha}^{0,1} \left([U_{\alpha}^-]^d - U_{\alpha}^1 + \frac{e^1}{2} \Phi_{\alpha}^1 \right) + \nu^{0,1} \left([U_z^-]^d - U_z^1 \right) \right] d\omega \\
& + \sum_{i=1}^n \int_{\partial\omega_U} \left[\left(N_{\alpha\beta}^i n_{\beta} \right) \left([U_{\alpha}^i]^d - U_{\alpha}^i \right) + \left(M_{\alpha\beta}^i n_{\beta} \right) \left([\Phi_{\alpha}^i]^d - \Phi_{\alpha}^i \right) + \left(Q_{\alpha}^i n_{\alpha} \right) \left([U_z^i]^d - U_z^i \right) \right] ds
\end{aligned} \tag{1.101}$$

La stationnarité de cette fonctionnelle par rapport aux efforts généralisés sur les bords donne les conditions aux limites en déplacement. Ainsi, ces conditions s'obtiennent comme suit:

- sur la face supérieure du multicouche ω_U^+ :

$$U_{\alpha}^n(x, y) + \frac{e^n}{2} \Phi_{\alpha}^n(x, y) = [U_{\alpha}^+]^d(x, y) \quad , \quad U_z^n(x, y) = [U_z^+]^d(x, y) \tag{1.102}$$

- sur la face inférieure du multicouche ω_U^- :

$$U_{\alpha}^1(x, y) - \frac{e^1}{2} \Phi_{\alpha}^1(x, y) = [U_{\alpha}^-]^d(x, y) \quad , \quad U_z^1(x, y) = [U_z^-]^d(x, y) \tag{1.103}$$

- sur le bord latéral du multicouche $\partial\omega_U$ pour $1 \leq i \leq n$:

$$U_{\alpha}^i(x_0, y_0) = [U_{\alpha}^i]^d(x_0, y_0) \tag{1.104}$$

$$\Phi_{\alpha}^i(x_0, y_0) = [\Phi_{\alpha}^i]^d(x_0, y_0) \tag{1.105}$$

$$U_z^i(x_0, y_0) = [U_z^i]^d(x_0, y_0) \tag{1.106}$$

1.A.8 Relations de comportement

Les relations de comportement du modèle s'obtiennent en calculant la stationnarité de la fonctionnelle T_2 par rapport à une variation des efforts généralisés sur ω . De

ce faire, il faut développer la première intégrale dans l'équation 1.101 qui est, en fait, l'expression de l'énergie élastique en contrainte. Le tenseur d'ordre quatre $\underline{\underline{S}}$ est le tenseur de souplesse qui est constant dans chaque couche. On note $\underline{\underline{S}}^i = S_{mnop}^i$ (avec $m, n, o, p \in \{1, 2, 3\}$) le tenseur de souplesse de la couche i . Dans le cadre de cette étude, on ne considère que des matériaux orthotropes. On suppose que l'axe $z = \underline{e}_3$ est l'axe normal d'orthotropie et donc, les composantes du tenseur de souplesse contenant un nombre impair d'indice 3 sont nulles. Les composantes non nulles du tenseur de souplesse sont notées comme suit:

$$\left(\underline{\underline{\tilde{S}}^i}\right)_{\alpha\beta\gamma\delta} = S_{\alpha\beta\gamma\delta}^i, \quad \left(\underline{\underline{\tilde{S}}_Q^i}\right)_{\alpha\beta} = 4S_{\alpha 3\beta 3}^i, \quad \left(\underline{\underline{\tilde{S}}_3^i}\right)_{\alpha\beta} = 2S_{\alpha\beta 33}^i, \quad \left(S_\nu^i\right) = S_{3333}^i$$

$\underline{\underline{\tilde{S}}^i}$ est un tenseur d'ordre quatre de souplesse lié aux contraintes membranaires. $\underline{\underline{\tilde{S}}_Q^i}$ et $\underline{\underline{\tilde{S}}_3^i}$ sont des tenseurs d'ordre deux de souplesse correspondant, respectivement, au cisaillement hors plan et au couplage entre les contraintes membranaires et d'arrachement. En fin, le scalaire S_ν^i représente la souplesse liée à la contrainte d'arrachement.

Maintenant, on peut décomposer l'énergie élastique sous la forme suivante:

$$W^{3D} = \frac{1}{2} \int_{\Omega} \underline{\underline{\sigma}}(\underline{x}) : \underline{\underline{S}}(\underline{x}) : \underline{\underline{\sigma}}(\underline{x}) d\Omega = \sum_{i=1}^n \int_{\omega} [w_c^i + w_Q^i + w_\nu^i + w_3^i] d\omega \quad (1.107)$$

où:

- w_c^i est l'énergie élastique des contraintes membranaires de la couche i :

$$w_c^i = \frac{1}{2} \int_{h_-^i}^{h_+^i} \sigma_{\alpha\beta}^i S_{\alpha\beta\gamma\delta}^i \sigma_{\gamma\delta}^i dz \quad (1.108)$$

- w_Q^i est l'énergie élastique du cisaillement hors plan de la couche i :

$$w_Q^i = \frac{1}{2} \int_{h_-^i}^{h_+^i} \sigma_{\alpha 3}^i S_{Q\alpha\beta}^i \sigma_{\beta 3}^i dz \quad (1.109)$$

- w_ν^i est l'énergie élastique de la contrainte normale transverse de la couche i :

$$w_\nu^i = \frac{1}{2} \int_{h_-^i}^{h_+^i} \sigma_{33}^i S_\nu^i \sigma_{33}^i dz \quad (1.110)$$

- w_3^i est l'énergie élastique de couplage entre les contraintes membranaires et la contrainte normale transverse de la couche i :

$$w_3^i = \frac{1}{2} \int_{h_-^i}^{h_+^i} \sigma_{\alpha\beta}^i (S_3^i)_{\alpha\beta} \sigma_{33}^i dz \quad (1.111)$$

Hypothèse 2: *On néglige l'énergie w_3^i liée au couplage entre les contraintes membranaires et la contrainte normale transverse. Cette hypothèse revient à négliger les effets de Poisson dus au pincement des couches qui est une hypothèse habituelle dans la plupart des théories des plaques.*

Grâce à l'orthogonalité des polynômes P_k^i , on peut facilement calculer les énergies mentionnées ci-avant. En injectant les expressions des contraintes 3D approchées (1.71 à 1.73) dans les équations précédentes on obtient:

$$w_c^i = \frac{1}{2} S_{\alpha\beta\gamma\delta}^i \left[\frac{1}{e^i} N_{\alpha\beta}^i N_{\gamma\delta}^i + \frac{12}{(e^i)^3} M_{\alpha\beta}^i M_{\gamma\delta}^i \right] \quad (1.112)$$

$$w_Q^i = \frac{1}{2} S_{Q\alpha\beta}^i \left[\begin{aligned} & \frac{1}{e^i} Q_\alpha^i Q_\beta^i + \frac{e^i}{12} (\tau_\alpha^{i,i+1} - \tau_\alpha^{i-1,i}) (\tau_\beta^{i,i+1} - \tau_\beta^{i-1,i}) \\ & + \frac{1}{5e^i} \left(Q_\alpha^i - \frac{e^i}{2} (\tau_\alpha^{i,i+1} + \tau_\alpha^{i-1,i}) \right) \left(Q_\beta^i - \frac{e^i}{2} (\tau_\beta^{i,i+1} + \tau_\beta^{i-1,i}) \right) \end{aligned} \right] \quad (1.113)$$

$$w_\nu^i = \frac{1}{2} S_\nu^i \left[\begin{aligned} & e^i \left[\frac{\nu^{i,i+1} + \nu^{i-1,i}}{2} + \frac{e^i}{12} (\tau_{\alpha,\alpha}^{i,i+1} - \tau_{\alpha,\alpha}^{i-1,i}) \right]^2 \\ & + \frac{e^i}{12} \left[\frac{6}{5} (\nu^{i,i+1} - \nu^{i-1,i}) + \frac{e^i}{10} (\tau_{\alpha,\alpha}^{i,i+1} + \tau_{\alpha,\alpha}^{i-1,i}) \right]^2 \\ & + \frac{e^i}{5} \left[\frac{e^i}{12} (\tau_{\alpha,\alpha}^{i,i+1} - \tau_{\alpha,\alpha}^{i-1,i}) \right]^2 \\ & + \frac{e^i}{700} \left[\nu^{i,i+1} - \nu^{i-1,i} + \frac{e^i}{2} (\tau_{\alpha,\alpha}^{i,i+1} + \tau_{\alpha,\alpha}^{i-1,i}) \right]^2 \end{aligned} \right] \quad (1.114)$$

Dans le calcul de w_ν^i on a remplacé $Q_{\alpha,\alpha}$ par $\nu^{i-1,i} - \nu^{i,i+1}$ d'après l'équation de l'équilibre 1.91.

Hypothèse 3: *Dans l'énergie w_ν^i , on néglige les termes en $\tau_{\alpha,\alpha}^{i,i+1} = \text{div } \tilde{\tau}^{i,i+1}$ car ils sont multipliés par $(e^i)^2$ et $(e^i)^3$ et donc, leur contribution à l'énergie est probablement faible.*

D'après cette hypothèse w_ν^i devient:

$$w_\nu^i = \frac{1}{2} S_\nu^i e^i \left[\frac{13}{35} \left((\nu^{i,i+1})^2 + (\nu^{i-1,i})^2 \right) + \frac{9}{35} \nu^{i-1,i} \nu^{i,i+1} \right] \quad (1.115)$$

En utilisant les expressions obtenues pour l'énergie élastique, la fonctionnelle T_2 prend la forme suivante:

$$\begin{aligned}
 T_2 = & \sum_{i=1}^n \int_{\omega} \left[N_{\alpha\beta}^i \varepsilon_{\alpha\beta}^i + M_{\alpha\beta}^i \chi_{\alpha\beta}^i + Q_{\alpha}^i d_{\Phi_{\alpha}}^i \right] d\omega + \sum_{i=1}^{n-1} \int_{\omega} \left[\tau_{\alpha}^{i,i+1} D_{\alpha}^{i,i+1} + \nu^{i,i+1} D_z^{i,i+1} \right] d\omega \\
 & - \frac{1}{2} \sum_{i=1}^n \int_{\omega} S_{\alpha\beta\gamma\delta}^i \left[\frac{1}{e^i} N_{\alpha\beta}^i N_{\gamma\delta}^i + \frac{12}{(e^i)^3} M_{\alpha\beta}^i M_{\gamma\delta}^i \right] d\omega \\
 & - \frac{1}{2} \sum_{i=1}^n \int_{\omega} S_{Q_{\alpha\beta}}^i \left[\begin{aligned} & \frac{1}{e^i} Q_{\alpha}^i Q_{\beta}^i + \frac{e^i}{12} (\tau_{\alpha}^{i,i+1} - \tau_{\alpha}^{i-1,i}) (\tau_{\beta}^{i,i+1} - \tau_{\beta}^{i-1,i}) \\ & + \frac{1}{5e^i} \left(Q_{\alpha}^i - \frac{e^i}{2} (\tau_{\alpha}^{i,i+1} + \tau_{\alpha}^{i-1,i}) \right) \left(Q_{\beta}^i - \frac{e^i}{2} (\tau_{\beta}^{i,i+1} + \tau_{\beta}^{i-1,i}) \right) \end{aligned} \right] d\omega \\
 & - \frac{1}{2} \sum_{i=1}^n \int_{\omega} S_{\nu}^i e^i \left[\frac{13}{35} \left((\nu^{i-1,i})^2 + (\nu^{i,i+1})^2 \right) + \frac{9}{35} \nu^{i-1,i} \nu^{i,i+1} \right] d\omega \\
 & + \int_{\omega_{\bar{U}}^+} \dots + \int_{\omega_{\bar{U}}^-} \dots + \int_{\partial\omega_U} \dots
 \end{aligned} \tag{1.116}$$

La stationnarité de la fonctionnelle T_2 sur ω conduit aux équations de comportement du modèle reliant les déformations généralisées aux efforts généralisés comme suit:

- Comportement de la couche i pour $1 \leq i \leq n$

- Loi de comportement des efforts membranaires:

$$\varepsilon_{\alpha\beta}^i = \frac{1}{e^i} S_{\alpha\beta\gamma\delta}^i N_{\alpha\beta}^i \tag{1.117}$$

- Loi de comportement des moments de flexion:

$$\chi_{\alpha\beta}^i = \frac{12}{(e^i)^3} S_{\alpha\beta\gamma\delta}^i M_{\alpha\beta}^i \tag{1.118}$$

- Loi de comportement des efforts de cisaillement hors plan de la couche:

$$d_{\Phi_{\alpha}}^i = \frac{6}{5e^i} S_{Q_{\alpha\beta}}^i Q_{\beta}^i - \frac{1}{10} S_{Q_{\alpha\beta}}^i (\tau_{\beta}^{i-1,i} + \tau_{\beta}^{i,i+1}) \tag{1.119}$$

- Comportement à l'interface $i, i + 1$ pour $1 \leq i \leq n - 1$

- Loi de comportement des contraintes de cisaillement:

$$D_{\alpha}^{i,i+1} = -\frac{1}{10} \left(S_{Q_{\alpha\beta}}^i Q_{\beta}^i + S_{Q_{\alpha\beta}}^{i+1} Q_{\beta}^{i+1} \right) - \frac{1}{30} \left(e^i S_{Q_{\alpha\beta}}^i \tau_{\beta}^{i-1,i} + e^{i+1} S_{Q_{\alpha\beta}}^{i+1} \tau_{\beta}^{i+1,i+2} \right) + \frac{2}{15} \left(e^i S_{Q_{\alpha\beta}}^i + e^{i+1} S_{Q_{\alpha\beta}}^{i+1} \right) \tau_{\beta}^{i,i+1} \quad (1.120)$$

- Loi de comportement des contraintes d'arrachement:

$$D_z^{i,i+1} = \frac{9}{70} \left(e^i S_{\nu}^i \nu^{i-1,i} + e^{i+1} S_{\nu}^{i+1} \nu^{i+1,i+2} \right) + \frac{13}{35} \left(e^i S_{\nu}^i + e^{i+1} S_{\nu}^{i+1} \right) \nu^{i,i+1} \quad (1.121)$$

Finalement, l'énergie élastique en terms des efforts généralisés et déformations généralisées du modèle peut s'écrire comm suit:

$$W^{LS1} = \frac{1}{2} \sum_{i=1}^n \int_{\omega} \left[N_{\alpha\beta}^i \varepsilon_{\alpha\beta}^i + M_{\alpha\beta}^i \chi_{\alpha\beta}^i + Q_{\alpha}^i d_{\Phi_{\alpha}}^i \right] d\omega + \frac{1}{2} \sum_{i=1}^{n-1} \int_{\omega} \left[\tau_{\alpha}^{i,i+1} D_{\alpha}^{i,i+1} + \nu^{i,i+1} D_z^{i,i+1} \right] d\omega \quad (1.122)$$

Chapter 2

Delaminated multilayered plates under uniaxial extension. Part I: Analytical analysis using a layerwise stress approach

Comme expliqué dans le chapitre 1, parmi les travaux qui ont été effectués sur le modèle LS1 ($M4 - 5n$), il n'y a pas beaucoup d'études sur l'analyse du délaminage. [Diaz Diaz \[2001\]](#) a étudié le délaminage dans des plaques composites mais ses travaux sont limités au cas des multicouches symétriques avec quatre fissures symétriques dans la section de la plaque. Ainsi, le problème étudié revient à l'étude d'un quart de la section avec une seule interface fissurée et le système d'équations obtenu est résolu numériquement. Dans ce chapitre, nous proposons une méthode systématique pour étudier le problème du multi-délaminage dans des plaques multicouches invariants dans le sens longitudinal symétriques ou non-symétriques. La méthode proposée permet d'analyser une configuration quelconque du délaminage (plusieurs interfaces délaminées avec des longueurs différentes) dans la section du multicouche. Le système d'équations obtenu est résolu analytiquement par la méthode de décomposition en vecteurs propres sachant que le multi-délaminage fait qu'il y a, en général, des valeurs propres nulles, répétitives, et complexes.

Ce chapitre est la première partie d'un article en deux parties publié dans la revue "International Journal of Solids and Structures" sous la référence [Saeedi et al. \[2012a\]](#).

Contents

2.1	Introduction	77
2.2	The LS1 model	79
2.2.1	Generalized stresses and 3D stress field	80
2.2.2	Generalized displacements and generalized strains	80
2.2.3	Constitutive and equilibrium equations	81
2.2.4	Boundary conditions	82
2.3	Analysis of non-delaminated multilayered plate	83
2.3.1	Problem description	83
2.3.2	LS1 problem formulation	83
2.4	Analysis of delaminated multilayered plate	86
2.4.1	Laminate with one interfacial crack	86
2.4.2	Laminate with several interfacial cracks	88
2.5	Finite element validation	89
2.5.1	Interlaminar stress distributions	91
2.5.2	3D-stress distributions at layers	91
2.5.2.1	Stress distributions at the middle plane of the layers	91
2.5.2.2	Stress distributions through the thickness	92
2.6	Conclusion	93
Appendix 2.A	Expression of the 3D stress field	100
Appendix 2.B	Analytical solution of non-delaminated multi-layered plate	101
Appendix 2.C	Analytical solution of delaminated multilayered plate - a single interfacial crack	104
Appendix 2.D	Analytical solution of delaminated multilayered plate - several interfacial cracks	105

Abstract

The aim of this two-part paper is to propose an efficient and accurate alternative to the computationally expensive three-dimensional finite element method (3D-FEM), for analyzing delaminated multilayered plates under uniaxial extension. Many of the existing models deal with the analysis of multilayered structures only in the non-delaminated state. The first part of the present study extends the application of a layerwise stress model, called the *LS1* model, to delaminated multilayered plates subjected to uniaxial extension. The analytical LS1 solutions are derived for general non-delaminated and delaminated multilayers and compared to 3D finite element solutions. The comparison gives a good agreement between the LS1 and 3D-FE models except near singularities (free edges, crack tips,...). In order to overcome this drawback, a refinement approach, called the *refined LS1*, is presented in Part II and applied to angle-ply rectangular composite laminates. The comparison between the refined LS1 and 3D-FE models reveals an excellent agreement, even in the vicinity of singularities, in terms of interlaminar stresses and strain energy release rate. The main conclusion of the second part is that the proposed refined LS1 model can be used as an accurate and very efficient model for evaluating the interfacial stress fields as well as the strain energy release rate in multi-delamination problems.

keyword: Multilayer; Layerwise model; Delamination; Interlaminar stresses

2.1 Introduction

Delamination is one of the most common failure modes in multilayered structures and especially in composite laminates. The delamination phenomenon can be induced by various factors such as stress concentration at free edges, poor adhesion of layers, object impacts, global or local buckling of layers, etc. This failure mode can cause stiffness reduction and strength degradation, which may lead to total failure of the structure. As a consequence, the analysis of delamination becomes quite essential for multilayered structures.

Various viewpoints are considered for the modeling of delaminated structures. Some investigations are based on damage mechanics using the imperfect interface and cohesive zone approaches for modeling the delamination [Allix and Ladevèze 1992, Allix et al. 1998, Greco et al. 2002, Borg et al. 2002, Harper and Hallett 2008, Qiu et al. 2001]. In these approaches, which are particularly efficient for the delamination nucleation, the delamination is represented as total damage of the imperfect interface. Some others approaches use fracture mechanics considering delamination as the propagation of a crack between two adjacent layers of the delaminated interface [Davidson 1990, Larsson 1991, Nilsson 1993, Ousset 1999]. The virtual crack closure, the virtual crack extension and the J-integral techniques are used for the simulation of delamination especially with finite element method.

Many methods have been proposed to predict the delamination in multilayered structures. However, because of the complexity of the stress fields in the vicinity of free edges and crack tips, there is always a need for an effective and accurate approach

for evaluating the initiation and the propagation of delamination in multilayered structures. The nucleation of delamination and its growth is a complicated process so that the problem is 3D in nature. Several 3D approaches have been proposed in the literature for the modeling of the delamination. In finite element models, in order to capture accurately the stress concentration, a large number of elements should be considered through the thickness of laminate in the vicinity of free edges and crack tips. Thus, the finite element model may become very large and computationally expensive which is not attractive to designers of composite structures. Consequently, efficient 1D or 2D methods are needed for the analysis of delamination problems. The beam (1D) and plate (2D) theories have been widely used in the analysis of delamination problems. The delamination in composite structures has primarily been modeled by classical laminate theory (CLT) in which transverse shears are completely ignored. The first-order shear deformation theories (FSDT), based on a shear correction factor, have also been used for the delamination problems. By applying the Timoshenko beam theory, [Shen and Grady \[1992\]](#) analyzed the dynamic characteristics of a delaminated composite beam. [Lee \[2000\]](#) used a layerwise theory for the free vibration analysis of a delaminated composite beam. [Chattopadhyay and Gu \[1994\]](#) developed a higher order theory for modeling delamination in composite plates and shells of moderately thick construction. Although the global results of the higher order theories are accurate, the stress continuity at interfaces is not achieved. To overcome this drawback, [Barbero and Reddy \[1991\]](#) and later [Dakshina Moorthya and Reddy \[1998\]](#) proposed a layerwise approach for the modeling of delamination in composite laminates. In [[Cho and Kim 2001](#), [Oh et al. 2008](#)], the authors used a higher order zigzag theory for the analysis of multi-delaminated composite plates. [Park and Sankar \[2002\]](#) presented a method, called the crack-tip force method, for evaluating the energy release rate in delaminated beams and plates. [Zou et al. \[2002\]](#) presented a two-dimensional model, as an assembly of sub-laminates connected through their interfaces, for modeling the progressive inter-laminar delamination in laminated composite structures. [Kim et al. \[2003\]](#) developed a new generalized layerwise approach for characterizing the delamination effects on the dynamic response of composite laminated structures with arbitrary stacking sequences. [Krueger and O'Brien \[2001\]](#) applied a three-dimensional shell modeling technique for delamination analysis of composite laminates using the commercial software Abaqus.

The objective of this work is to present an efficient and accurate alternative to 3D methods for analyzing non-delaminated and delaminated multilayered materials under uniaxial extension. A layerwise stress model, previously called the *Multiparticle Model of Multilayered Materials (M₄)* [[Naciri et al. 1998](#), [Carreira et al. 2002](#), [Diaz Diaz et al. 2002](#), [Caron et al. 2006](#), [Dallot and Sab 2008b](#), [Diaz Diaz and Caron 2006a](#), [Nguyen and Caron 2006](#)], is used to solve the problem. Based on Carrera's nomenclature [[Carrera 2004](#)], the M₄ model can be described as a *LS1* model (Layerwise Stress approach with first-order membrane stress approximations per layer in the thickness direction). In this model, each layer is considered as a Reissner-Mindlin plate and the layers are linked together by interfacial stresses considered as generalized stresses in the model. Consequently, the out-of-plane shear and normal stresses are continuous at the interfaces. The main difference between the LS1 model and the other layerwise

models is that, most often, the layerwise models are either displacement approaches or mixed displacement-stress approaches while the LS1 model, inspired from Pagano's model [Pagano 1978a], is a pure layerwise stress approach where there is no ad hoc hypothesis on displacement fields.

The analytical solutions of the LS1 model for uncracked symmetric laminates under uniaxial extension were obtained by Naciri et al. [1998] and validated by Carreira et al. [2002] in comparison with FEM. The present investigation applies, for the first time, the LS1 model to analyze multilayered materials in delaminated state. The method proposed in this study allows a full analysis of multi-delaminated symmetric or unsymmetric multilayered plates under uniaxial extension. The delaminated plate is divided into sub-laminates (zones) at each crack tips. Unlike the others methods proposed in the literature [Park and Sankar 2002, Zou et al. 2002, Qiao and Wang 2004] in which the division-plane is the delamination plane, herein the division-plane is perpendicular to the delamination plane. As a consequence, in this method the sub-laminates are connected together by layer forces and not by interfacial forces. The advantage of this method is that for all delaminations with the same length, there will be only one division (i.e. each sub-laminate can contain several delaminated interfaces). Therefore, there will be fewer sub-laminates and thus fewer equations compared to other methods. By setting to zero the interlaminar stresses at delaminated interfaces, the solution for different zones are obtained. The layer displacement and stress continuity conditions are enforced between the zones which provides the global solution for the delaminated plate.

Although the LS1 model provides satisfying estimations of 3D fields, in the vicinity of singularities (particularly near free edges or crack tips) its results are not satisfactory compared to detailed 3D analyses. This should be attributed to the 2D character of the model. In order to enhance the local estimation of interlaminar stresses and the energy release rate, a refinement mesh strategy will be proposed in the second part of this paper [Saeedi et al. 2012b]. In this way, the accuracy of the model increases as much as needed. It will be shown that not only this new approach, called the *refined LS1*, is efficient but also its results are in excellent agreement with the 3D results. Based on this method, a dedicated software has been developed which gives the analytical solutions of multilayered laminates under uniaxial extension in non-delaminated and delaminated states. This program is able to determine easily all the stress and displacement fields at interfaces and layers as well as the energy release rate even in laminates constituted of a large number of layers with several interfacial cracks. This efficient software can be used for the analysis of delaminated multilayered plates in problems dealing with the prediction and/or propagation of delamination.

2.2 The LS1 model

In this section, the formulation of the *LS1* model (Layerwise Stress model with first-order membrane stress approximation per layer), previously called *M4-5n* model, is briefly presented. In the next sections, this model will be used to solve the delamination problem in composite laminates under uniaxial extension. In the following formulation,

x and y represent the in-plane directions and z is the thickness coordinate. h_-^i , h_+^i and \bar{h}^i are respectively the bottom, the top and the mid-plane z coordinate of layer i and $e^i = h_+^i - h_-^i$ denotes the thickness of layer i . Greek alphabet subscripts (such as $\alpha, \beta, \gamma, \delta$) correspond to $\{x, y\}$ or $\{1, 2\}$.

2.2.1 Generalized stresses and 3D stress field

As explained, the LS1 model is a layerwise model with stress field approximations. Indeed, this model presents a stress approach based on Pagano's model [Pagano 1978a], in which there is no hypothesis on displacement fields. In this model, the 3D stress components are considered as polynomial functions of z whose coefficients are expressed in terms of generalized stresses of the model. The in-plane stress components $\sigma_{\alpha\beta}$ are chosen as linear functions of z . According to the 3D equilibrium equations, the shear stresses $\sigma_{\alpha z}$ and the normal stress σ_{zz} are respectively quadratic and cubic polynomial functions of z . The generalized internal stresses are defined as follows ($\alpha, \beta \in \{x, y\}$) :

- In-plane stress, moment and shear resultants of layer i , respectively:

$$N_{\alpha\beta}^i(x, y) = \int_{h_-^i}^{h_+^i} \sigma_{\alpha\beta}(x, y, z) dz \quad (2.1)$$

$$M_{\alpha\beta}^i(x, y) = \int_{h_-^i}^{h_+^i} (z - \bar{h}^i) \sigma_{\alpha\beta}(x, y, z) dz \quad (2.2)$$

$$Q_{\alpha}^i(x, y) = \int_{h_-^i}^{h_+^i} \sigma_{\alpha z}(x, y, z) dz \quad (2.3)$$

- Interlaminar shear and normal stresses at interface $i, i + 1$:

$$\tau_{\alpha}^{i,i+1}(x, y) = \sigma_{\alpha z}^i(x, y, h_+^i) = \sigma_{\alpha z}^{i+1}(x, y, h_-^{i+1}) \quad (2.4)$$

$$\nu^{i,i+1}(x, y) = \sigma_{zz}^i(x, y, h_+^i) = \sigma_{zz}^{i+1}(x, y, h_-^{i+1}) \quad (2.5)$$

The interlaminar stresses at interfaces are unknowns of the model. Therefore, the stress continuities at the interfaces are automatically satisfied and the interlaminar stresses can be evaluated directly without any postprocessing. If needed, the distributions of the 3D stresses can be calculated across the thickness of the layers. The 3D stress components are expressed in terms of the generalized stresses of the model as described in Appendix 2.A.

2.2.2 Generalized displacements and generalized strains

Since the LS1 model is a layerwise stress approach, there is no hypothesis on the form of the displacement fields and the displacements stem from the model. By introducing the assumed stress fields into the Hellinger-Reissner functional and integrating with respect to z over the thickness of each layer, the expressions of generalized displacements

are deduced. These generalized displacements are in fact weighted-averages of the 3D displacements [Naciri et al. 1998, Carreira et al. 2002]. In this way, five kinematic fields (three displacements and two rotations) are introduced for each layer:

$$U_\alpha^i(x, y) = \frac{1}{e^i} \int_{h_-^i}^{h_+^i} U_\alpha(x, y, z) dz \quad (2.6)$$

$$U_z^i(x, y) = \frac{1}{e^i} \int_{h_-^i}^{h_+^i} U_z(x, y, z) dz \quad (2.7)$$

$$\Phi_\alpha^i(x, y) = \frac{12}{(e^i)^2} \int_{h_-^i}^{h_+^i} \frac{z - \bar{h}^i}{e^i} U_\alpha(x, y, z) dz \quad (2.8)$$

Generalized strains which are deduced from the generalized displacements, are associated with the generalized stresses so that they appear as the energy conjugate to the generalized stresses in the Hellinger-Reissner functional. They are defined as follows:

$$\varepsilon_{\alpha\beta}^i = \frac{1}{2} (U_{\alpha,\beta}^i + U_{\beta,\alpha}^i) \quad (2.9)$$

$$\chi_{\alpha\beta}^i = \frac{1}{2} (\Phi_{\alpha,\beta}^i + \Phi_{\beta,\alpha}^i) \quad (2.10)$$

$$d_{\Phi_\alpha}^i = \Phi_\alpha^i + U_{z,\alpha}^i \quad (2.11)$$

$$D_\alpha^{i,i+1} = U_\alpha^{i+1} - U_\alpha^i - \left(\frac{e^i}{2} \Phi_\alpha^i + \frac{e^{i+1}}{2} \Phi_\alpha^{i+1} \right) \quad (2.12)$$

$$D_z^{i,i+1} = U_z^{i+1} - U_z^i \quad (2.13)$$

Accordingly, the generalized strains $\varepsilon_{\alpha\beta}^i$, $\chi_{\alpha\beta}^i$, $d_{\Phi_\alpha}^i$, $D_\alpha^{i,i+1}$ and $D_z^{i,i+1}$ are associated, respectively, with the generalized stresses $N_{\alpha\beta}^i$, $M_{\alpha\beta}^i$, Q_α^i , $\tau_\alpha^{i,i+1}$ and $\nu^{i,i+1}$.

2.2.3 Constitutive and equilibrium equations

The derivation of the Hellinger-Reissner functional with respect to generalized stresses yields the constitutive equations of the model.

Constitutive relations for layer i :

- Membrane and in-plane shear:

$$\varepsilon_{\alpha\beta}^i = \frac{1}{e^i} S_{\alpha\beta\gamma\delta}^i N_{\gamma\delta}^i \quad (2.14)$$

- Bending and torsion:

$$\chi_{\alpha\beta}^i = \frac{12}{(e^i)^3} S_{\alpha\beta\gamma\delta}^i M_{\gamma\delta}^i \quad (2.15)$$

- Out-of-plane shear:

$$d_{\Phi_\alpha}^i = \frac{6}{5e^i} S_{Q_{\alpha\beta}}^i Q_\beta^i - \frac{1}{10} S_{Q_{\alpha\beta}}^i (\tau_\beta^{i-1,i} + \tau_\beta^{i,i+1}) \quad (2.16)$$

Constitutive relations for interface $i, i + 1$:

- Interlaminar shear stress:

$$\begin{aligned} D_\alpha^{i,i+1} = & -\frac{1}{10} \left(S_{Q_{\alpha\beta}}^i Q_\beta^i + S_{Q_{\alpha\beta}}^{i+1} Q_\beta^{i+1} \right) - \frac{1}{30} \left(e^i S_{Q_{\alpha\beta}}^i \tau_\beta^{i-1,i} + e^{i+1} S_{Q_{\alpha\beta}}^{i+1} \tau_\beta^{i+1,i+2} \right) \\ & + \frac{2}{15} \left(e^i S_{Q_{\alpha\beta}}^i + e^{i+1} S_{Q_{\alpha\beta}}^{i+1} \right) \tau_\beta^{i,i+1} \end{aligned} \quad (2.17)$$

- Interlaminar normal stress:

$$D_z^{i,i+1} = \frac{9}{70} \left(e^i S_\nu^i \nu^{i-1,i} + e^{i+1} S_\nu^{i+1} \nu^{i+1,i+2} \right) + \frac{13}{35} \left(e^i S_\nu^i + e^{i+1} S_\nu^{i+1} \right) \nu^{i,i+1} \quad (2.18)$$

where $S_{\alpha\beta\gamma\delta}^i$, $S_{Q_{\alpha\beta}}^i$ and S_ν^i are components of the compliance matrix of layer i as expressed in Appendix 2.B.

The derivation of the Hellinger-Reissner functional with respect to generalized displacements leads to the equilibrium equations. Since there are 5 generalized displacements per layer, 5 equilibrium equations are obtained for each layer:

$$N_{\alpha\beta,\beta}^i + \tau_\alpha^{i,i+1} - \tau_\alpha^{i-1,i} = 0 \quad (2.19)$$

$$M_{\alpha\beta,\beta}^i + \frac{e^i}{2} \left(\tau_\alpha^{i,i+1} + \tau_\alpha^{i-1,i} \right) - Q_\alpha^i = 0 \quad (2.20)$$

$$Q_{\beta,\beta}^i + \nu^{i,i+1} - \nu^{i-1,i} = 0 \quad (2.21)$$

2.2.4 Boundary conditions

Since the model consists of $5n$ displacement fields, there are $5n$ boundary conditions at each edge. The boundary conditions of the model are written in terms of generalized stresses or generalized displacements. At point $p(x_0, y_0)$ on the lateral edge of the plate, the $5n$ boundary conditions are given as follows ($1 \leq i \leq n$):

$$\begin{aligned} N_{\alpha\beta}^i(x_0, y_0) n_\beta &= [N_\alpha^i]^d & \text{or} & & U_\alpha^i(x_0, y_0) &= [U_\alpha^i]^d \\ M_{\alpha\beta}^i(x_0, y_0) n_\beta &= [M_\alpha^i]^d & \text{or} & & \Phi_\alpha^i(x_0, y_0) &= [\Phi_\alpha^i]^d \\ Q_\alpha^i(x_0, y_0) n_\alpha &= [Q^i]^d & \text{or} & & U_z^i(x_0, y_0) &= [U_z^i]^d \end{aligned} \quad (2.22)$$

with

$$[N_\alpha^i]^d = \int_{h_i^-}^{h_i^+} T_\alpha^i(x_0, y_0, z) dz$$

$$[M_\alpha^i]^d = \int_{h_i^-}^{h_i^+} T_\alpha^i(x_0, y_0, z)(z - \bar{h}_i) dz$$

$$[Q^i]^d = \int_{h_i^-}^{h_i^+} T_z^i(x_0, y_0, z) dz$$

where the vector $\underline{n} = (n_\alpha, n_\beta)^t$ is the outward normal to the lateral edge and \underline{T} is the traction vector. The index d denotes determined (given) fields.

2.3 Analysis of non-delaminated multilayered plate

2.3.1 Problem description

A general $(\theta_1, \theta_2, \dots, \theta_n)$ composite plate is considered with a length of $2l$ and a width of $2b$ respectively in the x and y directions (Fig. 2.1). The thickness of the laminate following the z direction is equal to $\sum_{i=1}^n e^i = 2h$ and the middle plane of the plate is located at $z = 0$. The behavior of all layers is considered orthotropic. In order to apply a uniaxial extension, uniform displacements $\pm\Delta$ are imposed at the edges $x = \pm l$ while the other edges are free. It is assumed that the plate is long in the x direction ($l \gg b \gg h$) so that the strain components are independent of the x -coordinate far from the ends $x = \pm l$.

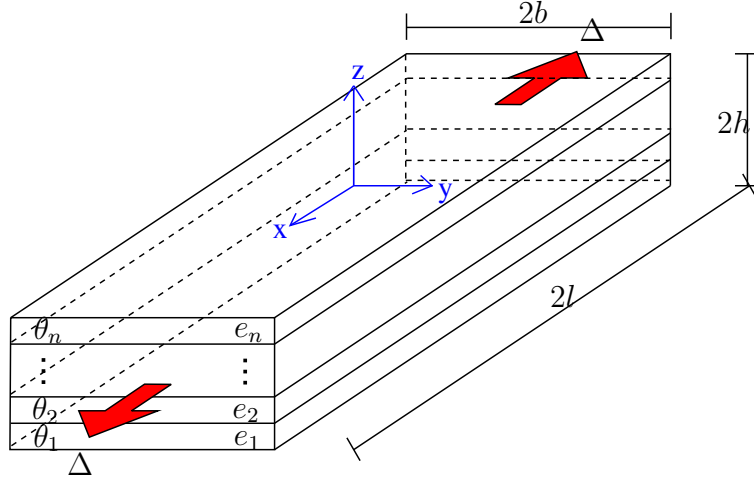


Figure 2.1: Laminate geometry, imposed displacements and coordinate system

2.3.2 LS1 problem formulation

Knowing that the strain field is independent of x , the generalized displacements can be written as follows:

$$U_x^i(x, y) = \frac{\Delta}{l}x + u_x^i(y) \quad , \quad U_y^i(x, y) = u_y^i(y) \quad , \quad U_z^i(x, y) = u_z^i(y) \quad (2.23)$$

$$\Phi_x^i(x, y) = \phi_x^i(y) \quad , \quad \Phi_y^i(x, y) = \phi_y^i(y)$$

By introducing these displacement fields into Eqs. 2.9 to 2.13, the generalized strain components are obtained as follows:

$$\begin{aligned}
 \varepsilon_{xx}^i &= \frac{\Delta}{l} \quad , \quad \varepsilon_{yy}^i = u_y^{i'} \quad , \quad \varepsilon_{xy}^i = \frac{1}{2}u_x^{i'} \\
 \chi_{xx}^i &= 0 \quad , \quad \chi_{yy}^i = \phi_y^{i'} \quad , \quad \chi_{xy}^i = \frac{1}{2}\phi_x^{i'} \\
 d_x^i &= \phi_x^i \quad , \quad d_y^i = \phi_y^i + u_z^{i'} \\
 D_x^{i,i+1} &= u_x^{i+1} - u_x^i - \left(\frac{e^i}{2}\phi_x^i + \frac{e^{i+1}}{2}\phi_x^{i+1} \right) \\
 D_y^{i,i+1} &= u_y^{i+1} - u_y^i - \left(\frac{e^i}{2}\phi_y^i + \frac{e^{i+1}}{2}\phi_y^{i+1} \right) \\
 D_z^{i,i+1} &= u_z^{i+1} - u_z^i
 \end{aligned} \tag{2.24}$$

where the prime sign denotes the derivation with respect to y .

By using Eqs. 2.14 to 2.18, the constitutive equations yield:

- Constitutive relation for layer i :

$$\begin{pmatrix} \frac{\Delta}{l} \\ u_y' \\ u_x \end{pmatrix}^i = \frac{\tilde{S}^i}{e^i} \cdot \begin{pmatrix} N_{xx} \\ N_{yy} \\ N_{xy} \end{pmatrix}^i \tag{2.25}$$

$$\begin{pmatrix} 0 \\ \phi_y' \\ \phi_x \end{pmatrix}^i = \frac{12}{(e^i)^3} \tilde{S}^i \cdot \begin{pmatrix} M_{xx} \\ M_{yy} \\ M_{xy} \end{pmatrix}^i \tag{2.26}$$

$$\begin{pmatrix} \phi_x \\ \phi_y + u_z' \end{pmatrix}^i = \frac{6}{5e^i} \tilde{S}_Q^i \cdot \begin{pmatrix} Q_x \\ Q_y \end{pmatrix}^i - \frac{1}{10} \tilde{S}_Q^i \cdot \begin{pmatrix} \tau_x^{i-1,i} + \tau_x^{i,i+1} \\ \tau_y^{i-1,i} + \tau_y^{i,i+1} \end{pmatrix} \tag{2.27}$$

- Constitutive relation for interface $i, i + 1$:

$$\begin{aligned}
 &\begin{pmatrix} u_x^{i+1} - u_x^i - \left(\frac{e^i}{2}\phi_x^i + \frac{e^{i+1}}{2}\phi_x^{i+1} \right) \\ u_y^{i+1} - u_y^i - \left(\frac{e^i}{2}\phi_y^i + \frac{e^{i+1}}{2}\phi_y^{i+1} \right) \end{pmatrix} = -\frac{1}{10} \left[\tilde{S}_Q^i \cdot \begin{pmatrix} Q_x \\ Q_y \end{pmatrix}^i + \tilde{S}_Q^{i+1} \cdot \begin{pmatrix} Q_x \\ Q_y \end{pmatrix}^{i+1} \right] \\
 &- \frac{1}{30} \left[e^i \tilde{S}_Q^i \cdot \begin{pmatrix} \tau_x \\ \tau_y \end{pmatrix}^{i-1,i} + e^{i+1} \tilde{S}_Q^{i+1} \cdot \begin{pmatrix} \tau_x \\ \tau_y \end{pmatrix}^{i+1,i+2} \right] + \frac{2}{15} (e^i \tilde{S}_Q^i + e^{i+1} \tilde{S}_Q^{i+1}) \begin{pmatrix} \tau_x \\ \tau_y \end{pmatrix}^{i,i+1}
 \end{aligned} \tag{2.28}$$

$$u_z^{i+1} - u_z^i = \frac{9}{70} (e^i S_\nu^i \nu^{i-1,i} + e^{i+1} S_\nu^{i+1} \nu^{i+1,i+2}) + \frac{13}{35} (e^i S_\nu^i + e^{i+1} S_\nu^{i+1}) \nu^{i,i+1} \quad (2.29)$$

where \tilde{S}^i and \tilde{S}_Q^i denote respectively the plane stress part and the out-of-plane shear stress part of the compliance matrix of layer i (see Appendix 2.B).

Moreover, according to Eqs. 2.19 to 2.21, five equilibrium equations are written for each layer as follows:

$$N_{xy}^{i'} + \tau_x^{i,i+1} - \tau_x^{i-1,i} = 0 \quad (2.30)$$

$$N_{yy}^{i'} + \tau_y^{i,i+1} - \tau_y^{i-1,i} = 0 \quad (2.31)$$

$$M_{xy}^{i'} + \frac{e}{2} (\tau_x^{i,i+1} + \tau_x^{i-1,i}) - Q_x^i = 0 \quad (2.32)$$

$$M_{yy}^{i'} + \frac{e}{2} (\tau_y^{i,i+1} + \tau_y^{i-1,i}) - Q_y^i = 0 \quad (2.33)$$

$$Q_y^{i'} + \nu^{i,i+1} - \nu^{i-1,i} = 0 \quad (2.34)$$

There are $16n - 3$ unknown fields and the same number of equations from which $10n$ are first-order differential equations and $6n - 3$ are algebraic. By condensing the system of equations, a system of $5n$ second-order differential equations is extracted which can be written as:

$$\underline{X}'' = \underline{M} \cdot \underline{X} \quad (2.35)$$

where \underline{X} is an unknown vector of dimension $5n$ and \underline{M} is a $5n \times 5n$ matrix which depends on the mechanical material properties, the orientation and the thickness of the layers (see Appendix 2.B for more details).

By applying the eigenvector expansion method, the obtained system of equations is solved. Knowing that there may be complex and repeated eigenvalues, the analytical solution of the system of equations will be in the form of exponential, trigonometric and polynomial functions as follows:

$$\underline{X} = \sum_{i=1}^{2n} e^{\alpha_i y} \left[\underline{P}_i(y) \sin(\beta_i y) + \underline{Q}_i(y) \cos(\beta_i y) \right] \quad (2.36)$$

where the components of the vectors $\underline{P}_i(y)$ and $\underline{Q}_i(y)$ are polynomial functions with constant coefficients. Since there are $5n$ second-order differential equations, $10n$ unknown constants of integration are obtained. In order to determine these constants $10n$ boundary conditions are needed. These boundary conditions are obtained by imposing free-edge conditions at the edge $y = \pm b$. For each layer i ($1 \leq i \leq n$) there are 10 equations:

$$N_{xy}^i(\pm b) = 0 \quad , \quad N_{yy}^i(\pm b) = 0 \quad , \quad M_{xy}^i(\pm b) = 0 \quad , \quad M_{yy}^i(\pm b) = 0 \quad , \quad Q_y^i(\pm b) = 0 \quad (2.37)$$

In this paper, we are interested in the free-edge problem but any boundary condition could be imposed at the edge $y = \pm b$ by replacing the boundary conditions 2.37 by the desired constraint conditions.

2.4 Analysis of delaminated multilayered plate

In this section, we are interested in the delaminated state of multilayered plates under uniaxial extension. The same laminate as considered in the previous section is discussed except that in the present case there are one or more interfacial cracks.

2.4.1 Laminate with one interfacial crack

At first, it is assumed that one delamination crack exists at an arbitrary interface such as $k, k + 1$. The crack initiates from the free edge $y = b$ with a length of a in the y direction and along the length of the laminate in the x direction (see Fig. 2.2). The invariance assumption following the x direction is still valid. Two zones are distinguished:

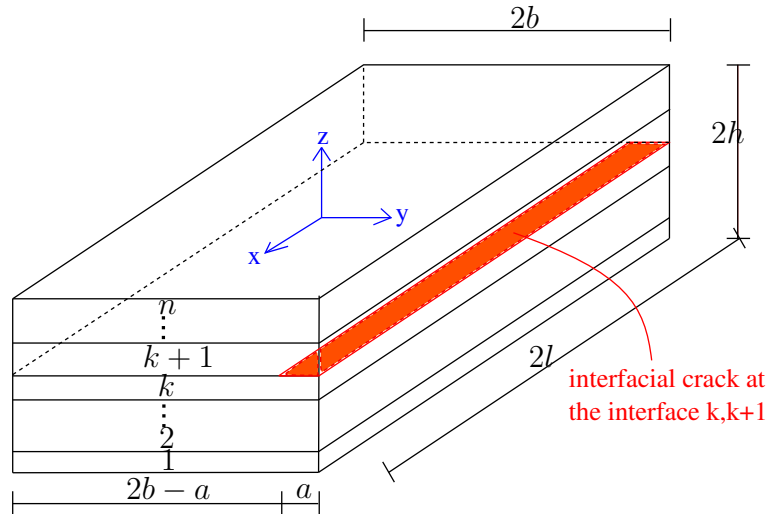


Figure 2.2: Laminate with an interfacial crack of length a at the interface $k, k + 1$

$$\text{Zone I} \quad : \quad -b \leq y \leq (b - a) \quad \text{non-delaminated zone}$$

$$\text{Zone II} \quad : \quad (b - a) \leq y \leq b \quad \text{delaminated zone}$$

To solve this problem, the expressions of the unknown fields in zone I (non-delaminated) and II (delaminated) are found separately; then, by enforcing continuity and boundary conditions, the general solution of the problem is obtained. The solution of the non-delaminated plate (zone I) has already been found in the previous section. In this section, the solution of the delaminated plate (zone II) is found. It is assumed

that the laminate is completely delaminated at the interface $k, k + 1$ in zone II. Thus the three following equations are imposed:

$$\tau_x^{k,k+1} = 0 \quad , \quad \tau_y^{k,k+1} = 0 \quad , \quad \nu^{k,k+1} = 0 \quad ; \quad (b - a) \leq y \leq b \quad (2.38)$$

On the other hand, there are three displacement discontinuity fields $\gamma_x^{k,k+1}$, $\gamma_y^{k,k+1}$ and $\gamma_z^{k,k+1}$ at the delaminated interface. The constitutive relation at the delaminated interface $k, k + 1$ can be written as follows:

- Interlaminar shear stress:

$$\begin{aligned} D_\alpha^{k,k+1} - \gamma_\alpha^{k,k+1} = & -\frac{1}{10} \left(S_{Q_{\alpha\beta}}^k Q_\beta^k + S_{Q_{\alpha\beta}}^{k+1} Q_\beta^{k+1} \right) - \frac{1}{30} \left(e^k S_{Q_{\alpha\beta}}^k \tau_\beta^{k-1,k} + e^{k+1} S_{Q_{\alpha\beta}}^{k+1} \tau_\beta^{k+1,k+2} \right) \\ & + \frac{2}{15} \left(e^k S_{Q_{\alpha\beta}}^k + e^{k+1} S_{Q_{\alpha\beta}}^{k+1} \right) \tau_\beta^{k,k+1} \end{aligned} \quad (2.39)$$

- Interlaminar normal stress:

$$D_z^{k,k+1} - \gamma_z^{k,k+1} = \frac{9}{70} \left(e^k S_\nu^k \nu^{k-1,k} + e^{k+1} S_\nu^{k+1} \nu^{k+1,k+2} \right) + \frac{13}{35} \left(e^k S_\nu^k + e^{k+1} S_\nu^{k+1} \right) \nu^{k,k+1} \quad (2.40)$$

where $\underline{\gamma}^{k,k+1}$ indicates the displacement discontinuity fields at the interface.

By writing the equations of the LS1 model and applying the same method used in the non-delaminated state, a similar system of $5n$ second-order differential equations is obtained as follows:

$$\underline{X}'' = \underline{M}_d \cdot \underline{X} \quad (2.41)$$

where \underline{X} is an unknown vector of dimension $5n$ with the same expression and \underline{M}_d is a $5n \times 5n$ matrix which depends on the mechanical material properties, the orientation, the thickness of the layers and also the position of the crack (see Appendix 2.C for the details).

It should be noted that the system of equations in non-delaminated state (2.35) and delaminated state (2.41) have the same form except that the matrix \underline{M} in the non-delaminated state changes to \underline{M}_d in the delaminated state.

To find the general solution of the problem, it is necessary to apply the boundary conditions. Since there are two systems of $5n$ second-order equations, there will be $2 \times 10n$ constants of integration; thus $2 \times 10n$ conditions are needed for determining these unknown constants. There are $10n$ boundary conditions at the free edges $y = \pm b$ (Eqs. 2.37). The $10n$ other conditions are deduced from the continuity of generalized displacements and stresses between zones I and II. There are five displacement continuity relations per layer as follows:

$$\begin{aligned} [u_x^i(y_p)]^I &= [u_x^i(y_p)]^{II} \quad , \quad [u_y^i(y_p)]^I = [u_y^i(y_p)]^{II} \quad , \quad [u_z^i(y_p)]^I = [u_z^i(y_p)]^{II} \\ [\phi_x^i(y_p)]^I &= [\phi_x^i(y_p)]^{II} \quad , \quad [\phi_y^i(y_p)]^I = [\phi_y^i(y_p)]^{II} \end{aligned} \quad (2.42)$$

The continuities of the generalized stresses are written as:

$$[[\underline{N}(y_p) \cdot \underline{e}_y]] = 0 \quad , \quad [[\underline{M}(y_p) \cdot \underline{e}_y]] = 0 \quad , \quad [[\underline{Q}(y_p) \cdot \underline{e}_y]] = 0 \quad (2.43)$$

This results to five conditions per layer as follows:

$$\begin{aligned} [N_{xy}^i(y_p)]^I &= [N_{xy}^i(y_p)]^{II} \quad , \quad [N_{yy}^i(y_p)]^I = [N_{yy}^i(y_p)]^{II} \\ [M_{xy}^i(y_p)]^I &= [M_{xy}^i(y_p)]^{II} \quad , \quad [M_{yy}^i(y_p)]^I = [M_{yy}^i(y_p)]^{II} \\ [Q_y^i(y_p)]^I &= [Q_y^i(y_p)]^{II} \end{aligned} \quad (2.44)$$

By using the constitutive equations, these continuity conditions can be expressed as a function of $(u_x^i)'$, $(u_y^i)'$, $(\phi_x^i)'$, $(\phi_y^i)'$ and $(Q_y^i)'$ which are the principal unknowns of the final system.

2.4.2 Laminate with several interfacial cracks

Now, we are interested in the general cracking configuration with several interfacial cracks. The problem is identical to the previous problem except that this time there are several interfacial cracks with different length as shown in Fig. 2.3.

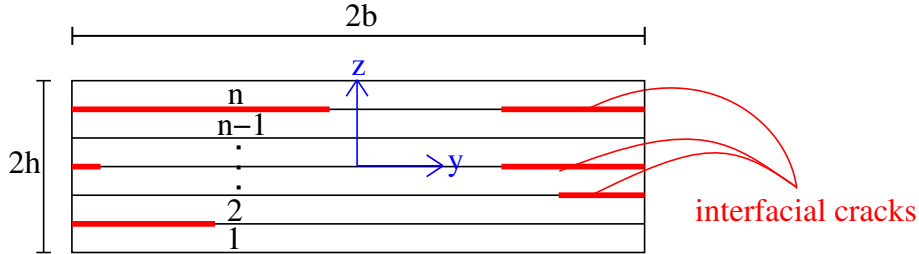


Figure 2.3: Laminate section with several cracks at different interfaces

Herein, the approach consists in generalizing the applied method for the single crack problem. Indeed, in the case of a single crack the laminate was divided into two zones at the crack tip. Similarly, in the presence of several cracks the laminate section is segmented following the y direction at every crack tip so that several zones are found as shown in Fig. 2.4.

The governing system of equations in each zone is the same as 2.35 for non-delaminated zones or 2.41 for delaminated zones knowing that the expression of the matrix \underline{M}_d is changed depending on the number and the position of the cracks (see Appendix 2.D for more details).

For q zones, there will be $5n \times q$ second-order differential equations. Therefore, there are $10n \times q$ unknown constants of integration. In order to determine these constants, $10n \times q$ conditions are needed. The free-edge conditions at the edges $y = \pm b$ yield $10n$ boundary conditions as Eq. 2.37. Regarding the continuity conditions, there are $10n$ conditions (five displacement continuity conditions per layer as Eq. 2.42 and five

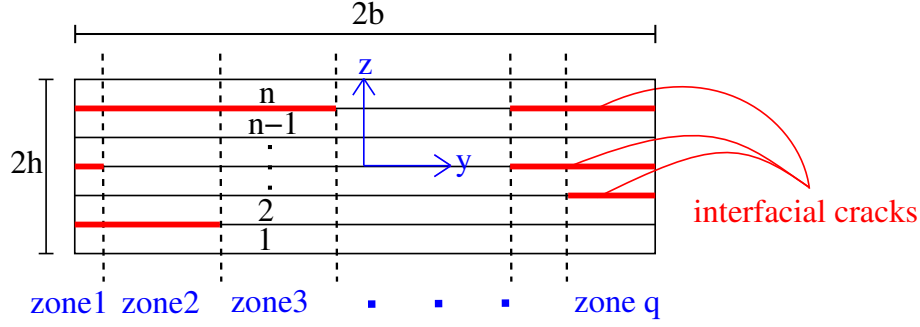


Figure 2.4: Solving method for the laminate with several cracks

stress continuity conditions per layer as Eq. 2.44) between every two adjacent zones. Therefore, totally $10n + 10n \times (q - 1) = 10n \times q$ boundary conditions are obtained. These conditions yield a system of $10n \times q$ linear algebraic equations with $10n \times q$ unknown constants which can be easily solved.

2.5 Finite element validation

Based on the proposed model, a special software was developed which gives the analytical LS1 solutions of the non-delaminated or delaminated multilayered plate under uniaxial extension. In order to validate the model, a case study is investigated and the results of the LS1 model are compared to those of a 3D finite element model.

A rectangular $(30^\circ, 60^\circ)_s$ composite laminate is considered for which the effect of all interfacial stresses is important. The width and the height of the laminate are $2b = 20 \text{ mm}$ and $2h = 4 \times 0.19 = 0.76 \text{ mm}$ respectively in the y and z directions. All plies are made up of the same carbon-epoxy material (G947/M18) whose mechanical properties are as follows:

$$\begin{aligned} E_L &= 97.6 \text{ GPa} , E_T = E_N = 8.0 \text{ GPa} \\ G_{LT} &= G_{LN} = 3.1 \text{ GPa} , G_{TN} = 2.7 \text{ GPa} \\ \nu_{LT} &= \nu_{LN} = 0.37 , \nu_{TN} = 0.5 , e = 0.19 \text{ mm} \end{aligned}$$

A uniaxial longitudinal strain $\varepsilon_{xx} = 0.001$ is imposed following the x direction. As shown in Fig. 2.5, the delamination is made up of four existing cracks of length $a = 1 \text{ mm}$ situated symmetrically at the interfaces $30^\circ/60^\circ$. It is assumed that the laminate is very long so that there is no variation in the x direction.

A 3D finite element modeling is performed by means of the commercial software Abaqus. By making use of the longitudinal invariance of the plate, the size of the domain can be significantly reduced. Indeed, instead of modeling a long plate, it is sufficient to use only one element in the x direction with the following invariance boundary conditions (Fig. 2.6):

$$\begin{aligned} U_x(x_1, y, z) &= U_x(x_0, y, z) + (x_1 - x_0)\varepsilon_{xx} \\ U_y(x_1, y, z) &= U_y(x_0, y, z) \\ U_z(x_1, y, z) &= U_z(x_0, y, z) \end{aligned} \quad (2.45)$$

2. DELAMINATED MULTILAYERED PLATES UNDER UNIAXIAL EXTENSION. PART I:
ANALYTICAL ANALYSIS USING A LAYERWISE STRESS APPROACH

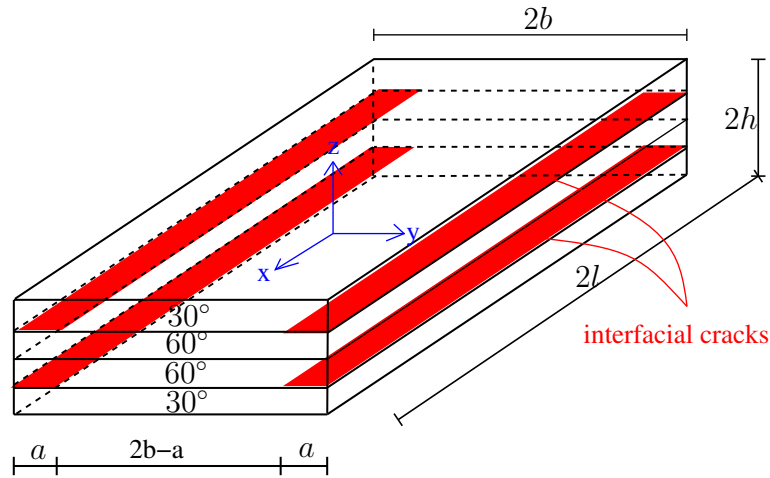


Figure 2.5: $(30^\circ, 60^\circ)_s$ laminate under uniaxial extension with delamination at the interfaces $30^\circ/60^\circ$

It should be noted that because of the invariance in the x direction, the 3D aspect ratio of the elements is not important and the size of the elements in the x direction does not play any role.

Due to the mirror symmetry of the laminate, only the half thickness of the laminate is modeled. In order to obtain accurate results, a strong refinement is applied near the crack tip (see Fig. 2.6). The size of the elements in this zone is almost $0.5 \mu\text{m}$ and the total number of nodes is about 10^5 .

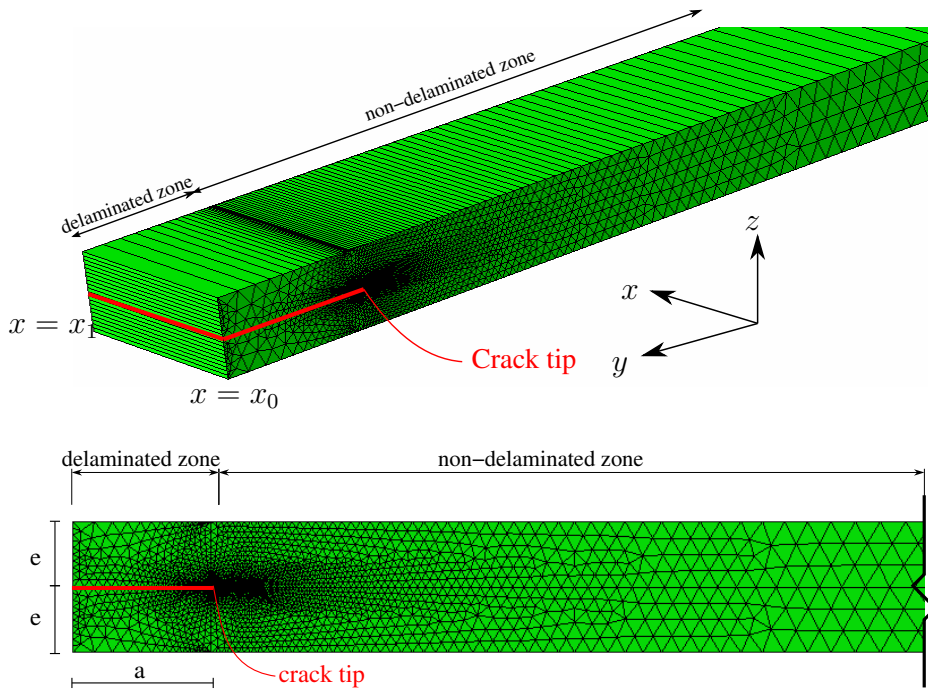


Figure 2.6: Finite element model of the laminate in delaminated state - 3D model (top); mesh in the yz plane (bottom)

2.5.1 Interlaminar stress distributions

At first, we are interested in the distributions of interlaminar stresses which are related to delamination. It should be mentioned that the interlaminar stresses are considered as generalized stresses in the LS1 model and they are evaluated directly without any postprocessing. In what follows, the abscissa axis y/b presents the dimensionless coordinate following the laminate width and the ordinate axis $k_{ij} = \frac{\sigma_{ij}}{E_x \varepsilon_{xx}}$; $i, j \in \{x, y, z\}$ signifies normalized dimensionless stress where ε_{xx} and E_x are respectively the imposed longitudinal strain and the longitudinal modulus of the laminate. Because of the symmetry following the y direction, the curves are plotted for $0 < y/b < 1$. Knowing that in the present problem $a = 1 \text{ mm}$ and $b = 10 \text{ mm}$, the abscissa $y/b = 0.9$ corresponds to the interfacial crack tip.

Fig. 2.7 shows the distributions of the interfacial shear stresses σ_{xz} , σ_{yz} and normal stress σ_{zz} at the $30^\circ/60^\circ$ interface. It is seen that the interlaminar stresses increase rapidly in the vicinity of the crack tip at $y/b = 0.9$ while being almost zero in the interior region of the laminate. The comparison between the LS1 and 3D-FE results shows that the two models give exactly the same results except very near the crack tip. More precisely, for $\bar{y} > e/4$ the LS1 and 3D-FE values are practically the same where \bar{y} denotes the distance from the crack tip and $e = 0.19 \text{ mm}$ is the thickness of a carbon-epoxy ply.

It should be noted that in the frame of classical elasticity theory, the interlaminar stress fields at the crack tip are singular. Thus the obtained stress values at the crack tip are meaningless in the LS1 model as well as in the 3D-FE model. In other words, in the FEM the more mesh is refined at the crack tip, the more the stress values increase. However, depending on the mesh refinement, there is a distance from singularity point after which the stress values become meaningful and the convergence is ensured. Indeed, although stress values at the singularity points are meaningless, the stress distributions in the vicinity of these points are important may be used as delamination stress criteria. For example, there are the stress criteria based on stress values at a specific distance from singularity point or the average stress criteria considering the average of interlaminar stresses over a characteristic distance from singularity point [Lagunegrand et al. 2006, Kim and Soni 1984, 1986, Brewer and Lagace 1988, Whitney and Nuismer 1974, Lorriot et al. 2003, Wimmer et al. 2009]. Since the LS1 stress values are not accurate enough very close to the crack tip, in the part two of this study, a refined layerwise mesh strategy will be proposed in order to increase the accuracy of the obtained stress distributions near the singularity zones even for a relatively coarse mesh. It will be shown that the stress fields become meaningful until a distance equal to $1/1000$ of the thickness of a carbon-epoxy ply ($\bar{y} > e/1000$).

2.5.2 3D-stress distributions at layers

2.5.2.1 Stress distributions at the middle plane of the layers

In this paragraph we compare the distributions of all 3D-stress fields at the middle of the layers. As it was previously explained, in the LS1 model the 3D stress components

2. DELAMINATED MULTILAYERED PLATES UNDER UNIAXIAL EXTENSION. PART I:
ANALYTICAL ANALYSIS USING A LAYERWISE STRESS APPROACH

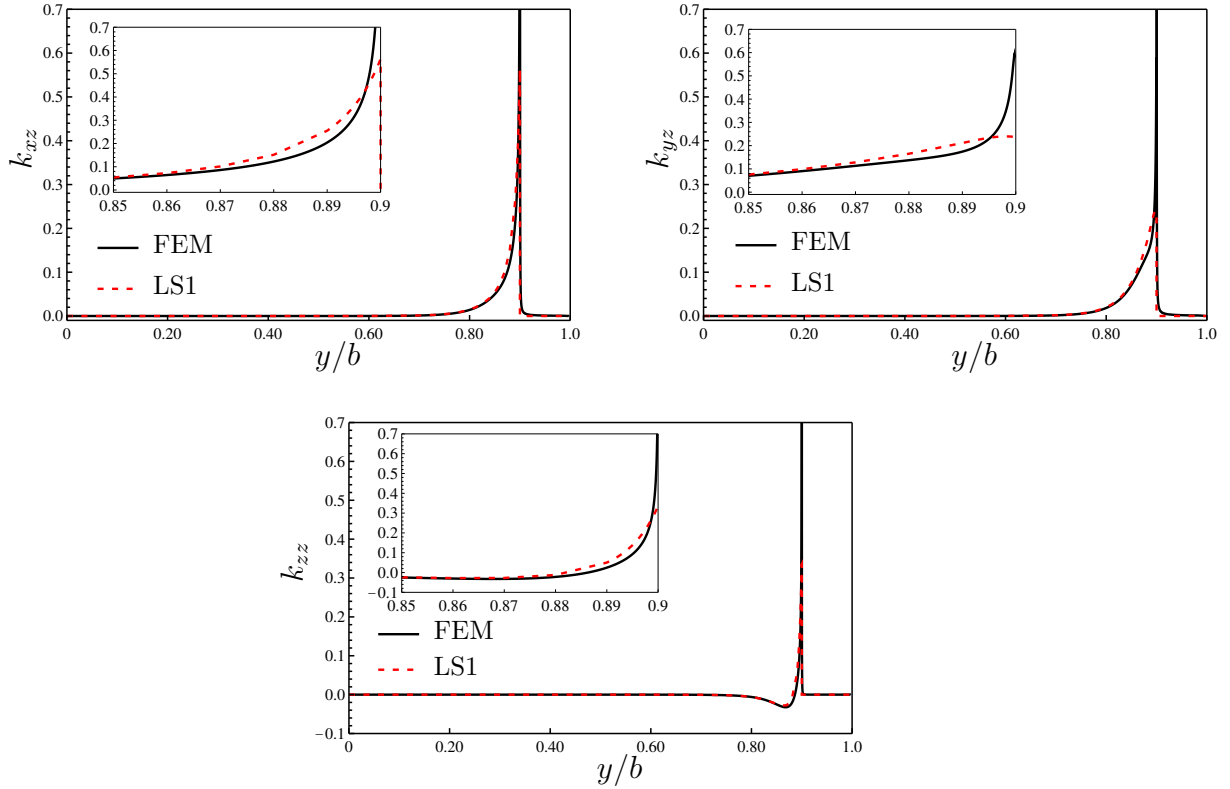


Figure 2.7: Distribution of the interlaminar stresses σ_{xz} , σ_{yz} and σ_{zz} at the $30^\circ/60^\circ$ interface of $(30^\circ, 60^\circ)_s$ laminate

can be expressed as functions of the generalized stresses of the model (see Appendix 2.A). Figs. 2.8 to 2.13 present the distributions of 3D-stresses in the middle plane of the 30° and 60° , layers. The comparison of the LS1 results with those of the 3D-FE model shows that the results of the two models are identical except in the vicinity of the crack tip ($y/b = 0.9$). Indeed, if the distance from the crack tip is greater than a fourth of the total thickness of the laminate ($\bar{y} > e/2$), the LS1 model is as accurate as the 3D-FE model; but very near the crack tip, the LS1 results are questionable. This conclusion is valid for all of the six 3D-stress components.

2.5.2.2 Stress distributions through the thickness

Finally, in order to show the consistency of our results, the stress distributions are plotted through the thickness at various distances away from the crack tip towards the inner region of the laminate. In the following figures, the through-the-thickness distributions are displayed for $\bar{y} = 0$; $\bar{y} = e/2$; $\bar{y} = e$ and $\bar{y} = 2e$ where \bar{y} signifies the distance from the crack tip following the y direction and $e = 0.19 \text{ mm}$ is the thickness of a single carbon-epoxy ply. The abscissa axis $k_{ij} = \frac{\sigma_{ij}}{E_x \varepsilon_{xx}}$; $i, j \in \{x, y, z\}$ indicates the normalized stress and the ordinate axis z/e_t denotes the normalized thickness coordinate where e_t is the total thickness of the laminate.

Figs. 2.14 to 2.19 show the distributions of all 3D stresses through the thickness of

the laminate. In each figure, the stress variation is displayed for four different distances from the crack tip. As it is demonstrated, at the crack tip position the stress estimations of the LS1 model are not accurate and even in some cases the LS1 results are totally different from the 3D-FEM results. However, it is clear that by moving slightly away from the crack tip, the LS1 model is consistent with the 3D-FE model. It is found that at the distance $\bar{y} = e/2$ from the crack tip, the global forms of the stress distributions are qualitatively captured by the LS1 model but the accuracy is not very satisfying. By moving a little more away from the crack tip, at $\bar{y} = e$ the accuracy of the LS1 model becomes acceptable, whereas the LS1 and 3D-FE models provide practically the same results for $\bar{y} > 2e$.

It is worth mentioning that the LS1 model is a very powerful model for the estimation of interlaminar stresses but it is not too appropriate for the evaluation of through-the-thickness stress fields near singularities. The reason is that in the LS1 formulation, the interlaminar stresses are the generalized stresses of the model while the 3D-stresses are obtained by linear, quadratic or cubic interpolations through the layer thickness. Due to local 3D effects in the vicinity of singularities, the LS1 estimations of 3D-stresses do not necessarily match the 3D-FEM values. However, by using the layerwise mesh strategy proposed in Part II of this paper, the LS1 estimations become quite satisfactory even very close to singularity points.

2.6 Conclusion

The delamination phenomenon is one of the major issues in design of multilayer structures. In order to apply a delamination failure criterion, it is necessary to analyze the delaminated structure. Since 3D finite element models are generally too expensive in terms of computational time and memory for such analysis, many researches are dedicated to approach delamination problems with alternative methods such as 2D layerwise models. This study uses a layerwise stress model, called the LS1 model, for analyzing multilayered plates. This model was already used and validated for analyzing multilayered plates under uniaxial extension in non-delaminated state [Carreira et al. 2002]. In the present work, the LS1 model was extended to the analysis of multilayered plates subjected to uniaxial extension in multi-delaminated state. This method allows us to model general multilayered long plates under uniaxial extension with any multi-delamination configuration in plate section plane.

The proposed method is based on the formulation of the LS1 model [Caron et al. 2006] which is a layerwise stress approach with first-order membrane stress approximation per layer. The model can be described as a stacking sequence of Reissner-Mindlin plates linked by interlaminar stresses. At first, the solution of an arbitrary $(\theta_1, \theta_2, \dots, \theta_n)$ laminate under uniaxial extension was obtained in non-delaminated state. Then the solving method was extended for multi-delaminated configuration in which there can be several interlaminar cracks with various length. The solving method consists in dividing the multi-delaminated plates at each crack tip into sub-laminates (zones); then imposing the displacement and stress continuity conditions between the adjacent zones. It should be noted that the division-plane in this method is not the delamination plane

2. DELAMINATED MULTILAYERED PLATES UNDER UNIAXIAL EXTENSION. PART I:
ANALYTICAL ANALYSIS USING A LAYERWISE STRESS APPROACH

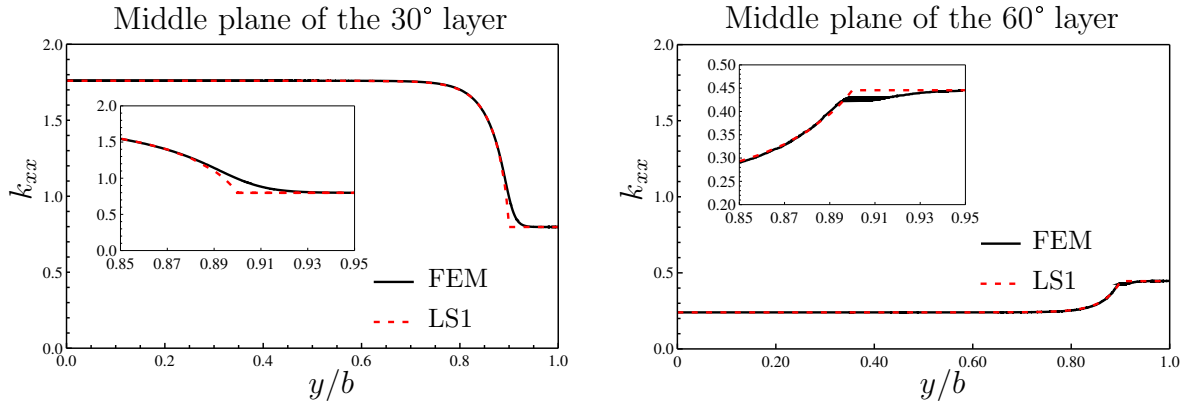


Figure 2.8: Distribution of the normal stress σ_{xx} at the middle of the layers in $(30^\circ, 60^\circ)_s$ laminate

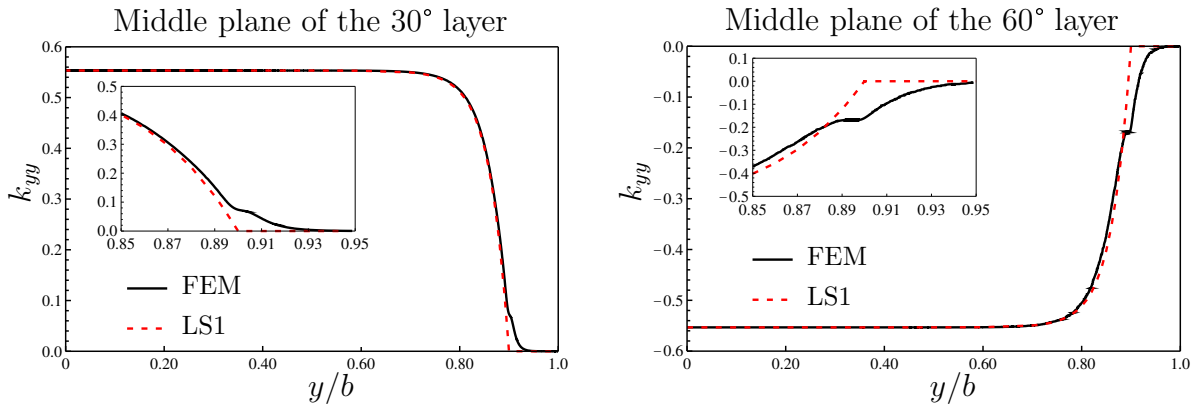


Figure 2.9: Distribution of the normal stress σ_{yy} at the middle of the layers in $(30^\circ, 60^\circ)_s$ laminate

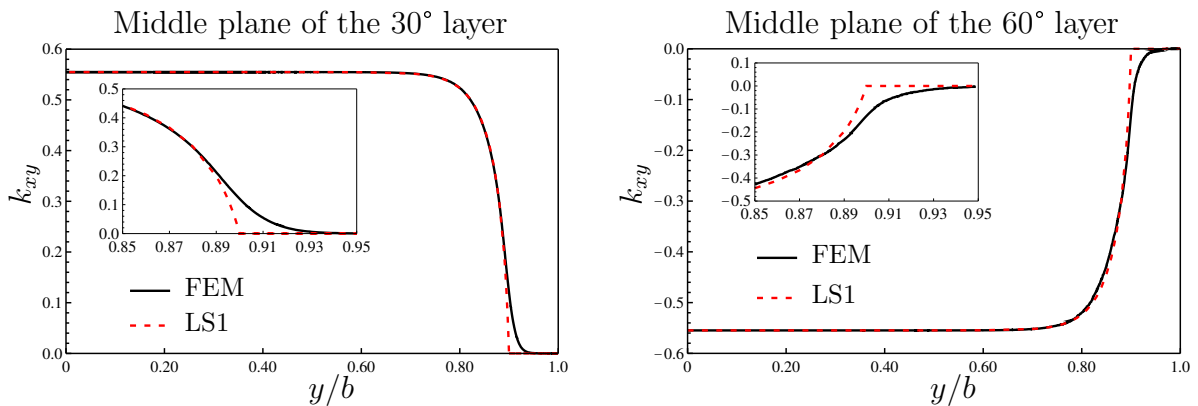


Figure 2.10: Distribution of the shear stress σ_{xy} at the middle of the layers in $(30^\circ, 60^\circ)_s$ laminate

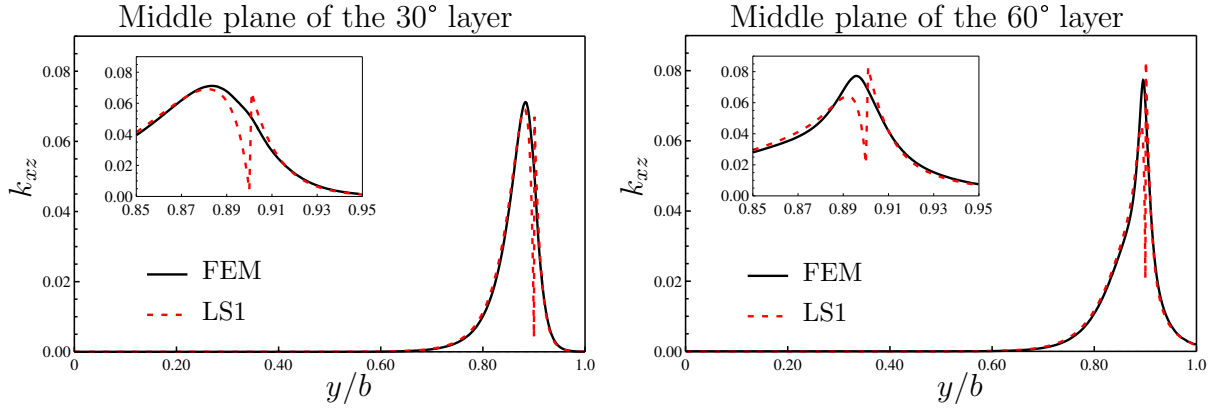


Figure 2.11: Distribution of the shear stress σ_{xz} at the middle of the layers in $(30^\circ, 60^\circ)_s$ laminate

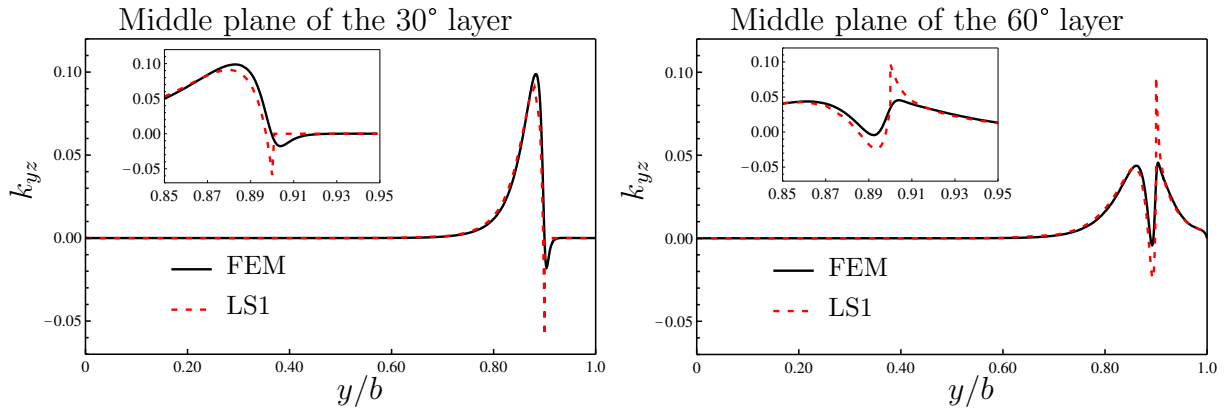


Figure 2.12: Distribution of the shear stress σ_{yz} at the middle of the layers in $(30^\circ, 60^\circ)_s$ laminate

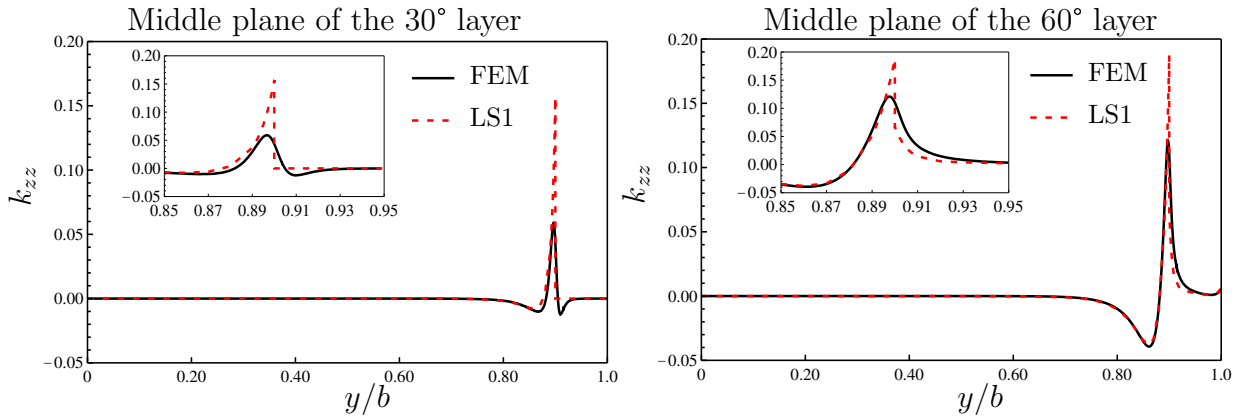


Figure 2.13: Distribution of the normal stress σ_{zz} at the middle of the layers in $(30^\circ, 60^\circ)_s$ laminate

2. DELAMINATED MULTILAYERED PLATES UNDER UNIAXIAL EXTENSION. PART I:
ANALYTICAL ANALYSIS USING A LAYERWISE STRESS APPROACH

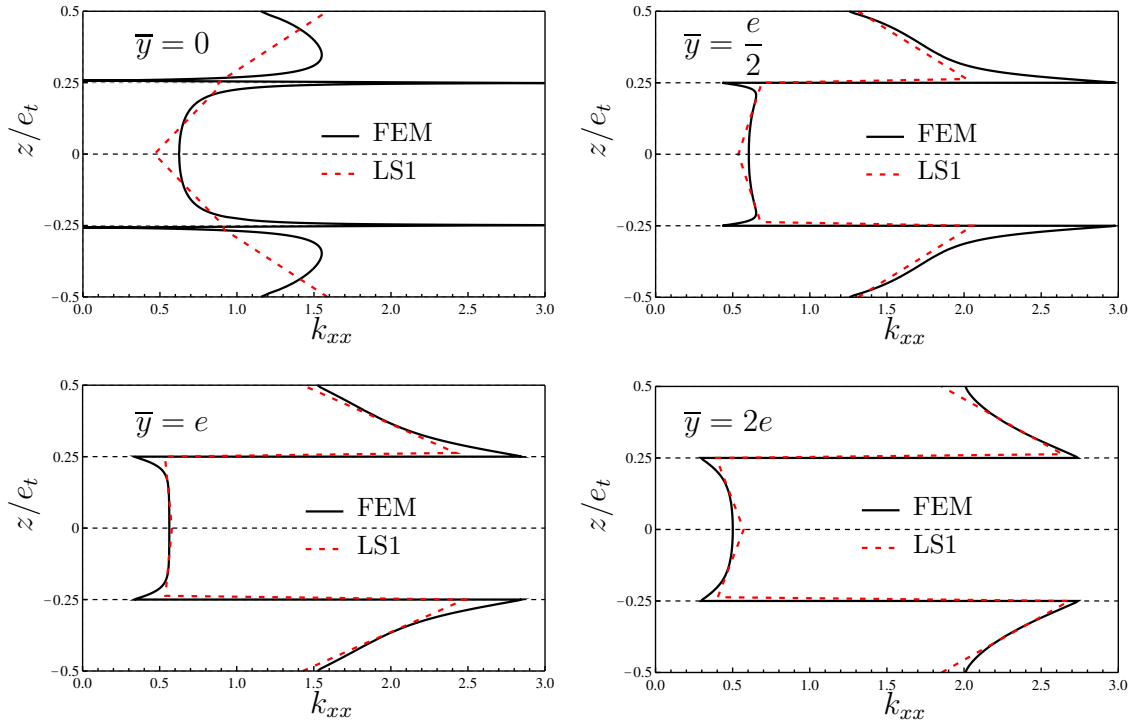


Figure 2.14: Distribution of the normal stress σ_{xx} through the thickness of $(30^\circ, 60^\circ)_s$ laminate

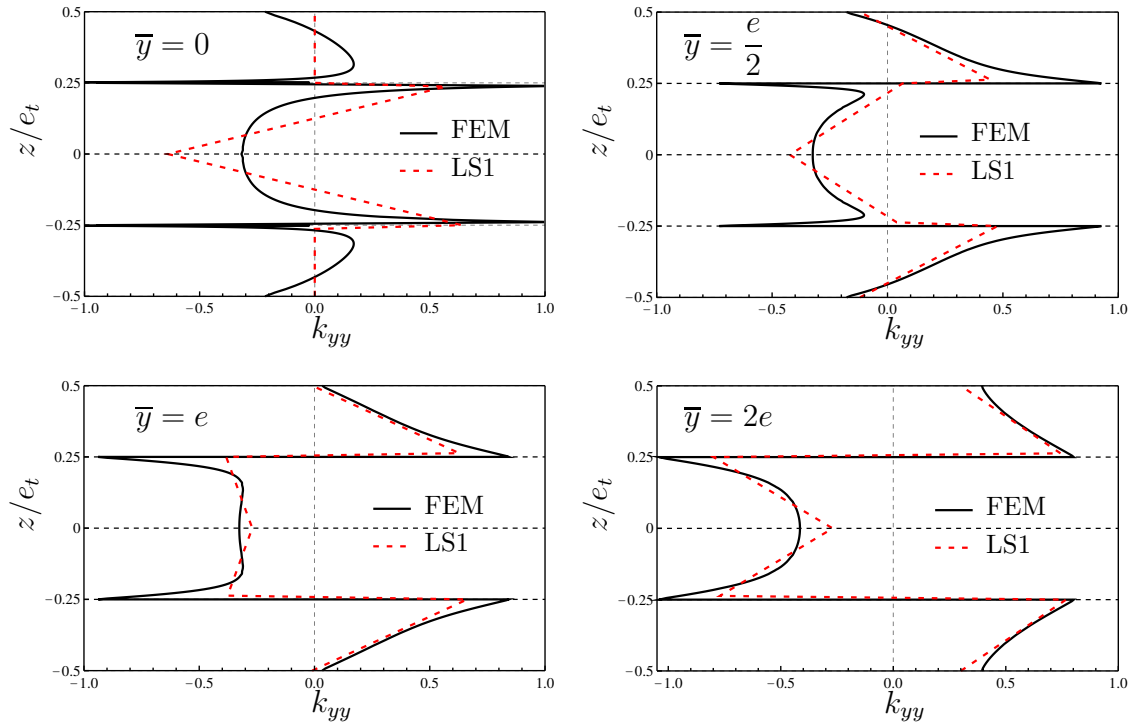


Figure 2.15: Distribution of the normal stress σ_{yy} through the thickness of $(30^\circ, 60^\circ)_s$ laminate

2.6. CONCLUSION

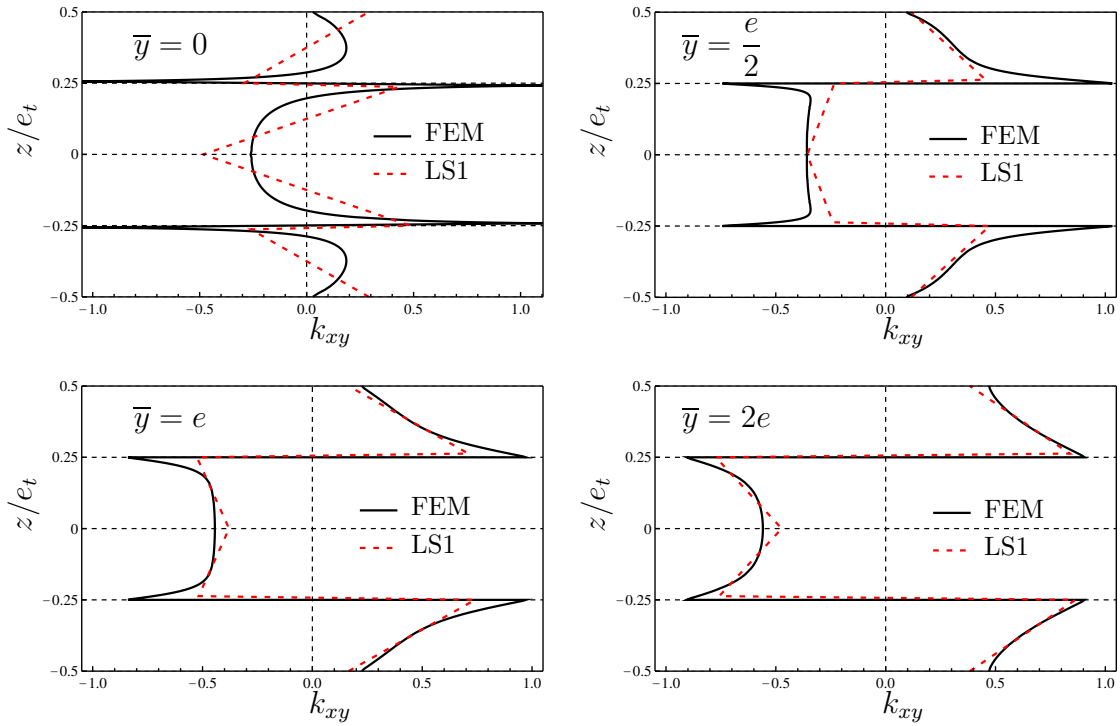


Figure 2.16: Distribution of the shear stress σ_{xy} through the thickness of $(30^\circ, 60^\circ)_s$ laminate

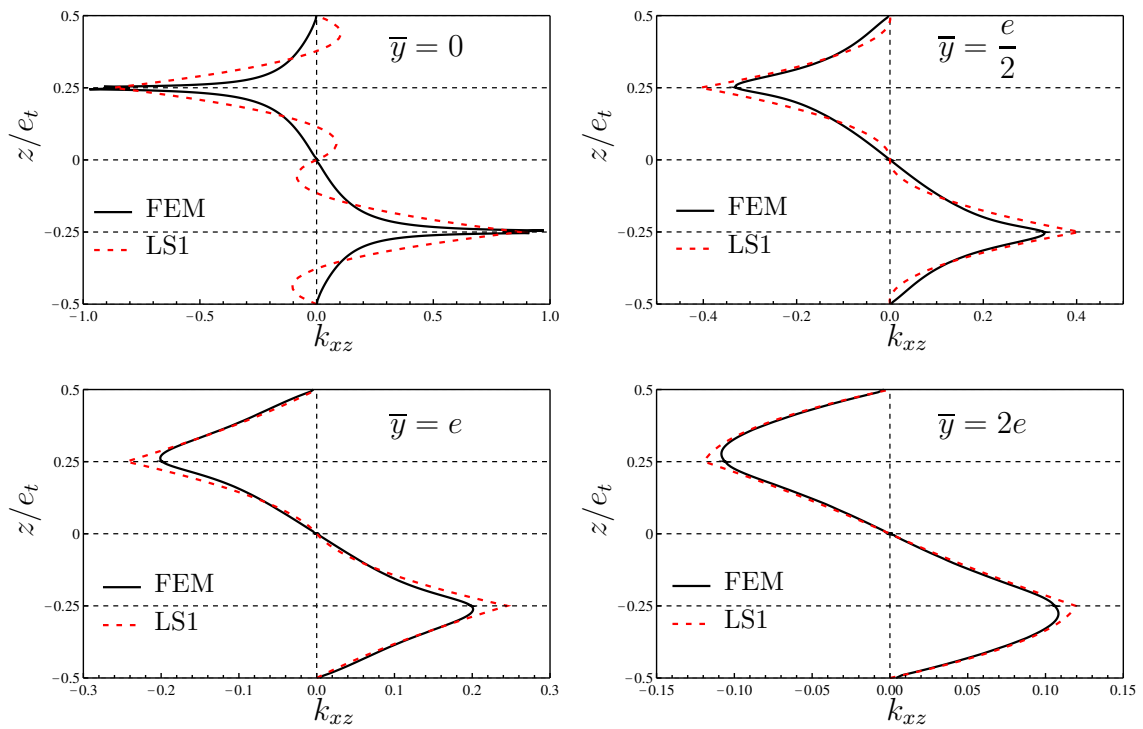


Figure 2.17: Distribution of the shear stress σ_{xz} through the thickness of $(30^\circ, 60^\circ)_s$ laminate

2. DELAMINATED MULTILAYERED PLATES UNDER UNIAXIAL EXTENSION. PART I:
ANALYTICAL ANALYSIS USING A LAYERWISE STRESS APPROACH

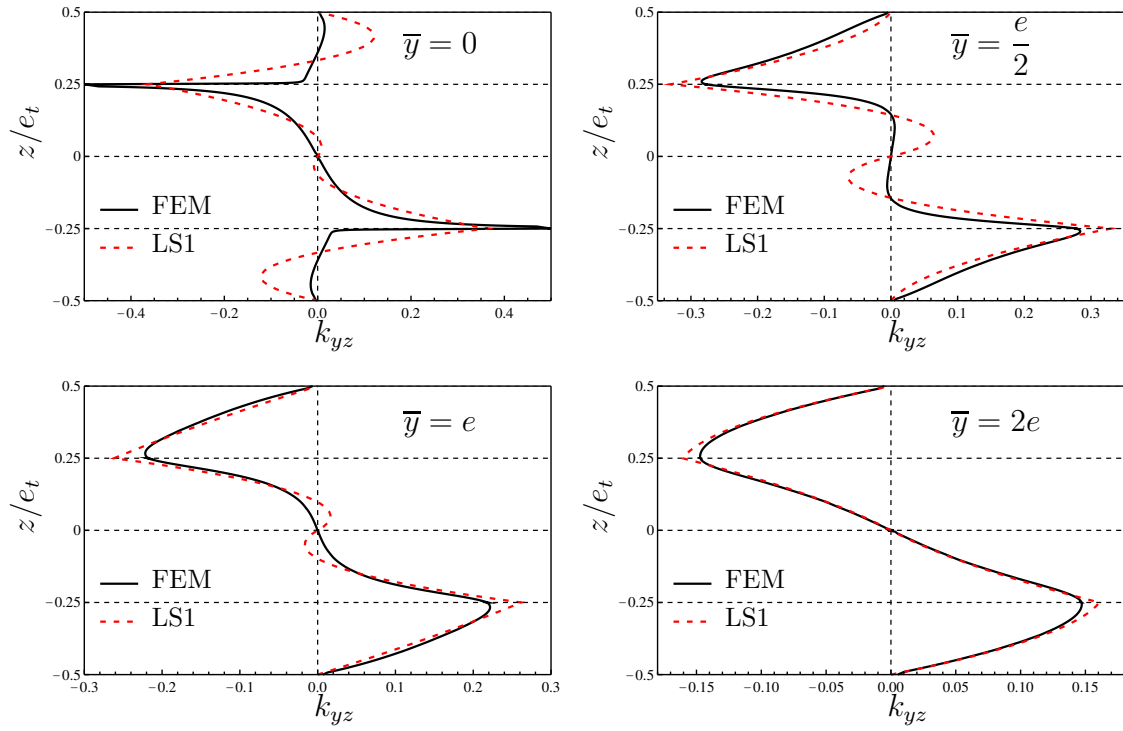


Figure 2.18: Distribution of the shear stress σ_{yz} through the thickness of $(30^\circ, 60^\circ)_s$ laminate

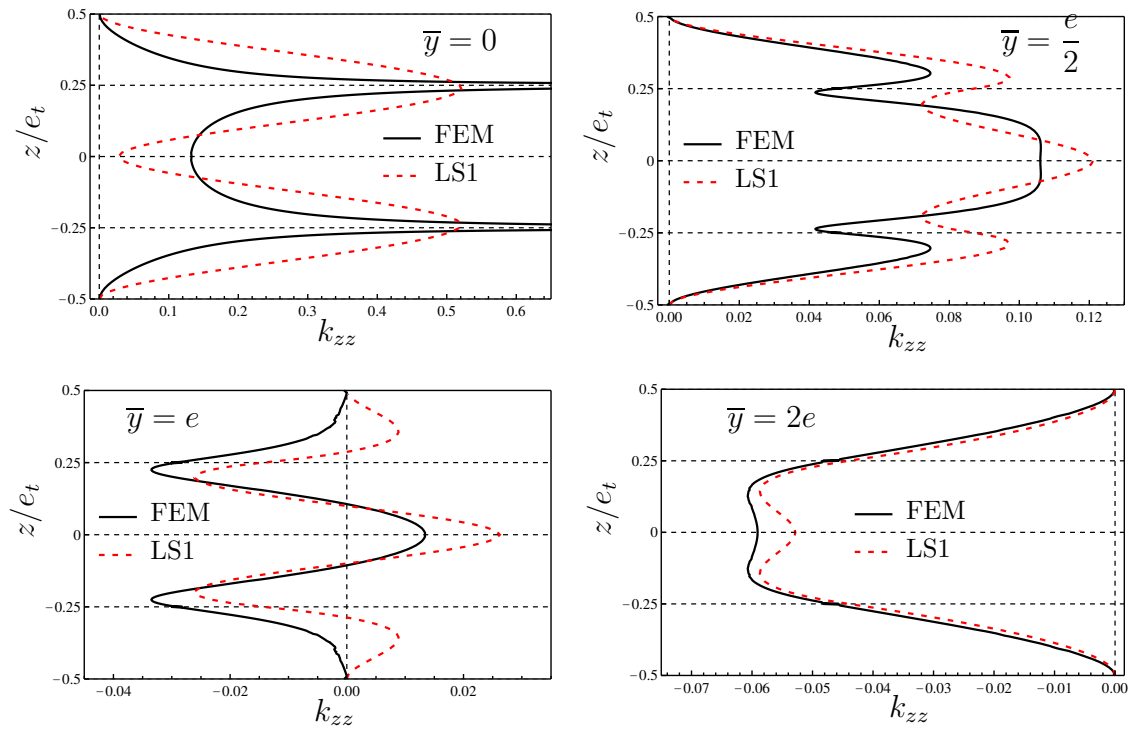


Figure 2.19: Distribution of the normal stress σ_{zz} through the thickness of $(30^\circ, 60^\circ)_s$ laminate

but it is perpendicular to the delamination plane. As a consequence, the continuity conditions are written at the level of the layers and not at the interfaces.

Based on the proposed model, a special software has been developed for the analysis of delamination in multilayered plates. This program gives quickly the analytical solution of the problem for any delamination configuration in the plate section. In order to validate the model, a $(30^\circ, 60^\circ)_s$ laminate was investigated and thorough stress comparisons were made between the LS1 model and a 3D-FEM. It was shown that the LS1 model accurately estimates all 3D stress fields everywhere except the region very close to the crack tip. Regarding the interlaminar stresses, the LS1 and 3D-FEM estimations are the same while $\bar{y} > e/4$ where \bar{y} signifies the distance from the crack tip and e is the thickness of a carbon-epoxy ply. Concerning the 3D stress fields at layers, it is concluded that for $\bar{y} > e$ (i.e. the distance from the crack tip is greater than the thickness of a carbon-epoxy ply), the LS1 results are acceptable. It should be kept in mind that the LS1 model, inspired from the Pagano's model [Pagano 1978a], is a layerwise stress model dedicated to the estimation of interlaminar stresses rather than a model for determining 3D-stress fields at layers. The comparisons between the LS1 model and the 3D-FEM regarding the interlaminar stresses, clearly show the usefulness and efficiency of the LS1 model as a layerwise stress model for delamination analyses. Nevertheless, very close to the crack tip ($\bar{y} < e/4$), the LS1 estimations of interlaminar stress singularities are not satisfying. Indeed, in the LS1 model the capture of stress singularities at free edges or crack tips is limited while in the 3D-FEM by refining the mesh, the capture of singularities can be improved.

In the second part of this paper [Saeedi et al. 2012b], it will be shown that this drawback of the LS1 model near singularities causes important errors in estimating the energy release rate for micro-cracks. A refined approach, called *refined LS1*, will be presented in the companion paper. In this approach, an efficient layerwise mesh strategy is proposed which improves extremely the 3D local estimations of the model. A complete comparison between a 3D-FE model and the refined LS1 model will show the accuracy and efficiency of the proposed model for delamination analysis of multilayered plates under uniaxial extension. It will be demonstrated that the refined LS1 model can be used as an accurate and very efficient model for evaluating the interlaminar stress fields as well as the energy release rate in the vicinity of stress singularity zones.

Appendix 2.A Expression of the 3D stress field

$$\sigma_{\alpha\beta}^i(x, y, z) = \left[\frac{1}{e^i} N_{\alpha\beta}^i(x, y) \right] P_0^i(z) + \left[\frac{12}{(e^i)^2} M_{\alpha\beta}^i(x, y) \right] P_1^i(z) \quad (2.46)$$

$$\begin{aligned} \sigma_{\alpha z}^i(x, y, z) &= \left[\frac{1}{e^i} Q_{\alpha}^i(x, y) \right] P_0^i(z) + \left[\tau_{\alpha}^{i,i+1}(x, y) - \tau_{\alpha}^{i-1,i}(x, y) \right] P_1^i(z) \\ &+ \left[\frac{1}{e^i} Q_{\alpha}^i(x, y) - \frac{1}{2} \left(\tau_{\alpha}^{i,i+1}(x, y) + \tau_{\alpha}^{i-1,i}(x, y) \right) \right] P_2^i(z) \end{aligned} \quad (2.47)$$

$$\begin{aligned} \sigma_{zz}^i(x, y, z) &= \left[\frac{\nu^{i,i+1}(x, y) + \nu^{i-1,i}(x, y)}{2} + \frac{e^i}{12} \operatorname{div} \left(\tilde{\tau}^{i,i+1}(x, y) - \tilde{\tau}^{i-1,i}(x, y) \right) \right] P_0^i(z) \\ &+ \left[-\frac{\operatorname{div} \tilde{Q}^i}{5} + \frac{e^i}{10} \operatorname{div} \left(\tilde{\tau}^{i,i+1}(x, y) + \tilde{\tau}^{i-1,i}(x, y) \right) + \left(\nu^{i,i+1}(x, y) - \nu^{i-1,i}(x, y) \right) \right] P_1^i(z) \\ &+ \left[\frac{e^i}{12} \operatorname{div} \left(\tilde{\tau}^{i,i+1}(x, y) - \tilde{\tau}^{i-1,i}(x, y) \right) \right] P_2^i(z) \\ &+ \left[-\operatorname{div} \tilde{Q}^i + \frac{e^i}{2} \operatorname{div} \left(\tilde{\tau}^{i,i+1}(x, y) + \tilde{\tau}^{i-1,i}(x, y) \right) \right] P_3^i(z) \end{aligned} \quad (2.48)$$

where:

$$\tilde{\tau}^i(x, y) = \begin{pmatrix} \tau_x(x, y) \\ \tau_y(x, y) \end{pmatrix}^i, \quad \tilde{Q}^i(x, y) = \begin{pmatrix} Q_x(x, y) \\ Q_y(x, y) \end{pmatrix}^i$$

and:

$$\begin{aligned} P_0^i(z) &= 1 \\ P_1^i(z) &= \frac{z - \bar{h}^i}{e^i} \\ P_2^i(z) &= -6 \left(\frac{z - \bar{h}^i}{e^i} \right)^2 + \frac{1}{2} \\ P_3^i(z) &= -2 \left(\frac{z - \bar{h}^i}{e^i} \right)^3 + \frac{3}{10} \left(\frac{z - \bar{h}^i}{e^i} \right) \end{aligned}$$

Appendix 2.B Analytical solution of non-delaminated multilayered plate

The 3D strain-stress relation for orthotropic linear elastic materials can be written in Voigt notation as:

$$\begin{pmatrix} \varepsilon_{xx} \\ \varepsilon_{yy} \\ \varepsilon_{zz} \\ 2\varepsilon_{yz} \\ 2\varepsilon_{xz} \\ 2\varepsilon_{xy} \end{pmatrix} = \underbrace{\begin{bmatrix} S_{11} & S_{12} & S_{13} & 0 & 0 & S_{16} \\ S_{12} & S_{22} & S_{23} & 0 & 0 & S_{26} \\ S_{13} & S_{23} & S_{33} & 0 & 0 & S_{36} \\ 0 & 0 & 0 & S_{44} & S_{45} & 0 \\ 0 & 0 & 0 & S_{45} & S_{55} & 0 \\ S_{16} & S_{26} & S_{36} & 0 & 0 & S_{66} \end{bmatrix}}_{\underline{\underline{S}}_{(x,y,z)}} \cdot \begin{pmatrix} \sigma_{xx} \\ \sigma_{yy} \\ \sigma_{zz} \\ \sigma_{yz} \\ \sigma_{xz} \\ \sigma_{xy} \end{pmatrix}$$

In the above relation, it is assumed that the normal direction is parallel to the z -axis and the longitudinal and transverse directions are located in the xy plane. The matrices $\tilde{\tilde{S}}$ and $\tilde{\tilde{S}}_Q$, and the scalar S_ν , deduced from the compliance matrix $\underline{\underline{S}}_{(x,y,z)}$, are defined as follows:

$$\tilde{\tilde{S}} = \begin{pmatrix} S_{11} & S_{12} & S_{16} \\ S_{12} & S_{22} & S_{26} \\ S_{16} & S_{26} & S_{66} \end{pmatrix} \quad ; \quad \tilde{\tilde{S}}_Q = \begin{pmatrix} S_{44} & S_{45} \\ S_{45} & S_{55} \end{pmatrix} \quad ; \quad S_\nu = S_{33}$$

As already stated, in total there are $16n - 3$ equations in which $6n - 3$ are algebraic. Therefore, it is possible to eliminate $6n - 3$ unknown fields. For this reason, the unknown fields $N_{xx}^i, M_{xx}^i, Q_x^i, \tau_x^{i,i+1}, \tau_y^{i,i+1}$ and $\nu^{i,i+1}$ are expressed in terms of the other unknown fields.

From Eq. 2.25, it is deduced:

$$N_{xx}^i = -\frac{S_{12}^i}{S_{11}^i} N_{yy}^i - \frac{S_{16}^i}{S_{11}^i} N_{xy}^i + \frac{e}{S_{11}^i} \frac{\Delta}{l} \quad ; \quad 1 \leq i \leq n \quad (2.49)$$

In the same way, from Eq. 2.26, the expression of M_{xx}^i is obtained as:

$$M_{xx}^i = -\frac{S_{12}^i}{S_{11}^i} M_{yy}^i - \frac{S_{16}^i}{S_{11}^i} M_{xy}^i \quad ; \quad 1 \leq i \leq n \quad (2.50)$$

The first equation of 2.27 and Eqs. 2.28 lead to $3n - 2$ algebraic equations. Thus, $3n - 2$ unknowns can be eliminated. To this end, the expressions of $Q_x^i, \tau_x^{i,i+1}$ and $\tau_y^{i,i+1}$ are derived as follows:

$$\underline{A} = \underline{\underline{N}}^{-1} \cdot \underline{B} \quad (2.51)$$

where:

$$\begin{aligned} (\underline{A})^t &= \left(\underbrace{Q_x^1, \dots, Q_x^n}_n, \underbrace{\tau_x^{1,2}, \dots, \tau_x^{n-1,n}}_{n-1}, \underbrace{\tau_y^{1,2}, \dots, \tau_y^{n-1,n}}_{n-1} \right) \\ (\underline{B})^t &= \left(\underbrace{\alpha^1, \dots, \alpha^n}_n, \underbrace{\beta^{1,2}, \dots, \beta^{n-1,n}}_{n-1}, \underbrace{\gamma^{1,2}, \dots, \gamma^{n,n-1}}_{n-1} \right) \end{aligned}$$

2. DELAMINATED MULTILAYERED PLATES UNDER UNIAXIAL EXTENSION. PART I:
ANALYTICAL ANALYSIS USING A LAYERWISE STRESS APPROACH

with:

$$\begin{aligned}\alpha^i &= \phi_x^i - \frac{6}{5e^i} S_{Q_{12}}^i Q_y^i \\ \beta^{i,i+1} &= u_x^{i+1} - u_x^i - \left(\frac{e^i}{2} \phi_x^i + \frac{e^{i+1}}{2} \phi_x^{i+1} \right) + \frac{1}{10} \left(S_{Q_{12}}^i Q_y^i + S_{Q_{12}}^{i+1} Q_y^{i+1} \right) \\ \gamma^{i,i+1} &= u_y^{i+1} - u_y^i - \left(\frac{e^i}{2} \phi_y^i + \frac{e^{i+1}}{2} \phi_y^{i+1} \right) + \frac{1}{10} \left(S_{Q_{22}}^i Q_y^i + S_{Q_{22}}^{i+1} Q_y^{i+1} \right)\end{aligned}$$

and $\underline{\underline{N}}$ is a $3n - 2 \times 3n - 2$ matrix as:

$$\underline{\underline{N}}_{(3n-2) \times (3n-2)} = \begin{bmatrix} \underline{\underline{N}}^1_{n \times n} & \underline{\underline{N}}^2_{n \times (n-1)} & \underline{\underline{N}}^3_{n \times (n-1)} \\ \left(\underline{\underline{N}}^2 \right)^t_{(n-1) \times n} & \underline{\underline{N}}^4_{(n-1) \times (n-1)} & \underline{\underline{N}}^5_{(n-1) \times (n-1)} \\ \left(\underline{\underline{N}}^3 \right)^t_{(n-1) \times n} & \underline{\underline{N}}^5_{(n-1) \times (n-1)} & \underline{\underline{N}}^6_{(n-1) \times (n-1)} \end{bmatrix}$$

where:

$$\begin{aligned}\underline{\underline{N}}^1_{ij} &= \frac{6}{5} \frac{S_{Q_{11}}^i}{e^i} \delta_{ij} & ; \quad (i, j) \in [1; n] \times [1; n] \\ \underline{\underline{N}}^2_{ij} &= -\frac{1}{10} S_{Q_{11}}^i (\delta_{ij} + \delta_{i,j+1}) & ; \quad (i, j) \in [1; n] \times [1; n-1] \\ \underline{\underline{N}}^3_{ij} &= -\frac{1}{10} S_{Q_{12}}^i (\delta_{ij} + \delta_{i,j+1}) & ; \quad (i, j) \in [1; n] \times [1; n-1] \\ \underline{\underline{N}}^4_{ij} &= -\frac{1}{30} \left[e^i S_{Q_{11}}^i \delta_{i,j+1} - 4 \left(e^i S_{Q_{11}}^i + e^{i+1} S_{Q_{11}}^{i+1} \right) \delta_{ij} + e^{i+1} S_{Q_{11}}^{i+1} \delta_{i,j-1} \right] & ; \quad (i, j) \in [1; n-1] \times [1; n-1] \\ \underline{\underline{N}}^5_{ij} &= -\frac{1}{30} \left[e^i S_{Q_{12}}^i \delta_{i,j+1} - 4 \left(e^i S_{Q_{12}}^i + e^{i+1} S_{Q_{12}}^{i+1} \right) \delta_{ij} + e^{i+1} S_{Q_{12}}^{i+1} \delta_{i,j-1} \right] & ; \quad (i, j) \in [1; n-1] \times [1; n-1] \\ \underline{\underline{N}}^6_{ij} &= -\frac{1}{30} \left[e^i S_{Q_{22}}^i \delta_{i,j+1} - 4 \left(e^i S_{Q_{22}}^i + e^{i+1} S_{Q_{22}}^{i+1} \right) \delta_{ij} + e^{i+1} S_{Q_{22}}^{i+1} \delta_{i,j-1} \right] & ; \quad (i, j) \in [1; n-1] \times [1; n-1]\end{aligned}$$

According to Eq. 2.29, the normal interlaminar stresses can be expressed as follows:

$$\underline{\underline{C}} = \underline{\underline{R}}^{-1} \cdot \underline{\underline{D}} \quad (2.52)$$

where:

$$\begin{aligned}(\underline{\underline{C}})^t &= (\nu^{1,2}, \nu^{2,3}, \dots, \nu^{n-1,n}) \\ (\underline{\underline{D}})^t &= (u_z^2 - u_z^1, u_z^3 - u_z^2, \dots, u_z^{n-1} - u_z^{n-2}, u_z^n - u_z^{n-1})\end{aligned}$$

and $\underline{\underline{R}}$ is a $n - 1 \times n - 1$ matrix with the following expression:

$$\begin{aligned}\underline{\underline{R}}_{ij} &= \frac{1}{70} [9 e^i S_{\nu}^i \delta_{i,j+1} + 26 (e^i S_{\nu}^i + e^{i+1} S_{\nu}^{i+1}) \delta_{ij} + 9 e^{i+1} S_{\nu}^{i+1} \delta_{i,j-1}] \\ &(i, j) \in [1; n-1] \times [1; n-1]\end{aligned}$$

Until now by using $6n - 3$ algebraic equations, the following $6n - 3$ unknown fields have been eliminated:

$$\begin{aligned} N_{xx}^i, M_{xx}^i, Q_x^i, & \quad ; \quad 1 \leq i \leq n \\ \tau_x^{i,i+1}, \tau_y^{i,i+1}, \nu^{i,i+1} & \quad ; \quad 1 \leq i \leq n - 1 \end{aligned}$$

Now, there are $10n$ first-order differential equations in terms of the following $10n$ unknown fields:

$$N_{xy}^i, N_{yy}^i, M_{xy}^i, M_{yy}^i, Q_y^i, u_x^i, u_y^i, u_z^i, \phi_x^i, \phi_y^i \quad ; \quad 1 \leq i \leq n$$

By rearranging Eqs. 2.25 and deriving with respect to y , we obtain:

$$(u_x^i)'' = \frac{1}{e^i} \left[c^i (N_{xy}^i)' + b^i (N_{yy}^i)' \right] \quad (2.53)$$

$$(u_y^i)'' = \frac{1}{e^i} \left[b^i (N_{xy}^i)' + a^i (N_{yy}^i)' \right] \quad (2.54)$$

with:

$$a^i = \left(S_{22} - \frac{(S_{12})^2}{S_{11}} \right)^i, \quad b^i = \left(S_{26} - \frac{S_{12} S_{16}}{S_{11}} \right)^i, \quad c^i = \left(S_{66} - \frac{(S_{16})^2}{S_{11}} \right)^i$$

In the same way, according to Eqs. 2.26 it is deduced:

$$(\phi_x^i)'' = \frac{12}{(e^i)^3} \left[c^i (M_{xy}^i)' + b^i (M_{yy}^i)' \right] \quad (2.55)$$

$$(\phi_y^i)'' = \frac{12}{(e^i)^3} \left[b^i (M_{xy}^i)' + a^i (M_{yy}^i)' \right] \quad (2.56)$$

Introducing the equilibrium equations (Eqs. 2.30 to 2.33) in the previous equations gives:

$$\boxed{(u_x^i)'' = \frac{1}{e^i} \left[c^i (\tau_x^{i-1,i} - \tau_x^{i,i+1}) + b^i (\tau_y^{i-1,i} - \tau_y^{i,i+1}) \right]} \quad (2.57)$$

$$\boxed{(u_y^i)'' = \frac{1}{e^i} \left[b^i (\tau_x^{i-1,i} - \tau_x^{i,i+1}) + a^i (\tau_y^{i-1,i} - \tau_y^{i,i+1}) \right]} \quad (2.58)$$

$$\boxed{(\phi_x^i)'' = \frac{12}{(e^i)^3} \left[c^i \left(Q_x^i - \frac{e^i}{2} (\tau_x^{i-1,i} + \tau_x^{i,i+1}) \right) + b^i \left(Q_y^i - \frac{e^i}{2} (\tau_y^{i-1,i} + \tau_y^{i,i+1}) \right) \right]} \quad (2.59)$$

$$\boxed{(\phi_y^i)'' = \frac{12}{(e^i)^3} \left[b^i \left(Q_x^i - \frac{e^i}{2} (\tau_x^{i-1,i} + \tau_x^{i,i+1}) \right) + a^i \left(Q_y^i - \frac{e^i}{2} (\tau_y^{i-1,i} + \tau_y^{i,i+1}) \right) \right]} \quad (2.60)$$

Now, the second equation of 2.27 is written as:

$$(u_z^i)' = -\phi_y^i + \frac{6}{5e^i} \left\{ S_{Q12}^i \left[Q_x^i - \frac{e^i}{12} (\tau_x^{i-1,i} + \tau_x^{i,i+1}) \right] + S_{Q22}^i \left[Q_y^i - \frac{e^i}{12} (\tau_y^{i-1,i} + \tau_y^{i,i+1}) \right] \right\}$$

To eliminate u_z^i , the system 2.52 is derived with respect to y in which the previous expression of $(u_z^i)'$ is introduced; so the expression of $(\nu^{i,i+1})'$ is obtained as:

$$(\underline{C})' = \underline{R}^{-1} \cdot (\underline{D})'$$

Deriving the last equilibrium equation (Eq. 2.34) yields:

$$\boxed{(Q_y^i)'' = (\nu^{i-1,i})' - (\nu^{i,i+1})'} \quad (2.61)$$

In which the expressions of $(\nu^{i,i+1})'$ is injected.

In this way, a system of $5n$ second-order equations is extracted as follows:

$$\underline{X}'' = \underline{M} \cdot \underline{X} \quad (2.62)$$

where:

$$\underline{X} = \left(\underbrace{\bar{u}_x^1, \dots, \bar{u}_x^n}_n, \underbrace{\bar{u}_y^1, \dots, \bar{u}_y^n}_n, \underbrace{\phi_x^1, \dots, \phi_x^n}_n, \underbrace{\phi_y^1, \dots, \phi_y^n}_n, \underbrace{\bar{Q}_y^1, \dots, \bar{Q}_y^n}_n \right)^t \quad (2.63)$$

where \underline{X} is the unknown vector of dimension $5n$ constituted of the following dimensionless variables:

$$\bar{u}_x^i = \frac{u_x^i}{\bar{e}} \quad , \quad \bar{u}_y^i = \frac{u_y^i}{\bar{e}} \quad , \quad \phi_x^i \quad , \quad \phi_y^i \quad , \quad \bar{Q}_y^i = \frac{Q_y^i}{\bar{e} \bar{G}}$$

with:

$$\bar{e} = \frac{1}{n} \sum_{i=1}^n e^i \quad , \quad \bar{G} = \frac{1}{n} \sum_{i=1}^n \frac{G_{LN}^i + G_{TN}^i}{2}$$

The components of the matrix \underline{M} are deduced from Eqs. 2.57 to 2.61. To impose the boundary conditions, they should be expressed in terms of principal unknowns of the final system of equations. Injecting the boundary conditions 2.37 into the constitutive equations 2.14 and 2.15 provides the following $10n$ boundary conditions:

$$\begin{aligned} (u_x^i)'(\pm b) &= \frac{\Delta S_{16}^i}{l S_{11}^i} \quad , \quad (u_y^i)'(\pm b) = \frac{\Delta S_{12}^i}{l S_{11}^i} \\ (\phi_x^i)'(\pm b) &= 0 \quad , \quad (\phi_y^i)'(\pm b) = 0 \quad , \quad Q_y^i(\pm b) = 0 \end{aligned} \quad (2.64)$$

Appendix 2.C Analytical solution of delaminated multilayered plate - a single interfacial crack

The interface $k, k + 1$ is completely delaminated, thus:

$$\tau_x^{k,k+1} = 0 \quad , \quad \tau_y^{k,k+1} = 0 \quad , \quad \nu^{k,k+1} = 0 \quad (2.65)$$

The interlaminar stresses $\tau_x^{k,k+1}$ and $\tau_y^{k,k+1}$ are known and should be eliminated from the system 2.51. Consequently, the system 2.51 is rewritten as:

$$\underline{A}_d = \underline{N}_d^{-1} \cdot \underline{B}_d \quad (2.66)$$

with:

$$\begin{aligned} (\underline{A}_d)^t &= \left(\underbrace{Q_x^1, \dots, Q_x^n}_n, \underbrace{\tau_x^{1,2}, \dots, \tau_x^{k-1,k}, \tau_x^{k+1,k+2}, \dots, \tau_x^{n-1,n}}_{n-2}, \underbrace{\tau_y^{1,2}, \dots, \tau_y^{k-1,k}, \tau_y^{k+1,k+2}, \dots, \tau_y^{n-1,n}}_{n-2} \right) \\ (\underline{B}_d)^t &= \left(\underbrace{\alpha^1, \dots, \alpha^n}_n, \underbrace{\beta^{1,2}, \dots, \beta^{k-1,k}, \beta^{k+1,k+2}, \dots, \beta^{n-1,n}}_{n-2}, \underbrace{\gamma^{1,2}, \dots, \gamma^{k-1,k}, \gamma^{k+1,k+2}, \dots, \gamma^{n,n-1}}_{n-2} \right) \end{aligned}$$

where the index d signifies the delaminated case. The matrix \underline{N}_d of dimensions $(3n - 4) \times (3n - 4)$ is deduced from the matrix \underline{N} by eliminating the lines and the columns corresponding to $\tau_x^{k,k+1}$ and $\tau_y^{k,k+1}$ (Lines and columns $n + k$ and $2n - 1 + k$).

Similarly, the interlaminar stress $\nu^{k,k+1}$ should be eliminated from the system 2.52 which gives:

$$\underline{C}_d = \underline{R}_d^{-1} \cdot \underline{D}_d \quad (2.67)$$

with:

$$\begin{aligned} (\underline{C}_d)^t &= (\nu^{1,2}, \dots, \nu^{k-1,k}, \nu^{k+1,k+2}, \dots, \nu^{n-1,n}) \\ (\underline{D}_d)^t &= (u_z^2 - u_z^1, \dots, u_z^k - u_z^{k-1}, u_z^{k+2} - u_z^{k+1}, \dots, u_z^n - u_z^{n-1}) \end{aligned}$$

The matrix \underline{R}_d of dimensions $(n - 2) \times (n - 2)$ is deduced from the matrix \underline{R} by eliminating the line and the column corresponding to $\nu^{k,k+1}$ (Line and column k).

By obtaining the expressions of the unknown fields Q_x^i , $\tau_x^{i,i+1}$, $\tau_y^{i,i+1}$ and $\nu^{i,i+1}$ via the systems 2.66 and 2.67, and introducing them into Eqs. 2.57 to 2.61 the system of equations 2.41 is derived. It is noted that the expression of the vector \underline{X} herein, is the same as 2.63.

Finally, the constitutive equations corresponding to the interface $k, k + 1$ (Eqs. 2.39 and 2.40) can be used in order to calculate the discontinuity displacements fields $\gamma_x^{k,k+1}$, $\gamma_y^{k,k+1}$ and $\gamma_z^{k,k+1}$.

Appendix 2.D Analytical solution of delaminated multilayered plate - several interfacial cracks

The solution of the problem in each zone is given in Eq. 2.35 for non-delaminated zones or in Eq. 2.41 for delaminated zones. For non-delaminated zones, the solution is

already obtained in Appendix 2.B. For the delaminated zones, the solution is found in the case of a single interfacial crack (see Appendix 2.C). Herein, there may be several delaminated interfaces in each zone. The solving method in multi-delaminated case is the same as that used in Appendix 2.C. In this way, there will be the same equations as 2.66 and 2.67 except that the expressions of the vectors \underline{A}_d , \underline{B}_d , \underline{C}_d , \underline{D}_d and the matrices $\underline{\underline{N}}_d$, $\underline{\underline{R}}_d$, which are obtained as follows:

For each delaminated interface such as $k, k + 1$:

- The vectors \underline{A}_d , \underline{B}_d are deduced from the vectors \underline{A} , \underline{B} by eliminating the components $n + k$ and $2n - 1 + k$
- The matrix $\underline{\underline{N}}_d$ is deduced from the matrix $\underline{\underline{N}}$ by eliminating the lines and the columns $n + k$ and $2n - 1 + k$
- The vectors \underline{C}_d , \underline{D}_d are deduced from the vectors \underline{C} , \underline{D} by eliminating the component k
- The matrix $\underline{\underline{R}}_d$ is deduced from the matrix $\underline{\underline{R}}$ by eliminating the line and the column k

Chapter 3

Delaminated multilayered plates under uniaxial extension. Part II: Efficient layerwise mesh strategy for the prediction of delamination onset

La solution analytique du modèle LS1 pour l'analyse des plaques multicouches délaminiées a été obtenue dans le chapitre 2. Nous avons montré que le modèle LS1 donne une bonne approximation des contraintes intralaminaires et interlaminaires dans des plaques délaminiées et non-délaminiées. Cependant, dans les zones où il y a des singularités de contraintes, comme les bords libres et les pointes de fissures, la précision du modèle est discutable par rapport à la solution 3D. Des contraintes interlaminaires ainsi que le taux de restitution d'énergie ne sont pas très précis et par conséquent, le modèle LS1 ne peut pas être utilisé facilement avec différents critères de délamination. C'est la raison pour laquelle, [Diaz Diaz and Caron \[2006a\]](#), [Diaz Diaz et al. \[2007b\]](#) ont proposé un critère d'initiation de délamination de type $\tau = \tau^c$ basé sur la valeur de contrainte interlaminaire au bord libre obtenue par le modèle. Cette valeur, théoriquement singulière, dépend du modèle et du raffinement considéré dans la modélisation. Par conséquent, la contrainte critique identifiée τ^c dépend de la modélisation. Afin d'améliorer les approximations du modèle LS1, nous proposons une sorte de discrétisation dans l'épaisseur de chaque couche physique, ce qu'on appelle le maillage layerwise. Le modèle raffiné, nommé le modèle LS1 raffiné, donne pratiquement les mêmes résultats que des éléments finis 3D en termes de contraintes interlaminaires et de taux de restitution d'énergie. Par conséquent, le modèle proposé peut être utilisé comme une alternative précise et efficace aux éléments finis 3D, ce qui nous permet d'utiliser sans problème des critères de délamination 3D en contrainte et/ou en énergie. Ici, un double critère à la fois en contrainte et en énergie [[Martin et al. 2010](#)] est utilisé pour étudier l'initiation de délamination en mode III dans des plaques composites.

Ce chapitre est la deuxième partie d'un article en deux parties publié dans la revue "International Journal of Solids and Structures" sous la référence [Saeedi et al. \[2012b\]](#).

Contents

3.1 Introduction	109
3.1.1 Analytical methods	110
3.1.2 Numerical methods	111
3.1.3 Present study	112
3.2 Problem description and LS1 Solution	114
3.3 An efficient layerwise mesh strategy	116
3.4 Numerical validation and discussion	118
3.4.1 Layerwise mesh influence	118
3.4.1.1 Free edge singularity	119
3.4.1.2 Crack tip singularity	119
3.4.1.3 Energy release rate	121
3.4.2 Finite element comparison	121
3.4.2.1 Non-delaminated state	124
3.4.2.2 Delaminated state	125
3.4.2.3 Delamination initiation criterion - Experimental comparison	127
3.4.3 Discussion	129
3.5 Conclusion	130
Appendix 3.A Crack tip stress singularity curves for $a = e$ and $a = 10e$	132

Abstract

In the first part [Saeedi et al. 2012a] of this two-part paper, a layerwise stress model, called the *LS1* model, has been extended to the analysis of delaminated multilayered plates subjected to uniaxial extension. The LS1 analytical solutions of general delaminated multilayered plates have been derived and compared to three-dimensional finite element method (3D-FEM) solutions. It has been proved that there is a good agreement between the LS1 and 3D-FEM models except very near singularities (free edges, crack tips,...). In order to overcome the drawback of the LS1 model in the vicinity of singularities, a refinement approach, called the *refined LS1* is proposed in this part. Based on an irregular layerwise mesh, the refined LS1 model is applied to the prediction of the delamination onset in angle-ply composite laminates. The comparison between the refined LS1 and 3D-FE models reveals an excellent agreement in terms of interlaminar stresses and strain energy release rate, even very close to singularities. The proposed refined LS1 model can be used as an accurate and very efficient model for the prediction of initiation and propagation of delamination in multilayered plates under uniaxial extension using stress based or energy release rate based criteria.

keyword: Multilayer; Layerwise model; Delamination; Interlaminar stresses; Energy release rate

3.1 Introduction

The free-edge delamination is one of the major issues in design and analysis of multilayered structures such as composite laminates. The difference of the elastic properties of two adjacent layers in composite materials can produce high interlaminar stresses in multilayered structures in the vicinity of free edges and crack tips. These stress concentrations that in theory are singular at free edges and crack tips, could trigger the delamination of the multilayer which might lead to global failure. One of the most widespread delamination cases in the literature is free-edge delamination in composite laminates under uniaxial tensile loading. Various approaches such as asymptotic analysis show that the free-edge effects in composite laminates provoke high interlaminar stresses at the free edges [Wang and Choi 1982a,b, Leguillon and Sanchez-Palencia 1987, Leguillon 1999]. Leguillon [1999] showed that in rectangular $(\pm\theta)_s$ laminates, the interlaminar stress components at the interface $\theta/ - \theta$ behave like $r^{\lambda-1}$ near the free edges where r is the distance from the free edge and λ is the singularity exponent ($0 < \lambda < 1$). According to [Martin et al. 2010], the singularity exponent λ takes values close to one. For $(\pm 10^\circ)_s$ and $(\pm 20^\circ)_s$ rectangular laminates with G947/M18 carbon-epoxy plies $\lambda = 0.999$ and $\lambda = 0.991$ respectively for $(\pm 10^\circ)_s$ and $(\pm 20^\circ)_s$ rectangular laminates with G947/M18 carbon-epoxy plies, which shows that the singularity is quite weak. It has already been shown that the classical lamination theory (CLT) is unable of predicting interlaminar stress singularities near the free edges of laminates. Therefore, a large amount of researches is dedicated to the study of interlaminar stresses at free edges of laminated materials. Due to the complexity of the problem in the general case, there is no exact solution to this problem except in some simple cases. Consequently, many

various approximate analytical and numerical methods have been developed worldwide to overcome this inability of CLT in calculating interlaminar stress concentrations in the vicinity of free edges and crack tips.

The delamination problem in multilayered structures has been studied by many investigators. In [Shen and Grady 1992], the authors analyzed the dynamic characteristics of a delaminated composite beam using the Timoshenko beam theory. Ju et al. [1995] presented a finite element formulation based on the Mindlin plate theory for the free vibration analysis of multi-delaminated composite plates. In [Amrutharaj et al. 1996], the authors used a fracture process zone to study the edge delamination of symmetrical angle-ply laminates under uniaxial tension. By using a layerwise theory, Lee [2000] developed a finite element method for the free vibration analysis of a delaminated composite beam. In [Lindemann and Becker 2002], different approaches were used for the assessment of the delamination tendency in laminates under extensional loading. In [Barbero and Reddy 1991], the layer-wise laminate theory of Reddy was extended to account for multiple delaminations between layers. Chattopadhyay and Gu [1994] used a higher order theory for modeling delamination in composite plates and shells of moderately thick construction. Dakshina Moorthya and Reddy [1998] developed a layerwise finite element with enhanced strains for the analysis of laminates with delaminations. Krueger and O'Brien [2001] carried out a three-dimensional shell modeling technique for the analysis of delamination in mode I, mode II and mixed mode I/II. In [Cho and Kim 2001, Kim and Cho 2002, Oh et al. 2008], the authors developed a shell finite element based on a higher order zigzag theory for the analysis of delaminated composite shells. By modeling laminated structures as an assembly of sub-laminates connected through their interfaces, Zou et al. [2002] presented a 2D model for progressive delamination in laminated composite structures. In [Lorriot et al. 2003], the authors studied the onset of free-edge delamination in composite laminates under tensile loading using the classical thin laminate theory with an asymptotic method for local stress tensor correction near the edge.

3.1.1 Analytical methods

In general, the analytical solutions can be classified as either equivalent single-layer theories (ESL) or layerwise theories. In both cases, the 3D elasticity problem is reduced to a 2D problem. The equivalent single-layer methods consist in treating the heterogeneous multilayered laminate as a homogeneous single-layer plate having equivalent effective elastic properties. Since the number of governing equations is independent of the total number of the layers, the ESL methods are relatively simple and computationally efficient. These methods generally provide acceptable results for global response of laminates but their results are not accurate enough near the edges. On the other hand, in layerwise methods the number of governing equations depends on the number of the layers. Thus, these methods are generally more sophisticated and computationally more intensive but they can provide very accurate results. Consequently, they are one of the best alternatives to 3D models. The reader can refer to [Carrera 2004] for a complete review of these approaches.

One of the first approximate solutions of interlaminar stresses was obtained by Pipes and Pagano [1974] for the analysis of interlaminar stresses in a uniformly extended symmetric angle-ply laminate. Later, Pagano [1974] applied a higher-order shear deformation theory to take into account the interlaminar normal stress in symmetric cross-ply laminates. By using an ESL method with simple stress approximations, Whitney and Sun [1973] evaluated the free-edge stresses in composite laminates. Tang and Levy [1975a] used a boundary-layer theory to analyze a symmetric angle-ply laminate under uniaxial tension, which could determine all the interlaminar stresses close to free edges. By means of complex series expansion method, Wang and Choi [1982a,b] studied the stress singularity at the boundary regions of a composite laminate. Whitney [1997] used higher-order plate theories for evaluating stress fields at free edges. By using the first-order shear deformation theory of plates and Reddy's layerwise theory, Nosier and Bahrami [2007] studied interlaminar stresses in antisymmetric angle-ply laminates under extensional and torsional loads. Nosier and Maleki [2008] employed an improved first-order shear deformation theory with Reddy's layerwise displacement approach to analyze free-edge stresses in general composite laminates subjected to extension loading. Pagano [1978a,b] also developed an approximate analytical stress approach based on Reissner variational principle to predict stress fields in composite laminates. By taking a direct inspiration from Pagano's model [Pagano 1978a], a layerwise stress model was proposed by Ehlacher et al., previously called the *Multiparticle Model of Multilayered Materials (M4)* [Naciri et al. 1998, Carreira et al. 2002, Diaz Diaz et al. 2002, Caron et al. 2006, Dallot and Sab 2008b, Diaz Diaz and Caron 2006a, Nguyen and Caron 2006]. Via this 2D layerwise model, the multilayered material is considered as a superposition of Reissner-Mindlin plates linked together by interfacial stresses. In order to make reference to Carrera's nomenclature proposed in [Carrera 2004], this model is described as a *LS1* approach which signifies a layerwise stress approach with first-order membrane stress approximations per layer in thickness direction. The main difference between the LS1 and other layerwise models is that, most often, the layerwise models are either displacement approaches or mixed displacement-stress approaches while the LS1 model, inspired from Pagano's model [Pagano 1978a], is a pure layerwise stress approach where there is no hypothesis on displacement fields. Diaz Diaz et al. [2002] used the LS1 model to evaluate interfacial stresses in symmetrical laminates under tensile loading with free edges. Caron et al. [2006] applied this model to the prediction of mode III delamination in multi-layered materials. In [Dallot and Sab 2008b], the authors employed the LS1 model for analyzing a sandwich plate under cylindrical bending and demonstrated the capacity of this model to capture the plastic collapse modes.

3.1.2 Numerical methods

The delamination problems have also been approached by various numerical methods such as finite difference methods, 2D and 3D finite element methods, combined 2D-3D finite element methods, boundary layer techniques, etc. Pipes and Pagano [1970] used a finite difference method in order to solve the two-dimensional governing equations. Wang and Crossman [1977a,b] suggested a quasi-three-dimensional finite element

method to calculate interlaminar stresses in the vicinity of free edges in symmetric laminates under uniaxial traction and uniform temperature variations. By using a layerwise laminate theory, [Robbins and Reddy \[1993\]](#) presented a displacement global-local finite element method for the modeling of thick composites. [Tian et al. \[2004\]](#) employed a hybrid finite element formulation to estimate interlaminar stresses in symmetric balanced laminates. [Carreira et al. \[2002\]](#) made use of 3D finite element calculations to validate the layerwise stress model (LS1) for the estimation of interlaminar stresses in symmetric composite laminates subjected to uniaxial extension. [Nguyen and Caron \[2006, 2009\]](#) presented a new finite element formulation based on the LS1 model for the analysis of free-edge stresses in composite laminates under mechanical and thermal loading. In [\[Duong et al. 2011\]](#) the authors proposed a layerwise finite element formulation for the analysis of multilayers with imperfect interfaces.

3.1.3 Present study

The objective of this two-part paper is to present an efficient and accurate model which can be used instead of 3D finite element models for the analysis of delaminated multilayered plates under tensile loading. In the first part of this study, the layerwise stress model (LS1) was extended to the analysis of multi-delaminated multilayered plates subjected to uniaxial extension and the analytical LS1 solutions were obtained. By means of a 3D-FE comparison, it was shown that the LS1 model reproduces quite well the 3D stress fields far from singularities. However, in the vicinity of singularities, the estimations are not accurate enough. Moreover, as it will be shown in the next sections, the LS1 model can result into large errors in the estimation of energy release rate for small cracks. Specifically, contrary to the theory of elasticity, the LS1 model yields a non-zero value of energy release rate for a crack of zero length ($G(a) \rightarrow 0$ if $a \rightarrow 0$). In order to overcome this drawback, an efficient layerwise mesh strategy for the LS1 model is adopted and proposed in this part. This refined approach, called *refined LS1*, improves considerably stress and energy release rate estimations.

According to the classical theory of elasticity, the stress fields at free edges and crack tips are singular and thus searching for the stress values by numerical methods at these points are meaningless. However, in the vicinity of singularity points, the stress values are finite so that by refining the mesh sufficiently, it is possible to obtain better approximation of the stress values. It should be noticed that many delamination criteria such as average stress criteria [[Lagunegrand et al. 2006](#), [Kim and Soni 1984, 1986](#), [Brewer and Lagace 1988](#), [Whitney and Nuismer 1974](#), [Lorriot et al. 2003](#), [Wimmer et al. 2009](#)] or the twofold strength and toughness delamination criterion proposed by [Martin et al. \[2010\]](#), are based on stress distribution close to singularity. To apply such delamination criteria, accurate estimations of stress fields near singularity points are necessary. As discussed in the first part, the LS1 model is very useful for estimating global response of multilayers; but its results are not accurate enough very close to singularities. Indeed, like the other 2D layerwise models, the LS1 model yields finite values for singular fields and the accuracy of the model in singularity zones is limited. In this part a layerwise mesh strategy is proposed which allows us to increase the accuracy

of the model as needed. The idea is to consider a layerwise mesh in which each *physical layer* is subdivided through the thickness and modeled by a number of *mathematical layers* to achieve the required accuracy (see Fig. 3.3). Indeed, there is a mesh concept in the thickness; it means that depending on the required accuracy, the layerwise mesh is chosen. The better the layerwise mesh is, the more accurate the results are. It should be remarked that the number of equations in layerwise models depends on the number of the layers. Therefore, there should not be a large number of mathematical layers in the model, because if an extremely refined mesh is used, the number of equations would increase enormously and the use of the layerwise model is not justified against 3D models. Consequently, the layerwise mesh strategy should take into consideration both efficiency and accuracy.

Concerning the LS1 model, Diaz Diaz and Caron [2006a] considered one mathematical layer per physical layer and proposed a maximum stress criterion of type $\tau^{max} = \tau^c$ for the delamination onset in which τ^{max} is the interlaminar shear stress at free edge. It is noted that contrary to the 3D theory, the stress field obtained by the LS1 model is not singular at free edge. In [Diaz Diaz et al. 2007a] by determining the energy release rate expression, the authors proposed an energetic criterion of type $G = G^c$ for the delamination initiation where G denotes the LS1 energy release rate value corresponding to an interfacial crack of length zero. They proved that for a mode III delamination problem, modeled by the LS1 model, the two criteria are equivalent. Since these criteria are based on the edge values in the model, the identified critical values G^c and τ^c depend on the model (specifically on the thickness of mathematical layers) and are not intrinsic to the material. As a consequence, if the layerwise mesh fineness changes, a new identification should be performed. Instead of using these delamination criteria which depend on the LS1 modeling, it is suggested in this work to use stress based or energy release rate based criteria which are intrinsic to the material. In fact, the refined LS1 model in this note is a calculation method like the 3D-FEM which can be used with any delamination criterion. In this paper, the twofold strength and toughness criterion proposed by Martin et al. [2010] is used for the prediction of delamination onset in composite laminates.

The initiation of delamination is studied in $(\pm\theta)_s$ carbon-epoxy composite laminates submitted to uniaxial extension loading. The LS1 modeling is performed by means of the dedicated software based on the LS1 analytical solution presented in the first part of this work. The influence of the proposed irregular layerwise mesh on convergence rate and accuracy is investigated by comparing the results of the LS1 model (with regular layerwise mesh) and the refined LS1 model (with the proposed irregular layerwise mesh). In order to validate our model, a 3D finite element modeling is performed using the commercial software Abaqus. Once the validity of the finite element calculations is ensured, the LS1, refined LS1 and 3D-FE results are compared in terms of interlaminar stresses and energy release rate. The comparisons reveal excellent agreements between the results of the refined LS1 and 3D-FE models even very close to singularity points. Consequently, the refined LS1 model (via the developed software for the analytical LS1 solutions) can be used as an accurate and very efficient alternative to the 3D-FEM for the prediction of delamination onset in multilayered plates under tensile loading.

3.2 Problem description and LS1 Solution

A general $(\theta_1, \theta_2, \dots, \theta_n)$ multilayered rectangular plate with a length of $2l$, a width of $2b$ and a thickness of $\sum_{i=1}^n e^i = 2h$, respectively, in the x , y and z directions is considered (Fig. 3.1). It is assumed that the middle plane of the plate is located at $z = 0$. The behavior of all layers is considered orthotropic. The plate is subjected to uniaxial strain $\varepsilon_{xx} = \Delta/l$. It is assumed that the plate is long in the x direction ($l \gg b \gg h$) so that the strain and stress components are independent of the x -coordinate far from the ends $x = \pm l$. The LS1 model (Layerwise Stress model with first-order membrane stress approximations per layer) is used to solve this problem. In this section, the LS1 model and its application for the analysis of multi-delaminated multilayered plates under uniaxial extension are briefly presented. The reader can refer to the first part of this paper for more details.

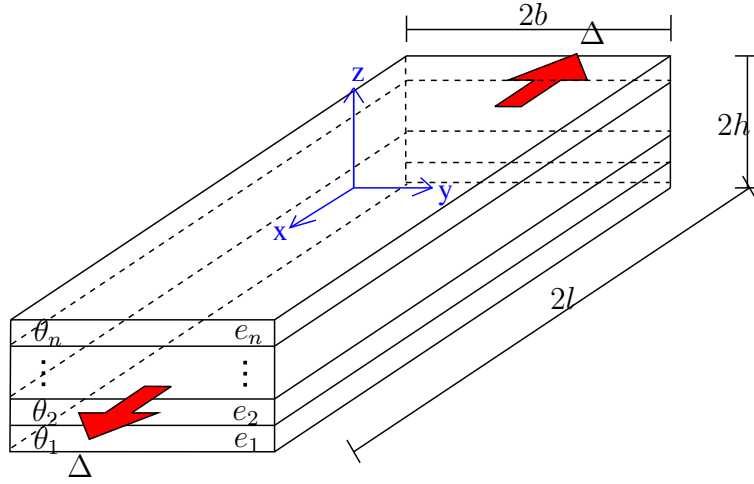


Figure 3.1: Laminate geometry; imposed displacements and coordinate system

The model is a superposition of Reissner-Mindlin plates linked together by interfacial stresses. Indeed, each layer i is considered as a Reissner-Mindlin plate with three displacement fields $U_x^i(x, y)$, $U_y^i(x, y)$, $U_z^i(x, y)$ and two rotation fields $\Phi_x^i(x, y)$, $\Phi_y^i(x, y)$. As presented in Table 3.1, the generalized stresses (in-plane stress resultants $N_{\alpha\beta}^i$, moment resultants $M_{\alpha\beta}^i$ and out-of-plane shear resultants Q_α^i) and the generalized strains of each layer are like to those of the Reissner-Mindlin plate theory. It is noted that Greek alphabet subscripts α and β correspond to $\{x, y\}$.

In addition to the generalized stresses through the thickness of layers, there are three interlaminar stresses (two shear interlaminar stresses $\tau_x^{i,i+1}$, $\tau_y^{i,i+1}$ and one normal interlaminar stress $\nu^{i,i+1}$) at each interface. Via interfacial constitutive relations of the model, these generalized interlaminar stresses are related to the generalized interlaminar strains defined in Table 3.2.

Now, a general multi-delamination state in the section of the plate is considered in which there can be several interfacial cracks with different lengths in the y direction. As shown schematically in Fig. 3.2, the solving method consists in dividing vertically the

Table 3.1: Generalized stresses and generalized strains of layer i

Generalized Stress	Generalized Strain
$N_{\alpha\beta}^i$	$\varepsilon_{\alpha\beta}^i = \frac{1}{2} (U_{\alpha,\beta}^i + U_{\beta,\alpha}^i)$
$M_{\alpha\beta}^i$	$\chi_{\alpha\beta}^i = \frac{1}{2} (\Phi_{\alpha,\beta}^i + \Phi_{\beta,\alpha}^i)$
Q_{α}^i	$d_{\Phi_{\alpha}}^i = \Phi_{\alpha}^i + U_{z,\alpha}^i$

Table 3.2: Generalized stresses and generalized strains of interface $i, i + 1$

Generalized Stress	Generalized Strain
$\tau_{\alpha}^{i,i+1}$	$D_{\alpha}^{i,i+1} = U_{\alpha}^{i+1} - U_{\alpha}^i - \left(\frac{e^i}{2} \Phi_{\alpha}^i + \frac{e^{i+1}}{2} \Phi_{\alpha}^{i+1} \right)$
$\nu^{i,i+1}$	$D_z^{i,i+1} = U_z^{i+1} - U_z^i$

laminated section following the y direction at every crack tip. In this way, the laminate is divided into some sublaminates (some zones).

Using the strain-displacement compatibility, constitutive and equilibrium equations, and enforcing the delamination conditions (zero interlaminar stresses at delaminated interfaces) leads to a system of $5n$ second-order differential equations for each zone. By applying the eigenvector expansion method, the governing system of equations in each zone is solved. Knowing that there may be complex and repeated eigenvalues, the analytical solution of the system of equations will be in the form of exponential, trigonometric and polynomial functions. For q zones, there are q systems of equations. Therefore, there will be $10n \times q$ second-order differential equations and so $10n \times q$ unknown integration constants. In order to determine these constants, $10n \times q$ conditions are needed. There are $10n$ limit conditions (herein, free-edge conditions) at the edges $y = \pm b$. Moreover, there are $10n$ stress and displacement continuity conditions between every two adjacent zones. Therefore, in total $10n + 10n \times (q - 1) = 10n \times q$ conditions are obtained. These conditions yield a system of $10n \times q$ linear algebraic equations with $10n \times q$ unknown constants which can be easily solved.

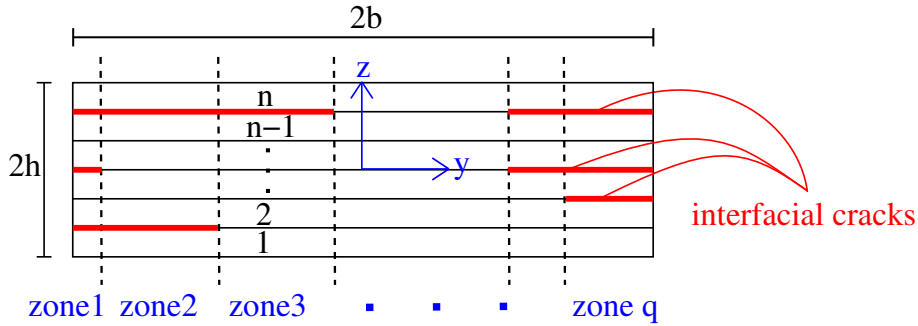


Figure 3.2: Laminate section with several cracks at different interfaces - Subdivision in the section

3.3 An efficient layerwise mesh strategy

In the first part of this paper, it was assumed that each physical layer corresponds to one layer in the LS1 model. It was shown that this modeling results to accurate estimations of the interlaminar stresses except in the vicinity of singularities. In the next section, it will be illustrated that this type of modeling also can produce significant errors in terms of energy release rate in the case of small cracks. This drawback of the LS1 model leads to a non-zero energy release rate for a crack of zero length ($G(a) \rightarrow 0$ if $a \rightarrow 0$). Thus, it is necessary to improve the LS1 estimations close to singularity points in order to be able to apply stress based or energy release rate based delamination criteria.

The approach consists in subdividing each *physical layer* through the thickness into a number of *mathematical layers* in the model. This refinement strategy through the thickness of the laminate, called *layerwise mesh* in this study, allows us to increase the accuracy of the model. It is clear that by refining the layerwise mesh (i.e., increasing the number of mathematical layers per physical layer), the accuracy of the model is improved so that if the layerwise mesh is infinitely refined, the LS1 solution will converge to the exact solution of the problem. However, both accuracy and efficiency concepts should be considered in the mesh refinement strategy. Some layerwise approaches in the literature used the subdivision of physical layers through the plate thickness [Nosier and Maleki 2008, Mittelstedt and Becker 2008, Malekzadeh et al. 2008a,b]. Based on the Reddy's layerwise theory, all these studies, used a regular layerwise mesh in which each physical layer is modeled by some mathematical layers with the same thickness. As regards the LS1 model, Diaz Diaz and Caron [2006a] proposed the same subdivision strategy for the LS1 model. Here we propose an irregular progressive mesh strategy in which the thicknesses of the mathematical layers are reduced in the vicinity of the physical interfaces as shown schematically in Fig. 3.3. This proposed strategy is the fruit of an investigation of different mesh topologies for the refinement in the thickness direction. According to this layerwise mesh strategy, the thicknesses of the mathematical layers are in the form of a geometric progression. In other words if the thickness of the mathematical layer beside the physical interface are set equal to h_{min} , the thicknesses of the next layers will be equal to $r \times h_{min}$, $r^2 \times h_{min}, \dots$ where r is the common

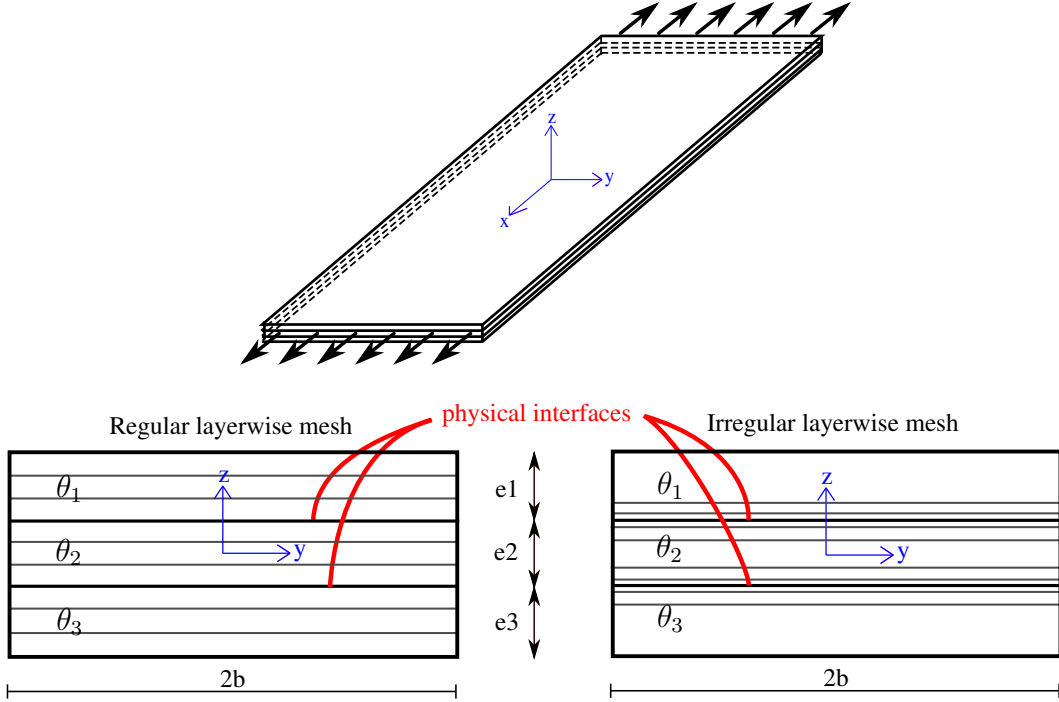


Figure 3.3: Laminate under uniaxial extension; irregular and regular layerwise mesh through the thickness

ratio of the geometric progression. It should be mentioned that if two adjacent physical layers are composed of the same material with identical orientation, it is not necessary to refine the mesh near the interface and such interface is not considered as a physical interface in the mesh strategy. By assuming that there are p mathematical layers per physical layer, two cases are distinguished:

- Physical layer with one physical interface

$$h_1 = h_{min} \ ; \ h_2 = r \times h_{min} \ \dots \ h_p = r^{p-1} \times h_{min}$$

$$\sum_{i=1}^p h_i = e \implies \boxed{1 + r + r^2 + \dots + r^{p-1} = \frac{e}{h_{min}}}$$

- Physical layer with two physical interfaces

– p is an even number

$$h_1 = h_p = h_{min} \ ; \ h_2 = h_{p-1} = r \times h_{min} \ \dots \ h_{\frac{p}{2}} = h_{\frac{p}{2}+1} = r^{\frac{p}{2}-1} \times h_{min}$$

$$\sum_{i=1}^p h_i = e \implies \boxed{2 \times \left(1 + r + r^2 + \dots + r^{\frac{p}{2}-1}\right) = \frac{e}{h_{min}}}$$

– p is an odd number

$$h_1 = h_p = h_{min} \ ; \ h_2 = h_{p-1} = r \times h_{min} \ \dots \ h_{\frac{p+1}{2}} = r^{\frac{p-1}{2}} \times h_{min}$$

$$\sum_{i=1}^p h_i = e \implies \boxed{2 \times \left(1 + r + r^2 + \dots + r^{\frac{p-3}{2}}\right) + r^{\frac{p-1}{2}} = \frac{e}{h_{min}}}$$

where e is the thickness of the physical layer. By choosing the ratio e/h_{min} and the number of mathematical layers per physical layer p (in the previous formulas), the thickness ratio r between the adjacent mathematical layers is easily calculated. Fig. 3.4 shows schematically the proposed progressive layerwise mesh through the physical layer thickness.

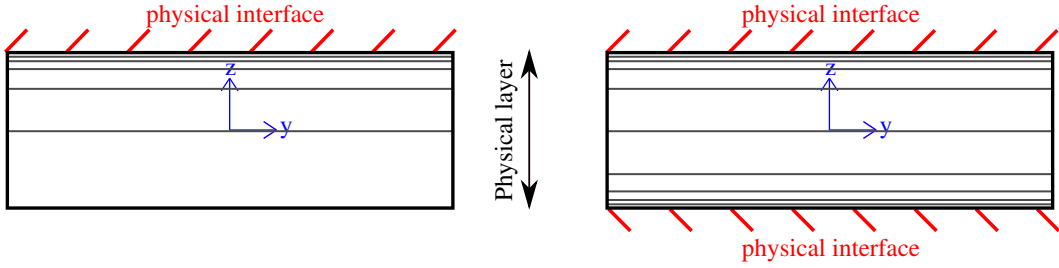


Figure 3.4: Progressive layerwise mesh through the physical layer thickness

3.4 Numerical validation and discussion

3.4.1 Layerwise mesh influence

Before comparing the results of the refined LS1 and 3D-FE models, the influence of the proposed layerwise mesh for the LS1 model is investigated. As a numerical example, a $(\pm 10^\circ)_s$ rectangular composite laminate with a width of $2b = 20 \text{ mm}$ and a total thickness of $e_t = 4e = 0.76 \text{ mm}$ is considered. The laminate is made up of four G947/M18 carbon-epoxy plies whose mechanical properties, tested by [Lagunegrand et al. \[2006\]](#), are reported in Table 3.3. The laminate is subjected to a uniaxial longitudinal strain $\varepsilon_{xx} = 0.001$ in the x direction. As shown in Fig. 3.5, the delamination consists of four interfacial cracks of length a located symmetrically at the interfaces $\theta/ - \theta$ (herein $\theta = 10^\circ$). Regarding the crack length, four cases are studied: $a = 0$ (non-delaminated state); $a = 0.1e$ (micro-crack); $a = e$ (meso-crack) and $a = 10e$ (macro-crack) where $e = 0.19 \text{ mm}$ is the thickness of a carbon-epoxy ply. Knowing that the interlaminar stresses σ_{yz} and σ_{zz} are negligible compared to σ_{xz} , we focus on the distribution of the interlaminar shear stress σ_{xz} . In what follows, p is the number of mathematical layers per physical layer, \bar{y} denotes the distance from the singularity point (free edge or crack tip) in the y direction and $k_{xz} = \frac{\sigma_{xz}}{E_x \varepsilon_{xx}}$ is the normalized dimensionless interlaminar shear stress where ε_{xx} and E_x are respectively the imposed longitudinal strain and the longitudinal modulus of the laminate. The thickness of the

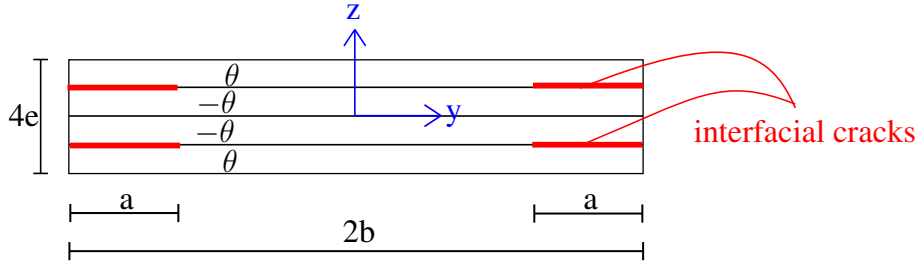


Figure 3.5: Laminate section with four interfacial cracks at the interfaces $\theta/ -\theta$

mathematical layer beside the physical interface $\theta/ -\theta$ is $1/100$ of the thickness of the physical layer ($e/h_{min} = 100$).

3.4.1.1 Free edge singularity

Fig. 3.6 shows the distributions of σ_{xz} at the interface $10^\circ/ -10^\circ$ in non-delaminated state ($a = 0$) for regular and irregular layerwise mesh. As seen, in the vicinity of the free edge ($0 < \bar{y} < 0.1e$) the rate of convergence for the regular layerwise mesh is very slow so that the more the mesh is refined, the more the interlaminar stress raises. On the other hand, for the proposed irregular layerwise mesh there is a rapid convergence rate in such a way that for $p \geq 3$ the convergence is ensured.

Knowing that the interlaminar stress σ_{xz} is theoretically singular at the free edge, there is no mesh-independent stress value at this point. However, except at the free edge point, the stress values are theoretically finite so that by refining the mesh sufficiently, it is possible to obtain converged stress values. By going away from the free edge, the mesh-dependency becomes negligible and the convergence is reached. Thus, there is always a *convergence distance* from which the results are not mesh-dependent. Fig. 3.7 compares the convergence of regular and irregular layerwise mesh for different distances from the free edge ($\bar{y} = e$, $\bar{y} = 0.1e$, $\bar{y} = 0.01e$ and $\bar{y} = 0.001e$). As shown, for $\bar{y} > 0.1e$ (e is the thickness of a carbon-epoxy ply), the influence of the layerwise mesh is negligible in a way that one mathematical layer per physical layer is sufficient to reach the converged value. Closer to the singularity ($\bar{y} < 0.1e$), the layerwise mesh plays an important role in the convergence. For the regular layerwise mesh, at the distance $\bar{y} = 0.01e$ from the singularity, the convergence is reached for $p = 8$ (i.e., eight mathematical layers per physical layer). It is clear that the regular layerwise mesh should be too much more refined in order to get convergence until $\bar{y} = 0.001e$. On the contrary, the convergence rate of the proposed irregular mesh herein is very rapid so that for $p = 3$ (three mathematical layers per physical layer), the convergence is easily reached even very close to the singularity point ($\bar{y} = 0.001e$).

3.4.1.2 Crack tip singularity

Now, the accuracy and the efficiency of the proposed layerwise mesh is investigated in the case of crack tip singularity. For this reason, three crack lengths $a = 0.1e$ (micro-crack), $a = e$ (meso-crack) and $a = 10e$ (macro-crack) are studied. Fig. 3.8 shows

3. DELAMINATED MULTILAYERED PLATES UNDER UNIAXIAL EXTENSION. PART II:
EFFICIENT LAYERWISE MESH STRATEGY FOR THE PREDICTION OF DELAMINATION ONSET

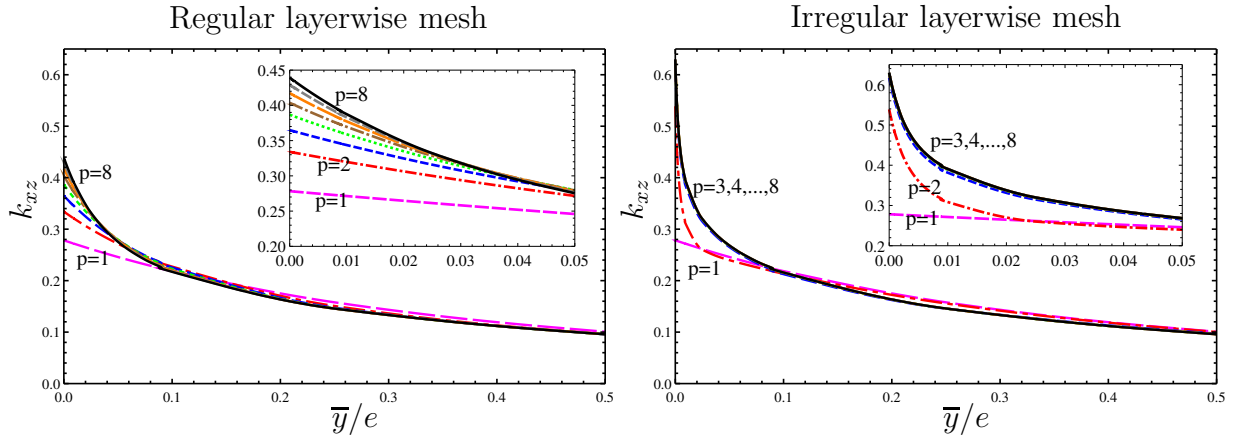


Figure 3.6: Distribution of the interlaminar shear stress σ_{xz} at the interface $10^\circ / -10^\circ$ - Free edge singularity ($a = 0$); (P is the number of mathematical layers per physical layer and k_{xz} denotes the normalized interlaminar stress)

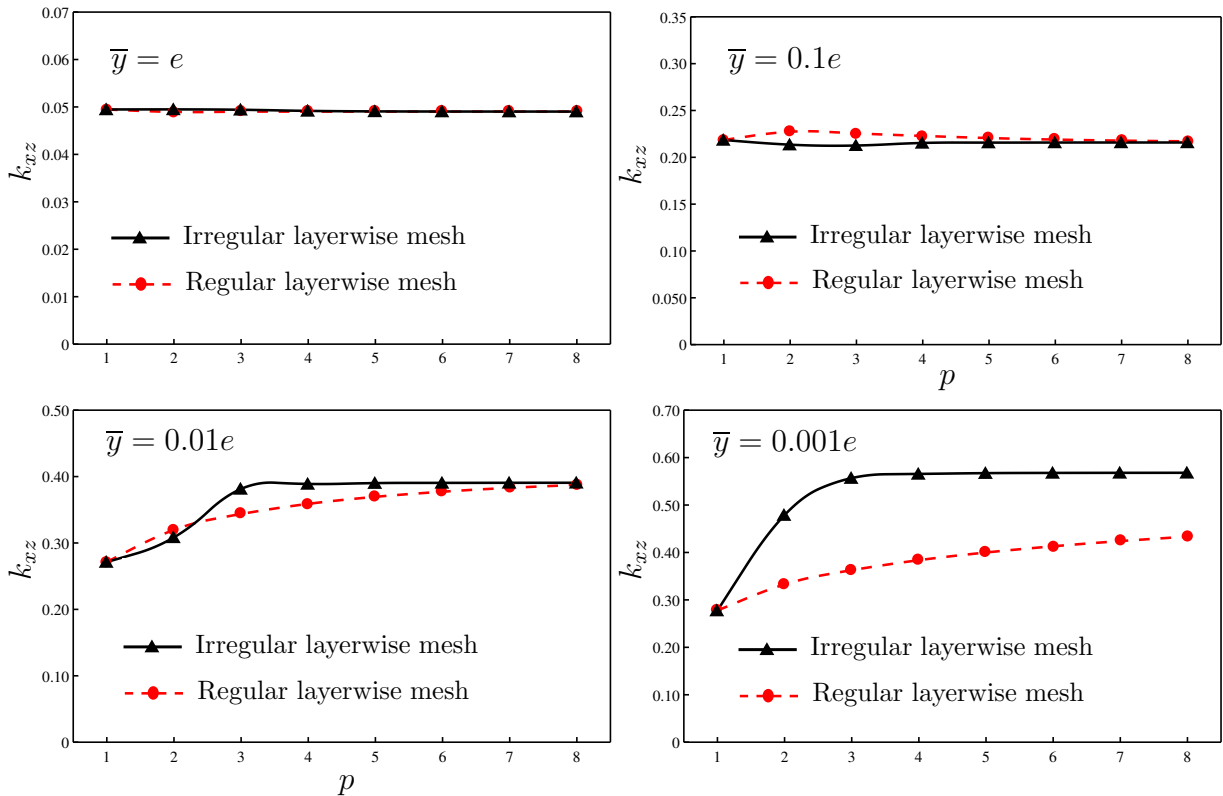


Figure 3.7: Convergence of the interlaminar shear stress σ_{xz} at different distances from the free edge

the distributions of σ_{xz} at the interface $10^\circ / -10^\circ$ for the crack length $a = 0.1e$. It is observed that the results of the irregular layerwise mesh converge for $p \geq 3$ while for the regular mesh, the convergence rate is very slow. As shown in Fig. 3.9, far from the crack tip ($\bar{y} = e$), the layerwise mesh has no effect and so $p = 1$ is sufficient (i.e., one mathematical layer per physical layer); but near the crack tip, the effect of the layerwise mesh strategy becomes important. In the case of the regular layerwise mesh, in order to obtain the converged value at the distance $\bar{y} = 0.1e$ from the crack tip, at least eight mathematical layers per physical layer are required ($p \geq 8$). This number should be very much higher for the convergence at $\bar{y} = 0.01e$ or $\bar{y} = 0.001e$. However, the proposed irregular layerwise mesh is very efficient so that only three mathematical layers per physical layer $p = 3$ are sufficient for convergence even very close to the crack tip ($\bar{y} = 0.001e = 0.19\mu m$). It should be noted that the same conclusion is drawn for the crack lengths $a = e$ and $a = 10e$ that were mentioned above (see Figs. 3.18 to 3.21 in Appendix 3.A for the curves corresponding to $a = e$ and $a = 10e$).

3.4.1.3 Energy release rate

Knowing that many delamination criteria are based on energy release rate, herein, the influence of the proposed LS1 mesh strategy on energy release rate estimations is investigated. Fig. 3.10 shows the convergence rate of energy release rate for the regular and irregular layerwise mesh. $\bar{G} = \frac{G}{e E_x \varepsilon_{xx}^2} = -\frac{\partial W / \partial a}{e E_x \varepsilon_{xx}^2}$ signifies the dimensionless energy release rate value for an interlaminar crack of length a . As seen, in the case of a large crack length ($a = e$), the energy release rate estimations with regular mesh are relatively acceptable. Nevertheless the irregular layerwise mesh provides a faster convergence. On the other side, in the case of a micro crack ($a \simeq 0$), the convergence of the regular mesh is too slow. Knowing that the theoretical value of the energy release rate is zero in this case ($G \rightarrow 0$ if $a \rightarrow 0$) [Leguillon et al. 2001], it seems that the regular mesh should be enormously refined to obtain the theoretical value and the results are not satisfying. On the contrary, the proposed irregular progressive mesh is very efficient so that for $p \geq 3$, the convergence is ensured and the results are stable.

As a conclusion, it is deduced that in the present case, an irregular layerwise mesh with three mathematical layers per physical layer ($p = 3$) is sufficient to evaluate accurately the energy release rate and the interlaminar stress fields.

3.4.2 Finite element comparison

In this section, in order to evaluate the accuracy and the efficiency of the *refined LS1* model in analyzing delamination problems, the results of this model are compared to those of a 3D finite element analysis performed with the commercial software Abaqus. The purpose of this investigation is to illustrate that, whatever the delamination criterion, the refined LS1 model is a powerful alternative to the 3D-FEM for the analysis of delaminations in multilayered plates. In this study, the focus is on the initiation of delamination. In general, the delamination criteria are based on interlaminar stress distribution and/or the energy release rate. In the present work, the twofold strength

3. DELAMINATED MULTILAYERED PLATES UNDER UNIAXIAL EXTENSION. PART II:
EFFICIENT LAYERWISE MESH STRATEGY FOR THE PREDICTION OF DELAMINATION ONSET

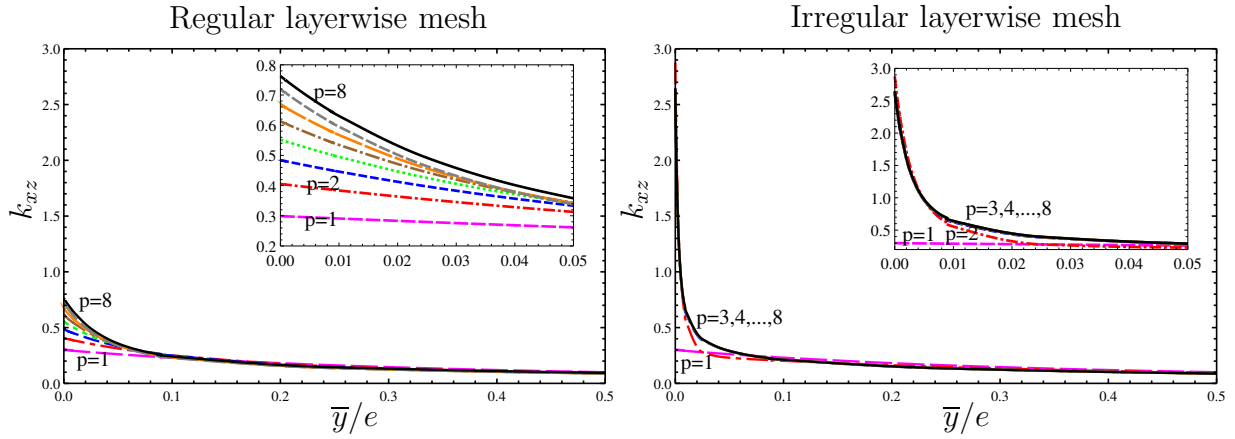


Figure 3.8: Distribution of the interlaminar shear stress σ_{xz} at the interface $10^\circ / -10^\circ$ - Crack tip singularity ($a=0.1e$); (P is the number of mathematical layers per physical layer and k_{xz} denotes the normalized interlaminar stress)

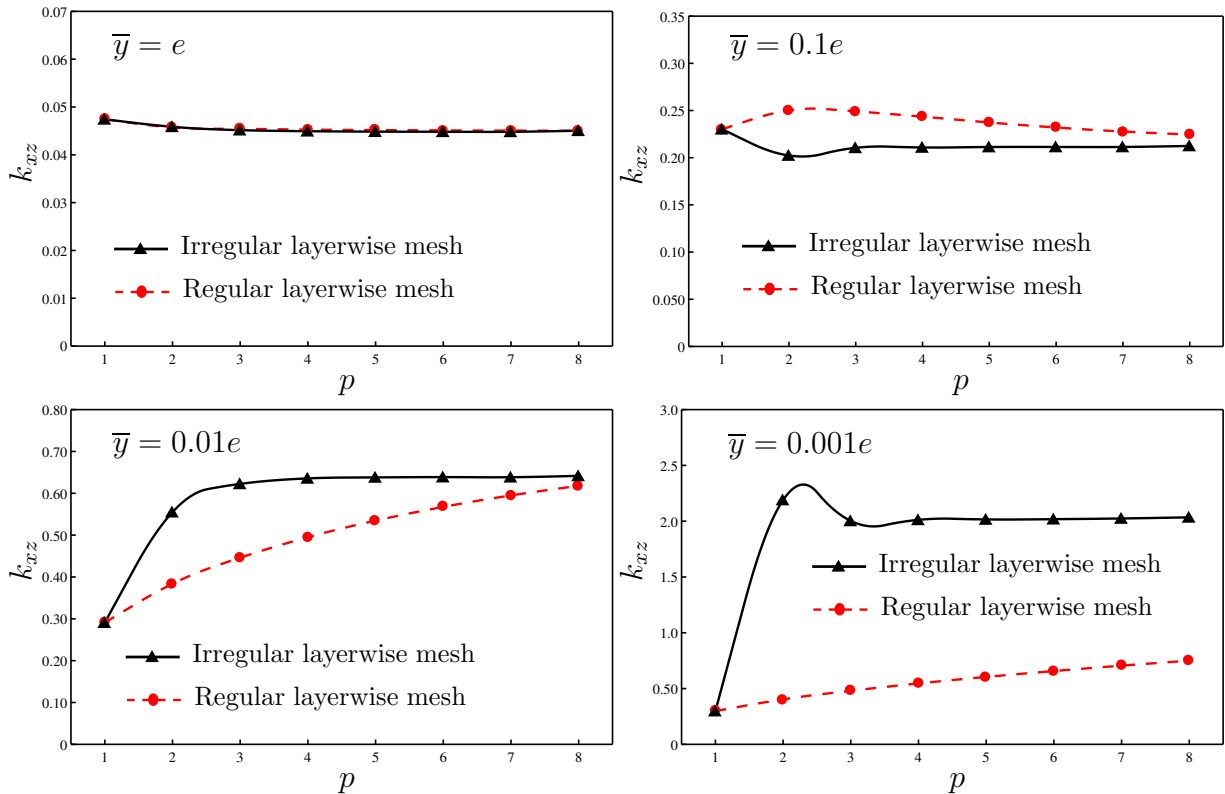


Figure 3.9: Convergence of the interlaminar shear stress σ_{xz} at different distances from the crack tip ($a = 0.1e$)

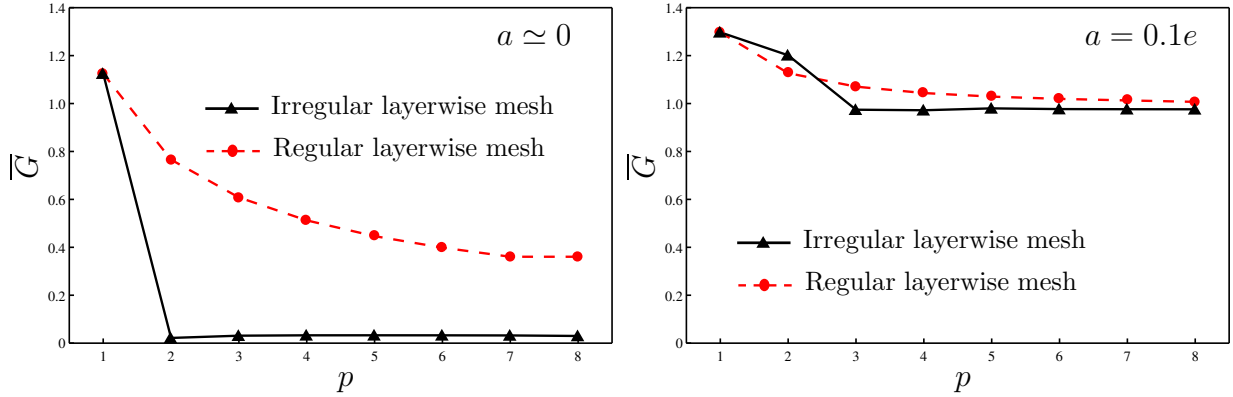


Figure 3.10: Convergence of the energy release rate for different interlaminar crack lengths a

and toughness criterion proposed by [Martin et al. \[2010\]](#) is used for the prediction of delamination onset in laminates. To use this criterion, the interlaminar stress distribution in non-delaminated state and the incremental energy release rate curve in the delaminated state are required.

To validate our model, the same numerical examples treated by [Martin et al. \[2010\]](#) are investigated in this study. Therefore, $(\pm 10^\circ)_s$ and $(\pm 20^\circ)_s$ rectangular composite laminates with G947/M18 and CTE1/T700 carbon-epoxy plies are considered as case studies. Mechanical properties of the two types of carbon-epoxy ply, tested by [Lagunegrand et al. \[2006\]](#) and [Diaz Diaz and Caron \[2006a\]](#), are reported in Table 3.3. The uniaxial longitudinal strain of $\varepsilon_{xx} = 0.001$ is imposed in the x direction. It is assumed that the laminate is very long so that there is no variation in the x direction far from the ends. It is noted that due to the mirror symmetry of the laminate, only the half thickness of the laminate is modeled.

Table 3.3: Mechanical material properties of the ply for G947/M18 and CTE1/T700 carbon-epoxy

carbon-epoxy	E_L (Gpa)	E_T (Gpa)	E_N (Gpa)	G_{LT} (Gpa)	G_{LN} (Gpa)	G_{TN} (Gpa)	ν_{LT}	ν_{LN}	ν_{TN}	e (mm)
G947/M18*	97.6	8.0	8.0	3.1	3.1	2.7	0.37	0.37	0.5	0.19
CTE1/T700**	153.82	10.61	10.61	5.58	5.58	5.58	0.315	0.315	0.315	0.13

** [Lagunegrand et al. \[2006\]](#)

** [Diaz Diaz and Caron \[2006a\]](#)

Three models are investigated: 3D finite element model, *LS1* model with regular layerwise mesh, refined *LS1* model with irregular progressive layerwise mesh. As proved in the previous section, an irregular progressive layerwise mesh with three mathematical layers per physical layer ($p = 3$) provides accurate estimations of interlaminar stress

fields and energy release rate. In order to have a reasonable comparison between the LS1 and refined LS1 models, the same number of mathematical layers is considered in both models. Therefore, the total number of equations that should be solved (i.e., the total number of unknowns) in the LS1 and the refined LS1 models is identical. It should be noted that in this study, the LS1 and refined LS1 solutions are obtained analytically by means of the dedicated software designed by the authors.

In the 3D-FE model, invariance conditions are exploited in order to reduce the size of the problem and ensure the longitudinal invariance. By making use of the invariance in the x direction, only one element in this direction is considered with the following invariance conditions (see Fig. 3.11):

$$\begin{aligned} U_x(x_1, y, z) &= U_x(x_0, y, z) + (x_1 - x_0)\varepsilon_{xx} \\ U_y(x_1, y, z) &= U_y(x_0, y, z) \\ U_z(x_1, y, z) &= U_z(x_0, y, z) \end{aligned} \quad (3.1)$$

It should be noted that because of the invariance in the x direction, the 3D aspect ratio of the elements is not important and the size of the elements in the x direction doesn't play any role.

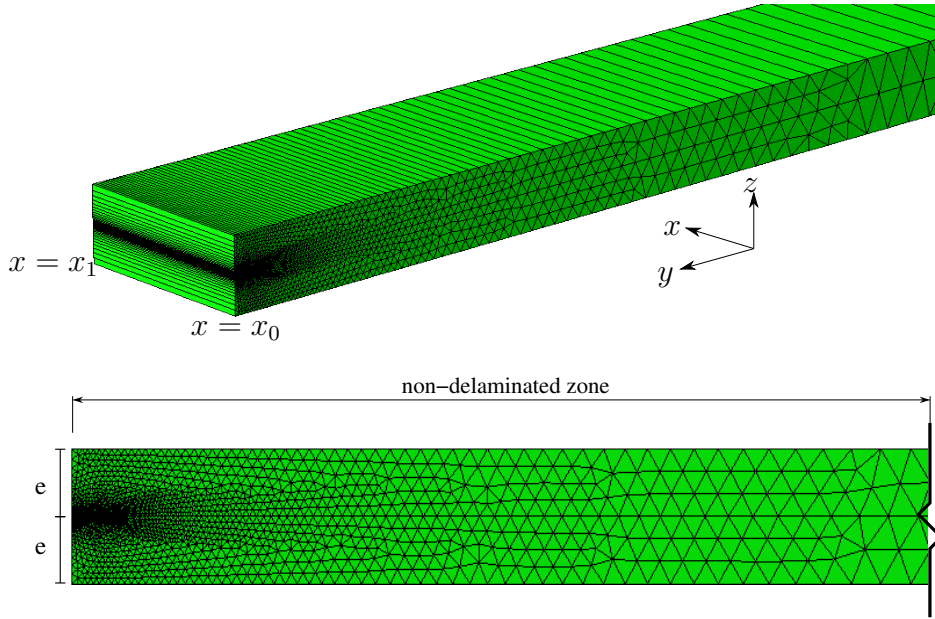


Figure 3.11: Finite element model of the laminate in non-delaminated state - 3D model (top); mesh in the yz plane (bottom)

3.4.2.1 Non-delaminated state

In the finite element model, we use the wedge elements. In order to obtain accurate results, the finite element mesh should be considerably refined at the interface near the free edges (see Fig. 3.11). The size of the elements in this zone is almost $1 \mu\text{m}$ and the total number of nodes is about 10000. As shown in Fig. 3.12, the interlaminar

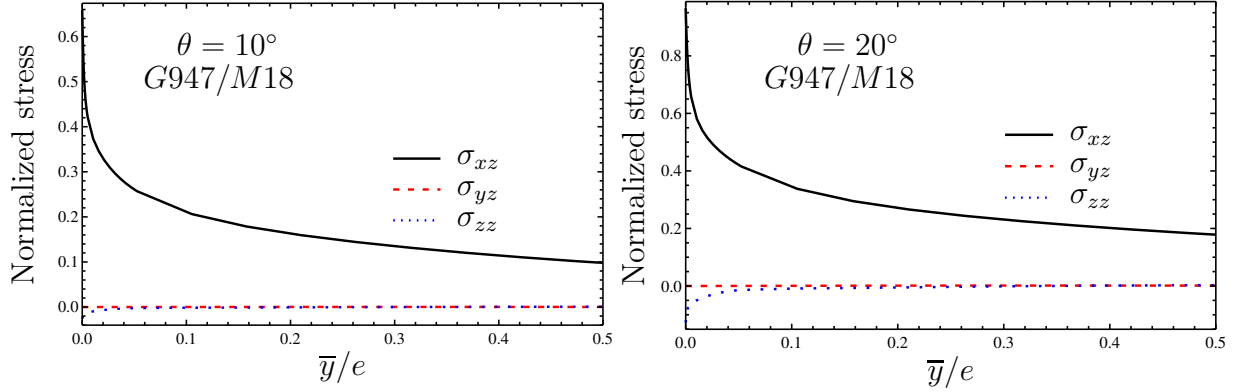


Figure 3.12: Distribution of the interlaminar stresses at the interface $\theta/ - \theta$ of $(\pm\theta)_s$ laminates

shear stress σ_{xz} is always dominant at the interface $\theta/ - \theta$ of $(\pm\theta)_s$ laminates ($\theta = 10^\circ$ or 20°). Therefore, the comparisons are made on the distribution of the interlaminar shear stress σ_{xz} .

Fig. 3.13 shows the distributions of the interlaminar shear stress σ_{xz} at the interface $\theta/ - \theta$ of $(\pm\theta)_s$ laminates. The ordinate axis $k_{xz} = \frac{\sigma_{xz}}{E_x \varepsilon_{xx}}$ indicates the normalized interlaminar shear stress and the abscissa axis \bar{y}/e denotes the normalized distance from the free edge where e is the thickness of a carbon-epoxy ply.

As seen in all cases, far from the free edge ($\bar{y} > 0.02e$) the three models give the same results. The smaller the distance from the free edge, the more the divergence between the curves. By comparing the curves very close to the free edge ($\bar{y} < 0.02e$), it is realized that the 3D finite element model is more accurate than the LS1 model (with the regular layerwise mesh); but the refined LS1 model (with the proposed irregular layerwise mesh) is more accurate than the 3D-FE model. Indeed, via the suggested refined LS1 model, the interlaminar stress singularity is much better captured compared with the LS1 model or the 3D-FE model. It should be mentioned that in the present case, the total degrees of freedom in the 3D-FE model are 200 times more than those (i.e., unknowns) in the refined LS1 model.

3.4.2.2 Delaminated state

In this section, the delamination state of $(\pm\theta)_s$ laminates is studied. It is assumed that there are four interfacial cracks of length a located symmetrically at the interfaces $\theta/ - \theta$ as shown in Fig. 3.5.

The same number of mathematical layers ($p = 3$) is used for the LS1 and refined LS1 models. Regarding the 3D-FE model, to obtain an appropriate accuracy, the mesh must be greatly refined near the crack tip (see Fig. 3.14). The size of the smallest elements near the crack tip is almost $1 \mu m$. In the delaminated state, the energy release rate estimations of the proposed model are investigated. In order to apply the mentioned twofold criterion [Martin et al. 2010], the curve of the incremental energy release rate as a function of crack length ($G^{inc}(a) = \frac{W(a=0) - W(a)}{a}$) should be extracted. By varying the crack length a and evaluating the incremental energy release rate for each crack length,

3. DELAMINATED MULTILAYERED PLATES UNDER UNIAXIAL EXTENSION. PART II:
EFFICIENT LAYERWISE MESH STRATEGY FOR THE PREDICTION OF DELAMINATION ONSET

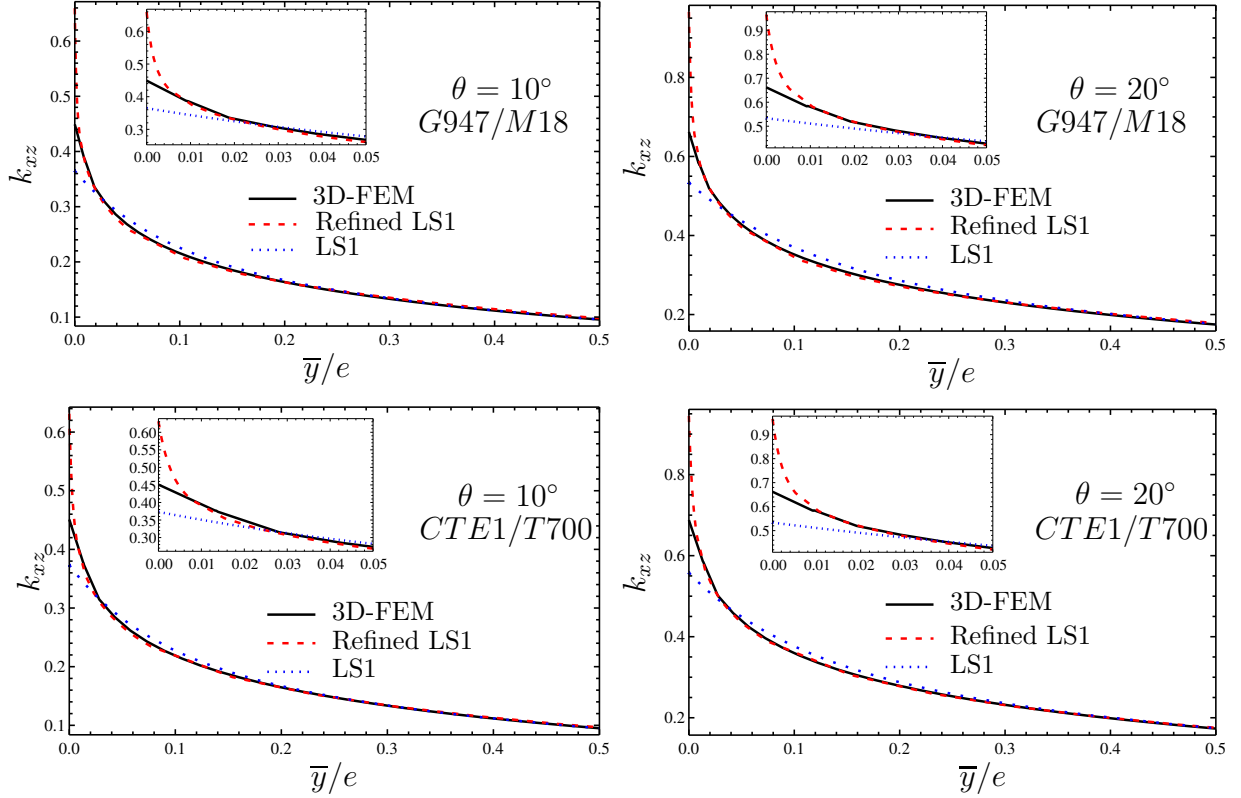


Figure 3.13: Distribution of the interlaminar shear stress σ_{xz} at the interface $\theta/ - \theta$ of $(\pm\theta)_s$ laminates

the incremental energy release rate curve is obtained. Fig. 3.15 plots the normalized incremental energy release rate $\bar{A}(a)$ versus the normalized crack length a/e for the $(\pm 10^\circ)_s$ and $(\pm 20^\circ)_s$ laminates with G947/M18 and CTE1/T700 carbon-epoxy plies. The normalized incremental energy release $\bar{A}(a)$ is obtained by:

$$\bar{A}(a) = \frac{G^{inc}(a)}{e E_x \varepsilon_{xx}^2} = \frac{W(a=0) - W(a)}{a e E_x \varepsilon_{xx}^2}$$

where a , e , E_{xx} , ε_{xx} and $W(a)$ indicate respectively the crack length, the carbon-epoxy ply thickness, the longitudinal effective modulus of the laminate, the imposed uniaxial deformation and the strain energy of delaminated laminate.

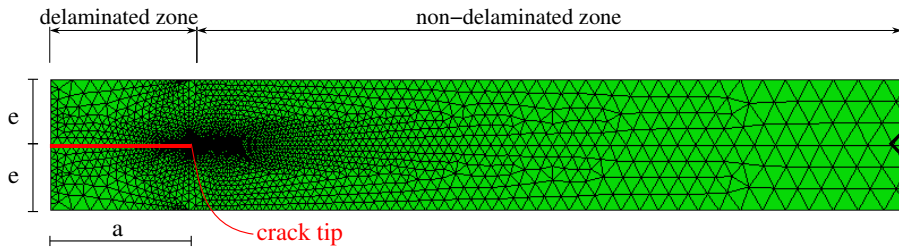


Figure 3.14: 3D-FE model: mesh in the yz plane in delaminated state

As expected, the incremental energy release rate is an increasing function of the interfacial crack length reaching a plateau for high values of a where the three models (3D Finite element, LS1 and refined LS1 models) present the same results. As seen in Fig. 3.15, for the small crack lengths ($a < e$) the estimations of the LS1 model are not accurate enough. The smaller the crack length is, the more significant the error becomes for this model. As a result, contrary to the 3D theory, the curve of the incremental energy release rate corresponding to the LS1 model does not pass through the origin ($\bar{A}(a \simeq 0) \neq 0$). This lack of accuracy may become problematic in applying energetic delamination criteria. To obtain accurate results via this model, the regular layerwise mesh should be extremely refined. This refinement greatly reduces the efficiency of the model. In the refined LS1 model with the irregular layerwise mesh strategy proposed in this study, this drawback is easily overcome. It is observed that the refined LS1 model is as accurate as the 3D-FE model even for too small crack lengths; knowing that the proposed model is enormously more efficient than the 3D-FEM.

Finally, as a verification, the distribution of the interlaminar stress σ_{xz} in the vicinity of the crack tip (in the delaminated state) is compared between the three models. Fig. 3.16 shows the distribution of σ_{xz} for $(\pm\theta)_s$ laminates with interlaminar cracks of length $a = e$ at the interfaces $\theta/-\theta$. The abscissa axis \bar{y}/e denotes the normalized distance from the crack tip where \bar{y} is the distance from the crack tip and e is the thickness of a carbon-epoxy ply. A comparison between the results of the three models, demonstrates that in delaminated state also, the refined LS1 model can evaluate accurately the interlaminar stresses so that the capture of the stress singularity at crack tip is even better than the 3D-FEM.

3.4.2.3 Delamination initiation criterion - Experimental comparison

Here, the quoted twofold strength and toughness criterion proposed by [Martin et al. \[2010\]](#), is used for the prediction of delamination onset in the investigated case studies. This combined criterion is written as follows:

$$\begin{cases} G^{inc}(a) = \bar{A}(a) e E_x \varepsilon_{xx}^2 \geq G^c \\ \sigma_{xz}(y) = k_{xz}(y) E_x \varepsilon_{xx} \geq \sigma^c \quad \text{for } y \leq a \end{cases} \quad (3.2)$$

For a monotonic and increasing applied loading, the crack increment at nucleation a^c is obtained by combining the previous equalities which leads to

$$\frac{\bar{A}(a^c)}{(k_{xz}(y = a^c))^2} = \frac{1 E_x G^c}{e (\sigma^c)^2} \quad (3.3)$$

Once the initiation length a^c is determined, the initiation strain ε^c derives from 3.2 as follows:

$$\varepsilon^c = \sqrt{\frac{G^c}{\bar{A}(a^c) e E_x}} \quad \text{or} \quad \varepsilon^c = \frac{\sigma^c}{E_x k_{xz}(y = a^c)} \quad (3.4)$$

The critical values σ^c and G^c are identified in a way that there is the best agreement with the experiments (tested by [Lagunegrand et al. \[2006\]](#) and [Diaz Diaz and Caron](#)

3. DELAMINATED MULTILAYERED PLATES UNDER UNIAXIAL EXTENSION. PART II:
EFFICIENT LAYERWISE MESH STRATEGY FOR THE PREDICTION OF DELAMINATION ONSET

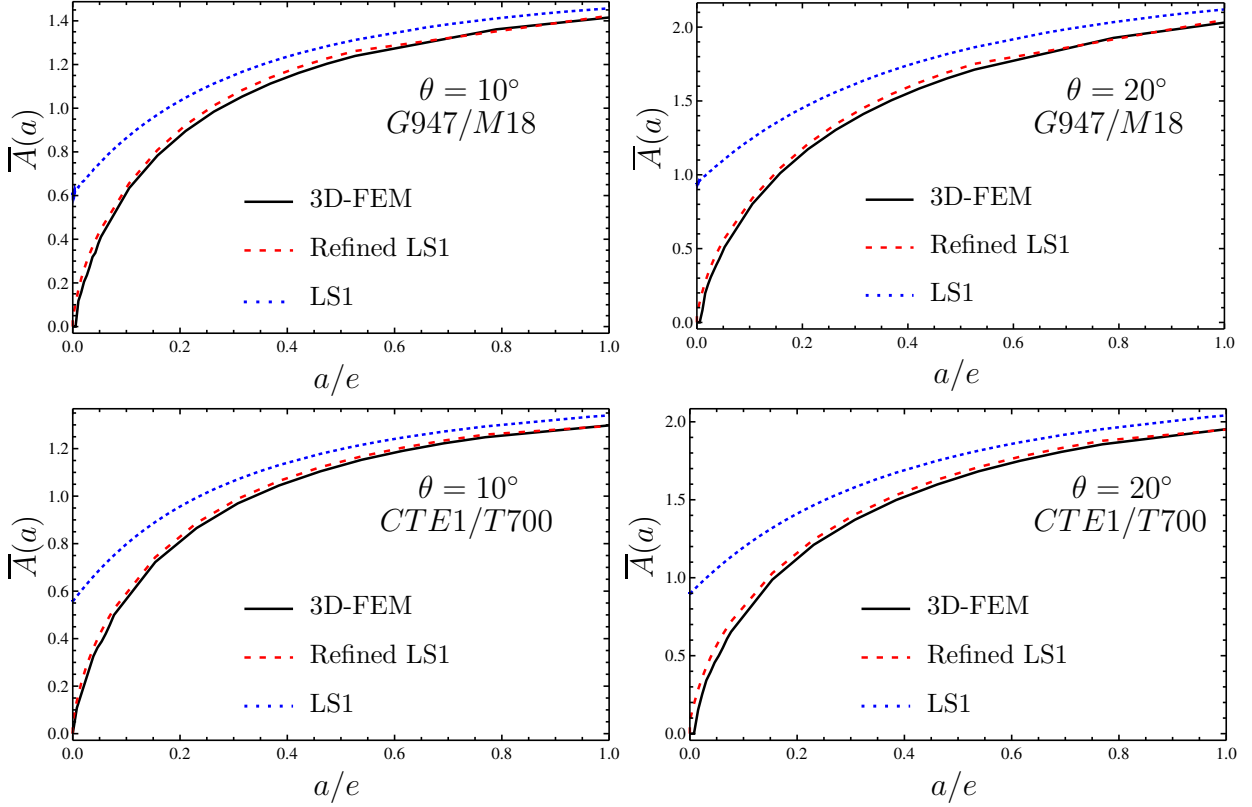


Figure 3.15: The normalized incremental energy release rate $\bar{A}(a)$ versus the normalized crack length a/e at the interface $\theta/ - \theta$ of $(\pm\theta)_s$ laminates

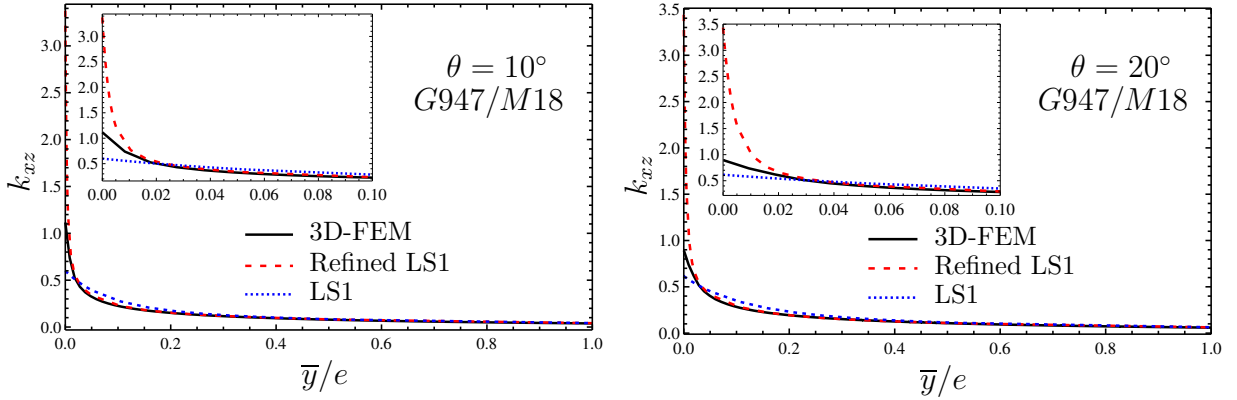


Figure 3.16: Distribution of the interlaminar shear stress σ_{xz} at the interface $\theta/ - \theta$ of $(\pm\theta)_s$ laminates in delaminated state

[2006a]). The same method used by Martin et al. [2010] is applied to identify σ^c and G^c knowing that, in this study, the proposed refined LS1 model is used instead of the finite element calculations. Fig. 3.17 shows the longitudinal stress at delamination onset versus the ply thickness and compares the predicted values with the experimental data for the G947/M18 and CTE1/T700 carbon-epoxy laminates. Good agreements

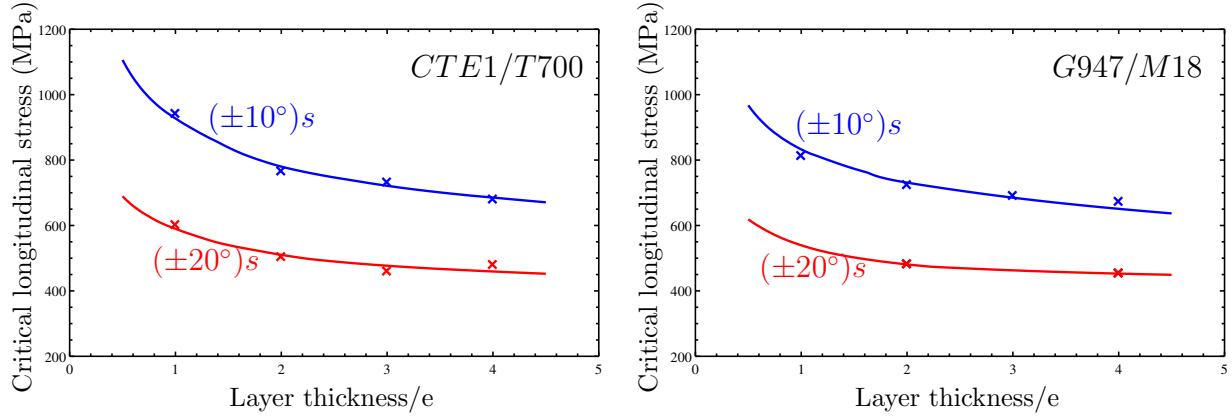


Figure 3.17: Comparison of the predicted critical longitudinal stress at delamination onset (continuous lines) with the experimental values (points) for $(\pm\theta)_s$ laminates

between the model and experiments confirm that; firstly, the applied criterion can predict accurately the delamination initiation; and secondly, the refined LS1 model can be used as an efficient and accurate alternative to 3D-FE calculations. It should be mentioned that since the refined LS1 model yields accurate estimations in terms of interlaminar stresses as well as energy release rate, this model can be used with any other delamination criterion based on stress or energy release rate.

3.4.3 Discussion

By studying both types of free-edge singularity and crack tip singularity (for different lengths of delamination), it is proved that the proposed refined LS1 model is capable of predicting accurately interlaminar stresses within the singularity zones. This implies that the proposed layerwise mesh is a kind of discretization through the thickness which implicitly takes into account the heterogeneity of laminated structures and is consistent with the physics of the problem. Indeed, the interpolation through the thickness is asymptotically precise and fits the order of stress singularity. That is why using the proposed refinement strategy in the thickness direction leads to an extremely fast convergence. It is worth mentioned that, in addition to stress singularities, the proposed layerwise mesh overcomes the drawback of calculating the energy release rate in the case of micro cracks.

In this work, the LS1 solutions of the delamination problem were obtained analytically for rectangular laminates under uniaxial extension. The proposed method can be used in other cases in which the x -invariance hypothesis is applicable such as multiple delaminations under cylindrical bending. However, in real structures with complicated geometries, this approach cannot be used. Indeed, the proposed model remains appropriate but the system of equations should be solved numerically. It is noted that a finite element program based on the LS1 formulation, called MPFEAP (MultiParticle Finite Element Analysis Program), has already been developed. This program can be used to analyze non-delaminated multilayered structures with complicated geometries [Duong et al. 2011, Nguyen and Caron 2006]. The software is capable of computing interlaminar stresses and other localized effects, which are impossible to calculate with

classical 2D finite element models. The proposed refined LS1 model for the analysis of delaminated multilayers can be implemented in MPFEAP. Although the formulation of the LS1 model may seem more complicated, it is much more efficient than the popular 3D-FEM.

3.5 Conclusion

In the present work, in order to improve the accuracy and the efficiency of the LS1 model, a layerwise mesh strategy (i.e., subdividing each physical layer into some mathematical layers through the thickness of the laminate) has been introduced. The proposed layerwise mesh is an irregular progressive layerwise mesh in which the mathematical layers become thinner by approaching the physical interfaces; while in a regular layerwise mesh, the thickness of all the mathematical layers is constant. In order to study the influence of the proposed layerwise mesh, a $(\pm 10^\circ)_s$ composite laminate was investigated in non-delaminated and delaminated states. The stress singularity at free-edge and crack tip for different crack lengths (micro-crack, meso-crack and macro-crack) were studied. It is found that the proposed refined LS1 model (based on the proposed irregular layerwise mesh) is much more efficient and accurate than the LS1 model (with regular layerwise mesh) and the proposed model converges very rapidly in terms of energy release rate and stress values. In the investigated examples, it is shown that an irregular layerwise mesh with three mathematical layers per physical layer ($p = 3$) converges in terms of interlaminar stresses (even very close to singularities) and energy release rate; whereas the LS1 model with regular layerwise mesh converges too slowly.

As application examples, $(\pm 10^\circ)_s$ and $(\pm 20^\circ)_s$ composite laminates with carbon-epoxy plies were investigated and the results of three models were compared: 3D-FEM (performed in Abaqus), LS1 and refined LS1 models. The comparison between the three models in non-delaminated state demonstrates the accuracy and the efficiency of the refined LS1 model to capture the stress singularity so that the proposed refined LS1 model predicts the singularity stress even better than the 3D-FEM. In delaminated situation, the influence of the layerwise mesh is significant. It is found that the LS1 estimations of the energy release rate are not accurate for small cracks (i.e., the crack length smaller than the ply thickness) and the LS1 model produces significant errors. On the other hand, the refined LS1 model estimates the energy release rate as accurately as the 3D-FEM. It is important to keep in mind that the total number of degrees of freedom (unknowns) in the refined LS1 model is less than 1/200 of the total number degrees of freedom in the 3D-FEM. This illustrates that the proposed model is an accurate and very efficient alternative to the 3D-FEM for delamination analyses. It is reminded that in this study, the twofold strength and toughness criterion proposed by [Martin et al. \[2010\]](#) was employed to predict delamination onset in the investigated examples but the refined LS1 model can be used with any other stress or energy release rate delamination criterion.

Because of its high efficiency in computational time and memory, the proposed approach is very useful for tackling computationally intensive problems. For example, stacking sequence optimization of composite laminates which is usually performed by

3.5. CONCLUSION

means of genetic algorithm or other technics, require a huge number of repetitive calculations. It is evident that for such problems, an efficient and fast approach for the analysis of laminates is necessary. The dedicated software described in this paper can be easily combined with optimization softwares. Another possible application is the propagation of delamination cracks in composite structures in which an extensive series of analyses for different delamination lengths should be carried out. It is noted that, the proposed software can also be used as a post-processor of a software based on the classical laminate theory for the design of multilayered structures. Obviously, the use of the proposed model instead of 3D-FEM calculations leads to a high reduction of computational cost.

Appendix 3.A Crack tip stress singularity curves for $a = e$ and $a = 10e$

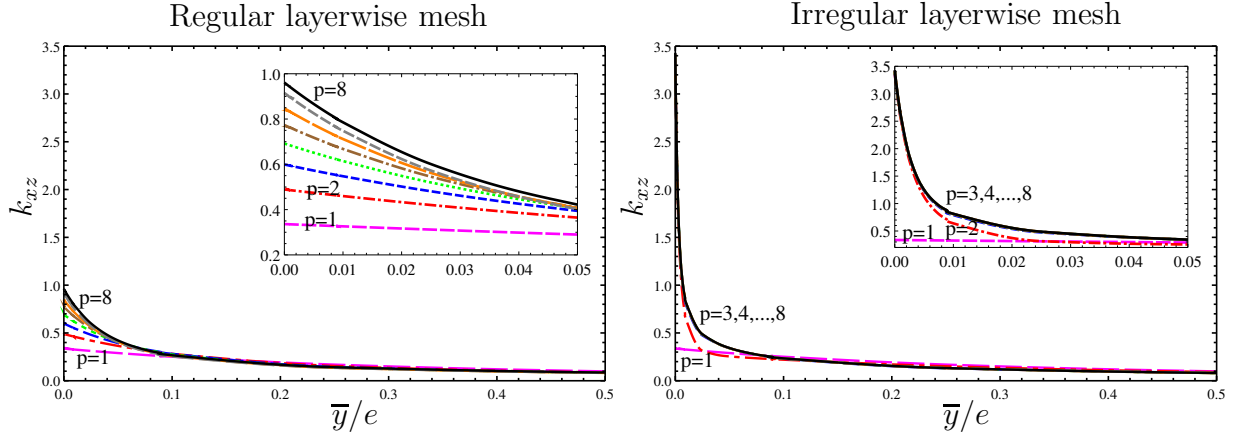


Figure 3.18: Distribution of the interlaminar shear stress σ_{xz} at the interface $10^\circ / -10^\circ$ - Crack tip singularity ($a=e$); (P is the number of mathematical layers per physical layer and k_{xz} denotes the normalized interlaminar stress)

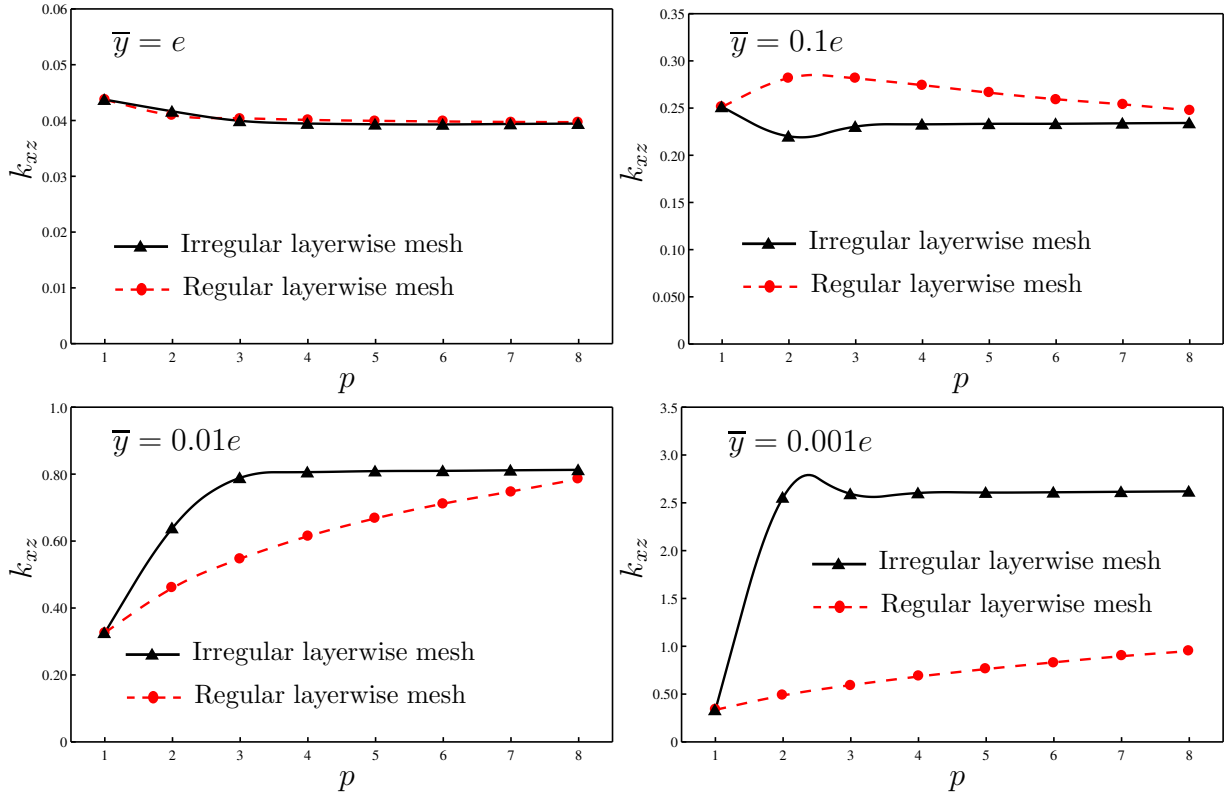


Figure 3.19: Distribution of the interlaminar shear stress σ_{xz} at the interface $10^\circ / -10^\circ$ - Crack tip singularity ($a = e$)

3.A. CRACK TIP STRESS SINGULARITY CURVES FOR $a = e$ AND $a = 10e$

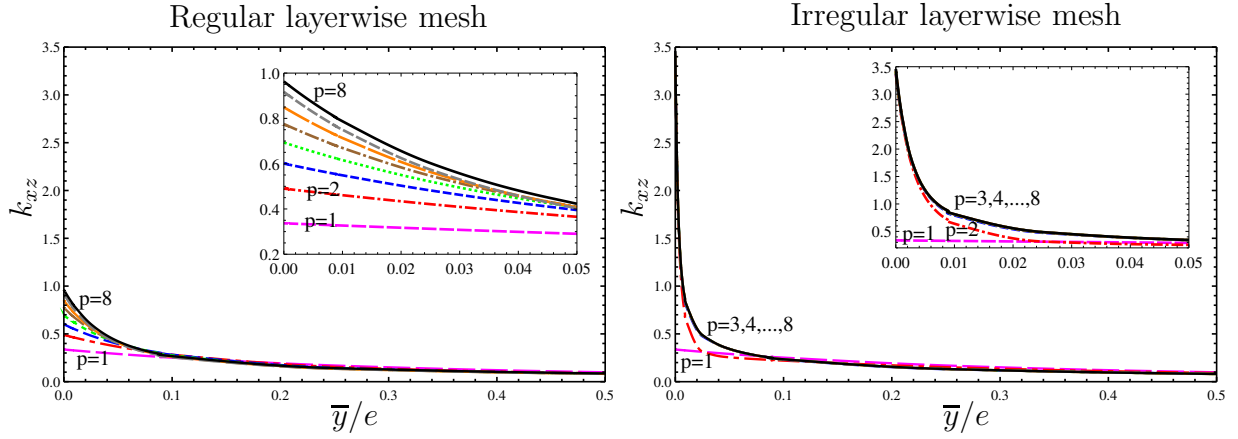


Figure 3.20: Distribution of the interlaminar shear stress σ_{xz} at the interface $10^\circ / -10^\circ$ - Crack tip singularity ($a=10e$); (P is the number of mathematical layers per physical layer and k_{xz} denotes the normalized interlaminar stress)

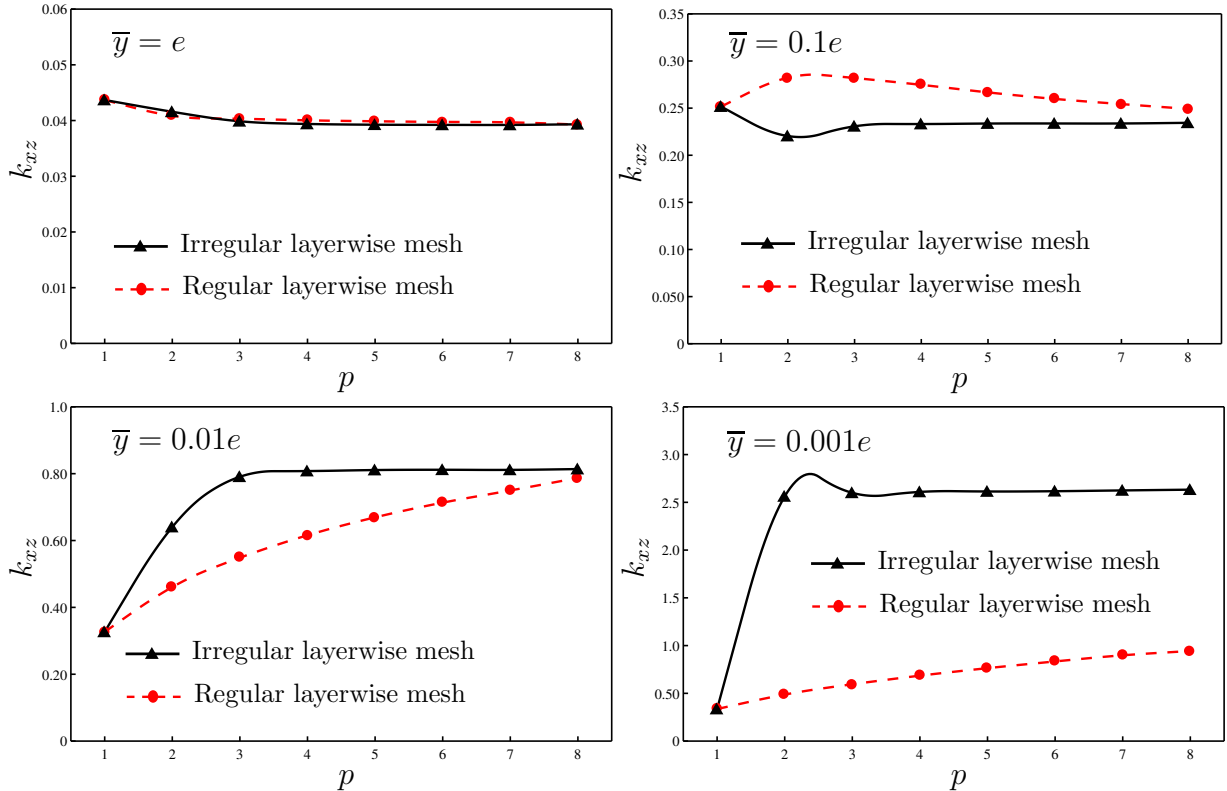


Figure 3.21: Distribution of the interlaminar shear stress σ_{xz} at the interface $10^\circ / -10^\circ$ - Crack tip singularity ($a = 10e$)

3. DELAMINATED MULTILAYERED PLATES UNDER UNIAXIAL EXTENSION. PART II:
EFFICIENT LAYERWISE MESH STRATEGY FOR THE PREDICTION OF DELAMINATION ONSET

Chapter 4

Cylindrical bending of multilayered plates with multi-delamination via a layerwise stress approach

Dans les chapitres 2 et 3 nous avons étudié des plaques multicouches délaminées en traction uniaxiale. Nous avons vu que ce type de chargement peut provoquer des délaminages en mode III. Le modèle LS1 a été utilisé pour la prédiction de l'amorçage du délaminage dans des plaques composites. Dans ce chapitre, nous étudions le problème du délaminage dans des plaques multicouches en flexion cylindrique. D'abord, nous trouvons la solution analytique du problème pour un chargement général (cylindrique) sur la face supérieure de la plaque. Ensuite, comme application, on étudie deux problèmes classiques de la propagation du délaminage en mode II et en mode III. Afin de valider notre méthode, nous comparons les approximations du modèle LS1 avec les résultats d'un modèle aux éléments finis 3D.

Ce chapitre est un article publié dans la revue "Composite Structures" sous la référence [Saeedi et al. \[2012c\]](#).

Contents

4.1	Introduction	137
4.2	Cylindrical bending problem	140
4.2.1	Problem description	140
4.2.2	Formulation of the LS1 model	140
4.2.3	x -invariance hypothesis	142
4.3	Analytical LS1 solution	143
4.3.1	Non-delaminated zone	143
4.3.2	Delaminated zone	145
4.3.3	Solution	147
4.4	Numerical examples	148
4.4.1	Mode I delamination - DCB like test	149
4.4.2	Mode II delamination - ENF like test	153
4.5	Conclusion	155
Appendix 4.A Definition of matrices		157
Appendix 4.B Solution of homogeneous system of second-order differential equations		158
4.B.1	Simple eigenvalues	158
4.B.2	Repeated and zero eigenvalues	158

Abstract

Three-dimensional finite element simulations of delamination propagation in multilayered plates are usually expensive in computational time and memory. In this paper, a two-dimensional layerwise model, called *the LS1 model*, is introduced as an accurate and effective alternative to the finite element method. The LS1 model is extended to the analysis of delamination growth in multilayered plates subjected to cylindrical bending loading. To this end, a general multilayered plate with arbitrary boundary conditions is investigated. By imposing the unilateral contact conditions at delaminated interfaces, analytical LS1 solutions to a general multi-delamination problem are obtained. As application examples, two classical mode I (Double Cantilever) and mode II (End Notched Flexure) delamination tests are investigated. By considering two types of crack resistance curve, the delamination propagation in composite laminates is studied. The LS1 results are found and compared to those of a finite element model. Very good agreements between the results of the two models prove the efficiency and accuracy of the LS1 model for the simulation of delamination propagation in laminates subjected to cylindrical bending.

keyword: Multilayer; Layerwise model; Multi-delamination; Cylindrical bending; Energy release rate

4.1 Introduction

Having high strength and stiffness-to-weight ratios, composite materials are extensively used in engineering applications such as aviation and aerospace, navigation, automotive, etc. However, these materials are susceptible to delaminations which can be caused by various factors such as manufacturing errors, edges effects, impact loading, etc. The delamination, often undetectable on the surface, can cause significant reduction in terms of strength and stiffness, and may lead to total failure of the structure without much warning in advance. Therefore, an accurate analysis of delamination is indispensable in order to determine the load carrying capacity and service effectiveness of laminated structures.

The modeling of the delamination in multilayered structures may be performed by means of fracture mechanics or damage mechanics approaches. In approaches based on fracture mechanics, the delamination is considered as the propagation of a crack between two adjacent layers of the delaminated interface; while damage approaches use the imperfect interface notion via an appropriate interface constitutive law. Many various approaches based on beam (1D) or plate (2D) theories [Kanninen 1973, Chang et al. 1976, Chai et al. 1981, Yin and Wang 1984, Yin et al. 1986, Grimaldi and Reddy 1985, Allix et al. 1995, Sridhar et al. 2002, Andrews et al. 2006, Raghu Prasada and Pavan Kumar 2008, De Morais 2011] or fully three-dimensional (3D) methods [Pagano 1969, 1970a, Chai 1990, Davidson et al. 1995, Chen and Lee 2004, She et al. 2009] have been proposed for the analysis of laminates subjected to different types of loading. Concerning the analysis of laminates under cylindrical bending loading, there are two well-known exact 3D solutions obtained by Pagano [1969, 1970a]. The first solution,

being for cross-ply laminates, can be considered as a special case of the second solution which is for angle-ply laminates. The 3D Pagano's solutions have been derived based on a set of simplifying assumptions, such as perfect interface conditions or simply supported boundary conditions. Many researches have attempted to study laminated structures with interfacial imperfections or damage. By extending Pagano's analysis and employing a spring-layer model, Williams and Addessio [1997] made a first attempt to obtain an exact 3D solution for laminated plates with delaminations. Williams [2001] studied cross-ply laminates in cylindrical bending with interlaminar imperfections and showed that there is a good agreement between plate theories and exact 3D solution. However, as shown in [Pagano 1970a], the accuracy of plate theory depends on many parameters like fiber orientation, thickness-to-span ratio, etc. As a matter of fact, in general cases such as thick angle-ply laminates with interfacial damage, the applicability of plate theories needs a careful verification.

Since the 3D modeling of laminated structures is always complex and computationally expensive in both memory and time, 2D approaches (equivalent single layer or layerwise) have been widely used as alternative methods. Although these 2D approaches are more efficient than 3D methods, their application is usually limited to simple cases of delamination, loading and boundary conditions. While the single-delamination problem in multilayered structures has been widely investigated, the multi-delamination problem of laminated structures has not been fully studied yet. Furthermore, most of the proposed methods and formulations in the literature deal with simple cases regarding the boundary conditions and type of loading. In this study, we seek to formulate and find a solution to a general multi-delamination problem under cylindrical bending loading. A general multilayered plate with arbitrary boundary conditions and multi-delaminations is considered (Fig. 4.1). The aim of this work is to obtain an accurate solution to this problem with a method which is much more effective than three-dimensional finite element method (3D-FEM). A layerwise stress model, inspired from Pagano's model [Pagano 1978a], is used to solve the problem. The model is called *LS1* which indicates layerwise stress approach with first-order membrane stress approximation per layer. In this model, each layer is considered as a Reissner-Mindlin plate with five generalized displacements (three displacements and two rotations). The layers are linked together by interfacial stresses (one normal and two shear interfacial stresses per interface). These interfacial stresses are considered as generalized stresses in the model which are related to corresponding generalized strains. The advantage of this model is that the stress continuities at interfaces are ensured. This model, previously called the *Multiparticle Model of Multilayered Materials (M₄)*, has been already used and validated in several studies [Naciri et al. 1998, Carreira et al. 2002, Diaz Diaz et al. 2002, Caron et al. 2006, Dallot and Sab 2008b, Diaz Diaz and Caron 2006a, Nguyen and Caron 2006].

In [Saeedi et al. 2012a,b], the authors focused on mode III delamination and applied the LS1 model to the analysis of delaminated multilayered plates subjected to uniaxial extension. It has been shown that the refined LS1 model is an accurate and efficient model for estimating energy release rate and also stress fields even very close to singularities. In this study, by tackling a general cylindrical bending problem, mode I and mode II delaminations are investigated. The unilateral contact conditions are imposed

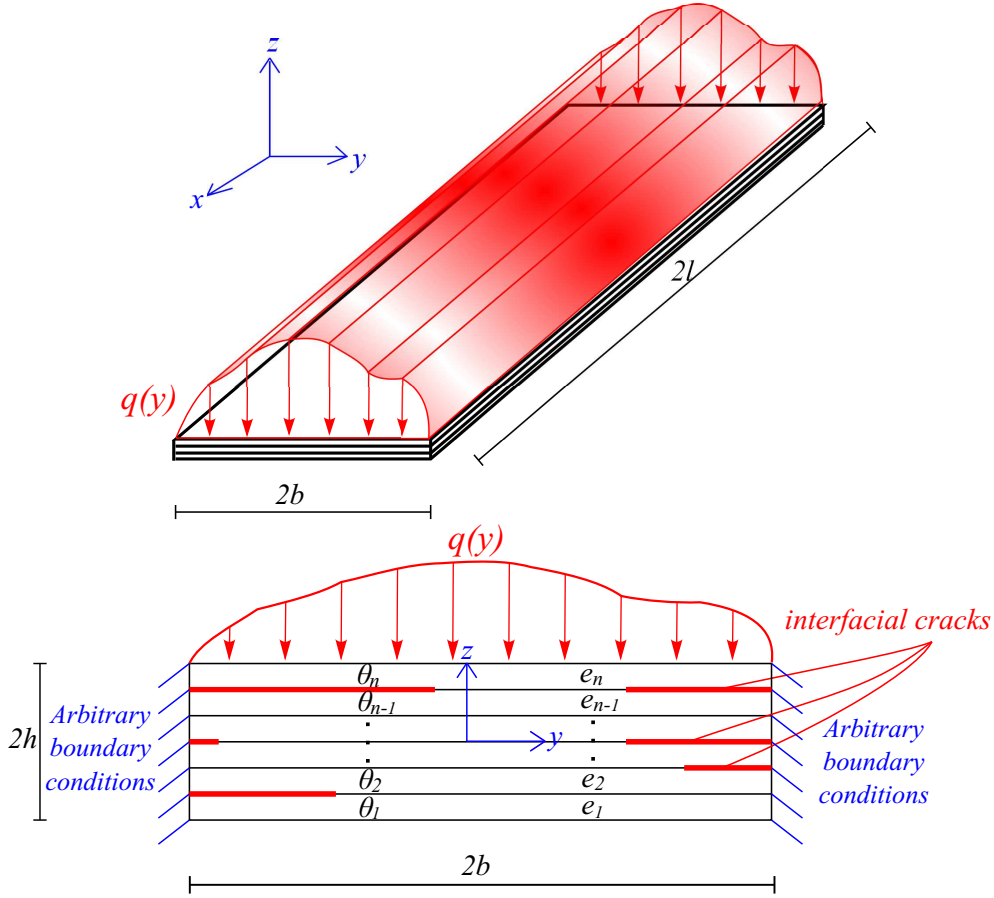


Figure 4.1: Laminate geometry, bending load and coordinate system (top); Laminate section in the yz plane

at delaminated interfaces between adjacent layers. At first, the problem is formulated for a general bending loading $q(y)$ (see Fig. 4.1). Then as application examples, classical mode I (Double Cantilever) and mode II (End Notched Flexure) delamination tests are investigated. In a previous work on the LS1 model [Saeedi et al. 2012b], the initiation of delamination was extensively studied. Herein, the LS1 model is applied to the propagation of modes I and II delamination in composite laminates. The proposed method has the advantage of being able to analyse multi-delamination situation. The solving method consists in dividing vertically the delaminated plate into sub-laminates (zones) at each crack tip; then deriving the solution of every zone separately. Finally, by enforcing displacement and stress continuity conditions between adjacent zones, the global solution of the delaminated plate is obtained. In order to validate the proposed method, two classical delamination tests (mode I and mode II) in composite laminates are studied. Results of the LS1 model are obtained using a dedicated program developed by the authors and compared with 3D-FEM results obtained by commercial finite element software Abaqus.

The paper is organized as follows: In section 2, cylindrical bending problem is described and the formulation of the LS1 model is briefly presented. In section 3, the

solving method is introduced and the governing system of equations on delaminated and non-delaminated zones are derived. Then, by applying the eigenvector expansion method, analytical LS1 solution of the problem is obtained. Comparisons between the LS1 and 3D-FE modeling, and discussion on results are provided in section 4.

4.2 Cylindrical bending problem

4.2.1 Problem description

A general $(\theta_1, \theta_2, \dots, \theta_n)$ composite plate with a length of $2l$ and a width of $2b$ respectively in the x and y directions is considered (Fig. 4.1). The thickness of the laminate following the z direction is equal to $\sum_{i=1}^n e^i = 2h$ and the middle plane of the plate is located at $z = 0$. The behavior of all layers is in general considered orthotropic. The laminate is subjected to cylindrical bending via an out-of-plane loading $q(y)$ applied on its top surface. It is assumed that the plate is long in the x direction ($l \gg b, h$) so that the strain components are independent of the x coordinate. Regarding the delamination, an arbitrary multi-delamination situation is considered in which there can be several interfacial cracks with different length as shown in Fig. 4.1.

4.2.2 Formulation of the LS1 model

In this section, the formulation of the *LS1* model is briefly presented. As explained in the introduction, the *LS1* model is a layerwise stress approach with first-order membrane stress approximation per layer. The model is a superposition of Reissner-Mindlin plates connected together by interfacial stresses. Since these interfacial stresses are considered as generalized stresses in the model, the stress continuities at interfaces are ensured. Unlike other layerwise models which are based on displacement or mixed displacement-stress approaches, the LS1 model, inspired from Pagano's model [Pagano 1978a], is a pure layerwise stress approach. As a matter of fact, in the LS1 formulation there is no hypothesis on displacement fields.

In what follows, x and y represent the in-plane directions while z is the thickness coordinate. h_-^i , h_+^i and \bar{h}^i are respectively the bottom, the top and the mid-plane z coordinates of layer i and $e^i = h_+^i - h_-^i$ denotes the layer thickness. Greek alphabet subscripts (such as $\alpha, \beta, \gamma, \delta$) correspond to $\{x, y\}$ or $\{1, 2\}$ and the Einstein summation convention is adopted for repeated indices.

Since each layer is considered as a Reissner-Mindlin plate, there are three displacement fields $U_x^i(x, y)$, $U_y^i(x, y)$, $U_z^i(x, y)$ and two rotation fields $\Phi_x^i(x, y)$, $\Phi_y^i(x, y)$ per layer for $1 \leq i \leq n$.

Generalized stresses of the model consist of three in-plane stress resultants $N_{\alpha\beta}^i$, three moment resultants $M_{\alpha\beta}^i$ (at the mid-plane of layer) and two out-of-plane shear resultants Q_α^i per layer i , also two shear stresses $\tau_x^{i,i+1}$, $\tau_y^{i,i+1}$ and one normal stress $\nu^{i,i+1}$ per interface $i, i + 1$. Generalized strains, corresponding to these generalizes stresses are as follows:

- for layer i

$$\begin{aligned}
 \varepsilon_{\alpha\beta}^i &= \frac{1}{2} (U_{\alpha,\beta}^i + U_{\beta,\alpha}^i) \longleftrightarrow N_{\alpha\beta}^i(x, y) \\
 \chi_{\alpha\beta}^i &= \frac{1}{2} (\Phi_{\alpha,\beta}^i + \Phi_{\beta,\alpha}^i) \longleftrightarrow M_{\alpha\beta}^i(x, y) \\
 d_{\Phi_\alpha}^i &= \Phi_\alpha^i + U_{z,\alpha}^i \longleftrightarrow Q_\alpha^i(x, y)
 \end{aligned} \tag{4.1}$$

- for interface $i, i + 1$

$$\begin{aligned}
 D_\alpha^{i,i+1} &= U_\alpha^{i+1} - U_\alpha^i - \left(\frac{e^i}{2} \Phi_\alpha^i + \frac{e^{i+1}}{2} \Phi_\alpha^{i+1} \right) \longleftrightarrow \tau_\alpha^{i,i+1}(x, y) \\
 D_z^{i,i+1} &= U_z^{i+1} - U_z^i \longleftrightarrow \nu^{i,i+1}(x, y)
 \end{aligned} \tag{4.2}$$

where $\varepsilon_{\alpha\beta}^i$, $\chi_{\alpha\beta}^i$ and $d_{\Phi_\alpha}^i$ are, respectively, in-plane strains, curvatures and out-of-plane shear strains of layer i . $D_\alpha^{i,i+1}$ and $D_z^{i,i+1}$ are relative displacements at interface $i, i + 1$.

Constitutive relations connect the generalized stresses to the generalized strains as follows:

- for layer i

$$\begin{aligned}
 \varepsilon_{\alpha\beta}^i &= \frac{1}{e^i} S_{\alpha\beta\gamma\delta}^i N_{\gamma\delta}^i \\
 \chi_{\alpha\beta}^i &= \frac{12}{(e^i)^3} S_{\alpha\beta\gamma\delta}^i M_{\gamma\delta}^i \\
 d_{\Phi_\alpha}^i &= \frac{6}{5e^i} S_{Q_{\alpha\beta}}^i Q_\beta^i - \frac{1}{10} S_{Q_{\alpha\beta}}^i (\tau_\beta^{i-1,i} + \tau_\beta^{i,i+1})
 \end{aligned} \tag{4.3}$$

- for interface $i, i + 1$

$$\begin{aligned}
 D_\alpha^{i,i+1} &= -\frac{1}{10} (S_{Q_{\alpha\beta}}^i Q_\beta^i + S_{Q_{\alpha\beta}}^{i+1} Q_\beta^{i+1}) - \frac{1}{30} (e^i S_{Q_{\alpha\beta}}^i \tau_\beta^{i-1,i} + e^{i+1} S_{Q_{\alpha\beta}}^{i+1} \tau_\beta^{i+1,i+2}) \\
 &\quad + \frac{2}{15} (e^i S_{Q_{\alpha\beta}}^i + e^{i+1} S_{Q_{\alpha\beta}}^{i+1}) \tau_\beta^{i,i+1} \\
 D_z^{i,i+1} &= \frac{9}{70} (e^i S_\nu^i \nu^{i-1,i} + e^{i+1} S_\nu^{i+1} \nu^{i+1,i+2}) + \frac{13}{35} (e^i S_\nu^i + e^{i+1} S_\nu^{i+1}) \nu^{i,i+1}
 \end{aligned} \tag{4.4}$$

where $S_{\alpha\beta\gamma\delta}^i$, $S_{Q_{\alpha\beta}}^i$ and S_ν^i are the components of the compliance matrix of layer i . They are respectively related to the plane stress, out-of-plane shear stress and normal stress components.

Regarding equilibrium equations, there are five equations for each layer:

$$\begin{aligned}
 N_{\alpha\beta,\beta}^i + \tau_\alpha^{i,i+1} - \tau_\alpha^{i-1,i} &= 0 \\
 M_{\alpha\beta,\beta}^i + \frac{e^i}{2} (\tau_\alpha^{i,i+1} + \tau_\alpha^{i-1,i}) - Q_\alpha^i &= 0 \\
 Q_{\beta,\beta}^i + \nu^{i,i+1} - \nu^{i-1,i} &= 0
 \end{aligned} \tag{4.5}$$

The boundary conditions of the model are written in terms of generalized stresses or generalized displacements. At point $p(x_0, y_0)$ on the lateral edge of the plate, the five boundary conditions are given as follows:

$$\begin{aligned} N_{\alpha\beta}^i(x_0, y_0) n_\beta &= [N_\alpha^i]^d & \text{or} & & U_\alpha^i(x_0, y_0) &= [U_\alpha^i]^d \\ M_{\alpha\beta}^i(x_0, y_0) n_\beta &= [M_\alpha^i]^d & \text{or} & & \Phi_\alpha^i(x_0, y_0) &= [\Phi_\alpha^i]^d \\ Q_\alpha^i(x_0, y_0) n_\alpha &= [Q^i]^d & \text{or} & & U_z^i(x_0, y_0) &= [U_z^i]^d \end{aligned} \quad (4.6)$$

where the vector $\underline{n} = (n_\alpha, n_\beta)^t$ is the outward normal to the lateral edge and the superscript d denotes determined (given) fields.

4.2.3 x -invariance hypothesis

The invariance in the x direction yields the generalized displacements as follows:

$$\begin{aligned} U_x^i(x, y) &= u_x^i(y) & ; & & U_y^i(x, y) &= u_y^i(y) & ; & & U_z^i(x, y) &= u_z^i(y) \\ \Phi_x^i(x, y) &= \phi_x^i(y) & ; & & \Phi_y^i(x, y) &= \phi_y^i(y) \end{aligned} \quad (4.7)$$

By introducing these displacement fields into Eqs. 4.1 and 4.2, the generalized strain components are obtained as follows:

- for layer i

$$\begin{aligned} \varepsilon_{xx}^i &= 0 & ; & & \varepsilon_{yy}^i &= u_y^{i'} & ; & & \varepsilon_{xy}^i &= \frac{1}{2}u_x^{i'} \\ \chi_{xx}^i &= 0 & ; & & \chi_{yy}^i &= \phi_y^{i'} & ; & & \chi_{xy}^i &= \frac{1}{2}\phi_x^{i'} \\ d_x^i &= \phi_x^i & ; & & d_y^i &= \phi_y^i + u_z^{i'} \end{aligned} \quad (4.8)$$

- for interface $i, i + 1$

$$\begin{aligned} D_x^{i,i+1} &= u_x^{i+1} - u_x^i - \left(\frac{e^i}{2}\phi_x^i + \frac{e^{i+1}}{2}\phi_x^{i+1} \right) \\ D_y^{i,i+1} &= u_y^{i+1} - u_y^i - \left(\frac{e^i}{2}\phi_y^i + \frac{e^{i+1}}{2}\phi_y^{i+1} \right) \\ D_z^{i,i+1} &= u_z^{i+1} - u_z^i \end{aligned} \quad (4.9)$$

where the prime denotes the differentiation with respect to y .

According to Eqs. 4.5, the equilibrium equations are written for each layer ($1 \leq i \leq n$) as follows:

$$N_{xy}^{i'} + \tau_x^{i,i+1} - \tau_x^{i-1,i} = 0 \quad (4.10)$$

$$N_{yy}^{i'} + \tau_y^{i,i+1} - \tau_y^{i-1,i} = 0 \quad (4.11)$$

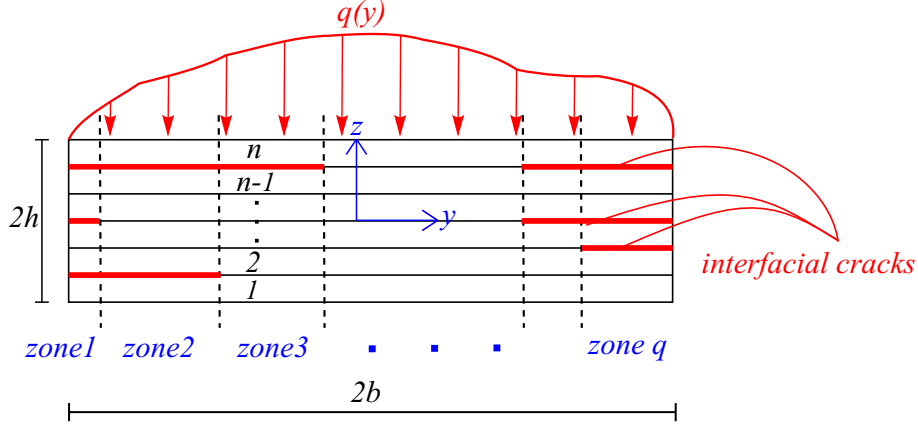


Figure 4.2: Solving method for laminate with several interfacial cracks

$$M_{xy}^i{}' + \frac{e}{2} (\tau_x^{i,i+1} + \tau_x^{i-1,i}) - Q_x^i = 0 \quad (4.12)$$

$$M_{yy}^i{}' + \frac{e}{2} (\tau_y^{i,i+1} + \tau_y^{i-1,i}) - Q_y^i = 0 \quad (4.13)$$

$$Q_y^i{}' + \nu^{i,i+1} - \nu^{i-1,i} = 0 \quad (4.14)$$

It should be noted that in the previous equations the interfaces 0, 1 and $n, n + 1$ denote respectively the bottom and the top surface of the plate. In view of the loading, the stress components on the bottom and the top surface are as:

$$\begin{aligned} \tau_x^{0,1} = \tau_y^{0,1} = \nu^{0,1} &= 0 \\ \tau_x^{n,n+1} = \tau_y^{n,n+1} &= 0 \quad ; \quad \nu^{n,n+1} = -q(y) \end{aligned}$$

4.3 Analytical LS1 solution

As shown in Fig. 4.1, there are several interfacial cracks with different length in the laminate section plane. The solving method consists in segmenting the laminate section vertically at every crack tip. In this way, depending on the crack tip positions along the y direction, several zones are found as shown in Fig. 4.2. On each zone, each of the $n - 1$ interfaces can be delaminated or not. To solve the problem, the governing system of equations is derived and solved for every zone. Then, by enforcing continuity conditions between adjacent zones and employing boundary conditions at the edges, the general solution is obtained.

4.3.1 Non-delaminated zone

At first, the problem solution is found for a non-delaminated zone in which no interface is delaminated. In the next step, this solution is extended to multi-delamination case.

By writing the compatibility, constitutive and equilibrium equations of the LS1 model, $16n - 3$ equations are obtained. Among them, $6n - 3$ are algebraic equations. Therefore, it is possible to eliminate $6n - 3$ unknown fields (N_{xx}^i , M_{xx}^i , Q_x^i , $\tau_x^{i,i+1}$, $\tau_y^{i,i+1}$ and $\nu^{i,i+1}$). By inserting the compatibility relations into the algebraic constitutive relations, these $6n - 3$ unknown fields are expressed in terms of the other unknown fields as follows:

$$N_{xx}^i = -\frac{S_{12}^i}{S_{11}^i}N_{yy}^i - \frac{S_{16}^i}{S_{11}^i}N_{xy}^i \quad ; \quad 1 \leq i \leq n \quad (4.15)$$

$$M_{xx}^i = -\frac{S_{12}^i}{S_{11}^i}M_{yy}^i - \frac{S_{16}^i}{S_{11}^i}M_{xy}^i \quad ; \quad 1 \leq i \leq n \quad (4.16)$$

$$\underline{A} = \underline{\underline{N}}^{-1} \cdot \underline{B} \quad (4.17)$$

where

$$\begin{aligned} (\underline{A})^t &= \left(\underbrace{Q_x^1, \dots, Q_x^n}_n, \underbrace{\tau_x^{1,2}, \dots, \tau_x^{n-1,n}}_{n-1}, \underbrace{\tau_y^{1,2}, \dots, \tau_y^{n-1,n}}_{n-1} \right) \\ (\underline{B})^t &= \left(\underbrace{\alpha^1, \dots, \alpha^n}_n, \underbrace{\beta^{1,2}, \dots, \beta^{n-1,n}}_{n-1}, \underbrace{\gamma^{1,2}, \dots, \gamma^{n,n-1}}_{n-1} \right) \end{aligned}$$

with

$$\alpha^i = \phi_x^i - \frac{6}{5e^i}S_{Q12}^i Q_y^i$$

$$\beta^{i,i+1} = u_x^{i+1} - u_x^i - \left(\frac{e^i}{2}\phi_x^i + \frac{e^{i+1}}{2}\phi_x^{i+1} \right) + \frac{1}{10} \left(S_{Q12}^i Q_y^i + S_{Q12}^{i+1} Q_y^{i+1} \right)$$

$$\gamma^{i,i+1} = u_y^{i+1} - u_y^i - \left(\frac{e^i}{2}\phi_y^i + \frac{e^{i+1}}{2}\phi_y^{i+1} \right) + \frac{1}{10} \left(S_{Q22}^i Q_y^i + S_{Q22}^{i+1} Q_y^{i+1} \right)$$

and $\underline{\underline{N}}$ is a $3n - 2 \times 3n - 2$ matrix.

$$\underline{C} = \underline{\underline{R}}^{-1} \cdot (\underline{D} - \underline{W}) \quad (4.18)$$

where

$$(\underline{C})^t = (\nu^{1,2}, \nu^{2,3}, \dots, \nu^{n-1,n})$$

$$(\underline{D})^t = (u_z^2 - u_z^1, u_z^3 - u_z^2, \dots, u_z^{n-1} - u_z^{n-2}, u_z^n - u_z^{n-1})$$

$$(\underline{W})^t = \left(\underbrace{0, 0, \dots, 0}_{n-2}, \frac{9}{70}e^n S_\nu^n q(y) \right)$$

and \underline{R} is a $n - 1 \times n - 1$ matrix. The expressions of the matrices \underline{N} and \underline{R} are given in Appendix 4.A.

Now, there are $10n$ first-order differential equations and the same number of unknowns fields ($N_{xy}^i, N_{yy}^i, M_{xy}^i, M_{yy}^i, Q_y^i, u_x^i, u_y^i, \phi_x^i, \phi_y^i, u_z^i$). These $10n$ equations are transformed into $5n$ second-order differential equations. Eliminating $N_{xy}^i, N_{yy}^i, M_{xy}^i, M_{yy}^i, u_z^i$ between the constitutive and equilibrium equations gives:

$$(u_x^i)'' = \frac{1}{e^i} [c^i (\tau_x^{i-1,i} - \tau_x^{i,i+1}) + b^i (\tau_y^{i-1,i} - \tau_y^{i,i+1})] \quad (4.19)$$

$$(u_y^i)'' = \frac{1}{e^i} [b^i (\tau_x^{i-1,i} - \tau_x^{i,i+1}) + a^i (\tau_y^{i-1,i} - \tau_y^{i,i+1})] \quad (4.20)$$

$$(\phi_x^i)'' = \frac{12}{(e^i)^3} \left[c^i \left(Q_x^i - \frac{e^i}{2} (\tau_x^{i-1,i} + \tau_x^{i,i+1}) \right) + b^i \left(Q_y^i - \frac{e^i}{2} (\tau_y^{i-1,i} + \tau_y^{i,i+1}) \right) \right] \quad (4.21)$$

$$(\phi_y^i)'' = \frac{12}{(e^i)^3} \left[b^i \left(Q_x^i - \frac{e^i}{2} (\tau_x^{i-1,i} + \tau_x^{i,i+1}) \right) + a^i \left(Q_y^i - \frac{e^i}{2} (\tau_y^{i-1,i} + \tau_y^{i,i+1}) \right) \right] \quad (4.22)$$

$$(Q_y^i)'' = (\nu^{i-1,i})' - (\nu^{i,i+1})' \quad (4.23)$$

where a^i, b^i and c^i are constants which depend on the material properties and the layer orientation. They are defined as follows (S_{ki}^i are the components of the plane stress compliance matrix of layer i):

$$a^i = \left(S_{22} - \frac{(S_{12})^2}{S_{11}} \right)^i, \quad b^i = \left(S_{26} - \frac{S_{12} S_{16}}{S_{11}} \right)^i, \quad c^i = \left(S_{66} - \frac{(S_{16})^2}{S_{11}} \right)^i$$

Substituting Eqs. 4.17 and 4.18 into the above equations, results a system of $5n$ second-order differential equations as follows:

$$\underline{X}''(y) = \underline{M} \cdot \underline{X}(y) + \underline{F}(y) \quad (4.24)$$

where \underline{X} is a vector consisting of the $5n$ unknown fields and \underline{M} is a $5n \times 5n$ matrix which depends on the mechanical material properties, the orientation and the thickness of layers. The vector \underline{F} is a function of external loading $q(y)$ on the top surface of the plate.

4.3.2 Delaminated zone

Now, it is assumed that there is one or more interfacial cracks. For every delaminated interface $k, k + 1$, three unknown displacement discontinuity fields $\gamma_x^{k,k+1}, \gamma_y^{k,k+1}$ and $\gamma_z^{k,k+1}$ are introduced. Therefore, three supplementary equations are needed. These equations are obtained by imposing the following conditions:

$$\tau_x^{k,k+1} = 0, \quad \tau_y^{k,k+1} = 0 \quad (4.25)$$

and the unilateral contact conditions:

$$\gamma_z^{k,k+1} \geq 0, \quad \nu^{k,k+1} \leq 0, \quad \nu^{k,k+1} \gamma_z^{k,k+1} = 0 \quad (4.26)$$

The first condition $\gamma_z^{k,k+1} \geq 0$ implies that no penetration can occur between two adjacent layers. The second condition $\nu^{k,k+1} \leq 0$ is related to the fact, that no tension force is allowed to occur within the delaminated interface (a positive value for the normal interfacial stress $\nu^{k,k+1}$ means tension, and a negative value compression). According to the third condition, if the normal interfacial stress is negative ($\nu^{k,k+1} < 0$), there is no crack opening displacement ($\gamma_z^{k,k+1} = 0$). Otherwise, if the crack opening displacement is not zero ($\gamma_z^{k,k+1} > 0$), the normal interface stress will be zero ($\nu^{k,k+1} = 0$).

The solution technique is as follows: first of all, it is assumed that the two adjacent layers are in contact ($\gamma_z^{k,k+1} = 0$) all over the delamination zone. After solving the problem according to the method described in the following, the condition $\nu^{k,k+1} \leq 0$ is checked over the delamination crack. In the zones in which $\nu^{k,k+1} > 0$, the unilateral conditions are not satisfied; therefore, the problem is resolved again assuming that there is no contact ($\nu^{k,k+1} = 0$) in these zones. Then, the condition $\gamma_z^{k,k+1} \geq 0$ is checked. In the zones in which $\gamma_z^{k,k+1} < 0$, the contact condition is assumed again and the problem is resolved. This iteration is continued until the unilateral conditions are satisfied all over the delamination zone.

The constitutive relations at delaminated interface $k, k + 1$ are the same as Eq. 4.9 except that on the left sides $D_\alpha^{k,k+1}$ and $D_z^{k,k+1}$ are substituted by $D_\alpha^{k,k+1} - \gamma_\alpha^{k,k+1}$ and $D_z^{k,k+1} - \gamma_z^{k,k+1}$ respectively.

The interlaminar stresses $\tau_x^{k,k+1}$, $\tau_y^{k,k+1}$ and $\nu^{k,k+1}$ (if $\nu^{k,k+1} \neq 0$) are known and should be eliminated from the systems 4.17 and 4.18. Consequently, these systems are rewritten as:

$$\begin{aligned} \underline{A}_d &= \underline{N}_d^{-1} \cdot \underline{B}_d \\ \underline{C}_d &= \underline{R}_d^{-1} \cdot (\underline{D}_d - \underline{W}_d) \end{aligned} \quad (4.27)$$

where the index d signifies the delaminated state (see Appendix 4.A for the expressions of the above vectors and matrices).

By applying the same method used in the non-delaminated state, a similar system of $5n$ second-order differential equations is obtained as follows:

$$\underline{X}''(y) = \underline{M}_d \cdot \underline{X}(y) + \underline{F}(y) \quad (4.28)$$

\underline{M}_d is a $5n \times 5n$ matrix which depends not only on the mechanical material properties, the orientation and the thickness of the layers but also on the positions of the interfacial cracks in each zone.

Remark: According to the vector $\underline{F}(y)$ in Eqs. 4.24 and 4.28, the systems of equations in both non-delaminated and delaminated zones are nonhomogeneous. The vector \underline{F} arises from the vectors \underline{W} and \underline{W}_d in Eqs. 4.18 and 4.27, and thus is a function of $q(y)$. It means that the cylindrical bending loading $q(y)$ gives rise to a nonhomogeneous system of equations. That is not the case for a uniaxial extension loading. In [Saeedi et al. 2012a], it has been shown that the corresponding system of equations is homogeneous if the laminate is only subjected to extension.

4.3.3 Solution

By applying the eigenvector expansion method, the obtained system of equations is solved analytically (see Appendix 4.B). Knowing that there may be real, complex and repeated eigenvalues, the general solution of the associated homogeneous system of equations will be in the form of exponential, trigonometric and polynomial functions as follows:

$$\underline{X}_h = \sum_{i=1}^{2n} e^{\alpha_i y} \left[\underline{P}_i(y) \sin(\beta_i y) + \underline{Q}_i(y) \cos(\beta_i y) \right] \quad (4.29)$$

where the components of the vectors $\underline{P}_i(y)$ and $\underline{Q}_i(y)$ are polynomial functions with constant coefficients. Degrees of these polynomials depend on the multiplicity of the eigenvalues. The general solution of the nonhomogeneous system is the sum of the general solution of the related homogeneous system and a particular solution:

$$\underline{X} = \underline{X}_h + \underline{X}_p \quad (4.30)$$

The form of the vector \underline{X}_p (a particular solution for the nonhomogeneous system) depends on the bending load $q(y)$. In this study, for polynomial, exponential and trigonometric functions $q(y)$, the method of undetermined coefficients is used to find the particular solution.

The governing system of equations in each zone consists of $5n$ second-order differential equations. Therefore, for q zones, there are $10n \times q$ unknown constants of integration which are determined using continuity and boundary conditions. The boundary conditions are obtained by writing stress or displacement conditions at the edges $y = \pm b$. For each layer i ($1 \leq i \leq n$) at each edge, there are five boundary conditions either on generalized stresses or on generalized displacements:

$$\begin{aligned} u_x^i(y_0) &\longleftrightarrow N_{xy}^i(y_0) & u_y^i(y_0) &\longleftrightarrow N_{yy}^i(y_0) & u_z^i(y_0) &\longleftrightarrow Q_y^i(y_0) \\ \phi_x^i(y_0) &\longleftrightarrow M_{xy}^i(y_0) & \phi_y^i(y_0) &\longleftrightarrow M_{yy}^i(y_0) \end{aligned} \quad (4.31)$$

where y_0 denotes the edge position (herein $y_0 = b$ and $y_0 = -b$). In this way, $10n$ boundary conditions corresponding to the edges $y = \pm b$ are obtained.

The continuity conditions are deduced from the continuity of generalized displacements and generalized stresses between adjacent zones. There are $5n$ displacement continuity relations between every two adjacent zones as follows:

$$\begin{aligned} [[u_x^i(y_p)]] &= 0, \quad [[u_y^i(y_p)]] = 0, \quad [[u_z^i(y_p)]] = 0 \\ [[\phi_x^i(y_p)]] &= 0, \quad [[\phi_y^i(y_p)]] = 0 \end{aligned} \quad (4.32)$$

The continuities of the generalized stresses are written as:

$$\begin{aligned} [[N_{xy}^i(y_p)]] &= 0, \quad [[N_{yy}^i(y_p)]] = 0, \quad [[Q_y^i(y_p)]] = 0 \\ [[M_{xy}^i(y_p)]] &= 0, \quad [[M_{yy}^i(y_p)]] = 0 \end{aligned} \quad (4.33)$$

By using the constitutive equations, these continuity conditions can be expressed in terms of $(u_x^i)'$, $(u_y^i)'$, $(\phi_x^i)'$, $(\phi_y^i)'$ and $(Q_y^i)'$ which are the principal unknowns of the final system.

Therefore, totally $10n + 10n \times (q - 1) = 10n \times q$ conditions are obtained. These conditions yield a system of $10n \times q$ linear algebraic equations with $10n \times q$ unknown constants which can be easily solved.

4.4 Numerical examples

In order to validate the proposed method and illustrate its accuracy, some classical delamination tests are carried out. The results of our model are compared with those of a 3D-FE model. The analytical solutions of the LS1 model are obtained by means of a dedicated program written in Mathematica (Wolfram Research) by the authors. The finite element modeling is performed in commercial finite element software Abaqus.

In [Saeedi et al. 2012a,b], mode III delamination has been fully discussed and the LS1 model has been applied to the prediction of delamination onset. Herein, we are interested in mode I and mode II delamination propagation under cylindrical bending. To this end, two classical mode I and mode II delamination tests on composite laminates are studied. The investigated laminates consist of G947/M18 carbon-epoxy plies whose mechanical properties, tested by Lagunegrand et al. [2006], are as follows:

$$\begin{aligned} E_L &= 97.6 \text{ GPa} ; E_T = E_N = 8.0 \text{ GPa} \\ G_{LT} &= G_{LN} = 3.1 \text{ GPa} ; G_{TN} = 2.7 \text{ GPa} \\ \nu_{LT} &= \nu_{LN} = 0.37 ; \nu_{TN} = 0.5 ; e = 0.19 \text{ mm} \end{aligned}$$

In investigated examples, the composite plate is under cylindrical bending and the length of the plate is assumed infinite in the x direction. Invariance conditions are exploited in the 3D-FE modeling in order to ensure the longitudinal invariance and reduce the computational cost. Since there is no variation in the x direction, it is sufficient to consider only one element in the x direction with the following invariance conditions:

$$\begin{aligned} U_x(x_1, y, z) &= U_x(x_0, y, z) \\ U_y(x_1, y, z) &= U_y(x_0, y, z) \\ U_z(x_1, y, z) &= U_z(x_0, y, z) \end{aligned} \tag{4.34}$$

It should be noted that the size of the elements in the x direction does not play any role (the elements will be taken to have unit size in this direction). Therefore, the 3D aspect ratio of the elements has no importance while the 2D aspect ratio in the yz plane should be taken into consideration.

In order to model the propagation of delamination, a crack extension resistance curve (R-curve) is required. The R-curve is a plot of the interlaminar fracture toughness G_c as a function of the crack extension. This curve is used to examine the processes

of crack growth. The fracture behavior is complex and fracture toughness cannot be characterized as intrinsic property of the laminate. Indeed, the R-curve behavior is not a material property but depends on the specimen shape. This is why in many research works on delamination, the R-curve effect is neglected and fracture toughness G_c is considered constant [Wang and Crossman 1980]. Various experimental tests show that the resistance to fracture increases with growing crack size in elastic-plastic materials. In general, the delamination propagation energy reaches a plateau for high values of crack extension (steady state). As a matter of fact, the interlaminar crack resistance varies between G_{ini}^c (fracture toughness associated to initiation of delamination growth) and G_{ss}^c (fracture toughness related to steady state delamination growth).

In this study, two typical R-curves will be used in order to model the propagation of delamination. As shown in Fig. 4.3, the first type is a constant law with $G^c = G_{ss}^c = 500 \text{ J/m}^2$. In this case, the interlaminar crack resistance remains constant during the crack propagation. The second is a bilinear law with $G_{ini}^c = 200 \text{ J/m}^2$ and $G_{ss}^c = 500 \text{ J/m}^2$. As already shown in the literature [Bui et al. 2000, Jacobsen and Sørensen 2001, Yan et al. 2001, Gutkin et al. 2011, De Souza et al. 2011], this fracture behavior is much more realistic in delamination tests. It should be mentioned that the aim of this work is not to investigate the form of the R-curve in different cases. In the present investigation, the R-curve is just an input for delamination modeling so that any other type of R-curve can be used in the models.

It is noted that in the LS1 modeling, the energy release rate is calculated via the virtual crack-closure technique (VCCT) while in the 3D-FE modeling, the J-Integral method is employed.

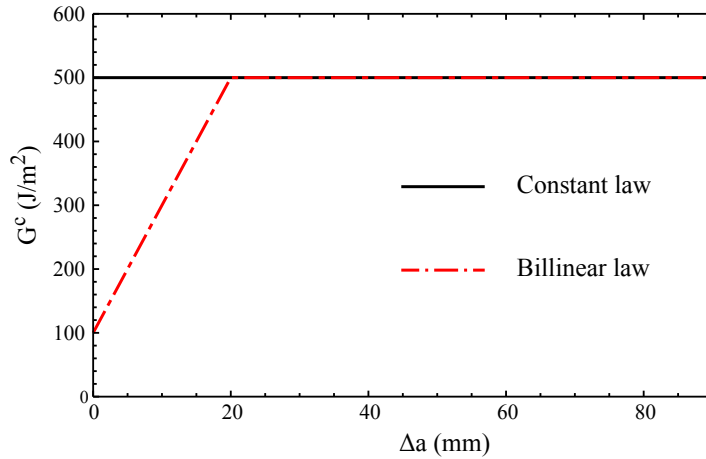


Figure 4.3: R-Curves (Resistance versus crack extension) used for mode I and mode II delamination

4.4.1 Mode I delamination - DCB like test

For mode I delamination, a double cantilever plate is studied. The test is the same as a double cantilever beam (DCB) test except that herein, there is an infinite plate

instead of a beam. The specimen is a $(45^\circ, -45^\circ)_{5s}$ composite laminate with a total thickness of $20e = 38mm$ and a width of $L = 2b = 100mm$ respectively in the z and y directions. As explained, the laminate is assumed to be long in the x direction so that there is no variation in this direction. Fig. 4.4 shows the plate geometry and applied loads in the yz plane. The delamination consists of an interlaminar crack of length a situated at the laminate mid-plane.

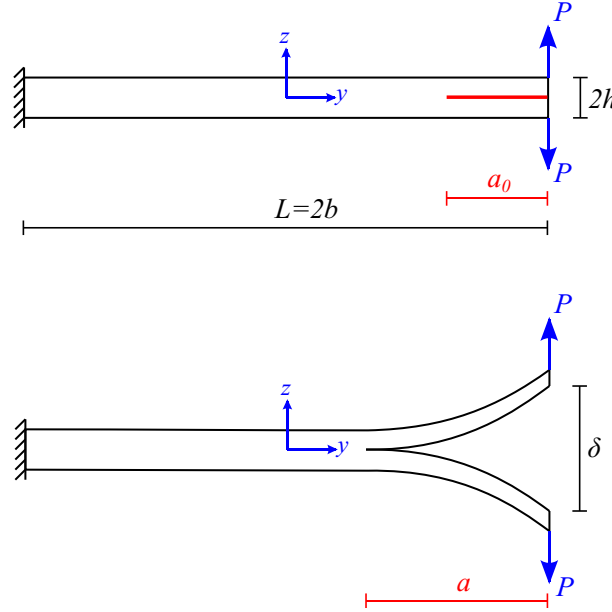


Figure 4.4: Mode I delamination : Undeformed State (Top); Deformed state (Bottom)

In the 3D-FE modeling, an appropriate mesh with hexahedral elements are used. In order to obtain accurate results, the mesh should be highly refined close to the crack tip (Fig. 4.5). The size of the smallest elements at the crack tip is about $1\mu m$ and the total number of nodes in the model is almost 60,000. Regarding the LS1 modeling, a *layerwise mesh* (i.e. the number of mathematical layers in the LS1 model corresponding to a physical layer) should be chosen. In [Saeedi et al. 2012b], the authors have proposed a specific layerwise mesh strategy for the LS1 model. It has been demonstrated that for the mode III delamination, this layerwise mesh strategy is very efficient and provides accurate estimations of energy release rate and interlaminar stresses near singularities. In this work, it will be shown that one mathematical layer per physical layer is sufficient to obtain accurate results for the propagation of delamination in modes I and II.

Fig. 4.6 plots the compliance $C = \delta/P$ and the energy release rate $G = -\partial W/\partial a$ versus the normalized crack length a/L . As expected, the compliance curve passes through the origin because for an interlaminar crack of length zero (i.e. $a = 0$), the crack opening displacement δ is zero. It is seen that the energy release rate corresponding to a zero-length delamination is also null. The results show that for all crack lengths, the compliance and energy release rate estimations of the LS1 model are as accurate as the 3D-FEM.

Now, the propagation of an existing delamination crack is investigated. The initial

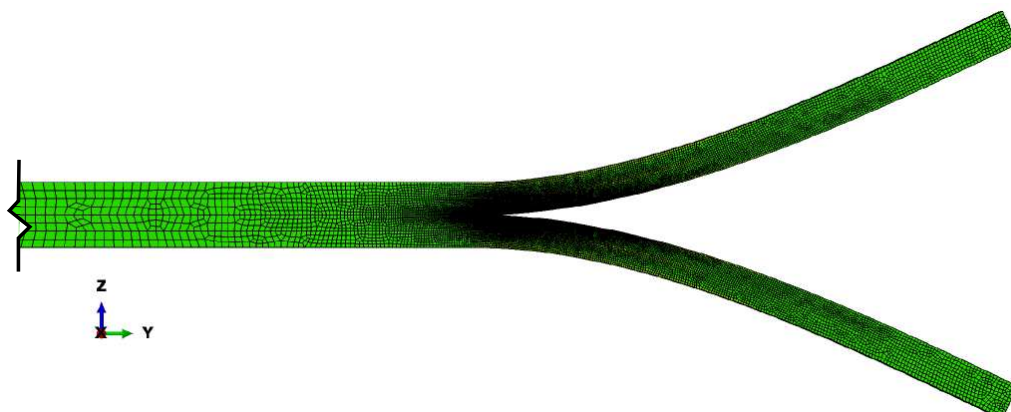


Figure 4.5: Mode I delamination - Finite element model

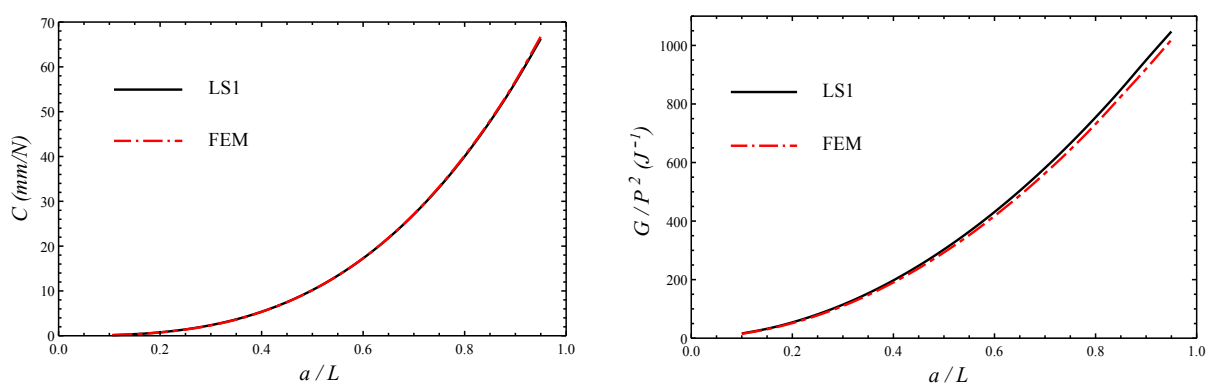


Figure 4.6: Compliance (Left) and energy release rate (right) versus crack length - Mode I delamination

crack length is taken as $a_0/L = 0.1$. As discussed above, two types of R-curve (constant and bilinear) are considered. Figs. 4.7 and 4.8 illustrate the crack opening displacement δ and the applied load P versus the normalized crack length. As seen, the two types of R-curve give almost the same results in terms of the crack opening displacement while the form of the load curves are different. As expected, for $0.1 < a/L < 0.3$ (i.e. $\Delta a < 20\text{mm}$), the R-curves are different and yield different values for the applied load P . It is observed that the values of P obtained by the constant R-curve are overestimated with respect to those calculated by the bilinear R-curve. Anyway, in both cases, the results of the LS1 model are as precise as those of the 3D-FEM.

The load-displacement curve is shown in Fig. 4.9 for the constant and bilinear R-curves. One can see that the first part of the $P - \delta$ curve is ascending reaching a peak; thereafter, the load decreases with increasing the displacement as the crack propagates. For the constant R-curve, the peak of the $P - \delta$ curve is much higher than the one obtained by the bilinear R-curve. This is due to the overestimation of the applied load obtained by the constant resistance curve. This overestimation causes that the descending part of the curve is more steeper in the case of the constant R-curve. By the way, it is clear to see that for both constant and bilinear R-curves, the LS1 and

4. CYLINDRICAL BENDING OF MULTILAYERED PLATES WITH MULTI-DELAMINATION VIA A LAYERWISE STRESS APPROACH

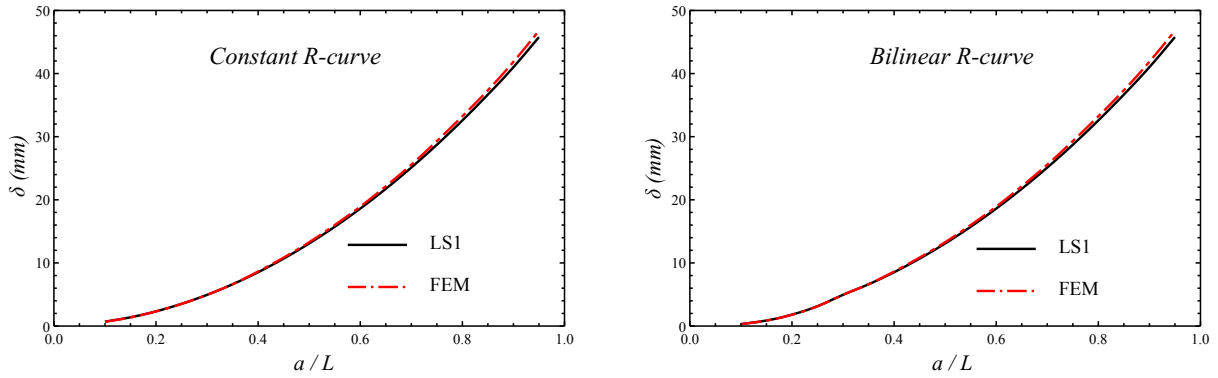


Figure 4.7: Crack opening displacement versus crack length - Mode I delamination

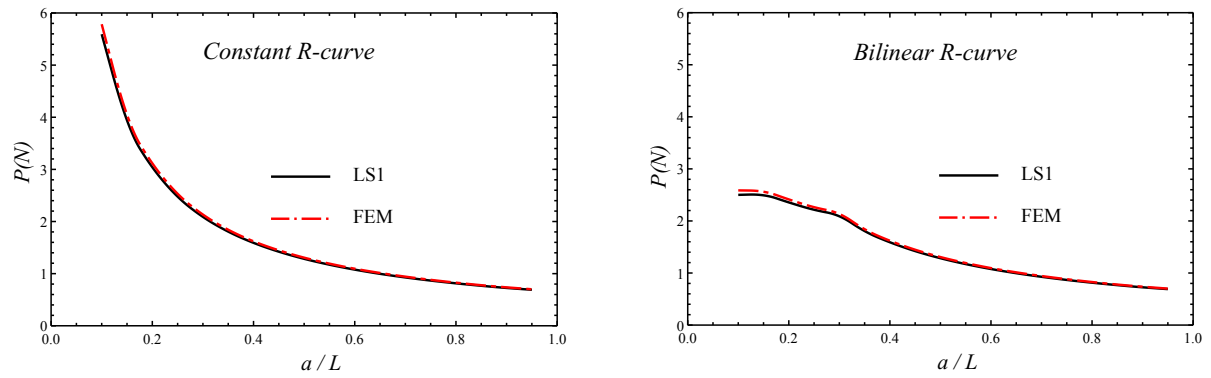


Figure 4.8: Applied load versus crack length - Mode I delamination

3D-FEM results are practically the same. It should be kept in mind that in the LS1 model, the total number of unknown constants is $10n \times q = 400$ while in the finite element model, there are about $3 \times 60,000 = 180,000$ degrees of freedom.

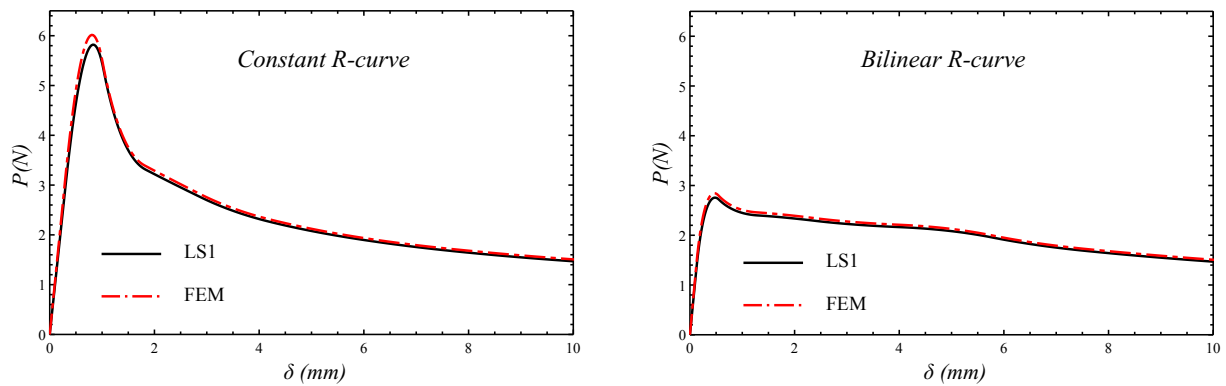


Figure 4.9: Applied load versus crack opening displacement - Mode I delamination

4.4.2 Mode II delamination - ENF like test

Now, mode II delamination is investigated via an End Notched Flexure (ENF) test. The specimen is a simple supported plate with a width of $L = 2b = 100mm$ and a thickness of $20e = 38mm$ respectively in the y and z directions while the length of the plate in the x direction is assumed infinite. The plate is a $(45^\circ, -45^\circ, 90^\circ, 0^\circ, -45^\circ, 45^\circ, 0^\circ, 90^\circ, -45^\circ, 45^\circ)_s$ composite laminate with an interlaminar crack at its mid-plane. Fig. 4.10 schematically shows the undeformed and deformed states of the specimen.

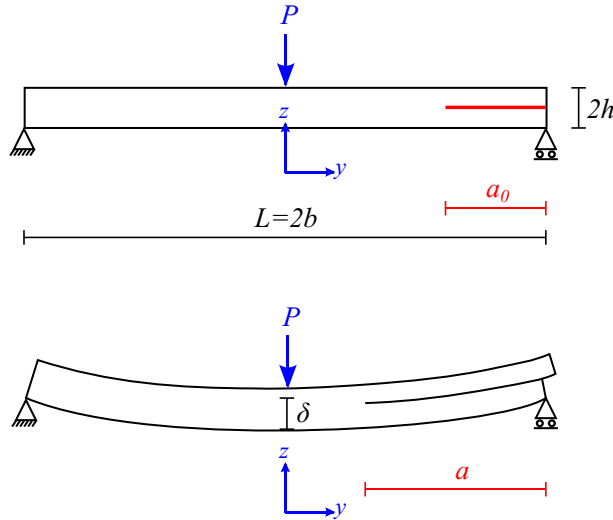


Figure 4.10: Mode II delamination : Undeformed State (Top); Deformed state (Bottom)

The finite element modeling is carried out using the invariance conditions discussed above. As shown in Fig. 4.11, the mesh should be extra refined at the crack tip in order to obtain accurate and reliable results.

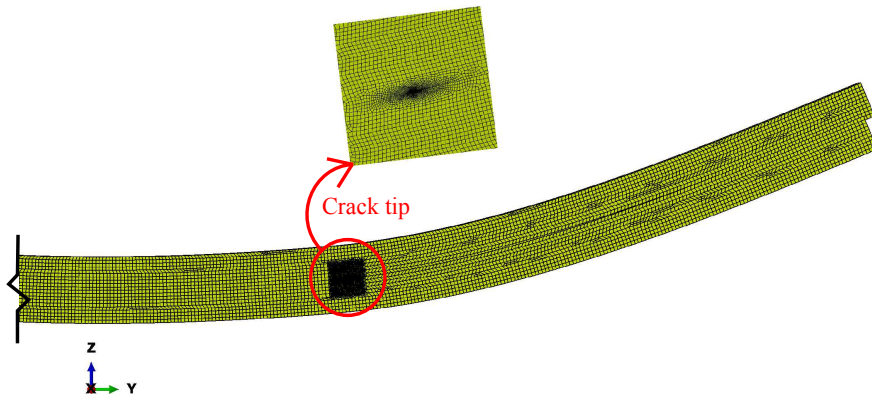


Figure 4.11: Mode II delamination - Finite element model

Fig. 4.12 shows the compliance $C = \delta/P$ and the energy release rate $G = -\partial W/\partial a$ as a function of the normalized crack length a/L . It should be noted that, herein, the

displacement δ corresponds to the deflection at the midspan of the plate. That is why the compliance curve does not pass through the origin. It is found that the convexity of the compliance curve changes at $a/L = 0.5$, which corresponds to the situation that the crack tip is at the midspan. As seen, the peak of the energy release rate curve is also observed at the same position.

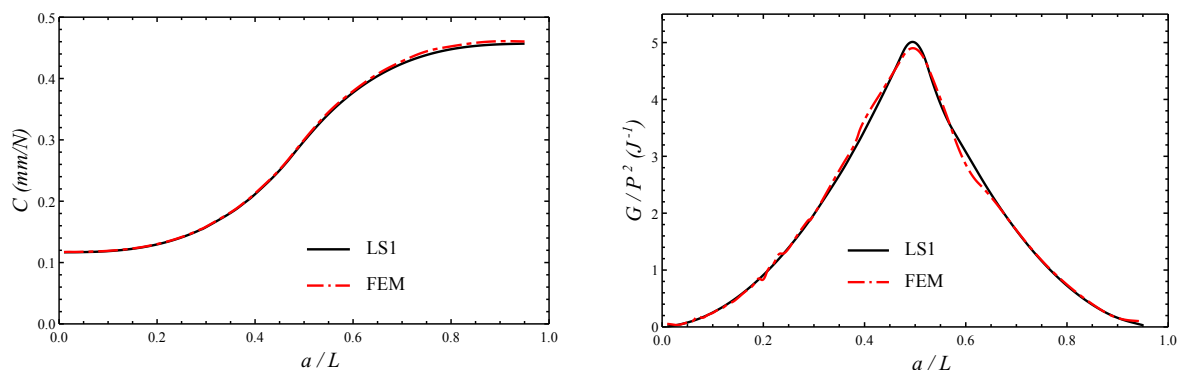


Figure 4.12: Compliance (Left) and energy release rate (right) versus crack length - Mode II delamination

Comparison between the LS1 and FEM results proves that the LS1 model provides accurate estimations in terms of compliance and energy release rate.

In order to examine the performance of the proposed model, a propagation study is carried out here. It is assumed that there is an existing interlaminar crack at the mid-plane of the laminate with an initial length of $a_0/L = 0.1$. As before, two types of R-curve (constant and bilinear) are investigated. Figs. 4.13 and 4.14 plot respectively the midspan deflection δ and the applied load P versus the normalized crack length a/L . As seen, in the case of the bilinear R-curve, the midspan deflection is constant for $0.1 < a/L < 0.5$. It means that the propagation of the delamination has no influence on the deflection. On the other hand, using a constant R-curve causes a decrease in the midspan deflection. Once the crack tip passes the midspan (i.e. $a/L > 0.5$), the deflection increases with the crack growth. Regarding the applied load, it is found that for $a/L < 0.5$ (i.e. the crack tip situated to the right of the load position), the applied load P decreases with the crack extension; while for $a/L > 0.5$ (i.e. the crack tip situated to the left of the load position), the crack propagation causes an increase in the applied load. As a matter of fact, the minimum value of the applied load occurs at $a/L = 0.5$ (i.e. the crack tip situated at the load position).

Fig. 4.15 shows the load-deflection curves. The descending parts of the curves correspond to the crack extension when $a/L < 0.5$. It is seen that the descending part is much steeper for the constant R-curve compared with the bilinear R-curve. The troughs in the curves correspond to $a/L = 0.5$. After that, the load-deflection curves ascend almost linearly.

It is clearly observed that in all cases, the LS1 model estimations are practically the same as the 3D-FEM results. This shows that the LS1 model can be used as an alternative model to the finite element modeling in delamination propagation problems.

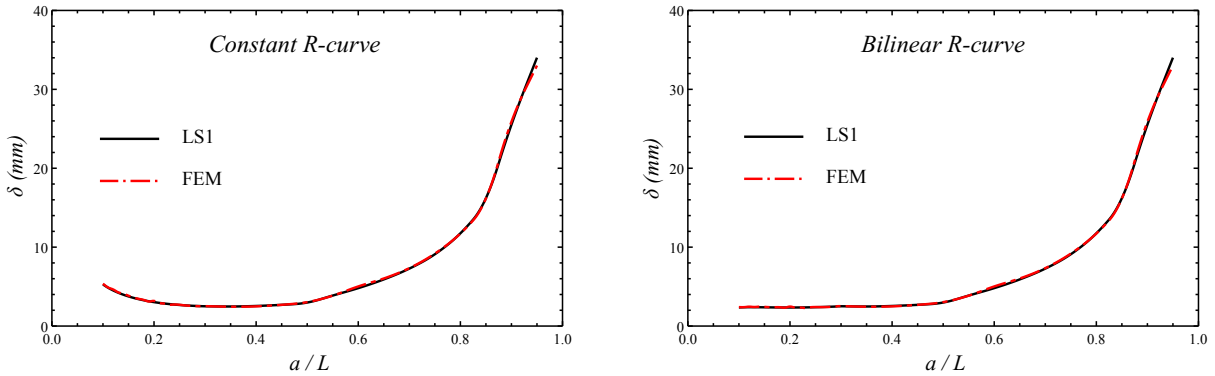


Figure 4.13: Midspan deflection versus crack length - Mode II delamination

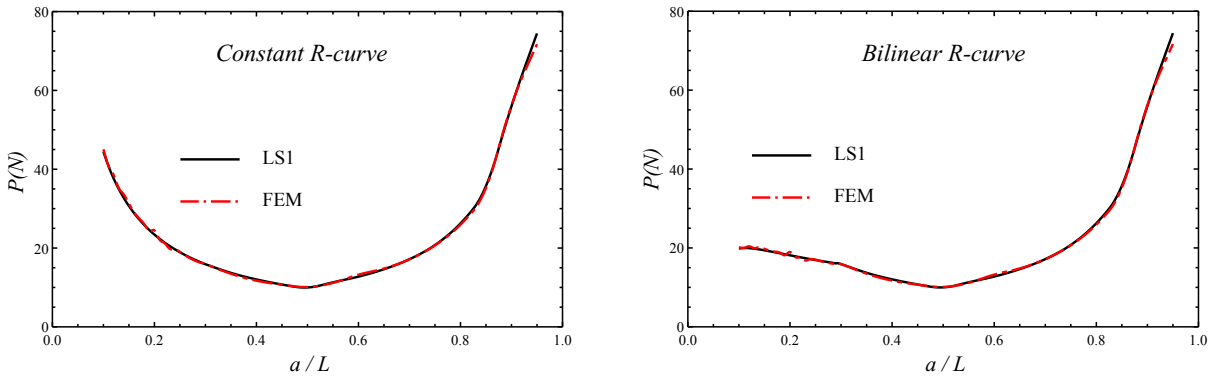


Figure 4.14: Applied load versus crack length - Mode II delamination

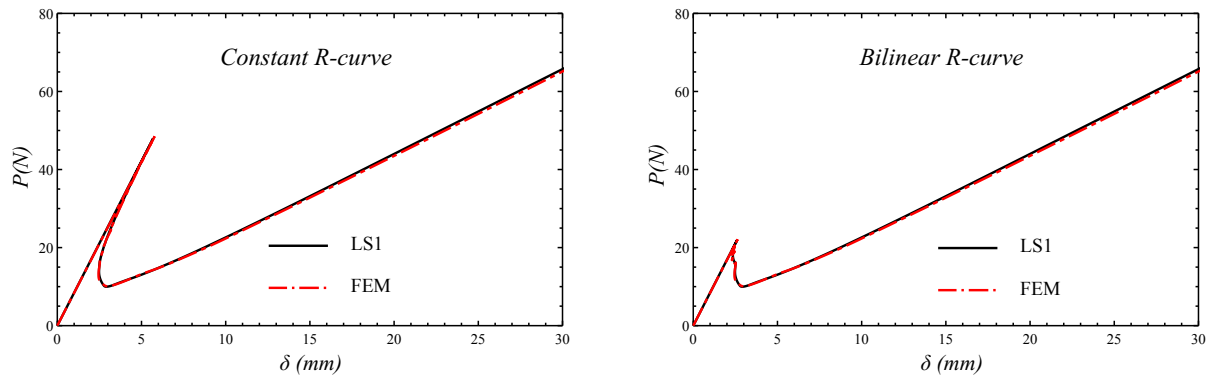


Figure 4.15: Applied load versus midspan deflection - Mode II delamination

4.5 Conclusion

This study deals with the delamination problem in multilayered plates subjected to cylindrical bending. The objective is to find an accurate and efficient model which can be used instead of sophisticated finite element simulations (too expensive in times and memory) to solve this problem. The LS1 model (layerwise stress approach with first-

order membrane stress approximations per layer in the thickness direction) was used to this end. The LS1 model was developed to analyse general delamination problems in multilayered plates under cylindrical bending. The proposed method permits the analysis of multi-delamination in laminates with arbitrary boundary conditions. The LS1 formulation for a general multi-delamination problem was written and the governing system of equations was derived. Analytical solution of the problem was obtained using the eigenvector expansion method.

As application examples, two classical mode I and mode II delamination tests were investigated. In order to studying the propagation of delamination, two types of crack resistance curve (R-curve) were considered: constant R-curve (fracture toughness remains constant during crack extension) and bilinear R-curve (fracture toughness increases with crack extension at first; then it becomes constant). For mode I delamination, a double cantilever test was carried out on a $(45^\circ, -45^\circ)_{5s}$ carbon-epoxy composite laminates. Mode II delamination was studied through an end notched flexure test on a $(45^\circ, -45^\circ, 90^\circ, 0^\circ, -45^\circ, 45^\circ, 0^\circ, 90^\circ, -45^\circ, 45^\circ)_s$ composite laminate. The LS1 modeling was done by means of a dedicated Mathematica program developed by the authors. In order to validate the proposed method, the results of the LS1 model were compared to those of a 3D finite element modeling performed in commercial software Abaqus. The comparisons revealed excellent agreements between the LS1 estimations and the 3D-FEM results. It was demonstrated that in such problems, the LS1 model is as accurate as the 3D-FEM while it is much more efficient (in this study, 400 unknowns in the LS1 modeling against 180,000 in the finite element model). As a conclusion, the LS1 model shows high accuracy and efficiency, and can be used as an effective and reliable alternative to finite element calculations for the analysis of multi-delamination in laminates under cylindrical bending.

Appendix 4.A Definition of matrices

$\underline{\underline{N}}$ is a $3n - 2 \times 3n - 2$ matrix as follows:

$$\underline{\underline{N}}_{(3n-2) \times (3n-2)} = \begin{bmatrix} \underline{\underline{N}}^1_{n \times n} & \underline{\underline{N}}^2_{n \times (n-1)} & \underline{\underline{N}}^3_{n \times (n-1)} \\ \left(\underline{\underline{N}}^2\right)^t_{(n-1) \times n} & \underline{\underline{N}}^4_{(n-1) \times (n-1)} & \underline{\underline{N}}^5_{(n-1) \times (n-1)} \\ \left(\underline{\underline{N}}^3\right)^t_{(n-1) \times n} & \underline{\underline{N}}^5_{(n-1) \times (n-1)} & \underline{\underline{N}}^6_{(n-1) \times (n-1)} \end{bmatrix}$$

where

$$\underline{\underline{N}}^1_{ij} = \frac{6}{5} \frac{S_{Q11}^i}{e^i} \delta_{ij} \quad ; \quad (i, j) \in [1; n] \times [1; n]$$

$$\underline{\underline{N}}^2_{ij} = -\frac{1}{10} S_{Q11}^i (\delta_{ij} + \delta_{i,j+1}) \quad ; \quad (i, j) \in [1; n] \times [1; n-1]$$

$$\underline{\underline{N}}^3_{ij} = -\frac{1}{10} S_{Q12}^i (\delta_{ij} + \delta_{i,j+1}) \quad ; \quad (i, j) \in [1; n] \times [1; n-1]$$

$$\underline{\underline{N}}^4_{ij} = -\frac{1}{30} \left[e^i S_{Q11}^i \delta_{i,j+1} - 4 \left(e^i S_{Q11}^i + e^{i+1} S_{Q11}^{i+1} \right) \delta_{ij} + e^{i+1} S_{Q11}^{i+1} \delta_{i,j-1} \right] \quad ; \quad (i, j) \in [1; n-1] \times [1; n-1]$$

$$\underline{\underline{N}}^5_{ij} = -\frac{1}{30} \left[e^i S_{Q12}^i \delta_{i,j+1} - 4 \left(e^i S_{Q12}^i + e^{i+1} S_{Q12}^{i+1} \right) \delta_{ij} + e^{i+1} S_{Q12}^{i+1} \delta_{i,j-1} \right] \quad ; \quad (i, j) \in [1; n-1] \times [1; n-1]$$

$$\underline{\underline{N}}^6_{ij} = -\frac{1}{30} \left[e^i S_{Q22}^i \delta_{i,j+1} - 4 \left(e^i S_{Q22}^i + e^{i+1} S_{Q22}^{i+1} \right) \delta_{ij} + e^{i+1} S_{Q22}^{i+1} \delta_{i,j-1} \right] \quad ; \quad (i, j) \in [1; n-1] \times [1; n-1]$$

$\underline{\underline{R}}$ is a $n - 1 \times n - 1$ matrix with the following expression:

$$\underline{\underline{R}}_{ij} = \frac{1}{70} \left[9 e^i S_{\nu}^i \delta_{i,j+1} + 26 \left(e^i S_{\nu}^i + e^{i+1} S_{\nu}^{i+1} \right) \delta_{ij} + 9 e^{i+1} S_{\nu}^{i+1} \delta_{i,j-1} \right]$$

$$(i, j) \in [1; n-1] \times [1; n-1]$$

The vectors $\underline{\underline{A}}_d, \underline{\underline{B}}_d, \underline{\underline{C}}_d, \underline{\underline{D}}_d, \underline{\underline{W}}_d$ and the matrices $\underline{\underline{N}}_d, \underline{\underline{R}}_d$ are obtained as follows:

For each delaminated interface such as $k, k + 1$:

- The vectors $\underline{\underline{A}}_d, \underline{\underline{B}}_d$ are deduced from the vectors $\underline{\underline{A}}, \underline{\underline{B}}$ by eliminating the components $n + k$ and $2n - 1 + k$
- The matrix $\underline{\underline{N}}_d$ is deduced from the matrix $\underline{\underline{N}}$ by eliminating the lines and the columns $n + k$ and $2n - 1 + k$

- The vectors \underline{C}_d , \underline{D}_d , \underline{W}_d are deduced from the vectors \underline{C} , \underline{D} , \underline{W} by eliminating the component k
- The matrix $\underline{\underline{R}}_d$ is deduced from the matrix $\underline{\underline{R}}$ by eliminating the line and the column k

Appendix 4.B Solution of homogeneous system of second-order differential equations

Consider a system of m second-order differential equations as follows:

$$\underline{\underline{X}}''(y) = \underline{\underline{M}} \cdot \underline{\underline{X}}(y) \quad (4.35)$$

The eigenvector expansion method is used to solve the system. The eigenvalues and eigenvectors of the matrix $\underline{\underline{M}}$ are calculated as follows:

$$(\underline{\underline{M}} - \lambda \underline{\underline{I}}) \cdot \underline{\underline{\phi}} = \underline{\underline{O}} \quad (4.36)$$

where λ is an eigenvalue of the matrix $\underline{\underline{M}}$ and $\underline{\underline{\phi}}$ is the corresponding eigenvector. The eigenvalues can be simple or repeated; real or complex. For different types of eigenvalues, the solution of the system will be different.

4.B.1 Simple eigenvalues

If λ is a real (nonzero) eigenvalue, the system will have two solutions as follows:

$$\begin{aligned} \lambda \in \mathbb{R} > 0 & \xrightarrow{\text{solutions}} \underline{\underline{\phi}} \left(C_1 e^{\sqrt{\lambda}y} + C_2 e^{-\sqrt{\lambda}y} \right) \\ \lambda \in \mathbb{R} < 0 & \xrightarrow{\text{solutions}} \underline{\underline{\phi}} \left(C_1 \cos(\sqrt{|\lambda|}y) + C_2 \sin(-\sqrt{|\lambda|}y) \right) \end{aligned} \quad (4.37)$$

If $\lambda = a + bi$ is a complex eigenvalue, then $\bar{\lambda} = a - bi$ is also an eigenvalue of the matrix. The four solutions corresponding to λ and $\bar{\lambda}$ can be written in real form as:

$$\begin{aligned} C_1 e^{ct} [\underline{U} \cos(dy) - \underline{V} \sin(dy)] + C_2 e^{ct} [\underline{U} \sin(dy) + \underline{V} \cos(dy)] + \\ C_3 e^{-ct} [\underline{U} \cos(dy) + \underline{V} \sin(dy)] + C_4 e^{-ct} [\underline{U} \sin(dy) - \underline{V} \cos(dy)] \end{aligned} \quad (4.38)$$

where $\sqrt{\lambda} = \pm(c + i d)$ and $\underline{\underline{\phi}} = \underline{U} + i \underline{V}$

4.B.2 Repeated and zero eigenvalues

As explained, the matrix $\underline{\underline{M}}$ can have repeated eigenvalues. We distinguish between the algebraic multiplicity (k) and the geometric multiplicity (k') of a repeated eigenvalue. The algebraic multiplicity of an eigenvalue is defined as the multiplicity of the

corresponding root of the characteristic polynomial. The geometric multiplicity of an eigenvalue is defined as the number of linearly independent eigenvectors corresponding to that eigenvalue (i.e. the dimension of the associated eigenspace). It is easy to realize that always $k' \leq k$.

If $k' = k$, then there are k linearly independent eigenvectors corresponding to the eigenvalue λ . In this case, each independent eigenvector leads to two solutions as expressed above. Therefore, $2k$ solutions corresponding to the repeated eigenvalue λ are obtained.

If $k' < k$ (the geometric multiplicity is smaller than the algebraic multiplicity), there is no basis of eigenvectors (i.e. there are not sufficient eigenvectors to span the entire space). Indeed, the matrix $\underline{\underline{M}}$ doesn't have k independent eigenvectors corresponding to λ and so the matrix is not diagonalizable. In this case, the notion of eigenvector can be generalized to *generalized eigenvectors*. To find the solutions of the system, the system of second-order differential equations is converted to a system of first-order differential equation as follows:

$$\underline{\underline{X}}''(y) = \underline{\underline{M}} \cdot \underline{\underline{X}}(y) \implies \underline{\underline{U}}'(y) = \underline{\underline{A}} \cdot \underline{\underline{U}}(y) \quad (4.39)$$

where

$$\underline{\underline{U}}(y) = \begin{pmatrix} X(y) \\ X'(y) \end{pmatrix}' \quad ; \quad \underline{\underline{A}} = \begin{bmatrix} \underline{\underline{O}} & \underline{\underline{I}} \\ \underline{\underline{M}} & \underline{\underline{O}} \end{bmatrix} \quad (4.40)$$

If λ is an eigenvalue of the matrix $\underline{\underline{M}}$, then $\sqrt{\lambda} = \pm\mu$ will be eigenvalues of the matrix $\underline{\underline{A}}$. Given μ an eigenvalue of the matrix $\underline{\underline{A}}$ with algebraic multiplicity k , there is an integer m_p ($1 \leq m_p \leq k$) such that:

$$\begin{aligned} \dim \text{null} [(\underline{\underline{A}} - \mu \underline{\underline{I}})^{m_p}] &= k \\ \dim \text{null} [(\underline{\underline{A}} - \mu \underline{\underline{I}})^{m_p-1}] &< k \end{aligned} \quad (4.41)$$

where $\dim \text{null}$ signifies the dimension of the null space of the matrix. Any nonzero vector $\underline{\underline{\phi}}$ satisfying the next relation, is a generalized eigenvector for μ :

$$(\underline{\underline{A}} - \mu \underline{\underline{I}})^{m_p} \cdot \underline{\underline{\phi}} = \underline{\underline{O}} \quad (4.42)$$

Since the dimension of the null space of $(\underline{\underline{A}} - \mu \underline{\underline{I}})^{m_p}$ is equal to k , the previous relation results k generalized eigenvectors $\underline{\underline{\phi}}_1, \underline{\underline{\phi}}_2, \dots, \underline{\underline{\phi}}_k$ which are linearly independent. There are k linearly independent solutions corresponding to these generalized eigenvectors. These solution are obtained by:

$$e^{\mu y} \sum_{j=0}^{m_p-1} \frac{y^j}{j!} (\underline{\underline{A}} - \mu \underline{\underline{I}})^j \cdot (C_1 \underline{\underline{\phi}}_1 + C_2 \underline{\underline{\phi}}_2 + \dots + C_k \underline{\underline{\phi}}_k) \quad (4.43)$$

It should be mentioned that if μ is a complex number, the corresponding solutions can be written in real form (like the method already used for simple complex eigenvalues). In this way, $2k$ independent solutions (k solutions corresponding to μ and k solutions corresponding to $-\mu$) are obtained.

The same approach is used for zero eigenvalues. If $\lambda = 0$ is an eigenvalue of the matrix \underline{M} with algebraic multiplicity k , then the matrix \underline{A} will have $2k$ zero eigenvalues. Therefore, it is necessary to find $2k$ generalized eigenvectors in order to find $2k$ independent solutions for the system $\underline{U}'(y) = \underline{A} \cdot \underline{U}(y)$.

Chapter 5

Stress analysis of long multilayered plates subjected to invariant loading: Analytical solutions by a layerwise stress model

Dans les chapitres précédents, nous avons utilisé le modèle LS1 pour analyser des plaques multicouches soumises à la traction uniaxiale et à la flexion cylindrique. Pour ces deux types de chargement, la solution analytique du modèle LS1 a été obtenue. Ici, nous généralisons la méthode analytique proposée en prenant en considération tous les chargements possibles dans le cadre des plaques multicouches soumises à des chargements invariants dans le sens longitudinal. Ainsi, le champ des déformations peut être supposé invariant dans le sens longitudinal. Basé sur cette hypothèse, nous identifions tous les chargements possibles aux extrémités longitudinales de la plaque. Le problème consiste à analyser une plaque multicouche rectangulaire soumise à tous les chargements invariants possibles à ses extrémités, ses bords latéraux et sur ses faces supérieure et inférieure. La formulation du modèle LS1 est écrite sur la forme matricielle pour ce problème et la solution analytique du problème est présentée.

Ce chapitre est un article publié dans la revue “Composite Structures” sous la référence [Saeedi et al. \[2013\]](#).

Contents

5.1	Introduction	163
5.2	x-invariance condition	165
5.2.1	Problem description	165
5.2.2	3D formulation	166
5.2.3	LS1 model formulation	169
5.3	LS1 solution	171
5.3.1	System of equations	172
5.3.2	Solution	172
5.4	Numerical examples	173
5.4.1	Overall stiffness matrix	174
5.4.2	Interfacial stresses	176
5.4.3	Effects of end constraint	179
5.5	Conclusion	181
Appendix 5.A	Reduced form of 3D displacement field	183
Appendix 5.B	General formulation of the LS1 model	185
Appendix 5.C	Definition of scalars, vectors and matrices	187
Appendix 5.D	LS1 system of equations	190
Appendix 5.E	Kirchhoff-Love solution	194

Abstract This paper deals with the analysis of long multilayered plates subjected to invariant loading along the longitudinal direction. By assuming that the strain field is independent of the longitudinal coordinate, the general form of the displacement field is obtained for a rectangular plate. It is shown that there are only four types of loading which can be applied at the longitudinal ends of the plate: traction, out-of-plane bending, torsion and in-plane bending. In addition to these loads, the plate can be subjected to any loading on its top/bottom surfaces and any force/displacement boundary conditions at its lateral edges provided that these loads and boundary conditions are invariant along the longitudinal direction. Based on the obtained displacement field, a layerwise stress model, called the LS1 model, is used to solve the problem. The analytical LS1 solutions are obtained for general long multilayered plates with arbitrary lateral boundary conditions subjected to all types of invariant loads. Various numerical examples, related to different load conditions, are investigated and the LS1 results are compared to those obtained by a three-dimensional finite element (3D-FE) analysis. Excellent agreements in terms of overall stiffness matrix and free-edge interlaminar stresses are found between the LS1 and 3D-FE models.

keyword: Multilayer; Layerwise model; Free edge; Interlaminar stresses

5.1 Introduction

Multilayered structures such as composites laminates have, in general, high strength and stiffness-to-weight ratios. That is why they are increasingly used in a wide variety of engineering structures particularly in aerospace and automotive industries. Along with the increase in the use of these materials, various analytical or numerical methods have been developed for the analysis of multilayered structures. One of the major issues in design and analysis of these structures is related to free-edge effects. It has been demonstrated that differences in elastic properties of adjacent layers generally result in a highly concentrated interlaminar stresses near free edges [Ting and Chou 1981, Wang and Choi 1982a, Leguillon 1999, Chue and Liu 2002, Mittelstedt and Becker 2005]. This phenomenon can lead to interlaminar failures (delaminations) which may cause global failure of the multilayered structure.

Highly detailed three-dimensional (3D) models are usually very expensive in terms of computational time and memory. By taking into account the relatively small thickness of multilayered structures, different one or two-dimensional methods based on beam or plate theories have been proposed in the literature for the analysis of multilayered structures. Beam theories have been widely used for analyzing layered composite structures having beam geometry subjected to various conditions [Salari et al. 1998, Dall'Asta and Zona 2002, Murthy et al. 2005, Schnabl et al. 2006, Degiovanni et al. 2010, Sousa and da Silva 2010]. Two-dimensional models (2D) based on plate theories can be classified as equivalent single layer (ESL) theories or layerwise theories. In ESL theories, the multilayer is considered as a one-layer homogeneous plate with an equivalent global behavior. Therefore, the number of governing equations is independent of the number of plate layers. Classical laminate theory (CLT) based on

Kirchhoff-Love hypotheses and first-order shear deformation theory (FSDT) based on Reissner-Mindlin assumptions are the most widely used ESL theories. Many other ESL models based on higher order theories have been proposed in the literature [Whitney and Sun 1973, Reddy 1984a, Cho and Parmerter 1993, Swaminathan and Ragounadin 2004, Cecchi and Sab 2007, Nguyen et al. 2008]. Recently, Lebée and Sab [Lebée and Sab 2011a,b, 2012] have proposed a new plate theory for the analysis of thick plates under out-of-plane loading. This theory, called the Bending-Gradient plate theory, is an extension to the Reissner-Mindlin plate theory and improves the predictions of shear stress distributions in laminated plates. Although ESL models can provide acceptable results for global response of multilayers, they may lead to very inaccurate estimations of local response especially in thick plates. Layerwise models have been proposed to overcome the drawbacks of ESL models [Barbero and Reddy 1991, Robbins and Reddy 1993, Gaudenzi et al. 1995, Dakshina Moorthya and Reddy 1998, Carrera 1998a, Botello et al. 1999]. In these approaches, each layer of the multilayered structure is considered as an independent plate. Therefore, the number of governing equations depends on the number of the layers. This increases significantly the computational cost in layerwise approaches. However, thanks to their accuracy with respect to ESL models and their efficiency with respect to full 3D models, layerwise models have been proven to be very good alternatives to 3D models.

Regarding interlaminar stress analysis in laminated plates, several analytical or numerical studies have been published in the literature. The works of Hayashi [1967], Puppo and Evensen [1970], Tang and Levy [1975b], Pagano [1978a, 1974], Pipes and Pagano [1970, 1974], Wang and Crossman [1977b, 1980] can be considered as the first efforts. Over the past decades, many other studies have been carried out to evaluate interlaminar stresses in laminated plates. The interested reader is referred to [Carrera 2002, Zhang and Yang 2009] for complete reviews of different theories.

In the present work, a layerwise model, called the LS1 model, is used for the analysis of interlaminar stresses in long multilayered plates. Inspired from the Pagano's model [Pagano 1978a], the LS1 model is based on a stress approach with first-order membrane stress approximations per layer in the thickness direction. Each layer of the laminate is considered as a Reissner-Mindlin plate while the layers are connected together by interfacial stresses. The LS1 model has been used and validated by finite element calculations in some studies [Carreira et al. 2002, Diaz Diaz et al. 2002, Dallot and Sab 2008b, Diaz Diaz and Caron 2006a, Nguyen and Caron 2009, Duong et al. 2011]. In our previous works [Saeedi et al. 2012a,b,c], the LS1 model has been used for the analytical analysis of multilayered plates under uniaxial traction and cylindrical bending. The present investigation deals with the analysis of general long multilayered plates under all possible types of loading based on the assumption that the strain field is independent of the longitudinal (x) direction. For a long rectangular laminate, three categories of loading can be distinguished:

- Loading at the longitudinal ends
- Loading at the lateral edges
- Loading on the top and bottom surfaces

By obtaining the reduced form of 3D displacement field, it is identified that the first type of loading at the ends of the laminate is a combination of uniaxial traction, out-of-plane bending, torsion and in-plane bending among which the traction loading has been extensively investigated in [Saeedi et al. 2012a,b]. The second group of loading consists of arbitrary loads or displacements applied at the lateral edges which represent, in fact, the lateral boundary conditions. Finally, the third group of loading is related to applied stresses on the top and bottom surfaces of the laminate provided that these stresses are invariant along the longitudinal direction (i.e., cylindrical loading). As a particular case of this loading, one can mention the cylindrical bending problem which has been studied in [Saeedi et al. 2012c]. In this study, the analytical solutions of the LS1 model are obtained for a general angle/ply $(\theta_1, \theta_2, \dots, \theta_n)$ laminate subjected to all types of invariant loading. In order to investigate the accuracy and the efficiency of the LS1 model, edge-effects are investigated in an unsymmetric composite laminate. For various load conditions, the LS1 results in terms of interlaminar stresses and overall stiffness matrix are compared to those of a 3D-FE analysis performed with the commercial finite element software Abaqus. Finally, end constraint conditions and coupling effects between different load conditions are investigated.

5.2 x -invariance condition

5.2.1 Problem description

A general $(\theta_1, \theta_2, \dots, \theta_m)$ composite plate with a length of $2l$ and a width of $2b$ respectively in the x and y directions is considered. The thickness of the laminate following the z direction is equal to $\sum_{i=1}^m e^i = 2h$ and the $z = 0$ plane is located at the middle of the plate. The behavior of all layers is considered to be orthotropic. It is assumed that the plate is long in the x direction so that the strain and stress fields are independent of the x coordinate. The laminate is subjected to all possible loads based on the x -invariance condition. For a rectangular laminate which occupies the domain $(-l \leq x \leq l, -b \leq y \leq b, -h \leq z \leq h)$ the possible types of loading can be categorized into three groups:

- Loading at the ends of the laminate ($x = \pm l$)
- Loading at the lateral edges of the laminate ($y = \pm b$)
- Loading at the top and bottom surfaces of the laminate ($z = \pm h$)

Regarding the loading at $z = \pm h$, the laminate can be subjected to applied stresses on its top and bottom surfaces provided that these loads are invariant along the x direction (Fig. 5.1a). The loading at the lateral edges of the laminate is taken into account in the LS1 model by means of arbitrary boundary conditions at $y = \pm b$ (Fig. 5.1b). These boundary conditions, which are expressed in terms of imposed generalized displacements or generalized stresses of the model, should be invariant in the x direction. In order to identify the most general form of the loading at the longitudinal ends

$x = \pm l$, the linearized three-dimensional strain-displacement relations are used. By assuming that the strain field is independent of the x coordinate, the reduced form of the displacement field is derived. Then, the obtained form of the displacement field is applied to long multilayered plates and the LS1 model is used to solve the problem.

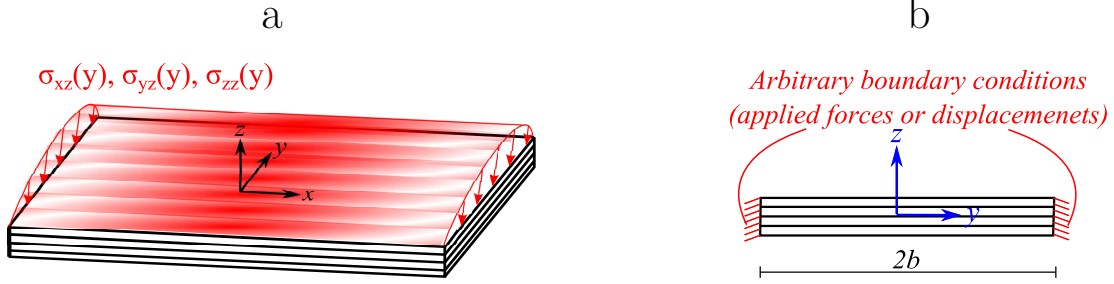


Figure 5.1: (a) Loading on the top/bottom surfaces of the laminate ($z = \pm h$) - (b) Arbitrary boundary conditions at the lateral edges ($y = \pm b$)

5.2.2 3D formulation

By assuming that the strain field is independent of the x coordinate, it is shown in 5.A that the most general linearized form of the displacement field (up to a rigid body motion) is given by (see also [Lekhnitskii 1981]):

$$U_x^{3D}(x, y, z) = u_x^{3D}(y, z) + (\varepsilon_{xx}^0 + \chi_{xx}^0 z + \chi_{zz}^0 y) x + \chi_{xy}^0 y z \quad (5.1)$$

$$U_y^{3D}(x, y, z) = u_y^{3D}(y, z) + \chi_{xy}^0 x z - \chi_{zz}^0 \frac{x^2}{2} \quad (5.2)$$

$$U_z^{3D}(x, y, z) = u_z^{3D}(y, z) - \chi_{xy}^0 x y - \chi_{xx}^0 \frac{x^2}{2} \quad (5.3)$$

where $\varepsilon_{xx}^0, \chi_{xx}^0, \chi_{zz}^0$ and χ_{xy}^0 are four given constants. This displacement field generates the following strain field:

$$\varepsilon_{xx}^{3D}(y, z) = \varepsilon_{xx}^0 + \chi_{xx}^0 z + \chi_{zz}^0 y \quad (5.4)$$

$$\varepsilon_{yy}^{3D}(y, z) = u_{y,y}^{3D}(y, z) \quad (5.5)$$

$$\varepsilon_{zz}^{3D}(y, z) = u_{z,z}^{3D}(y, z) \quad (5.6)$$

$$\varepsilon_{xy}^{3D}(y, z) = \frac{1}{2} u_{x,y}^{3D}(y, z) + \chi_{xy}^0 z \quad (5.7)$$

$$\varepsilon_{xz}^{3D}(y, z) = \frac{1}{2} u_{x,z}^{3D}(y, z) \quad (5.8)$$

$$\varepsilon_{yz}^{3D}(y, z) = \frac{1}{2} [u_{y,z}^{3D}(y, z) + u_{z,y}^{3D}(y, z)] \quad (5.9)$$

which indicates that $\varepsilon_{xx}^0, \chi_{xx}^0, \chi_{zz}^0$ and χ_{xy}^0 represent, respectively, the uniaxial extension

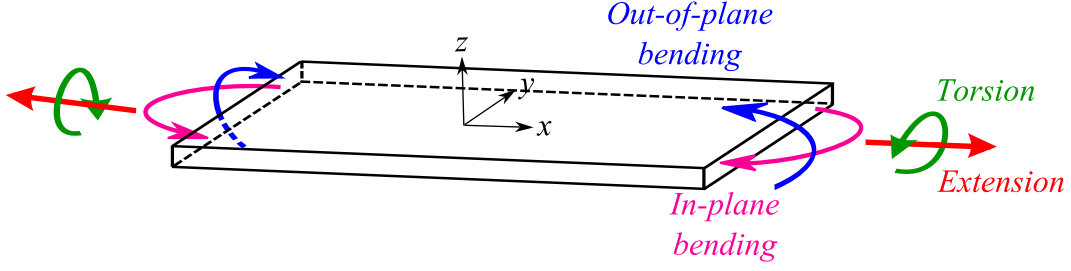


Figure 5.2: A long plate under different types of loading at its longitudinal ends

in the x direction, the bending about the y axis, the torsion about the x axis and the bending about the z axis (Fig. 5.2).

To analyze the plate, it is sufficient to consider a unit-cell with a length of $\Delta L = 2l$ in the x direction knowing that the solution of the problem is independent of this length. Using $x = \pm l$ in Eqs. 5.1 to 5.3 leads to the following conditions between opposite nodes in the x direction:

$$\Delta U_x^{3D} = (\varepsilon_{xx}^0 + \chi_{xx}^0 z + \chi_{zz}^0 y) \times \Delta L \quad (5.10)$$

$$\Delta U_y^{3D} = \chi_{xy}^0 z \times \Delta L \quad (5.11)$$

$$\Delta U_z^{3D} = -\chi_{xy}^0 y \times \Delta L \quad (5.12)$$

where $\Delta U_k^{3D} = U_k^{3D}(l, y, z) - U_k^{3D}(-l, y, z)$ for $k \in \{x, y, z\}$.

The stress conditions between the opposite faces should be imposed as follows:

$$\sigma_{xx}(l, y, z) = \sigma_{xx}(-l, y, z) \quad (5.13)$$

$$\sigma_{xy}(l, y, z) = \sigma_{xy}(-l, y, z) \quad (5.14)$$

$$\sigma_{xz}(l, y, z) = \sigma_{xz}(-l, y, z) \quad (5.15)$$

It should be mentioned that the stress field is independent of the x coordinate because the strain field and the elasticity properties are invariant in the x direction.

Now, in order to identify the resultant force/moments related to strain/curvatures ε_{xx}^0 , χ_{xx}^0 , χ_{zz}^0 and χ_{xy}^0 , the expression of the elastic strain energy of the body is derived. In linear elasticity, the strain energy must equal the external work performed on the structure:

$$W_t = \frac{1}{2} \int_V \underline{\underline{\sigma}} : \underline{\underline{\varepsilon}} dV = \frac{1}{2} \int_{\partial V} (\underline{\underline{\sigma}} \cdot \underline{n}) \cdot \underline{U} dS \quad (5.16)$$

where \underline{n} is the outward normal to the plate's boundary. Here, we are interested in the loading at the ends of the plate ($x = \pm l$). Therefore, the external work on the top and bottom surfaces ($z = \pm h$) and at the lateral edges ($y = \pm b$) are not taken into account. The energy corresponding to the loading at the ends of the plate is obtained as follows:

$$W_t = \frac{1}{2} \int_S [\underline{\underline{\sigma}}(l, y, z) \cdot \underline{e}_x] \cdot \underline{U} dS - \frac{1}{2} \int_S [\underline{\underline{\sigma}}(-l, y, z) \cdot \underline{e}_x] \cdot \underline{U} dS \quad (5.17)$$

in which S denotes the cross section of the body perpendicular to the x direction. Knowing that the stress field is independent of the x coordinate, the above equation takes the following form:

$$W_t = \frac{1}{2} \int_S (\sigma_{xx} \Delta U_x + \sigma_{xy} \Delta U_y + \sigma_{xz} \Delta U_z) dy dz \quad (5.18)$$

By substituting Eqs. 5.10 to 5.12 in this equation, the strain energy per unit length is obtained as:

$$\overline{W} = \frac{W_t}{\Delta L} = \frac{1}{2} (F_x^0 \varepsilon_{xx}^0 + M_{xx}^0 \chi_{xx}^0 + T_x^0 \chi_{xy}^0 + M_{zz}^0 \chi_{zz}^0) \quad (5.19)$$

where

$$F_x^0 = \int_S \sigma_{xx}(y, z) dy dz \quad (5.20)$$

$$M_{xx}^0 = \int_S z \sigma_{xx}(y, z) dy dz \quad (5.21)$$

$$T_x^0 = \int_S (z \sigma_{xy}(y, z) - y \sigma_{xz}(y, z)) dy dz \quad (5.22)$$

$$M_{zz}^0 = \int_S y \sigma_{xx}(y, z) dy dz \quad (5.23)$$

F_x^0 , M_{xx}^0 , T_x^0 and M_{zz}^0 are, respectively, the axial force, the bending moment about the y axis, the torque about the x axis and the bending moment about the z axis. According to the duality between strains and stresses, each of the four types of loading can be applied in terms of either strains or force/moment resultants (Fig. 5.3). Indeed, the loading conditions at the ends of the body ($x = \pm l$) can be expressed as follows:

$$\varepsilon_{xx}^0 \xleftrightarrow{or} F_x^0 \quad , \quad \chi_{xx}^0 \xleftrightarrow{or} M_{xx}^0 \quad , \quad \chi_{xy}^0 \xleftrightarrow{or} T_x^0 \quad , \quad \chi_{zz}^0 \xleftrightarrow{or} M_{zz}^0$$

To illustrate, let us take two examples. The loading case $\varepsilon_{xx}^0 \neq 0, \chi_{xx}^0 = \chi_{xy}^0 = \chi_{zz}^0 = 0$ is the uniform extension of the body in which the rotations about the x , y and z axes are blocked. In this case, the moment resultants M_{xx}^0 , T_x^0 and M_{zz}^0 are, in general, not zero. On the other hand, the loading case $F_x^0 \neq 0, M_{xx}^0 = T_x^0 = M_{zz}^0 = 0$ denotes the uniform traction in the x direction in which the body is free to rotate about the x , y and z axes. In this case, the conditions $M_{xx}^0 = T_x^0 = M_{zz}^0 = 0$ require that χ_{xx}^0 , χ_{xy}^0 and χ_{zz}^0 have, in general, nonzero values. The imposed strains and force/moment resultants can be related together as follows:

$$\begin{pmatrix} F_x^0 \\ M_{xx}^0 \\ T_x^0 \\ M_{zz}^0 \end{pmatrix} = \underline{\underline{K}} \cdot \begin{pmatrix} \varepsilon_{xx}^0 \\ \chi_{xx}^0 \\ \chi_{xy}^0 \\ \chi_{zz}^0 \end{pmatrix} \quad (5.24)$$

where the matrix $\underline{\underline{K}}$ denotes the overall stiffness matrix of the multilayered plate.

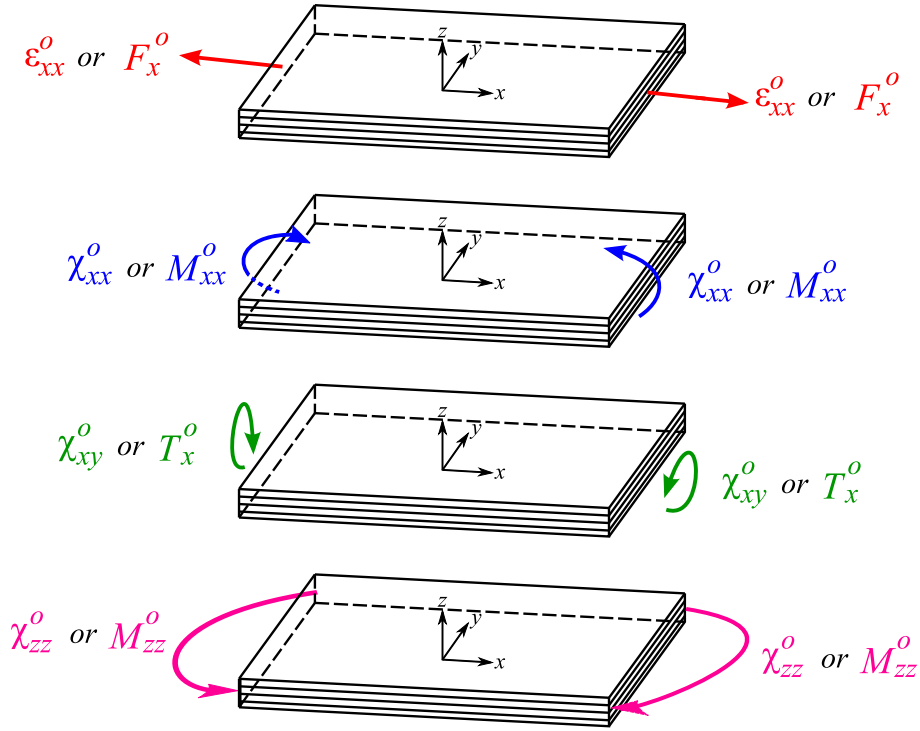


Figure 5.3: Laminate under different types of loading at the ends $x = \pm l$

Remark 1. Given that the strain and stress fields are independent of the x coordinate, the strain energy per unit length (\overline{W}) should also be independent of the x coordinate. Calculating \overline{W} for an arbitrary segment between $x = x_0$ and $x = x_1$ and imposing that \overline{W} is independent of x_0 and x_1 , it is deduced that:

$$\begin{aligned} F_y^0 &= \int_S \sigma_{xy}(y, z) dy dz = 0 \\ F_z^0 &= \int_S \sigma_{xz}(y, z) dy dz = 0 \end{aligned} \quad (5.25)$$

which indicates that the resultant shear forces on the cross section of the plate are null. These relations imply the static equilibrium of the plate in the y and z directions given that the stress field is invariant in the x direction.

5.2.3 LS1 model formulation

The general formulation of the *LS1* model (layerwise stress model with first-order membrane stress approximations per layer) is presented in 5.B. The LS1 model is, in fact, a superposition of Reissner-Mindlin plates which are linked together by interfacial stresses. Generalized stresses of each layer i consist of three in-plane stress resultants $N_{\alpha\beta}^i$, three moment resultants $M_{\alpha\beta}^i$ (at the mid-plane of layer) and two out-of-plane shear resultants Q_{α}^i ($\alpha, \beta \in \{x, y\}$). In addition to these generalized stresses, the model comprises two shear stresses $\tau_x^{i,i+1}$, $\tau_y^{i,i+1}$ and one normal stress $\nu^{i,i+1}$ per interface

$i, i + 1$. Since these interfacial stresses are considered as generalized stresses, the stress continuities at interfaces are guaranteed. The generalized displacements are three displacement fields $U_x^i(x, y)$, $U_y^i(x, y)$, $U_z^i(x, y)$ and two rotation fields $\Phi_x^i(x, y)$, $\Phi_y^i(x, y)$ per layer i . Generalized strains consist of $\varepsilon_{\alpha\beta}^i$, $\chi_{\alpha\beta}^i$ and $d_{\Phi_\alpha}^i$ which are, respectively, in-plane strains, curvatures and out-of-plane shear strains of layer i . With regard to interfaces, $D_\alpha^{i,i+1}$ and $D_z^{i,i+1}$ are considered as relative displacements at interface $i, i + 1$. Constitutive relations of the model connect these generalized strains to the generalized stresses (see 5.B for more details).

In the case of invariance in the x direction, substitution of the 3D-displacement field (Eqs. 5.1 to 5.3) into Eqs. 5.86 to 5.88 gives:

$$U_x^i(x, y) = u_x^i(y) + (\varepsilon_{xx}^0 + \bar{h}^i \chi_{xx}^0 + \chi_{zz}^0 y) x + \bar{h}^i \chi_{xy}^0 y \quad (5.26)$$

$$U_y^i(x, y) = u_y^i(y) + \bar{h}^i \chi_{xy}^0 x - \chi_{zz}^0 \frac{x^2}{2} \quad (5.27)$$

$$U_z^i(x, y) = u_z^i(y) - \chi_{xy}^0 xy - \chi_{xx}^0 \frac{x^2}{2} \quad (5.28)$$

$$\Phi_x^i(x, y) = \phi_x^i(y) + \chi_{xx}^0 x + \chi_{xy}^0 y \quad (5.29)$$

$$\Phi_y^i(x, y) = \phi_y^i(y) + \chi_{xy}^0 x \quad (5.30)$$

where:

$$u_\alpha^i(y) = \frac{1}{e^i} \int_{h_-^i}^{h_+^i} u_\alpha^{3D}(y, z) dz$$

$$u_z^i(y) = \frac{1}{e^i} \int_{h_-^i}^{h_+^i} u_z^{3D}(y, z) dz$$

$$\phi_\alpha^i(y) = \frac{12}{(e^i)^2} \int_{h_-^i}^{h_+^i} \frac{z - \bar{h}^i}{e^i} u_\alpha^{3D}(y, z) dz$$

Generalized strains are deduced from the generalized displacements. Injecting the previous generalized displacements into the displacement-strain relations (Eqs. 5.89 to 5.93) yields:

$$\varepsilon_{xx}^i = \varepsilon_{xx}^0 + \bar{h}^i \chi_{xx}^0 + \chi_{zz}^0 y, \quad \varepsilon_{yy}^i = u_y^{i'}, \quad \varepsilon_{xy}^i = \frac{1}{2} u_x^{i'} + \bar{h}^i \chi_{xy}^0 \quad (5.31)$$

$$\chi_{xx}^i = \chi_{xx}^0, \quad \chi_{yy}^i = \phi_y^{i'}, \quad \chi_{xy}^i = \frac{1}{2} \phi_x^{i'} + \chi_{xy}^0 \quad (5.32)$$

$$d_{\Phi_x}^i = \phi_x^i, \quad d_{\Phi_y}^i = \phi_y^i + u_z^{i'} \quad (5.33)$$

$$D_x^{i,i+1} = u_x^{i+1} - u_x^i - \left(\frac{e^i}{2} \phi_x^i + \frac{e^{i+1}}{2} \phi_x^{i+1} \right) \quad (5.34)$$

$$D_y^{i,i+1} = u_y^{i+1} - u_y^i - \left(\frac{e^i}{2} \phi_y^i + \frac{e^{i+1}}{2} \phi_y^{i+1} \right) \quad (5.35)$$

$$D_z^{i,i+1} = u_z^{i+1} - u_z^i \quad (5.36)$$

where a prime denotes derivative with respect to y .

Regarding the equilibrium equations, the model consists of five equations per layer i . Assuming that there is no variation in the x direction, these equations for each layer are written as ($1 \leq i \leq m$):

$$N_{xy}^i{}' + \tau_x^{i,i+1} - \tau_x^{i-1,i} = 0 \quad (5.37)$$

$$N_{yy}^i{}' + \tau_y^{i,i+1} - \tau_y^{i-1,i} = 0 \quad (5.38)$$

$$M_{xy}^i{}' + \frac{e^i}{2} (\tau_x^{i,i+1} + \tau_x^{i-1,i}) - Q_x^i = 0 \quad (5.39)$$

$$M_{yy}^i{}' + \frac{e^i}{2} (\tau_y^{i,i+1} + \tau_y^{i-1,i}) - Q_y^i = 0 \quad (5.40)$$

$$Q_y^i{}' + \nu^{i,i+1} - \nu^{i-1,i} = 0 \quad (5.41)$$

It should be noted that in the previous equations, $\tau_x^{m,m+1}$, $\tau_y^{m,m+1}$, $\nu^{m,m+1}$, $\tau_x^{0,1}$, $\tau_y^{0,1}$ and $\nu^{0,1}$ are given as follows:

$$\begin{aligned} \tau_x^{m,m+1}(y) &= T_x^+(y) \quad , \quad \tau_y^{m,m+1}(y) = T_y^+(y) \quad , \quad \nu^{m,m+1}(y) = T_z^+(y) \\ \tau_x^{0,1}(y) &= -T_x^-(y) \quad , \quad \tau_y^{0,1}(y) = -T_y^-(y) \quad , \quad \nu^{0,1}(y) = -T_z^-(y) \end{aligned}$$

where $\underline{T}^+(y)$ and $\underline{T}^-(y)$ represent the traction vector ($\underline{T} = \underline{\sigma} \cdot \underline{n}$) respectively on the top and bottom surfaces of the laminate.

5.3 LS1 solution

If the laminate and loading are symmetric with respect to the $z = 0$ plane, for $1 \leq i \leq m/2$ one can write:

$$u_\alpha^{m-i+1}(y) = u_\alpha^i(y) \quad , \quad u_z^{m-i+1}(y) = -u_z^i(y) \quad , \quad \phi_\alpha^{m-i+1}(y) = -\phi_\alpha^i(y) \quad (5.42)$$

where m is the total number of layers. Using the previous relations, for the generalized strains one obtains:

$$\varepsilon_{\alpha\beta}^{m-i+1}(y) = \varepsilon_{\alpha\beta}^i(y) \quad , \quad \chi_{\alpha\beta}^{m-i+1}(y) = -\chi_{\alpha\beta}^i(y) \quad , \quad d_{\Phi_\alpha}^{m-i+1}(y) = -d_{\Phi_\alpha}^i(y) \quad (5.43)$$

$$D_\alpha^{m-i,m-i+1}(y) = -D_\alpha^{i,i+1}(y) \quad , \quad D_z^{m-i,m-i+1}(y) = D_z^{i,i+1}(y) \quad (5.44)$$

and for the generalized stresses:

$$N_{\alpha\beta}^{m-i+1}(y) = N_{\alpha\beta}^i(y) \quad , \quad M_{\alpha\beta}^{m-i+1}(y) = -M_{\alpha\beta}^i(y) \quad , \quad Q_{\Phi_\alpha}^{m-i+1}(y) = -Q_{\Phi_\alpha}^i(y) \quad (5.45)$$

$$\tau_\alpha^{m-i,m-i+1}(y) = -\tau_\alpha^{i,i+1}(y) \quad , \quad \nu^{m-i,m-i+1}(y) = \nu^{i,i+1}(y) \quad (5.46)$$

It is deduced, from the above relation for $i = m/2$, that the interfacial shear stresses are zero at the mid-plane of symmetric laminates.

According to the previous equations, in the case of mirror symmetry the analysis can be limited to $1 \leq i \leq m/2$. In the following formulation n and n_I are, respectively, the number of layers and the number of interfaces considered in the calculation. In the case of mirror symmetry, $n = n_I = m/2$; otherwise $n = m$ and $n_I = m - 1$.

5.3.1 System of equations

Eqs. 5.31 to 5.41 form a system of $16n - 3$ equations in which there are $6n - 3$ algebraic equations and $10n$ first-order differential equations. We try to reduce this system of equations by eliminating $6n - 3$ unknown fields. To this end, the unknown fields $N_{xx}^i, M_{xx}^i, Q_x^i$ for $1 \leq i \leq n$, $\tau_x^{i,i+1}, \tau_y^{i,i+1}$ for $1 \leq i \leq n - 1$ and $\nu^{i,i+1}$ for $1 \leq i \leq n_I$ are expressed in terms of the other unknown fields. In this way, a system of $10n$ first-order differential equations is obtained. Then, the obtained system is transformed to a system of simpler form which consists of $5n$ second-order differential equations. In matrix form, the system of equations is written as follows (see 5.D for details):

$$\underline{X}_{(5n)}'' = \underline{M} \cdot \underline{X}_{(5n)} + \underline{F}_{(5n)} \quad (5.47)$$

where \underline{X} is a vector of $5n$ unknown fields $u_x^i, u_y^i, \phi_x^i, \phi_y^i$ and Q_y^i ($1 \leq i \leq n$), the matrix \underline{M} depends on the mechanical material properties, the orientation and the thickness of the layers, and the vector \underline{F} is a function of loadings.

5.3.2 Solution

The solution of the nonhomogeneous system 5.47 is the sum of the general solution of the associated homogeneous system and a particular solution:

$$\underline{X} = \underline{X}_h + \underline{X}_p \quad (5.48)$$

The eigenvector expansion method is used to find the general solution (\underline{X}_h) of the associated homogeneous system of equations. The general solution is in the form of exponential, trigonometric and polynomial functions as follows:

$$\underline{X}_h = \sum_{i=1}^{2n} e^{\alpha_i y} \left[\underline{P}_i(y) \sin(\beta_i y) + \underline{Q}_i(y) \cos(\beta_i y) \right] \quad (5.49)$$

where the vectors $\underline{P}_i(y)$ and $\underline{Q}_i(y)$ consist of polynomial functions with unknown constant coefficients. The degrees of these polynomials depend on the multiplicity of the eigenvalues.

The form of the particular solution \underline{X}_p depends on the vector \underline{F} . This vector has, in general, the following form:

$$\begin{aligned} \underline{F} = & \underline{C}_1 \cdot T_x^+(y) + \underline{C}_2 \cdot T_x^-(y) + \underline{C}_3 \cdot T_y^+(y) + \underline{C}_4 \cdot T_y^-(y) \\ & + \underline{C}_5 \cdot [T_z^+(y)]' + \underline{C}_6 \cdot [T_z^-(y)]' + \underline{C}_7 \chi_{zz}^0 \end{aligned} \quad (5.50)$$

where the vectors \underline{C}_1 to \underline{C}_7 consist of constant coefficients. Therefore, the form of the vector \underline{F} depends on the form of the applied stresses on the top and bottom surfaces of the plate. For polynomial, exponential and trigonometric load functions, the method of undetermined coefficients is used to find the particular solution. For any other load function, the Fourier series is used to decompose the load function into a sum of trigonometric functions.

Since the governing system of equations consists of $5n$ second-order differential equations, there are $10n$ unknown constants of integration. These unknowns are determined using boundary conditions at the edges $y = \pm b$. For each layer i ($1 \leq i \leq n$) at each edge, there are five boundary conditions either on generalized stresses or on generalized displacements:

$$u_x^i(y_0) \overset{or}{\longleftrightarrow} N_{xy}^i(y_0) , \quad u_y^i(y_0) \overset{or}{\longleftrightarrow} N_{yy}^i(y_0) , \quad u_z^i(y_0) \overset{or}{\longleftrightarrow} Q_y^i(y_0) \quad (5.51)$$

$$\phi_x^i(y_0) \overset{or}{\longleftrightarrow} M_{xy}^i(y_0) , \quad \phi_y^i(y_0) \overset{or}{\longleftrightarrow} M_{yy}^i(y_0) \quad (5.52)$$

where y_0 denotes the edge position (herein $y_0 = \pm b$). In this way, $10n$ boundary conditions are obtained. These boundary conditions yield a system of $10n$ linear algebraic equations with $10n$ unknown constants which can be easily solved.

Remark 2. For a free edge, the boundary conditions are as follows:

$$N_{xy}^i(y_0) = N_{yy}^i(y_0) = M_{xy}^i(y_0) = M_{yy}^i(y_0) = Q_y^i(y_0) = 0 \quad (5.53)$$

Remark 3. Using the constitutive equations, the boundary conditions defined on N_{xy}^i , N_{yy}^i , M_{xy}^i , M_{yy}^i and u_z^i can be expressed in terms of $u_x^{i'}$, $u_y^{i'}$, $\phi_x^{i'}$, $\phi_y^{i'}$ and $Q_y^{i'}$ which are the principal unknowns in the system of equations.

5.4 Numerical examples

In this section, some numerical examples are investigated in order to evaluate the accuracy and the efficiency of the proposed method in predicting free-edge effects. Comparisons are made between the results of the LS1 model and those obtained by a 3D-FEM. The LS1 results are obtained by means of a dedicated program written in Mathematica (Wolfram Research) by the authors. The finite element calculations are carried out using the commercial finite element software Abaqus.

In order to study the effects of coupling between different types of loading, an unsymmetric angle-ply composite laminate is selected. The investigated specimen is a $(0^\circ, -60^\circ, 45^\circ, -30^\circ)$ laminate with a total thickness of $h^t = 2h = 4 \times 0.19 = 0.76mm$. The mechanical properties of each ply are taken to be those of G947/M18 carbon-epoxy as given in [Lagunegrand et al. 2006]:

$$\begin{aligned} E_L &= 97.6 \text{ GPa} , \quad E_T = E_N = 8.0 \text{ GPa} \\ G_{LT} &= G_{LN} = 3.1 \text{ GPa} , \quad G_{TN} = 2.7 \text{ GPa} \\ \nu_{LT} &= \nu_{LN} = 0.37 , \quad \nu_{TN} = 0.5 , \quad e = 0.19 \text{ mm} \end{aligned}$$

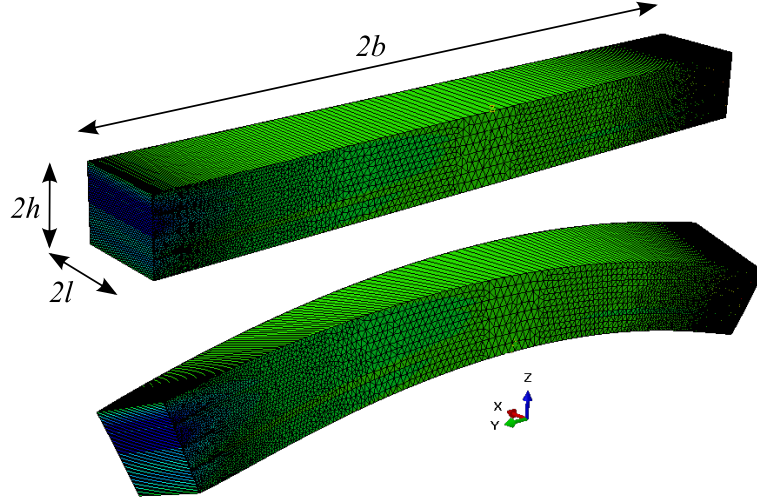


Figure 5.4: Finite element model of the laminate: undeformed state (top); deformed state in torsion (bottom)

It is assumed that strains and stresses are independent of the x coordinate. Therefore, in the 3D-FEM, it is sufficient to use only one element with an arbitrary length of $\Delta L = 2l$ in the x direction (Fig. 5.4). The invariance conditions 5.10 to 5.12 should be imposed between all opposite nodes in the x direction. The quadratic 15-nodes wedge elements are used in Abaqus with a highly refined mesh near the edges. The size of the smallest elements is about $1\mu m$ and the total number of nodes is almost 340000 (i.e., more than one million degrees of freedom).

5.4.1 Overall stiffness matrix

In this section, we are interested in the matrix $\underline{\underline{K}}$ defined in Eq. 5.24 which represents the overall stiffness matrix. Eq. 5.24 can be rewritten in a normalized form as:

$$\begin{pmatrix} \frac{F_x^0}{b^t h^t} \\ \frac{M_{xx}^0}{b^t (h^t)^2} \\ \frac{T_x^0}{b^t (h^t)^2} \\ \frac{M_{zz}^0}{(b^t)^2 h^t} \end{pmatrix} = \underline{\underline{\hat{K}}} \cdot \begin{pmatrix} \varepsilon_{xx}^0 \\ \chi_{xx}^0 h^t \\ \chi_{xy}^0 h^t \\ \chi_{zz}^0 b^t \end{pmatrix} \quad (5.54)$$

in which $b^t = 2b$ and h^t are, respectively, the total width and the total thickness of the laminate. The strains vector at the right side of the above equation is dimensionless while the vector at the left side and the matrix $\underline{\underline{\hat{K}}}$ have the dimension of stress. It is clear that the matrix $\underline{\underline{\hat{K}}}$ differs from one model to another. Here, this matrix is computed with the following three models: Kirchhoff-Love model, LS1 model and 3D-FEM. The

Table 5.1: Overall stiffness matrix of $(0^\circ, -60^\circ, 45^\circ, -30^\circ)$ laminate: comparison between the Kirchhoff-Love, LS1 and 3D-FE models

	Model	\hat{k}_{11} (GPa)	\hat{k}_{22} (GPa)	\hat{k}_{33} (GPa)	\hat{k}_{12} (GPa)	\hat{k}_{13} (GPa)	\hat{k}_{23} (GPa)	\hat{k}_{44} (GPa)	ϵ_{rel} (%)
$b^t/h^t = 5$	KL	37631.0	4749.3	2688.6	-6099.9	-2400.1	-917.7	3135.9	15.27
	LS1	36747.2	4643.1	2076.5	-6394.6	-1828.5	-704.7	2958.1	0.08
	FEM	36743.6	4642.9	2077.3	-6395.7	-1824.2	-703.0	2958.3	-
$b^t/h^t = 10$	KL	37631.0	4749.3	2688.6	-6099.9	-2400.1	-917.7	3135.9	6.82
	LS1	37189.0	4696.2	2382.4	-6247.3	-2114.1	-811.1	3036.2	0.04
	FEM	37187.0	4696.1	2382.8	-6247.8	-2111.9	-810.3	3036.1	-
$b^t/h^t = 20$	KL	37631.0	4749.3	2688.6	-6099.9	-2400.1	-917.7	3135.9	3.24
	LS1	37410.0	4722.8	2535.5	-6173.6	-2257.1	-864.4	3083.4	0.02
	FEM	37409.1	4722.7	2535.7	-6173.9	-2256.0	-864.0	3083.2	-
$b^t/h^t = 50$	KL	37631.0	4749.3	2688.6	-6099.9	-2400.1	-917.7	3135.9	1.26
	LS1	37542.6	4738.7	2627.4	-6129.4	-2342.9	-896.4	3114.3	0.01
	FEM	37542.2	4738.7	2627.5	-6129.5	-2342.5	-896.2	3114.2	-
$b^t/h^t = 100$	KL	37631.0	4749.3	2688.6	-6099.9	-2400.1	-917.7	3135.9	0.62
	LS1	37586.9	4744.0	2658.0	-6114.6	-2371.5	-907.0	3125.0	0.01
	FEM	37586.6	4745.4	2658.0	-6114.7	-2371.2	-907.0	3125.0	-

analytical expression of this matrix for the Kirchhoff-Love model is given in 5.E. In the 3D-FEM, the energy method (see Eq. 5.19) is used to calculate the matrix elements. In the LS1 model, according to Eqs. 5.20 to 5.23, the force and moment resultants can be calculated as follows:

$$F_x^0 = \sum_{i=1}^n \int_{-b}^b N_{xx}^i(y) dy \quad (5.55)$$

$$M_{xx}^0 = \sum_{i=1}^n \int_{-b}^b [M_{xx}^i(y) + \bar{h}^i N_{xx}^i(y)] dy \quad (5.56)$$

$$T_x^0 = \sum_{i=1}^n \int_{-b}^b [M_{xy}^i(y) + \bar{h}^i N_{xy}^i(y) - Q_x^i(y) y] dy \quad (5.57)$$

$$M_{zz}^0 = \sum_{i=1}^n \int_{-b}^b N_{xx}^i(y) y dy \quad (5.58)$$

In the investigated case, it is found that $\widehat{k}_{14} = \widehat{k}_{24} = \widehat{k}_{34} = 0$. It means that there is no coupling effect between the in-plane bending about the z axis and the other types of loading. The other matrix elements are not zero which signifies that coupling between the traction, the out-of-plane bending and the torsion can occur. In Table 5.1 the nonzero elements of the matrix $\widehat{\underline{K}}$ are reported for the three models. ϵ_{rel} denotes the average relative error of the Kirchhoff-Love or LS1 model with respect to the 3D-FEM. As expected, for all width-to-thickness ratios of b^t/h^t the results of the Kirchhoff-Love model are the same while in the LS1 model and FEM the matrix $\widehat{\underline{K}}$ depends on the width-to-thickness ratio b^t/h^t . The more the laminate is thick, the more the error of the Kirchhoff-Love model is significant. The drawback of the Kirchhoff-Love model is especially severe in predicting \widehat{k}_{13} , \widehat{k}_{23} and \widehat{k}_{33} which correspond to the torsion mode and its coupling with the other modes. For $b^t/h^t = 5, 10$ and 20 , the relative errors of these elements in the Kirchhoff-Love model are of the order of 30%, 13% and 6% respectively. These errors in the LS1 models are of the order of 0.2%, 0.1%, and 0.05% respectively. It is concluded that the LS1 model is as accurate as the 3D-FEM in predicting the stiffness matrix of the laminate.

5.4.2 Interfacial stresses

In order to study free-edge effects, the distributions of the interfacial stresses are compared between the LS1 and 3D-FE models. The width-to-thickness ratio of the laminate is taken to be $b^t/h^t = 10$. The laminate is investigated under different load conditions:

- Traction
 - Load condition 1: $F_x^0 = F^0, M_{xx}^0 = T_x^0 = M_{zz}^0 = 0$
 - Load condition 2: $F_x^0 = F^0, \chi_{xx}^0 = \chi_{xy}^0 = \chi_{zz}^0 = 0$
- Out-of-plane bending
 - Load condition 3: $M_{xx}^0 = M^0, F_x^0 = T_x^0 = M_{zz}^0 = 0$
 - Load condition 4: $M_{xx}^0 = M^0, \varepsilon_{xx}^0 = \chi_{xy}^0 = \chi_{zz}^0 = 0$
- Torsion
 - Load condition 5: $T_x^0 = T^0, F_x^0 = M_{xx}^0 = M_{zz}^0 = 0$
 - Load condition 6: $T_x^0 = T^0, \varepsilon_{xx}^0 = \chi_{xx}^0 = \chi_{zz}^0 = 0$
- In-plane bending
 - Load condition 7: $M_{zz}^0 = M^0, F_x^0 = M_{xx}^0 = T_x^0 = 0$
 - Load condition 8: $M_{zz}^0 = M^0, \varepsilon_{xx}^0 = \chi_{xx}^0 = \chi_{xy}^0 = 0$

In the load conditions 1, 3, 5 and 7 the laminate is subjected to a given force/moment while the other force/moment resultants are zero. In these cases, the laminate is free

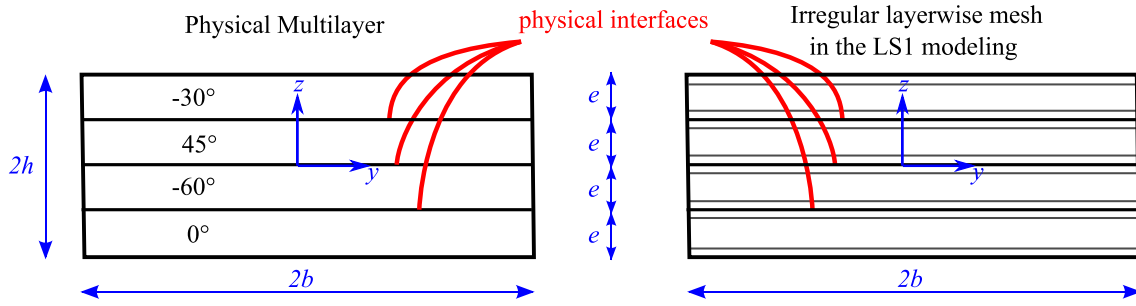


Figure 5.5: Layerwise mesh used in the LS1 model

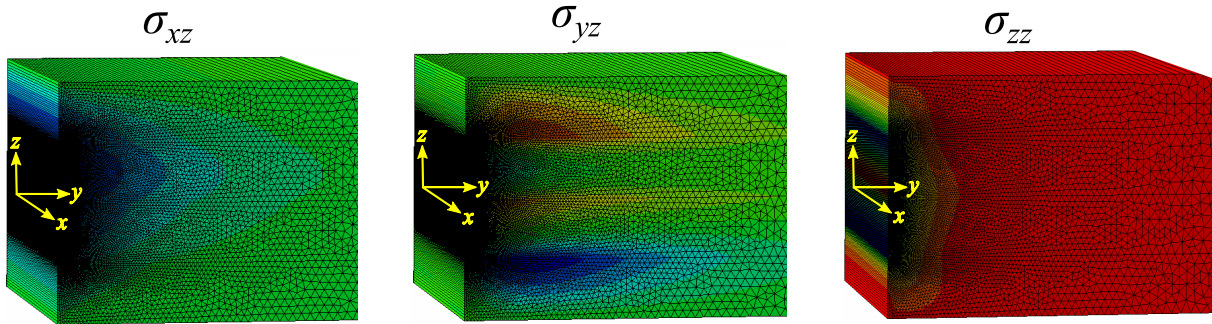


Figure 5.6: Free-edge stresses in the 3D-FEM for the load condition 6

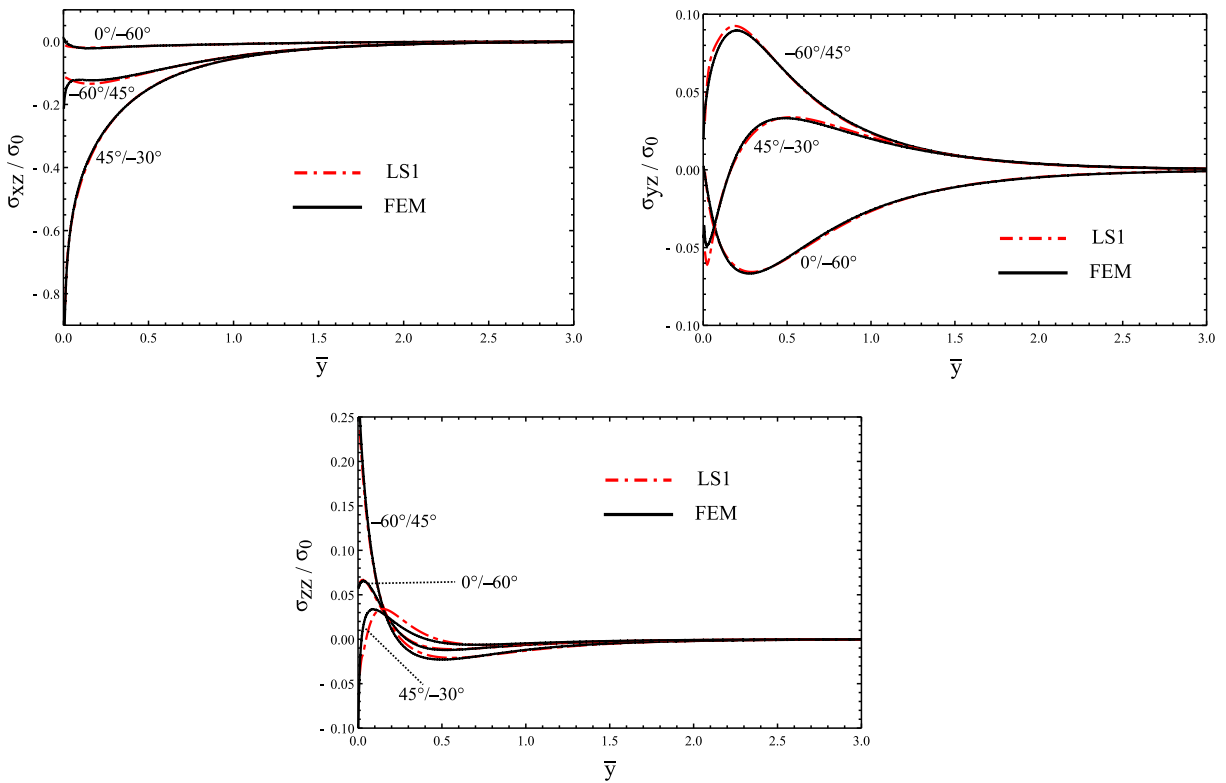


Figure 5.7: Distribution of interfacial stresses for the load condition 4

5. STRESS ANALYSIS OF LONG MULTILAYERED PLATES SUBJECTED TO INVARIANT LOADING: ANALYTICAL SOLUTIONS BY A LAYERWISE STRESS MODEL

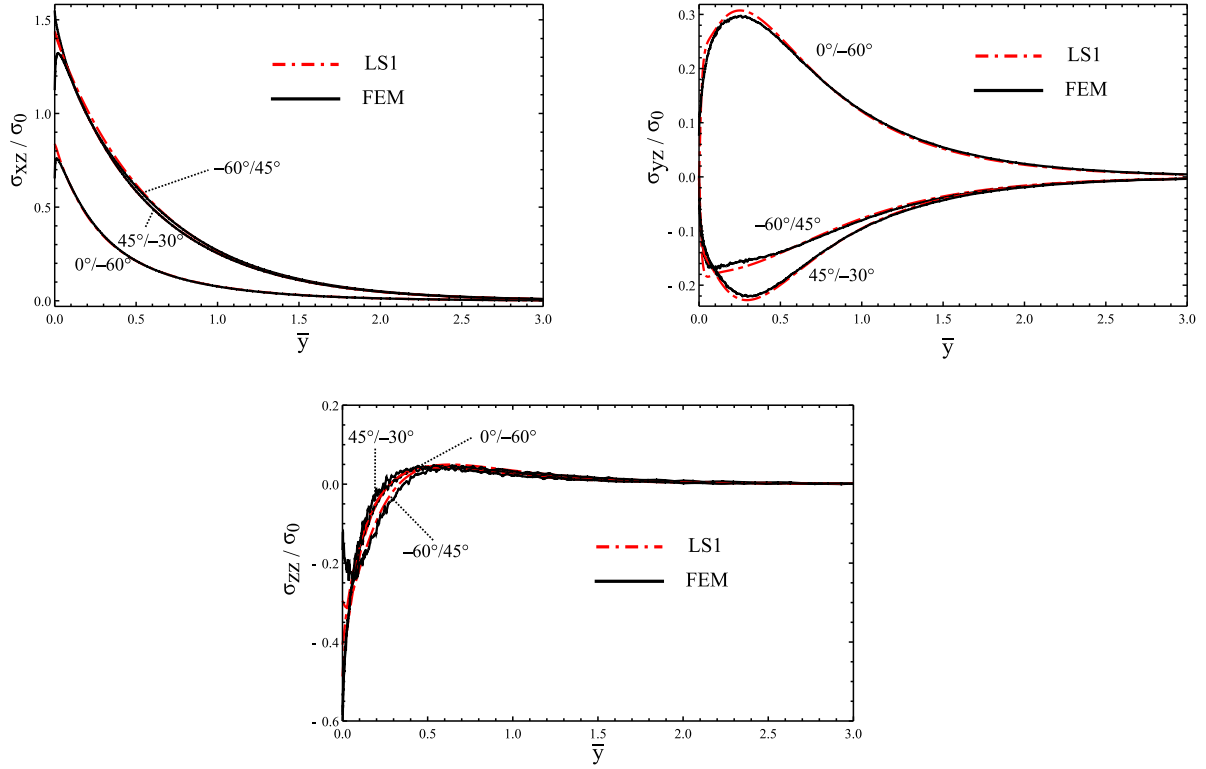


Figure 5.8: Distribution of interfacial stresses for the load condition 6

to move or rotate. On the contrary, in the load conditions 2, 4, 6 and 8, the laminate is under an imposed strain/curvature while all the other strains/curvatures are zero. As discussed in the previous section, in the present case there is no coupling effect between the in-plane bending about the z axis and the other types of loading. This means that the load conditions 7 and 8 are equivalent.

According to Eq. 5.54 it is clear that, in the framework of the linear elasticity theory, any load condition can be written as a linear combination of the load conditions 2, 4, 6 and 8. The load condition 2, which corresponds to the uniaxial extension mode, has been widely discussed in [Saeedi et al. 2012a,b]. It has been shown that in this case, the LS1 model can be used as an efficient and accurate alternative to the 3D-FEM. Herein, interlaminar stresses are studied in the load conditions 4, 6 and 8. In the LS1 model, a layerwise mesh (i.e., discretization in the thickness direction) with three mathematical layers per physical layer is used. The type of discretization is chosen according to [Saeedi et al. 2012b] which is an irregular progressive layerwise mesh more refined near the physical interfaces (Fig. 5.5).

The effects of the free-edge boundary conditions on the distributions of σ_{xz} , σ_{yz} , and σ_{zz} can be seen in Fig. 5.6. As explained, in order to capture these effects, the finite element mesh should be very refined near the free edge. Figs. 5.7 to 5.9 compare the distributions of interfacial stresses between the LS1 and 3D-FE models for the load conditions 4, 6 and 8. In these figures, the abscissa axes (\bar{y}) are the distance (in the y direction) from the free edge normalized by the total thickness of the laminate. The

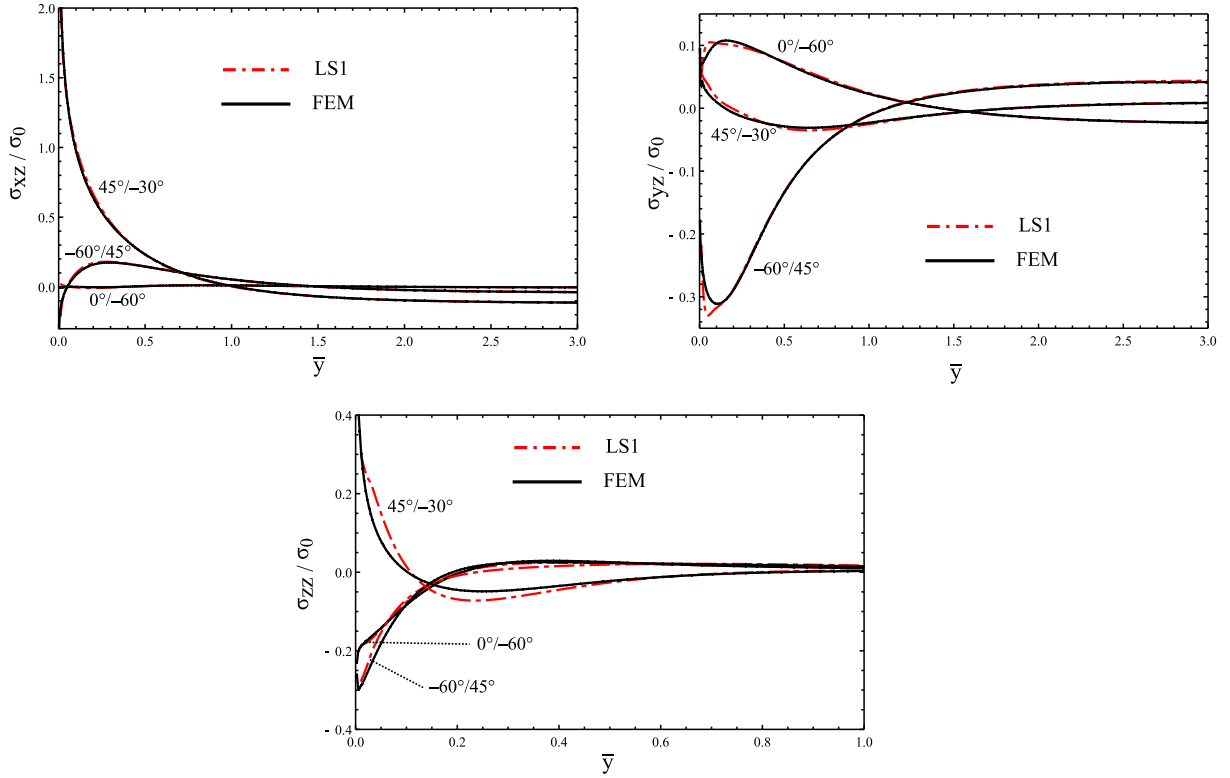


Figure 5.9: Distribution of interfacial stresses for the load condition 8

ordinate axes represent the normalized interfacial stresses. In each case, σ_0 is defined according to the left side of Eq. 5.54. For example, in the load condition 4, σ_0 is defined as $\sigma_0 = M_{xx}^0 / (b^t h^t)$. As seen, excellent agreements are observed between the LS1 and 3D-FE results. In all the interfaces, the LS1 model estimations of the three interfacial stresses σ_{xz} , σ_{yz} and σ_{zz} are as accurate as the 3D-FEM. It should be noted that in the present example, the total number of unknowns (i.e., degrees of freedom) in the LS1 model is 120 (against 10^6 in the 3D-FEM).

5.4.3 Effects of end constraint

Now, the effects of end constraint at the ends $x = \pm l$ on interfacial stresses are investigated. At first, the distributions of interlaminar stresses are compared between the load conditions 1 and 2. In both load conditions, the laminate is subjected to a tensile force F^0 in the x direction. In the load condition 1, the laminate is free to rotate about the x and y axes ($M_{xx}^0 = T_x^0 = 0 \implies \chi_{xx}^0 \neq 0, \chi_{xy}^0 \neq 0$). On the other hand, in the load condition 2, the rotations of the laminate about these axes are blocked ($\chi_{xx}^0 = \chi_{xy}^0 = 0 \implies M_{xx}^0 \neq 0, T_x^0 \neq 0$).

Fig. 5.10 compares all the interfacial stresses between the load conditions 1 and 2. The abscissa axes (\bar{y}) denote the distance (in the y direction) from the free edge normalized by the total thickness of the laminate. The ordinate axes are the normalized interfacial stresses in which $\sigma_0 = F_x^0 / (b^t h^t)$ denotes the uniform tensile stress at the

5. STRESS ANALYSIS OF LONG MULTILAYERED PLATES SUBJECTED TO INVARIANT LOADING: ANALYTICAL SOLUTIONS BY A LAYERWISE STRESS MODEL

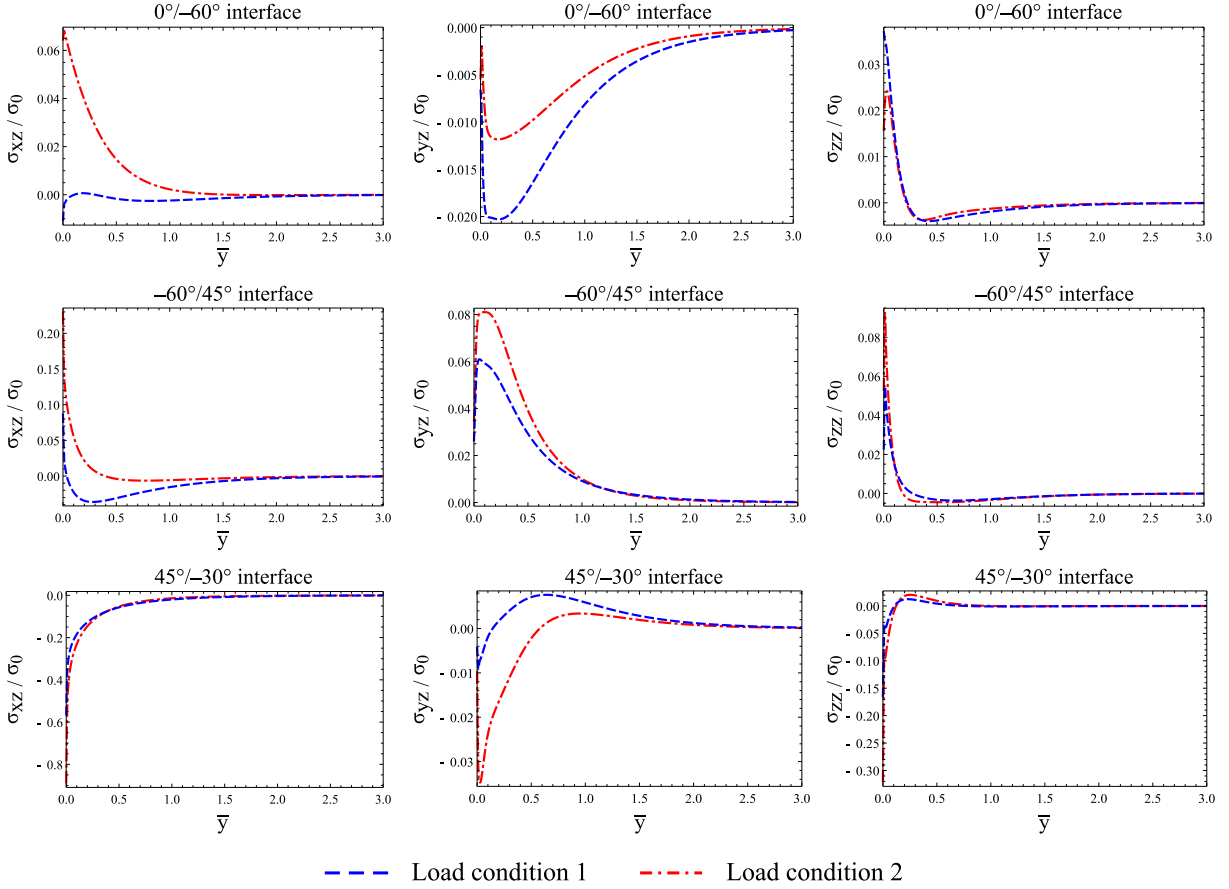


Figure 5.10: Distribution of interfacial stresses: comparison between the load conditions 1 and 2

end. It is observed that the influence of end constraint on the normal interlaminar stress σ_{zz} is negligible at all the interfaces. Regarding the shear interlaminar stresses σ_{xz} and σ_{yz} , the differences between the load conditions 1 and 2 are significant (except for σ_{xz} at the $45^\circ / -30^\circ$ interface). For example, the fact of constraining the laminate against the rotations in the load condition 2 leads to a significant increase in σ_{xz} at the $0^\circ / -60^\circ$ interface (with respect to the load condition 1 in which the laminate is free to rotate). Concerning the shear stress σ_{yz} at this interface, it is seen that the maximum value in the load condition 1 is almost twice the one in the load condition 2. On the contrary, at the other interfaces σ_{yz} is greater in the load condition 2.

In Fig. 5.11 comparisons between interfacial stresses in the load conditions 5 and 6 are shown. In both load conditions, the laminate is subjected to a constant torque T^0 . In the load condition 5, the laminate is free to move in the x direction or to rotate about the y axis ($F_x^0 = M_{xx}^0 = 0 \implies \varepsilon_{xx}^0 \neq 0, \chi_{xx}^0 \neq 0$). On the contrary, in the load condition 6, the laminate is constrained against the displacement in the x direction and the rotation about the y axis ($\varepsilon_{xx}^0 = \chi_{xx}^0 = 0 \implies F_x^0 \neq 0, M_{xx}^0 \neq 0$). According to Fig. 5.11, the normal interfacial stresses are approximately the same in both load conditions. With regard to the shear stresses σ_{xz} and σ_{yz} , one cannot draw a general

5.5. CONCLUSION

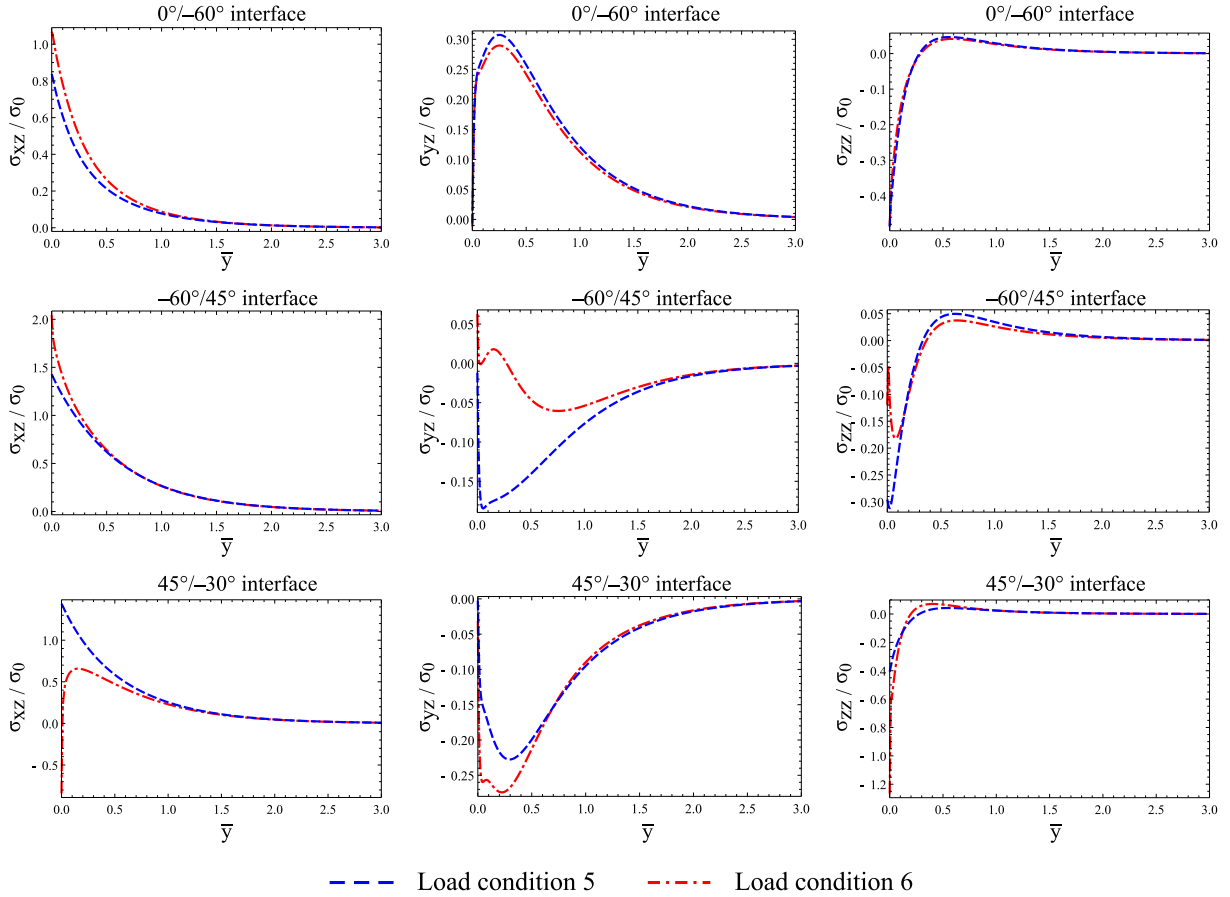


Figure 5.11: Distribution of interfacial stresses: comparison between the load conditions 5 and 6

conclusion. For example, the difference of σ_{yz} at the $0^\circ/-60^\circ$ interface is inconsiderable while this difference at the $-60^\circ/45^\circ$ and $45^\circ/-30^\circ$ interfaces near the free edge is very significant.

5.5 Conclusion

A layerwise stress model, called the LS1 model, is used for the analysis of long rectangular multilayered plates. Based on the assumption that the strain field is independent of the longitudinal coordinate, all possible types of loading are taken into account. By obtaining the reduced form of the displacement field for a rectangular multilayered plate, it is shown that the loading at the longitudinal ends is expressed as a linear combination of uniaxial traction, out-of-plane bending, torsion and in-plane bending. In addition to the loading at the longitudinal ends, the plate can be subjected to any invariant loading on its top and bottom surfaces. Concerning the lateral edges, arbitrary boundary conditions in terms of applied forces or displacements are considered. The analytical solutions of the LS1 model are obtained for a general $(\theta_1, \theta_2, \dots, \theta_n)$ laminate subjected to all of these invariant loads.

In order to investigate the efficiency and the accuracy of the LS1 model, some numerical examples are studied. Different load conditions (traction, out-of-plane bending, torsion and in-plane loading) and coupling effects are investigated in an unsymmetric ($0^\circ, -60^\circ, 45^\circ, -30^\circ$) composite laminate. The overall stiffness matrix of the laminate is compared between the Kirchhoff-Love, LS1 and 3D-FE models. As expected, in the case of thick laminate, the Kirchhoff-Love theory leads to significant errors especially in terms of the out-of-plane stiffnesses. In contrast, it is found that the estimations of the LS1 model are completely consistent with those obtained by the 3D-FEM (for example, for a width-to-thickness ratio of $b^t/h^t = 5$, the average relative error of the LS1 model is less than 0.01%). Regarding the interfacial stresses, the results of the LS1 are compared with the 3D-FEM approximations for different load conditions. Excellent agreements prove that the LS1 model can be used as an accurate and very efficient alternative to the 3D-FEM for the analysis of long multilayered plates. Finally, the effects of end constraint are studied. It is found that the fact of constraining or not the laminate against rotating and/or translating movements can have a significant influence on the distributions of interlaminar stresses near free edges.

The method proposed in this paper can be extended to the analysis of delamination in multilayered plates. Some special load conditions such as delamination of laminated plates under uniaxial traction and cylindrical bending have been investigated in [Saeedi et al. 2012a,b,c]. Future work will focus on multi-delamination problems in long laminated plates and will try to cover all possible types of loading. It is clear that for delamination propagation problems which require incremental simulations, such an efficient model is very useful and provides a great gain in computational cost with respect to the 3D-FEM.

Appendix 5.A Reduced form of 3D displacement field

For an arbitrary body in the Cartesian coordinates, it is assumed that all strain components are independent of the x coordinate. By integrating the three-dimensional strain-displacement relations in the frame of the infinitesimal strain theory, the most general form of displacements are obtained. Integrating ε_{xx} , ε_{yy} and ε_{zz} leads to:

$$U_x(x, y, z) = \int \varepsilon_{xx}(y, z)dx = u_x(y, z) + x f_1(y, z) \quad (5.59)$$

$$U_y(x, y, z) = \int \varepsilon_{yy}(y, z)dy = u_y(y, z) + f_2(x, z) \quad (5.60)$$

$$U_z(x, y, z) = \int \varepsilon_{zz}(y, z)dz = u_z(y, z) + f_3(x, y) \quad (5.61)$$

From the previous displacements ε_{xy} is obtained as follows:

$$\varepsilon_{xy}(y, z) = \frac{1}{2} [u_{x,y}(y, z) + x f_{1,y}(y, z) + f_{2,x}(x, z)] \quad (5.62)$$

Differentiating with respect to x and y gives:

$$f_{1,yy}(y, z) = 0 \Rightarrow f_1(y, z) = g_1(z) + g_2(z) y \quad (5.63)$$

By injecting $f_1(y, z)$ in Eq. 5.62 and differentiating with respect to x , the function $f_2(x, z)$ is found as:

$$g_2(z) + f_{2,xx}(x, z) = 0 \Rightarrow f_2(x, z) = -g_2(z) \frac{x^2}{2} + g_3(z) x + g_4(z) \quad (5.64)$$

According to Eq. 5.60 the function $g_4(z)$ can be omitted. Now ε_{xz} is calculated as follows:

$$\varepsilon_{xz}(y, z) = \frac{1}{2} [u_{x,z}(y, z) + x (g_{1,z}(z) + g_{2,z}(z) y) + f_{3,x}(x, y)] \quad (5.65)$$

By differentiating with respect to x and z , the functions $g_1(z)$ and $g_2(z)$ are found as:

$$g_1(z) = c_1 + c_2 z, \quad g_2(z) = c_3 + c_4 z \quad (5.66)$$

where c_i is an arbitrary constant. By differentiating Eq. 5.65 with respect to x , the function $f_3(x, y)$ is obtained as follows:

$$c_2 + c_4 y + f_{3,xx}(x, y) = 0 \Rightarrow f_3(x, y) = -(c_2 + c_4 y) \frac{x^2}{2} + g_5(y) x + g_6(y) \quad (5.67)$$

According to Eq. 5.61 the function $g_6(y)$ can be omitted. Finally ε_{yz} is expressed as:

$$\varepsilon_{yz}(y, z) = \frac{1}{2} [u_{y,z}(y, z) + u_{z,y}(y, z) - c_4 x^2 + x (g_{3,z}(z) + g_{5,y}(y))] \quad (5.68)$$

This leads to:

$$c_4 = 0 ; g_{3,z}(z) + g_{5,y}(y) = 0 \quad (5.69)$$

Therefore, the functions $g_3(z)$ and $g_5(y)$ are found as:

$$g_3(z) = c_6 + c_5z ; g_5(y) = c_7 - c_5y \quad (5.70)$$

By substituting $c_1, c_2, c_3, c_5, c_6, c_7$, respectively, with $\alpha_1, \alpha_2, \alpha_3, \alpha_4, \alpha_5, \alpha_6$ the displacement field is expressed as follows:

$$\begin{aligned} U_x(x, y, z) &= u_x(y, z) + (\alpha_1 + \alpha_2z + \alpha_3y) x \\ U_y(x, y, z) &= u_y(y, z) + (\alpha_5 + \alpha_4z) x - \alpha_3 \frac{x^2}{2} \\ U_z(x, y, z) &= u_z(y, z) + (\alpha_6 - \alpha_4y) x - \alpha_2 \frac{x^2}{2} \end{aligned} \quad (5.71)$$

According to this displacement field, the three-dimensional strains are obtained as follows:

$$\varepsilon_{xx}(y, z) = \alpha_1 + \alpha_2z + \alpha_3y \quad (5.72)$$

$$\varepsilon_{yy}(y, z) = u_{y,y}(y, z) \quad (5.73)$$

$$\varepsilon_{zz}(y, z) = u_{z,z}(y, z) \quad (5.74)$$

$$\varepsilon_{xy}(y, z) = \frac{1}{2} [u_{x,y}(y, z) + \alpha_5 + \alpha_4z] \quad (5.75)$$

$$\varepsilon_{xz}(y, z) = \frac{1}{2} [u_{x,z}(y, z) + \alpha_6 - \alpha_4y] \quad (5.76)$$

$$\varepsilon_{yz}(y, z) = \frac{1}{2} [u_{y,z}(y, z) + u_{z,y}(y, z)] \quad (5.77)$$

Replacing $u_x(y, z)$ with $u_x(y, z) - \alpha_5y - \alpha_6z$ reveals that no strains are produced by α_5 and α_6 . Indeed, the constants α_5 and α_6 correspond to the rigid-body rotations about the z and y axes respectively. Therefore, the terms related to these constants can be omitted. The constants $\alpha_1, \alpha_2, \alpha_3$ and α_4 correspond, respectively, to the uniform extension in the x direction, the out-of-plane bending about the y axis, the in-plane bending about the z axis and the torsion about the x axis (see Fig. 5.2). By replacing $u_x(y, z)$ with $u_x(y, z) + \alpha_4yz$ and inserting $\alpha_1 = \varepsilon_{xx}^0, \alpha_2 = \chi_{xx}^0, \alpha_3 = \chi_{zz}^0, \alpha_4 = \chi_{xy}^0$ the displacement field is expressed as follows:

$$U_x(x, y, z) = u_x(y, z) + (\varepsilon_{xx}^0 + \chi_{xx}^0z + \chi_{zz}^0y) x + \chi_{xy}^0yz \quad (5.78)$$

$$U_y(x, y, z) = u_y(y, z) + \chi_{xy}^0xz - \chi_{zz}^0 \frac{x^2}{2} \quad (5.79)$$

$$U_z(x, y, z) = u_z(y, z) - \chi_{xy}^0xy - \chi_{xx}^0 \frac{x^2}{2} \quad (5.80)$$

Appendix 5.B General formulation of the LS1 model

For an orthotropic elastic material whose normal direction coincides with the z axis, the linear relation between three dimensional strains and stresses can be written in Voigt notation as follows:

$$\begin{pmatrix} \varepsilon_{xx} \\ \varepsilon_{yy} \\ \varepsilon_{zz} \\ 2\varepsilon_{yz} \\ 2\varepsilon_{xz} \\ 2\varepsilon_{xy} \end{pmatrix} = \underbrace{\begin{bmatrix} S_{11} & S_{12} & S_{13} & 0 & 0 & S_{16} \\ S_{12} & S_{22} & S_{23} & 0 & 0 & S_{26} \\ S_{13} & S_{23} & S_{33} & 0 & 0 & S_{36} \\ 0 & 0 & 0 & S_{44} & S_{45} & 0 \\ 0 & 0 & 0 & S_{45} & S_{55} & 0 \\ S_{16} & S_{26} & S_{36} & 0 & 0 & S_{66} \end{bmatrix}}_{\underline{\underline{S}}_{(x,y,z)}} \cdot \begin{pmatrix} \sigma_{xx} \\ \sigma_{yy} \\ \sigma_{zz} \\ \sigma_{yz} \\ \sigma_{xz} \\ \sigma_{xy} \end{pmatrix}$$

In the formulation of the LS1 model, the matrices $\tilde{\tilde{S}}$ and $\tilde{\tilde{S}}_Q$, and the scalar S_ν are, respectively, related to the plane stress, out-of-plane shear stress and normal stress components of the compliance matrix. They are deduced from the compliance matrix $\underline{\underline{S}}_{(x,y,z)}$ as follows:

$$\tilde{\tilde{S}} = \begin{pmatrix} S_{11} & S_{12} & S_{16} \\ S_{12} & S_{22} & S_{26} \\ S_{16} & S_{26} & S_{66} \end{pmatrix}, \quad \tilde{\tilde{S}}_Q = \begin{pmatrix} S_{44} & S_{45} \\ S_{45} & S_{55} \end{pmatrix}, \quad S_\nu = S_{33}$$

In what follows, the formulation of the LS1 model is presented. In the following formulation, x and y represent the in-plane directions and z is the thickness coordinate. h_-^i , h_+^i and \bar{h}^i are the bottom, the top and the mid-plane z coordinates of layer i and $e^i = h_+^i - h_-^i$ denotes the thickness of layer i . Greek alphabet subscripts (such as $\alpha, \beta, \gamma, \delta$) correspond to $\{x, y\}$ or $\{1, 2\}$ and the Einstein summation convention is adopted for repeated indices.

Generalized stresses:

- for layer i

$$N_{\alpha\beta}^i(x, y) = \int_{h_-^i}^{h_+^i} \sigma_{\alpha\beta}(x, y, z) dz \quad (5.81)$$

$$M_{\alpha\beta}^i(x, y) = \int_{h_-^i}^{h_+^i} (z - \bar{h}^i) \sigma_{\alpha\beta}(x, y, z) dz \quad (5.82)$$

$$Q_\alpha^i(x, y) = \int_{h_-^i}^{h_+^i} \sigma_{\alpha z}(x, y, z) dz \quad (5.83)$$

- for interface $i, i + 1$

$$\tau_\alpha^{i,i+1}(x, y) = \sigma_{\alpha z}^i(x, y, h_+^i) = \sigma_{\alpha z}^{i+1}(x, y, h_-^{i+1}) \quad (5.84)$$

$$\nu^{i,i+1}(x, y) = \sigma_{zz}^i(x, y, h_+^i) = \sigma_{zz}^{i+1}(x, y, h_-^{i+1}) \quad (5.85)$$

Generalized displacements:

$$U_{\alpha}^i(x, y) = \frac{1}{e^i} \int_{h_-^i}^{h_+^i} U_{\alpha}^{3D}(x, y, z) dz \quad (5.86)$$

$$U_z^i(x, y) = \frac{1}{e^i} \int_{h_-^i}^{h_+^i} U_z^{3D}(x, y, z) dz \quad (5.87)$$

$$\Phi_{\alpha}^i(x, y) = \frac{12}{(e^i)^2} \int_{h_-^i}^{h_+^i} \frac{z - \bar{h}^i}{e^i} U_{\alpha}^{3D}(x, y, z) dz \quad (5.88)$$

Generalized strains:

- for layer i

$$\varepsilon_{\alpha\beta}^i = \frac{1}{2} (U_{\alpha,\beta}^i + U_{\beta,\alpha}^i) \quad (5.89)$$

$$\chi_{\alpha\beta}^i = \frac{1}{2} (\Phi_{\alpha,\beta}^i + \Phi_{\beta,\alpha}^i) \quad (5.90)$$

$$d_{\Phi_{\alpha}}^i = \Phi_{\alpha}^i + U_{z,\alpha}^i \quad (5.91)$$

- for interface $i, i + 1$

$$D_{\alpha}^{i,i+1} = U_{\alpha}^{i+1} - U_{\alpha}^i - \left(\frac{e^i}{2} \Phi_{\alpha}^i + \frac{e^{i+1}}{2} \Phi_{\alpha}^{i+1} \right) \quad (5.92)$$

$$D_z^{i,i+1} = U_z^{i+1} - U_z^i \quad (5.93)$$

Constitutive relations:

- for layer i

$$\varepsilon_{\alpha\beta}^i = \frac{1}{e^i} S_{\alpha\beta\gamma\delta}^i N_{\gamma\delta}^i \quad (5.94)$$

$$\chi_{\alpha\beta}^i = \frac{12}{(e^i)^3} S_{\alpha\beta\gamma\delta}^i M_{\gamma\delta}^i \quad (5.95)$$

$$d_{\Phi_{\alpha}}^i = \frac{6}{5e^i} S_{Q_{\alpha\beta}}^i Q_{\beta}^i - \frac{1}{10} S_{Q_{\alpha\beta}}^i (\tau_{\beta}^{i-1,i} + \tau_{\beta}^{i,i+1}) \quad (5.96)$$

- for interface $i, i + 1$

$$\begin{aligned} D_{\alpha}^{i,i+1} = & -\frac{1}{10} \left(S_{Q_{\alpha\beta}}^i Q_{\beta}^i + S_{Q_{\alpha\beta}}^{i+1} Q_{\beta}^{i+1} \right) - \frac{1}{30} \left(e^i S_{Q_{\alpha\beta}}^i \tau_{\beta}^{i-1,i} + e^{i+1} S_{Q_{\alpha\beta}}^{i+1} \tau_{\beta}^{i+1,i+2} \right) \\ & + \frac{2}{15} \left(e^i S_{Q_{\alpha\beta}}^i + e^{i+1} S_{Q_{\alpha\beta}}^{i+1} \right) \tau_{\beta}^{i,i+1} \end{aligned} \quad (5.97)$$

$$D_z^{i,i+1} = \frac{9}{70} \left(e^i S_{\nu}^i \nu^{i-1,i} + e^{i+1} S_{\nu}^{i+1} \nu^{i+1,i+2} \right) + \frac{13}{35} \left(e^i S_{\nu}^i + e^{i+1} S_{\nu}^{i+1} \right) \nu^{i,i+1} \quad (5.98)$$

Equilibrium equations:

$$N_{\alpha\beta,\beta}^i + \tau_\alpha^{i,i+1} - \tau_\alpha^{i-1,i} = 0 \quad (5.99)$$

$$M_{\alpha\beta,\beta}^i + \frac{e^i}{2} (\tau_\alpha^{i,i+1} + \tau_\alpha^{i-1,i}) - Q_\alpha^i = 0 \quad (5.100)$$

$$Q_{\beta,\beta}^i + \nu^{i,i+1} - \nu^{i-1,i} = 0 \quad (5.101)$$

Boundary conditions:

The boundary conditions of the model are written in terms of generalized stresses or generalized displacements. At point $p(x_0, y_0)$ on the lateral edge of the laminate, five boundary conditions are given as follows:

$$\begin{aligned} N_{\alpha\beta}^i(x_0, y_0) n_\beta &= [N_\alpha^i]^d & \text{or} & & U_\alpha^i(x_0, y_0) &= [U_\alpha^i]^d \\ M_{\alpha\beta}^i(x_0, y_0) n_\beta &= [M_\alpha^i]^d & \text{or} & & \Phi_\alpha^i(x_0, y_0) &= [\Phi_\alpha^i]^d \\ Q_\alpha^i(x_0, y_0) n_\alpha &= [Q^i]^d & \text{or} & & U_z^i(x_0, y_0) &= [U_z^i]^d \end{aligned} \quad (5.102)$$

where the vector $\underline{n} = (n_\alpha, n_\beta)^t$ is the outward normal to the lateral edge and the superscript d denotes determined (given) field.

Appendix 5.C Definition of scalars, vectors and matrices

The constants a^i , b^i and c^i for layer i are defined as:

$$a^i = \left(S_{22} - \frac{(S_{12})^2}{S_{11}} \right)^i, \quad b^i = \left(S_{26} - \frac{S_{12} S_{16}}{S_{11}} \right)^i, \quad c^i = \left(S_{66} - \frac{(S_{16})^2}{S_{11}} \right)^i$$

The scalar functions v_i ($1 \leq i \leq 20$) are defined as follows:

$$\begin{aligned} \begin{pmatrix} v_1 \\ v_2 \end{pmatrix} &= \frac{1}{10} \tilde{S}_Q^1 \cdot \begin{pmatrix} T_x^- \\ T_y^- \end{pmatrix}, & \begin{pmatrix} v_3 \\ v_4 \end{pmatrix} &= -\frac{1}{10} \tilde{S}_Q^n \cdot \begin{pmatrix} T_x^+ \\ T_y^+ \end{pmatrix} \\ \begin{pmatrix} v_5 \\ v_6 \end{pmatrix} &= \frac{e^1}{3} \begin{pmatrix} v_1 \\ v_2 \end{pmatrix}, & \begin{pmatrix} v_7 \\ v_8 \end{pmatrix} &= \frac{e^n}{3} \begin{pmatrix} v_3 \\ v_4 \end{pmatrix} \\ \begin{pmatrix} v_9 \\ v_{10} \end{pmatrix} &= -\frac{1}{e^1} \begin{pmatrix} c^1 & b^1 \\ b^1 & a^1 \end{pmatrix} \cdot \begin{pmatrix} T_x^- \\ T_y^- \end{pmatrix}, & \begin{pmatrix} v_{11} \\ v_{12} \end{pmatrix} &= -\frac{1}{e^n} \begin{pmatrix} c^n & b^n \\ b^n & a^n \end{pmatrix} \cdot \begin{pmatrix} T_x^+ \\ T_y^+ \end{pmatrix} \\ \begin{pmatrix} v_{13} \\ v_{14} \end{pmatrix} &= -\frac{6}{e^1} \begin{pmatrix} v_9 \\ v_{10} \end{pmatrix}, & \begin{pmatrix} v_{15} \\ v_{16} \end{pmatrix} &= \frac{6}{e^n} \begin{pmatrix} v_{11} \\ v_{12} \end{pmatrix} \\ v_{17} &= -\frac{9}{70} e^1 S_\nu^1 T_z^-, & v_{18} &= \frac{9}{70} e^n S_\nu^n T_z^+ \end{aligned}$$

5. STRESS ANALYSIS OF LONG MULTILAYERED PLATES SUBJECTED TO INVARIANT LOADING: ANALYTICAL SOLUTIONS BY A LAYERWISE STRESS MODEL

$$v_{19} = -T_z^- \quad , \quad v_{20} = -T_z^+$$

In the case of mirror symmetry, the analysis is limited to layers $1 \leq i \leq m/2$. In such case, one should consider $v_3 = v_4 = v_7 = v_8 = v_{11} = v_{12} = v_{15} = v_{16} = v_{18} = v_{20} = 0$.

The matrices $\underline{\underline{T}}$ are obtained as follows:

$$\underline{\underline{T}}^{1a} = \left[\frac{6 S_{Q11}^i}{5 e^i} \delta_{ij} \right]_{n \times n} \quad ; \quad \underline{\underline{T}}^{1b} = \left[\frac{6 S_{Q12}^i}{5 e^i} \delta_{ij} \right]_{n \times n} \quad ; \quad \underline{\underline{T}}^{1c} = \left[\frac{6 S_{Q22}^i}{5 e^i} \delta_{ij} \right]_{n \times n}$$

$$\underline{\underline{T}}^{2a} = \left[-\frac{1}{10} S_{Q11}^j (\delta_{ij} + \delta_{i+1,j}) \right]_{(n-1) \times n}$$

$$\underline{\underline{T}}^{2b} = \left[-\frac{1}{10} S_{Q12}^j (\delta_{ij} + \delta_{i+1,j}) \right]_{(n-1) \times n}$$

$$\underline{\underline{T}}^{2c} = \left[-\frac{1}{10} S_{Q22}^j (\delta_{ij} + \delta_{i+1,j}) \right]_{(n-1) \times n}$$

$$\underline{\underline{T}}^{3a} = -\frac{1}{30} \left[e^i S_{Q11}^i \delta_{i,j+1} - 4 \left(e^i S_{Q11}^i + e^{i+1} S_{Q11}^{i+1} \right) \delta_{ij} + e^{i+1} S_{Q11}^{i+1} \delta_{i,j-1} \right]_{(n-1) \times (n-1)}$$

$$\underline{\underline{T}}^{3b} = -\frac{1}{30} \left[e^i S_{Q12}^i \delta_{i,j+1} - 4 \left(e^i S_{Q12}^i + e^{i+1} S_{Q12}^{i+1} \right) \delta_{ij} + e^{i+1} S_{Q12}^{i+1} \delta_{i,j-1} \right]_{(n-1) \times (n-1)}$$

$$\underline{\underline{T}}^{3c} = -\frac{1}{30} \left[e^i S_{Q22}^i \delta_{i,j+1} - 4 \left(e^i S_{Q22}^i + e^{i+1} S_{Q22}^{i+1} \right) \delta_{ij} + e^{i+1} S_{Q22}^{i+1} \delta_{i,j-1} \right]_{(n-1) \times (n-1)}$$

$$\underline{\underline{T}}^{4a} = \left[\frac{a^i}{e^i} (\delta_{i,j+1} - \delta_{ij}) \right]_{n \times (n-1)}$$

$$\underline{\underline{T}}^{4b} = \left[\frac{b^i}{e^i} (\delta_{i,j+1} - \delta_{ij}) \right]_{n \times (n-1)}$$

$$\underline{\underline{T}}^{4c} = \left[\frac{c^i}{e^i} (\delta_{i,j+1} - \delta_{ij}) \right]_{n \times (n-1)}$$

$$\underline{\underline{T}}^{5a} = \left[-6 \frac{a^i}{(e^i)^2} (\delta_{i,j+1} + \delta_{ij}) \right]_{n \times (n-1)}$$

$$\underline{\underline{T}}^{5b} = \left[-6 \frac{b^i}{(e^i)^2} (\delta_{i,j+1} + \delta_{ij}) \right]_{n \times (n-1)}$$

$$\underline{\underline{T}}^{5c} = \left[-6 \frac{c^i}{(e^i)^2} (\delta_{i,j+1} + \delta_{ij}) \right]_{n \times (n-1)}$$

$$\underline{\underline{T}}^{6a} = \left[12 \frac{a^i}{(e^i)^3} \delta_{ij} \right]_{n \times n} \quad ; \quad \underline{\underline{T}}^{6b} = \left[12 \frac{b^i}{(e^i)^3} \delta_{ij} \right]_{n \times n} \quad ; \quad \underline{\underline{T}}^{6c} = \left[12 \frac{c^i}{(e^i)^3} \delta_{ij} \right]_{n \times n}$$

$$\underline{\underline{T}}^7 = [\delta_{i+1,j} - \delta_{ij}]_{(n-1) \times n} \quad ; \quad \underline{\underline{T}}^{7R} = [\delta_{i+1,j} - \delta_{ij}]_{n_I \times n}$$

Note: If there is no mirror symmetry $\underline{T}_7 = \underline{T}_7^R$.

$$\underline{T}^8 = \left[-\frac{e^j}{2} (\delta_{ij} + \delta_{i+1,j}) \right]_{(n-1) \times n}$$

$$\underline{T}^9 = [t_{ij}^9]_{n_I \times n_I} \quad ; \quad t_{ij}^9 = \begin{cases} 1 & i \geq j \\ 0 & i < j \end{cases}$$

The matrices \underline{H} are obtained as follows:

$$\underline{H}^1_{(3n-2) \times (5n)} = \left[\begin{array}{c|c|c|c|c} \underline{Q}_{n \times n} & \underline{Q}_{n \times n} & \underline{I}_{n \times n} & \underline{Q}_{n \times n} & -\underline{T}^{1b}_{n \times n} \\ \hline \underline{T}^7_{(n-1) \times n} & \underline{Q}_{(n-1) \times n} & \underline{T}^8_{(n-1) \times n} & \underline{Q}_{(n-1) \times n} & -\underline{T}^{2b}_{(n-1) \times n} \\ \hline \underline{Q}_{(n-1) \times n} & \underline{T}^7_{(n-1) \times n} & \underline{Q}_{(n-1) \times n} & \underline{T}^8_{(n-1) \times n} & -\underline{T}^{2c}_{(n-1) \times n} \end{array} \right]$$

$$\underline{H}^2_{n \times (3n-2)} = \left[\underline{Q}_{n \times n} \mid \underline{T}^{4c}_{n \times (n-1)} \mid \underline{T}^{4b}_{n \times (n-1)} \right]$$

$$\underline{H}^3_{n \times (3n-2)} = \left[\underline{Q}_{n \times n} \mid \underline{T}^{4b}_{n \times (n-1)} \mid \underline{T}^{4a}_{n \times (n-1)} \right]$$

$$\underline{H}^4_{n \times (3n-2)} = \left[\underline{T}^{6c}_{n \times n} \mid \underline{T}^{5c}_{n \times (n-1)} \mid \underline{T}^{5b}_{n \times (n-1)} \right]$$

$$\underline{H}^5_{n \times (3n-2)} = \left[\underline{T}^{6b}_{n \times n} \mid \underline{T}^{5b}_{n \times (n-1)} \mid \underline{T}^{5a}_{n \times (n-1)} \right]$$

$$\underline{H}^6_{n \times 5n} = \left[\underline{Q}_{n \times 4n} \mid \underline{T}^{6b}_{n \times n} \right]$$

$$\underline{H}^7_{n \times 5n} = \left[\underline{Q}_{n \times 4n} \mid \underline{T}^{6a}_{n \times n} \right]$$

$$\underline{H}^8_{n \times (3n-2)} = \left[\underline{T}^{1b}_{n \times n} \mid (\underline{T}^{2b})^t_{n \times (n-1)} \mid (\underline{T}^{2c})^t_{n \times (n-1)} \right]$$

$$\underline{H}^9_{n \times 5n} = \left[\underline{Q}_{n \times 3n} \mid -\underline{I}_{n \times n} \mid \underline{T}^{1c}_{n \times n} \right]$$

where \underline{Q} and \underline{I} are zero matrix and identity matrix respectively.

The matrix \underline{N} has the form:

$$\underline{N}_{(3n-2) \times (3n-2)} = \left[\begin{array}{c|c|c} \underline{T}^{1a}_{n \times n} & (\underline{T}^{2a})^t_{n \times (n-1)} & (\underline{T}^{2b})^t_{n \times (n-1)} \\ \hline \underline{T}^{2a}_{(n-1) \times n} & \underline{T}^{3a}_{(n-1) \times (n-1)} & \underline{T}^{3b}_{(n-1) \times (n-1)} \\ \hline \underline{T}^{2b}_{(n-1) \times n} & \underline{T}^{3b}_{(n-1) \times (n-1)} & \underline{T}^{3c}_{(n-1) \times (n-1)} \end{array} \right]$$

The matrix $\underline{\underline{R}}$ is obtained as:

$$\underline{\underline{R}} = \frac{1}{70} [9 e^i S_\nu^i \delta_{i,j+1} + 26 (e^i S_\nu^i + e^{i+1} S_\nu^{i+1}) \delta_{ij} + 9 e^{i+1} S_\nu^{i+1} \delta_{i,j-1}]_{n_I \times n_I}$$

Appendix 5.D LS1 system of equations

The expressions of the constants S_ν^i , a^i , b^i , c^i , the matrices \tilde{S}^i , \tilde{S}_Q^i , $\underline{\underline{N}}$, $\underline{\underline{R}}$ and also all of the scalar functions v and matrices $\underline{\underline{T}}$, $\underline{\underline{H}}$ used in the formulation of this section are defined in 5.C.

By substituting Eqs. 5.33 to 5.35 into Eqs. 5.96 for $\alpha = x$ and 5.97, the latter equations can be written in matrix form as follows:

$$\underline{\underline{N}}_{(3n-2) \times (3n-2)} \cdot \underline{\underline{A}}_{(3n-2)} + \underline{\underline{V}}_{(3n-2)} = \underline{\underline{B}}_{(3n-2)} \quad (5.103)$$

where:

$$\underline{\underline{A}}_{(3n-2)} = \begin{pmatrix} \left(\underline{\underline{Q}}_x^i \right)_{(n)} \\ \left(\underline{\underline{\tau}}_x^{i,i+1} \right)_{(n-1)} \\ \left(\underline{\underline{\tau}}_y^{i,i+1} \right)_{(n-1)} \end{pmatrix}, \quad \underline{\underline{B}}_{(3n-2)} = \begin{pmatrix} \left(\underline{\underline{\alpha}}^i \right)_{(n)} \\ \left(\underline{\underline{\beta}}^{i,i+1} \right)_{(n-1)} \\ \left(\underline{\underline{\gamma}}^{i,i+1} \right)_{(n-1)} \end{pmatrix}$$

with:

$$\begin{aligned} \alpha^i &= \phi_x^i - \frac{6}{5e^i} S_{Q_{12}}^i Q_y^i \\ \beta^{i,i+1} &= u_x^{i+1} - u_x^i - \left(\frac{e^i}{2} \phi_x^i + \frac{e^{i+1}}{2} \phi_x^{i+1} \right) + \frac{1}{10} \left(S_{Q_{12}}^i Q_y^i + S_{Q_{12}}^{i+1} Q_y^{i+1} \right) \\ \gamma^{i,i+1} &= u_y^{i+1} - u_y^i - \left(\frac{e^i}{2} \phi_y^i + \frac{e^{i+1}}{2} \phi_y^{i+1} \right) + \frac{1}{10} \left(S_{Q_{22}}^i Q_y^i + S_{Q_{22}}^{i+1} Q_y^{i+1} \right) \end{aligned}$$

$\underline{\underline{V}}$ is a vector of dimensions $3n-2$ which is related to given loads on the top and bottom surfaces of the laminate. It is defined as:

$$(\underline{\underline{V}})^t = \begin{cases} (v_1 + v_3) & ; \quad n = 1 \\ (v_1, v_3, v_5 + v_7, v_6 + v_8) & ; \quad n = 2 \\ \left(\underbrace{v_1, 0, \dots, 0, v_3}_n, \underbrace{v_5, 0, \dots, 0, v_7}_{n-1}, \underbrace{v_6, 0, \dots, 0, v_8}_{n-1} \right) & ; \quad n \geq 3 \end{cases}$$

The vector $\underline{\underline{B}}$ in matrix form can be expressed as:

$$\underline{\underline{B}}_{(3n-2)} = \underline{\underline{H}}_{(3n-2) \times 5n}^1 \cdot \underline{\underline{X}}_{(5n)} \quad (5.104)$$

where \underline{X} is a vector of dimension $5n$ as:

$$\underline{X}_{(5n)} = \begin{pmatrix} \left(\underline{u}_x^i \right)_{(n)} \\ \left(\underline{u}_y^i \right)_{(n)} \\ \left(\underline{\phi}_x^i \right)_{(n)} \\ \left(\underline{\phi}_y^i \right)_{(n)} \\ \left(\underline{Q}_y^i \right)_{(n)} \end{pmatrix}, \quad 1 \leq i \leq n \quad (5.105)$$

According to Eqs. 5.103 and 5.104, the vector \underline{A} is obtained as:

$$\underline{A}_{(3n-2)} = \underline{L}_{(3n-2) \times 5n} \cdot \underline{X}_{(5n)} + \underline{f}_{(3n-2)}^N \quad (5.106)$$

where

$$\underline{L}_{(3n-2) \times 5n} = \underline{N}_{(3n-2) \times (3n-2)}^{-1} \cdot \underline{H}_{(3n-2) \times 5n}^1$$

$$\underline{f}_{(3n-2)}^N = -\underline{N}_{(3n-2) \times (3n-2)}^{-1} \cdot \underline{V}_{(3n-2)}$$

By substituting Eq. 5.31 into Eq. 5.94, it can be deduced ($1 \leq i \leq n$):

$$N_{xx}^i = \frac{1}{S_{11}^i} [e^i (\varepsilon_{xx}^0 + \bar{h}^i \chi_{xx}^0 + \chi_{zz}^0 y) - S_{12}^i N_{yy}^i - S_{16}^i N_{xy}^i] \quad (5.107)$$

$$u_x^{i'} = \frac{1}{e^i} [c^i N_{xy}^i + b^i N_{yy}^i] + \frac{S_{16}^i}{S_{11}^i} (\varepsilon_{xx}^0 + \bar{h}^i \chi_{xx}^0 + \chi_{zz}^0 y) - 2\bar{h}^i \chi_{xy}^0 \quad (5.108)$$

$$u_y^{i'} = \frac{1}{e^i} [b^i N_{xy}^i + a^i N_{yy}^i] + \frac{S_{12}^i}{S_{11}^i} (\varepsilon_{xx}^0 + \bar{h}^i \chi_{xx}^0 + \chi_{zz}^0 y) \quad (5.109)$$

By differentiating Eqs. 5.108 and 5.109 with respect to y and using Eqs. 5.37 and 5.38, one obtains:

$$u_x^{i''} = \frac{1}{e^i} [c^i (\tau_x^{i-1,i} - \tau_x^{i,i+1}) + b^i (\tau_y^{i-1,i} - \tau_y^{i,i+1})] + \frac{S_{16}^i}{S_{11}^i} \chi_{zz}^0 \quad (5.110)$$

$$u_y^{i''} = \frac{1}{e^i} [b^i (\tau_x^{i-1,i} - \tau_x^{i,i+1}) + a^i (\tau_y^{i-1,i} - \tau_y^{i,i+1})] + \frac{S_{12}^i}{S_{11}^i} \chi_{zz}^0 \quad (5.111)$$

In the same way, by substituting Eq. 5.32 into Eq. 5.95, it is deduced ($1 \leq i \leq n$):

$$M_{xx}^i = \frac{1}{S_{11}^i} \left[\frac{(e^i)^3}{12} \chi_{xx}^0 - S_{12}^i M_{yy}^i - S_{16}^i M_{xy}^i \right] \quad (5.112)$$

$$\phi_x^{i'} = \frac{12}{(e^i)^3} [c^i M_{xy}^i + b^i M_{yy}^i] + \frac{S_{16}^i}{S_{11}^i} \chi_{xx}^0 - 2\chi_{xy}^0 \quad (5.113)$$

$$\phi_y^{i'} = \frac{12}{(e^i)^3} [b^i M_{xy}^i + a^i M_{yy}^i] + \frac{S_{12}^i}{S_{11}^i} \chi_{xx}^0 \quad (5.114)$$

By differentiating the previous equations with respect to y and using Eqs. 5.39 and 5.40, one finds:

$$\phi_x^{i''} = \frac{12}{(e^i)^3} \left[c^i \left(Q_x^i - \frac{e^i}{2} (\tau_x^{i-1,i} + \tau_x^{i,i+1}) \right) + b^i \left(Q_y^i - \frac{e^i}{2} (\tau_y^{i-1,i} + \tau_y^{i,i+1}) \right) \right] \quad (5.115)$$

$$\phi_y^{i''} = \frac{12}{(e^i)^3} \left[b^i \left(Q_x^i - \frac{e^i}{2} (\tau_x^{i-1,i} + \tau_x^{i,i+1}) \right) + a^i \left(Q_y^i - \frac{e^i}{2} (\tau_y^{i-1,i} + \tau_y^{i,i+1}) \right) \right] \quad (5.116)$$

Eqs. 5.110, 5.111, 5.115 and 5.116 in matrix form can be expressed as:

$$\left(\underline{u}_x'' \right)_{(n)} = \underline{H}^2_{n \times (3n-2)} \cdot \underline{A}_{(3n-2)} + \underline{f}_{1(n)} + \widehat{\underline{f}}_{1(n)} \quad (5.117)$$

$$\left(\underline{u}_y'' \right)_{(n)} = \underline{H}^3_{n \times (3n-2)} \cdot \underline{A}_{(3n-2)} + \underline{f}_{2(n)} + \widehat{\underline{f}}_{2(n)} \quad (5.118)$$

$$\left(\underline{\phi}_x'' \right)_{(n)} = \underline{H}^4_{n \times (3n-2)} \cdot \underline{A}_{(3n-2)} + \underline{T}^{6b} \cdot \left(\underline{Q}_y \right)_{(n)} + \underline{f}_{3(n)} \quad (5.119)$$

$$\left(\underline{\phi}_y'' \right)_{(n)} = \underline{H}^5_{n \times (3n-2)} \cdot \underline{A}_{(3n-2)} + \underline{T}^{6a} \cdot \left(\underline{Q}_y \right)_{(n)} + \underline{f}_{4(n)} \quad (5.120)$$

where

$$\underline{f}_{1(n)} = (\delta_{i1} v_9 + \delta_{in} v_{11}) \quad , \quad \underline{f}_{2(n)} = (\delta_{i1} v_{10} + \delta_{in} v_{12})$$

$$\underline{f}_{3(n)} = (\delta_{i1} v_{13} + \delta_{in} v_{15}) \quad , \quad \underline{f}_{4(n)} = (\delta_{i1} v_{14} + \delta_{in} v_{16})$$

$$\widehat{\underline{f}}_{1(n)} = \left(\frac{S_{16}^i}{S_{11}^i} \chi_{zz}^0 \right) \quad , \quad \widehat{\underline{f}}_{2(n)} = \left(\frac{S_{12}^i}{S_{11}^i} \chi_{zz}^0 \right)$$

in which $1 \leq i \leq n$ and δ_{ij} is the Kronecker's delta.

Introducing Eq. 5.106 into the previous equations gives:

$$\left(\underline{u}_x'' \right)_{(n)} = \underline{H}^2_{n \times (3n-2)} \cdot \underline{L}_{(3n-2) \times 5n} \cdot \underline{X}_{(5n)} + \underline{H}^2_{n \times (3n-2)} \cdot \underline{f}_{(3n-2)}^N + \underline{f}_{1(n)} + \widehat{\underline{f}}_{1(n)} \quad (5.121)$$

$$\left(\underline{u}_y'' \right)_{(n)} = \underline{H}^3_{n \times (3n-2)} \cdot \underline{L}_{(3n-2) \times 5n} \cdot \underline{X}_{(5n)} + \underline{H}^3_{n \times (3n-2)} \cdot \underline{f}_{(3n-2)}^N + \underline{f}_{2(n)} + \widehat{\underline{f}}_{2(n)} \quad (5.122)$$

$$\left(\underline{\phi}_x'' \right)_{(n)} = \left(\underline{H}^4_{n \times (3n-2)} \cdot \underline{L}_{(3n-2) \times 5n} + \underline{H}^6_{n \times 5n} \right) \cdot \underline{X}_{(5n)} + \underline{H}^4_{n \times (3n-2)} \cdot \underline{f}_{(3n-2)}^N + \underline{f}_{3(n)} \quad (5.123)$$

$$\left(\underline{\phi''}_y\right)_{(n)} = \left(\underline{H}^5_{n \times (3n-2)} \cdot \underline{L}_{(3n-2) \times 5n} + \underline{H}^7_{n \times 5n}\right) \cdot \underline{X}_{(5n)} + \underline{H}^5_{n \times (3n-2)} \cdot \underline{f}_{(3n-2)}^N + \underline{f}_{4(n)} \quad (5.124)$$

Eq. 5.98 in matrix form is written as:

$$\underline{R}_{n_I \times n_I} \cdot \underline{C}_{(n_I)} + \underline{W}_{(n_I)} = \underline{D}_{(n_I)} \quad (5.125)$$

where:

$$\begin{aligned} \left(\underline{C}_{(n_I)}\right)^t &= \left(\nu^{1,2}, \nu^{2,3}, \dots, \nu^{n_I, n_I+1}\right) \\ \left(\underline{D}_{(n_I)}\right)^t &= \left(u_z^2 - u_z^1, u_z^3 - u_z^2, \dots, u_z^{n_I+1} \delta_{n_I+1, n} - u_z^{n_I}\right) \\ \underline{W}_{(n_I)} &= \left(v_{17} \delta_{i1} + v_{18} \delta_{in}\right), \quad 1 \leq i \leq n_I \end{aligned}$$

Eq. 5.41 in matrix representation has the form:

$$\left(\underline{Q}'_y\right)_{(n)} = \left(\underline{T}^{7R}\right)^t_{n \times n_I} \cdot \underline{C}_{(n_I)} + \underline{f}_{5(n)} \quad (5.126)$$

where

$$\underline{f}_{5(n)} = \left(\delta_{i1} v_{19} + \delta_{in} v_{20}\right), \quad 1 \leq i \leq n$$

Combining this equation with Eq. 5.125 results in:

$$\left(\underline{Q}'_y\right)_{(n)} = \left(\underline{T}^{7R}\right)^t_{n \times n_I} \cdot \underline{R}^{-1}_{n_I \times n_I} \cdot \left(\underline{D}_{(n_I)} - \underline{W}_{(n_I)}\right) + \underline{f}_{5(n)} \quad (5.127)$$

The vector \underline{D} can be written as:

$$\underline{D}_{(n_I)} = \underline{T}^{7R}_{n_I \times n} \cdot \left(\underline{u}_z\right)_{(n)} \quad (5.128)$$

By injecting this equation into Eq. 5.127 and differentiating with respect to y one can write:

$$\left(\underline{Q}''_y\right)_{(n)} = \left(\underline{T}^{7R}\right)^t_{n \times n_I} \cdot \underline{R}^{-1}_{n_I \times n_I} \cdot \left(\underline{T}^{7R}_{n_I \times n} \cdot \left(\underline{u}'_z\right)_{(n)} - \underline{W}'_{(n_I)}\right) + \underline{f}'_{5(n)} \quad (5.129)$$

Now, from Eq. 5.96 for $\alpha = y$ one obtains:

$$\left(\underline{u}'_z\right)_{(n)} = -\left(\underline{\phi}_y\right)_{(n)} + \underline{T}^{1c}_{n \times n} \cdot \left(\underline{Q}_y\right)_{(n)} + \underline{H}^8_{n \times (3n-2)} \cdot \underline{A}_{(3n-2)} \quad (5.130)$$

Injecting Eq. 5.106 into this equation yields:

$$\left(\underline{u}'_z\right)_{(n)} = \left[\underline{H}^9_{n \times 5n} + \underline{H}^8_{n \times (3n-2)} \cdot \underline{L}_{(3n-2) \times 5n}\right] \cdot \underline{X}_{(5n)} + \underline{H}^8_{n \times (3n-2)} \cdot \underline{f}_{(3n-2)}^N + \underline{f}_{6(n)} \quad (5.131)$$

where

$$\underline{f}_{6(n)} = (\delta_{i1} v_2 + \delta_{in} v_4) \quad 1 \leq i \leq n$$

Finally, by substituting the above equation into Eq. 5.129 we obtain:

$$\left(\underline{Q}_y'' \right)_{(n)} = \left(\underline{T}^{7R} \right)_{n \times n_I}^t \cdot \widehat{\underline{L}}_{n_I \times 5n} \cdot \underline{X}_{(5n)} + \left(\underline{T}^{7R} \right)_{n \times n_I}^t \cdot \underline{f}_{(n_I)}^R + \underline{f}_{5(n)}' \quad (5.132)$$

where

$$\begin{aligned} \widehat{\underline{L}}_{n_I \times 5n} &= \underline{R}_{n_I \times n_I}^{-1} \cdot \underline{T}_{n_I \times n}^{7R} \cdot \left[\underline{H}_{n \times 5n}^9 + \underline{H}_{n \times (3n-2)}^8 \cdot \underline{L}_{(3n-2) \times 5n} \right] \\ \underline{f}_{(n_I)}^R &= \underline{R}_{n_I \times n_I}^{-1} \cdot \left[\underline{T}_{n_I \times n}^{7R} \cdot \left(\underline{H}_{n \times (3n-2)}^8 \cdot \underline{f}_{(3n-2)}^N + \underline{f}_{6(n)} \right) - \left(\underline{W}_{(n_I)} \right)' \right] \end{aligned}$$

Eqs. 5.121 to 5.124 and Eq. 5.132 form a system of $5n$ second-order differential equations as follows:

$$\underline{X}_{(5n)}'' = \underline{M} \cdot \underline{X}_{(5n)} + \underline{F}_{(5n)} \quad (5.133)$$

where:

$$\underline{F}_{(5n)} = \underline{F}_{1(5n)} + \underline{F}_{2(5n)}$$

with:

$$\underline{F}_{1(5n)} = \begin{pmatrix} \underline{f}_{1(n)} + \underline{H}_{n \times (3n-2)}^2 \cdot \underline{f}_{(3n-2)}^N \\ \underline{f}_{2(n)} + \underline{H}_{n \times (3n-2)}^3 \cdot \underline{f}_{(3n-2)}^N \\ \underline{f}_{3(n)} + \underline{H}_{n \times (3n-2)}^4 \cdot \underline{f}_{(3n-2)}^N \\ \underline{f}_{4(n)} + \underline{H}_{n \times (3n-2)}^5 \cdot \underline{f}_{(3n-2)}^N \\ \underline{f}_{5(n)}' + \left(\underline{T}^{7R} \right)_{n \times n_I}^t \cdot \underline{f}_{(n_I)}^R \end{pmatrix}, \quad \underline{F}_{2(5n)} = \begin{pmatrix} \widehat{\underline{f}}_{1(n)} \\ \widehat{\underline{f}}_{2(n)} \\ \underline{Q}_{(n)} \\ \underline{Q}_{(n)} \\ \underline{Q}_{(n)} \end{pmatrix}$$

Appendix 5.E Kirchhoff-Love solution

According to Eqs. 5.4, 5.5 and 5.7, it can be deduced:

$$E_{xx}^{KL}(y) = \varepsilon_{xx}^0 + \chi_{zz}^0 y, \quad E_{yy}^{KL}(y) = u_{y,y}^{KL}(y), \quad E_{xy}^{KL}(y) = \frac{1}{2} u_{x,y}^{KL}(y) \quad (5.134)$$

$$\chi_{xx}^{KL}(y) = \chi_{xx}^0, \quad \chi_{yy}^{KL}(y) = \phi_{y,y}^{KL}(y), \quad \chi_{xy}^{KL}(y) = \chi_{xy}^0 \quad (5.135)$$

where $\phi_y^{KL}(y) = -u_{z,y}^{KL}(y)$.

Equilibrium equations of the Kirchhoff-Love theory are as follows:

$$N_{xx,x} + N_{xy,y} = 0 \quad (5.136)$$

$$N_{xy,x} + N_{yy,y} = 0 \quad (5.137)$$

$$M_{xx,xx} + 2M_{xy,xy} + M_{yy,yy} = 0 \quad (5.138)$$

Since there is no variation in the x direction, we obtain:

$$N_{xy} = C_1, \quad N_{yy} = C_2, \quad M_{yy} = C_3 + C_4 y \quad (5.139)$$

where C_1 to C_4 are constant. Free-edge conditions give rise to $C_1 = C_2 = C_3 = C_4 = 0$.

Constitutive relations are written as:

$$\begin{pmatrix} N_{xx}^{KL} \\ N_{yy}^{KL} \\ N_{xy}^{KL} \\ M_{xx}^{KL} \\ M_{yy}^{KL} \\ M_{xy}^{KL} \end{pmatrix} = \begin{bmatrix} \underline{\underline{A}} & \underline{\underline{B}} \\ \underline{\underline{B}} & \underline{\underline{D}} \end{bmatrix} \cdot \begin{pmatrix} E_{xx}^{KL} \\ E_{yy}^{KL} \\ 2E_{xy}^{KL} \\ \chi_{xx}^{KL} \\ \chi_{yy}^{KL} \\ 2\chi_{xy}^{KL} \end{pmatrix} \quad (5.140)$$

In order to express the unknown fields in terms of the known fields, the constitutive relations are arranged as follows:

$$\underline{\underline{Y}}_1 = \underline{\underline{K}} \cdot \underline{\underline{Y}}_2 \quad (5.141)$$

where

$$\underline{\underline{Y}}_1 = \begin{pmatrix} N_{xx}^{KL}(y) \\ E_{yy}^{KL}(y) \\ 2E_{xy}^{KL}(y) \\ M_{xx}^{KL}(y) \\ \chi_{yy}^{KL}(y) \\ M_{xy}^{KL}(y) \end{pmatrix}, \quad \underline{\underline{Y}}_2 = \begin{pmatrix} \varepsilon_{xx}^0 + \chi_{zz}^0 y \\ 0 \\ 0 \\ \chi_{xx}^0 \\ 0 \\ 2\chi_{xy}^0 \end{pmatrix}, \quad \underline{\underline{K}} = (\underline{\underline{K}}^1)^{-1} \cdot \underline{\underline{K}}^2$$

$$\underline{\underline{K}}^1 = \begin{bmatrix} 1 & -A_{12} & -A_{16} & 0 & -B_{12} & 0 \\ 0 & -A_{22} & -A_{26} & 0 & -B_{22} & 0 \\ 0 & -A_{26} & -A_{66} & 0 & -B_{26} & 0 \\ 0 & -B_{12} & -B_{16} & 1 & -D_{12} & 0 \\ 0 & -B_{22} & -B_{26} & 0 & -D_{22} & 0 \\ 0 & -B_{26} & -B_{66} & 0 & -D_{26} & 1 \end{bmatrix}, \quad \underline{\underline{K}}^2 = \begin{bmatrix} A_{11} & 0 & 0 & B_{11} & 0 & B_{16} \\ A_{12} & -1 & 0 & B_{12} & 0 & B_{26} \\ A_{16} & 0 & -1 & B_{16} & 0 & B_{66} \\ B_{11} & 0 & 0 & D_{11} & 0 & D_{16} \\ B_{12} & 0 & 0 & D_{12} & -1 & D_{26} \\ B_{16} & 0 & 0 & D_{16} & 0 & D_{66} \end{bmatrix}$$

Now, we are interested in relations between the imposed strains and stresses at the ends (Eq. 5.54). From the previous equation, it can be deduced:

$$\begin{pmatrix} N_{xx}^{KL}(y) \\ M_{xx}^{KL}(y) \\ M_{xy}^{KL}(y) \end{pmatrix} = \begin{bmatrix} K_{11} & K_{14} & K_{16} \\ K_{14} & K_{44} & K_{46} \\ K_{16} & K_{46} & K_{66} \end{bmatrix} \cdot \begin{pmatrix} \varepsilon_{xx}^0 + \chi_{zz}^0 y \\ \chi_{xx}^0 \\ 2\chi_{xy}^0 \end{pmatrix} \quad (5.142)$$

In this model, the force and moment resultants defined in Eqs. 5.20 to 5.23 can be obtained as follows:

$$F_x^0 = \int_{-b}^b N_{xx}^{KL}(y) dy, \quad M_{zz}^0 = \int_{-b}^b N_{xx}^{KL}(y) y dy$$

$$M_{xx}^0 = \int_{-b}^b M_{xx}^{LK}(y) dy, \quad T_x^0 = 2 \int_{-b}^b M_{xy}^{KL}(y) dy$$

By integrating Eq. 5.142 and normalizing, relations between the imposed stresses and strains are obtained as:

$$\begin{pmatrix} \frac{F_x^0}{b^t h^t} \\ \frac{M_{xx}^0}{b^t (h^t)^2} \\ \frac{T_x^0}{b^t (h^t)^2} \\ \frac{M_{zz}^0}{(b^t)^2 h^t} \end{pmatrix} = \underbrace{\begin{bmatrix} \frac{K_{11}}{h^t} & \frac{K_{14}}{(h^t)^2} & \frac{2K_{16}}{(h^t)^2} & 0 \\ \frac{K_{14}}{(h^t)^2} & \frac{K_{44}}{(h^t)^3} & \frac{2K_{46}}{(h^t)^3} & 0 \\ \frac{2K_{16}}{(h^t)^2} & \frac{2K_{46}}{(h^t)^3} & \frac{4K_{66}}{(h^t)^3} & 0 \\ 0 & 0 & 0 & \frac{K_{11}}{12h^t} \end{bmatrix}}_{\underline{\underline{\hat{K}}}} \cdot \begin{pmatrix} \varepsilon_{xx}^0 \\ \chi_{xx}^0 h^t \\ \chi_{xy}^0 h^t \\ \chi_{zz}^0 b^t \end{pmatrix} \quad (5.143)$$

where b^t and h^t are the total width and the total thickness of the laminate.

Conclusion générale et perspectives

Ce travail de doctorat a été l'occasion d'étudier certains phénomènes locaux comme les singularités de contraintes et le délaminage dans des stratifiés multicouches. Nous avons expliqué dans le chapitre 1 que pour étudier la réponse locale des structures multicouches, des modèles bidimensionnels (2D) de type layerwise sont l'une des meilleures alternatives aux approches tridimensionnelles (3D) qui sont très coûteuses en temps de calcul et en mémoire. Bien que ces modèles soient plus efficaces que les approches 3D, la précision de leurs résultats n'est pas toujours satisfaisante. En plus, ils ont parfois certaines limites dans la modélisation de la rupture et de la fissuration. Dans cette thèse, nous avons présenté une approche alternative précise et très efficace aux éléments finis 3D pour l'analyse du délaminage dans des stratifiés multicouches soumis à des chargements invariants dans le sens de la longueur. L'approche est basée sur un modèle layerwise en contrainte, appelé le *modèle LS1*, qui a été développé au sein du Laboratoire Navier.

Contrairement aux travaux précédents effectués sur le modèle LS1 qui ont été majoritairement numériques, nous avons présenté une approche analytique systématique pour l'analyse du multi-délaminage. Le point de départ de ce travail porte sur le délaminage en traction uniaxiale (mode III) qui a été étudié au chapitre 2. Le problème du multi-délaminage a été abordé par le modèle LS1 et la solution analytique du problème a été présentée. La méthode de décomposition en vecteurs propres a été appliquée pour trouver la solution analytique du problème sachant que, dans le cas général, il y a des valeurs propres nulles, répétitives, et complexes en raison du multi-délaminage. Pour vérifier la précision de la méthode proposée dans les zones de singularités de contraintes, nous avons étudié des stratifiés composites dans les cas non-délaminé (singularités au bord libre) et délaminé (singularités en pointe de fissure). En comparant avec la méthode des éléments finis 3D, nous avons montré que les résultats du modèle LS1 sont précis sauf très près des bords libres et des pointes de fissures. En effet, au niveau des contraintes interlaminaires, les singularités ne sont pas bien captées par le modèle. En plus, en ce qui concerne le taux de restitution d'énergie, l'erreur du modèle dans le cas de petites fissures (de longueur inférieure à l'épaisseur d'un pli) est significative. Plus la taille de fissure est faible, plus l'erreur du modèle devient importante. Cela conduit à une valeur non-nulle du taux de restitution d'énergie pour une fissure de longueur zéro, ce qui n'est pas justifié d'après la théorie de l'élasticité linéaire.

Il est clair que la précision dans les zones de singularités est très importante car ce sont des informations locales (contraintes interlaminaires, taux de restitution d'énergie,...) dans ces zones-là qui sont nécessaires pour prédire le délaminage. Pour

améliorer la précision du modèle au voisinage des singularités, on a proposé au chapitre 3 un modèle raffiné, nommé le modèle LS1 raffiné, dans lequel on utilise une sorte de maillage layerwise dans l'épaisseur des couches physiques. Cela consiste à modéliser chaque couche physique par plusieurs couches dans le modèle d'une façon irrégulière de telle sorte que les épaisseurs des couches fictives diminuent progressivement en approchant des interfaces physiques. Avec cette stratégie, la précision du modèle n'est plus limitée et on est capable de l'augmenter selon le besoin (comme un raffinement du maillage en éléments finis). Nous avons montré que ce type de maillage irrégulier est beaucoup plus efficace par rapport à un maillage régulier dans lequel les épaisseurs des couches fictives sont les mêmes. En utilisant un double critère en contrainte/énergie, l'initiation du délaminage a été étudiée dans des plaques composites. Des comparaisons entre le modèle LS1 (avec le maillage layerwise régulier), le modèle LS1 raffiné (avec le maillage irrégulier proposé) et la méthode des éléments finis 3D ont montré que contrairement au modèle LS1 classique, le modèle raffiné donne quasiment les mêmes résultats que l'approche 3D en termes de contraintes interlaminaires et de taux de restitution d'énergie, ce qui permet d'utiliser ce modèle avec n'importe quel type de critères tridimensionnels de délaminage.

Après l'étude de l'initiation de délaminage, nous avons proposé au chapitre 4 d'étudier la propagation de délaminage. Pour ce faire, la propagation de délaminage en flexion cylindrique a été abordée. Nous avons considéré une plaque multicouche longue avec un chargement quelconque de flexion cylindrique (invariant dans la direction longitudinale) sur la face supérieure et avec des conditions aux limites arbitraires aux bords latéraux. Le modèle LS1 a été utilisé et l'approche analytique utilisée dans le cas de traction uniaxiale a été développée pour la résolution de ce problème. Deux exemples classiques de la propagation du délaminage en mode I (DCB) et en mode II (ENF) ont été traités. En comparant les résultats du modèle LS1 avec ceux des éléments finis 3D, nous avons démontré la précision et l'efficacité du modèle dans l'analyse de la propagation du délaminage en modes I et II.

Ayant étudié deux types de chargement (traction uniaxiale et flexion cylindrique), nous avons étendu, au chapitre 5, notre approche analytique à d'autres types de chargement. On reste dans le cadre des plaques multicouches pour lesquelles le champ de déformation peut être considéré indépendant de la coordonnée longitudinale. Basé sur cette hypothèse, nous avons identifié tous les chargements possibles sur les extrémités longitudinales, les faces supérieure et inférieure et les bords latéraux. En utilisant les relations déformation-déplacement 3D, nous avons montré que, dans le cas général, le chargement aux extrémités d'une telle plaque consiste en une traction uniaxiale, une flexion hors plan, une torsion et une flexion dans le plan. Le chargement sur les bords latéraux consiste à des forces ou déplacements imposés qui se traduisent par des conditions aux limites arbitraires dans notre approche LS1. En ce qui concerne les faces supérieure et inférieure, la plaque peut être soumise à un chargement quelconque dans la largeur mais invariant dans la longueur. Le modèle LS1 a été étendu pour analyser des plaques multicouches soumises à tous ces types de chargement. La formulation matricielle du problème a été écrite et la solution analytique dans le cas général a été présentée. Plusieurs types de chargement ont été étudiés dans des stratifiés composites

non-symétriques. Afin de valider l'approche proposée, nous avons comparé les résultats du modèle LS1 avec ceux obtenus par un calcul par éléments finis, ce qui a clairement montré la précision et l'efficacité significative de l'approche proposée.

A la fin, comme une brève synthèse, nous remarquons que la méthode proposée dans ce travail:

- permet de trouver la solution analytique du modèle LS1;
- est à la fois précise et très efficace par rapport aux méthodes numériques tridimensionnelles;
- permet de prendre en compte différents types de chargement;
- permet d'aborder facilement des problèmes de multi-délaminage.

Grâce à ces avantages, la méthode proposée peut être utilisée comme une alternative fiable à la méthode des éléments finis 3D dans l'analyse des plaques multicouches. Il est évident que dans des problèmes nécessitant un grand nombre de calculs comme la propagation de fissure, l'optimisation des séquences d'empilement,... une telle approche est très utile.

Enfin, à la suite de ce travail nous proposons quelques perspectives:

- La méthode analytique proposée peut être appliquée à d'autres géométries que des plaques. Une application intéressante est le cas des tubes multicouches qui peut être traité en écrivant la formulation du problème en coordonnées cylindriques.
- Étant donné que la méthode proposée est limitée aux plaques rectangulaires invari-antes, une approche de type global-local peut être utilisée pour d'autres géométries de plaque. En effet, on pourrait raccorder un modèle monocouche simple (Kirchhoff-Love, Reissner-Mindlin,...) pour l'analyse globale avec le modèle analytique proposé pour l'analyse locale. Cela permettrait d'aborder des géométries plus compliquées comme des plaques multicouches trouées.
- Le maillage layerwise proposé pour l'analyse du multi-délaminage pourrait être implémenté dans le code de calcul MPFEAP qui est basé sur la formulation d'éléments finis du modèle LS1. Ainsi, dans le cas des géométries compliquées où le problème ne peut pas être résolu analytiquement, on pourrait utiliser des éléments finis du modèle LS1 raffiné à la place des éléments finis 3D très coûteux.

Références bibliographiques

- E. A. Abdallah, C. Bouvet, S. Rivallant, B. Broll, and J. J. Barrau. Experimental analysis of damage creation and permanent indentation on highly oriented plates. *Composites Science and Technology*, 69:1238–1245, 2009.
- O. Allix and P. Ladevèze. Interlaminar interface modelling for the prediction of delamination. *Composite Structures*, 22:235–242, 1992.
- O. Allix, P. Ladevèze, and A. Corigliano. Damage analysis of interlaminar fracture specimens. *Composite Structures*, 31:61–74, 1995.
- O. Allixa, D. Lévêquea, and L. Perret. Identification and forecast of delamination in composite laminates by an interlaminar interface model. *Composites Science and Technology*, 58:671–678, 1998.
- S. A. Ambartsumian. On the theory of bending plates. *Izv Otd Tech Nauk AN SSSR*, 5:69–77, 1958a.
- S. A. Ambartsumian. On a general theory of anisotropic shells. *PMM*, 22:226–237, 1958b.
- S. A. Ambartsumian. *Theory of anisotropic shells*. Fizmatzig, Moskwa, 1961.
- S. A. Ambartsumian. Contributions to the theory of anisotropic layered shells. *Applied Mechanics Reviews*, 15:245–249, 1962.
- G. S. Amrutharaj, K. Y. Lam, and B. Cotterell. Delaminations at the free edge of a composite laminate. *Composites Part B: Engineering*, 27:475–483, 1996.
- M. G. Andrews, R. Massabò, and B. N. Cox. Elastic interaction of multiple delaminations in plates subject to cylindrical bending. *International Journal of Solids and Structures*, 43:855–886, 2006.
- M. Aydogdu. A new shear deformation theory for laminated composite plates. *Composite Structures*, 89:94–101, 2009.
- D. Ballhause, M. D’Ottavio, B. Kröplin, and E. Carrera. A unified formulation to assess multilayered theories for piezoelectric plates. *Computers and Structures*, 83:1217–1235, 2005.

RÉFÉRENCES BIBLIOGRAPHIQUES

- E. J. Barbero and J. N. Reddy. Modeling of delamination in composite laminates using a layerwise plate theory. *International Journal of Solids and Structures*, 28:373–388, 1991.
- E. J. Barbero, J. N. Reddy, and J. L. Teply. General two-dimensional theory of laminated cylindrical shells. *American Institute of Aeronautics and Astronautics Journal*, 28:544–553, 1990.
- A. Beakou and M. Touratier. A rectangular finite element for analysis composite multilayered shallow shells in static, vibration and buckling. *International Journal for Numerical Methods in Engineering*, 36:627–653, 1993.
- M. L. Benzeggagh and M. Kenane. Measurement of mixed-mode delamination fracture toughness of unidirectional glass/epoxy composites with mixed-mode bending apparatus. *Composites Science and Technology*, 56:439–449, 1996.
- B. Bhaskar and T. K. Varadan. Refinement of higher-order laminated plate theories. *American Institute of Aeronautics and Astronautics Journal*, 27:1830–1831, 1989.
- A. Bhimaraddi and L. K. Stevens. A higher order theory for free vibration of orthotropic, homogeneous, and laminated rectangular plates. *Journal of Applied Mechanics*, 51:195–198, 1984.
- R. Borg, L. Nilsson, and K. Simonsson. Modeling of delamination using a discretized cohesive zone and damage formulation. *Composites Science and Technology*, 62:1299–1314, 2002.
- S. Botello, E. Onate, and J. M. Canet. A layer-wise triangle for analysis of laminated composite plates and shells. *Computers and Structures*, 70:635–646, 1999.
- C. Bouvet, B. Castanié, M. Bizeul, and J. J. Barrau. Low velocity impact modelling in laminate composite panels with discrete interface elements. *International Journal of Solids and Structures*, 46:2809–2821, 2009.
- C. Bouvet, S. Rivallant, and J. J. Barrau. Low velocity impact modeling in composite laminates capturing permanent indentation. *Composites Science and Technology*, 72:1977–1988, 2012.
- J. C. Brewer and P. A. Lagace. Quadratic stress criterion for initiation of delamination. *Journal of Composite Materials*, 22:1141–1155, 1988.
- V. Q. Bui, E. Marechal, and H. Nguyen-Dang. Imperfect interlaminar interfaces in laminated composites: delamination with the r-curve effect. *Composites Science and Technology*, 60:2619–2630, 2000.
- D. Caillerie and J. C. Nedelec Communicator. Thin elastic and periodic plates. *Mathematical Methods in the Applied Sciences*, 6:159–191, 1984.

RÉFÉRENCES BIBLIOGRAPHIQUES

- D. Caillerie and E. Sanchez-Palencia. Elastic thin shells: Asymptotic theory in the anisotropic and heterogeneous cases. *Mathematical Models and Methods in Applied Sciences*, 5:473–496, 1995.
- J. F. Caron, A. Diaz Diaz, R. P. Carreira, A. Chabot, and A. Ehrlacher. Multi-particle modelling for the prediction of delamination in multi-layered materials. *Composites Science and Technology*, 66:755–765, 2006.
- R. P. Carreira. *Validations par éléments finis des Modèles Multiparticulaires de Matériaux Multicouches (M4)*. PhD thesis, Ecole Nationale des Ponts et Chaussées, France, 1998.
- R. P. Carreira, J. F. Caron, and A. Diaz Diaz. Model of multilayered materials for interface stresses estimation and validation by finite element calculations. *Mechanics of Materials*, 34:217–230, 2002.
- E. Carrera. A class of two-dimensional theories for anisotropic multilayered plates analysis. *Accademia delle Scienze di Torino, Memorie Scienze Fisiche*, 19;20:1–39, 1995.
- E. Carrera. Mixed layer-wise models for multilayered plates analysis. *Composite Structures*, 43:57–70, 1998a.
- E. Carrera. Layer-wise mixed models for accurate vibration analysis of multilayered plates. *Journal of Applied Mechanics*, 65:820–828, 1998b.
- E. Carrera. A reissner’s mixed variational theorem applied to vibration analysis of multilayered shell. *Journal of Applied Mechanics*, 66:69–78, 1999a.
- E. Carrera. A study of transverse normal stress effects on vibration of multilayered plates and shells. *Journal of Sound and Vibration*, 225:803–829, 1999b.
- E. Carrera. Multilayered shell theories that account for a layer-wise mixed description. part I. governing equations. *American Institute of Aeronautics and Astronautics Journal*, 37:1107–1116, 1999c.
- E. Carrera. Multilayered shell theories that account for a layer-wise mixed description. part II. numerical evaluations. *American Institute of Aeronautics and Astronautics Journal*, 37:1117–1124, 1999d.
- E. Carrera. Single-layer vs multi-layers plate modelings on the basis of reissner’s mixed theorem. *American Institute of Aeronautics and Astronautics Journal*, 38:342–343, 2000.
- E. Carrera. Theories and finite elements for multilayered, anisotropic composite plates and shells. *Archives of Computational Methods in Engineering*, 9:87–140, 2002.
- E. Carrera. On the use of the murakami’s zig-zag function in the modeling of layered plates and shells. *Computers and Structures*, 82:541–554, 2004.

RÉFÉRENCES BIBLIOGRAPHIQUES

- A. Cecchi and K. Sab. A homogenized reissner-mindlin model for orthotropic periodic plates: Application to brickwork panels. *International Journal of Solids and Structures*, 44:6055–6079, 2007.
- A. Chabot. *Analyse des efforts à l'interface entre les couches des matériaux composites à l'aide de modèles multiparticulaires de matériaux multicouches (M4)*. PhD thesis, Ecole Nationale des Ponts et Chaussées, France, 1997.
- H. Chai. Three-dimensional fracture analysis of thin-film debonding. *International Journal of Fracture*, 46:237–256, 1990.
- H. Chai, C. D. Babcock, and W. G. Knauss. One dimensional modelling of failure in laminated plates by delamination buckling. *International Journal of Solids and Structures*, 17:1069–1083, 1981.
- D. J. Chang, R. Muki, and R. A. Westmann. Double cantilever beam models in adhesive mechanics. *International Journal of Solids and Structures*, 12:13–26, 1976.
- A. Chattopadhyay and H. Gu. A new higher order plate theory in modeling delamination buckling of composite laminates. *American Institute of Aeronautics and Astronautics Journal*, 32:1709–1716, 1994.
- W. Q. Chen and K. Y. Lee. Three-dimensional exact analysis of angle-ply laminates in cylindrical bending with interfacial damage via state-space method. *Composite Structures*, 64:275–283, 2004.
- M. Cho and J. S. Kim. Higher-order zig-zag theory for laminated composites with multiple delaminations. *Journal of Applied Mechanics*, 68:869–877, 2001.
- M. Cho and R. R. Parmerter. Efficient higher order composite plate theory for general lamination configurations. *American Institute of Aeronautics and Astronautics Journal*, 31:1299–1305, 1993.
- H. Y. Choi and F. K. Chang. A model for predicting damage in graphite/epoxy laminated composites resulting from low-velocity point impact. *Journal of Composite Materials*, 26:2134–2169, 1992.
- P. C. Chou and J. Carleone. Transverse shear in laminated plate theories. *American Institute of Aeronautics and Astronautics Journal*, 11:1333–1336, 1973.
- W. T. Chow and S. N. Atluri. Prediction of post-buckling strength of stiffened laminated composite panels based on the criterion of mixed-mode stress intensity factors. *Computational Mechanics*, 18:215–224, 1996.
- W. T. Chow and S. N. Atluri. Stress intensity factors as the fracture parameters for delamination crack growth in composite laminates. *Composites Part B: Engineering*, 28:375–384, 1997.

RÉFÉRENCES BIBLIOGRAPHIQUES

- C. H. Chue and C. I. Liu. Disappearance of free-edge stress singularity in composite laminates. *Composite Structures*, 56:111–129, 2002.
- A. Chyanbin, C. J. Kao, and L. E. Chang. Delamination fracture criteria for composite laminates. *Journal of Composite Materials*, 29:1962–1987, 1995.
- P.G. Ciarlet. *Introduction to linear shell theory*. Series in applied mathematics N°1, France, 1998.
- P.G. Ciarlet and P. Destuynder. A justification of a nonlinear model in plate theory. *Computer Methods in Applied Mechanics and Engineering*, 17-18:227–258, 1979.
- P.G. Ciarlet and V. Lods. Asymptotic analysis of linearly elastic shells. I. justification of membrane shell equations. *Archive for Rational Mechanics and Analysis*, 136:119–161, 1996a.
- P.G. Ciarlet and V. Lods. Asymptotic analysis of linearly elastic shells. III. justification of koiter’s shell equations. *Archive for Rational Mechanics and Analysis*, 136:191–200, 1996b.
- P.G. Ciarlet and V. Lods. Asymptotic analysis of linearly elastic shells: Generalized membrane shells. *Journal of Elasticity*, 43:147–188, 1996c.
- P.G. Ciarlet and J.C. Paumier. A justification of the marguerre-von karman equations. *Computational Mechanics*, 1:177–202, 1986.
- P.G. Ciarlet, V. Lods, and B. Miara. Asymptotic analysis of linearly elastic shells. II. justification of flexural shell equations. *Archive for Rational Mechanics and Analysis*, 136:163–190, 1996.
- P. Cicala. *Systematic approach to linear shell theory*. Levrotto & Bella, Torino, 1965.
- A. H. Cottrell. Theoretical aspects of radiation damage and brittle fracture in steel pressure vessels. *Iron Steel Institute Special Report*, 69:281–296, 1961.
- C. M. Dakshina Moorthya and J. N. Reddy. Modeling of delamination using a layer-wise element with enhanced strains. *International Journal for Numerical Methods in Engineering*, 43:755–779, 1998.
- A. Dall’Asta and A. Zona. Nonlinear analysis of composite beams by a displacement approach. *Computers and Structures*, 80:2217–2228, 2002.
- J. Dallot and K. Sab. Limit analysis of multilayered plates. part I: The homogenized Love-Kirchhoff model. *Journal of the Mechanics and Physics of Solids*, 56:581–612, 2008a.
- J. Dallot and K. Sab. Limit analysis of multi-layered plates. part II: Shear effects. *Journal of the Mechanics and Physics of Solids*, 56:561–580, 2008b.

RÉFÉRENCES BIBLIOGRAPHIQUES

- F. Dau, O. Polita, and M. Touratier. c^1 plate and shell finite elements for geometrically nonlinear analysis of multilayered structures. *Computers and Structures*, 84:1264–1274, 2006.
- B. D. Davidson. An analytical investigation of delamination front curvature in double cantilever beam specimens. *Journal of Composite Materials*, 24:1124–1137, 1990.
- B. D. Davidson, R. Krüger, and M. König. Three-dimensional analysis of center-delaminated unidirectional and multidirectional single-leg bending specimens. *Composites Science and Technology*, 54:385–394, 1995.
- A. B. De Morais. Novel cohesive beam model for the end-notched flexure (enf) specimen. *Engineering Fracture Mechanics*, 78:3017–3029, 2011.
- J. A. De Souza, S. Goutianos, M. Skovgaard, and B. F. Sørensen. Fracture resistance curves and toughening mechanisms in polymer based dental composites. *Journal of the Mechanical Behavior of Biomedical Materials*, 4:558–571, 2011.
- M. Degiovanni, M. Gherlone, M. Mattone, and M. Di Sciuva. A sub-laminates fem approach for the analysis of sandwich beams with multilayered composite faces. *Composite Structures*, 92:2299–2306, 2010.
- L Demasi. ∞^6 mixed plate theories based on the generalized unified formulation. part III: Advanced mixed high order shear deformation theories. *Composite Structures*, 87:183–194, 2009.
- M. Di Sciuva. A refinement of the transverse shear deformation theory for multilayered orthotropic plates. *Aerotecnica Missili e Spazio*, 63:84–92, 1984.
- M. Di Sciuva. An improved shear-deformation theory for moderately thick multilayered anisotropic shells and plates. *Journal of Applied Mechanics*, 54:589–596, 1987.
- M. Di Sciuva and E. Carrera. Elastodynamic behavior of relatively thick, symmetrically, laminated, anisotropic circular cylindrical shells. *Journal of Applied Mechanics*, 59:222–224, 1992.
- M. Di Sciuva, A. Cicorello, and E. Dalle Mura. A class of multilayered anisotropic plate elements including the effects of transverse shear deformability. *AIDAA Conference (Torino)*, pages 877–892, 1984.
- A. Diaz Diaz. *Délamination des matériaux multicouches : Phénomènes, Modèles et Critères*. PhD thesis, Ecole Nationale des Ponts et Chaussées, France, 2001.
- A. Diaz Diaz and J. F. Caron. Prediction of the onset of mode III delamination in carbon-epoxy laminates. *Composite Structures*, 72:438–445, 2006a.
- A. Diaz Diaz and J. F. Caron. Interface plasticity and delamination onset prediction. *Mechanics of Materials*, 38:648–663, 2006b.

RÉFÉRENCES BIBLIOGRAPHIQUES

- A. Diaz Diaz, J. F. Caron, and R. P. Carreira. Software application for evaluating interfacial stresses in inelastic symmetrical laminates with free edges. *Composite Structures*, 58:195–208, 2002.
- A. Diaz Diaz, J. F. Caron, and A. Ehrlacher. Analytical determination of the modes I, II and III energy release rates in a delaminated laminate and validation of a delamination criterion. *Composite Structures*, 78:424–432, 2007a.
- A. Diaz Diaz, J. F. Caron, and A. Ehrlacher. Analytical determination of the modes I, II and III energy release rates in a delaminated laminate and validation of a delamination criterion. *Composite Structures*, 78:424–432, 2007b.
- S. L. Donaldson. Fracture toughness testing of graphite/epoxy and graphite/peek composites. *Composites*, 16:103–112, 1985.
- S. L. Donaldson. The effect of interlaminar fracture properties on the delamination buckling of composite laminates. *Composites Science and Technology*, 28:33–44, 1987.
- V. A. Duong. *Développement en dynamique d'un élément fini multicouche avec interfaces imparfaites*. PhD thesis, Ecole Nationale des Ponts et Chaussées, France, 2008.
- V. A. Duong, A. Diaz Diaz, S. Chataigner, and J. F. Caron. A layerwise finite element for multilayers with imperfect interfaces. *Composite Structures*, 93:3262–3271, 2011.
- L. L. Durocher and R. Solechi. Bending and vibration of isotropic two-layer plates. *American Institute of Aeronautics and Astronautics Journal*, 13:1522–1523, 1975.
- A. Ehrlacher, T. Naciri, A. Chabot, and J. F. Caron. Analyse des efforts d'interface à l'aide d'une modélisation multiphasique des matériaux multicouches (M4). *Comptes Rendus des 9ièmes Journées Nationales sur les Composites*, 1994.
- M. Epstein and P. G. Glockner. Nonlinear analysis of multilayered shells. *International Journal of Solids and Structures*, 13:1081–1089, 1977.
- M. Epstein and H. P. Huttelmaier. A finite element formulation for multilayered and thick plates. *Computers and Structures*, 16:645–650, 1983.
- D. Fang, Z. K. Zhang, A. K. Soh, and K. L. Lee. Fracture criteria of piezoelectric ceramics with defects. *Mechanics of Materials*, 36:917–928, 2004.
- A. J. M. Ferreira, C. M. C. Roque, and P. A. L. S. Martins. Analysis of composite plates using higher-order shear deformation theory and a finite point formulation based on the multiquadric radial basis function method. *Composites Part B: Engineering*, 34:627–636, 2003.
- K. O. Friedrichs and R. F. Dressler. A boundary-layer theory for elastic plates. *Communications on Pure and Applied Mathematics*, 14:1–33, 1961.

RÉFÉRENCES BIBLIOGRAPHIQUES

- P. Gaudenzi. A general formulation of higher order theories for the analysis of laminated plates. *Composite Structures*, 20:103–112, 1992.
- P. Gaudenzi, R. Barboni, and A. Mannini. A finite element evaluation of single-layer and multi-layer theories for the analysis of laminated plates. *Computers and Structures*, 30:427–440, 1995.
- P. H. Geubelle and J. S. Baylor. Impact-induced delamination of composites: a 2d simulation. *Composites Part B: Engineering*, 29:589–602, 1998.
- J. W. Gillespie, L. A. Carlsson, B. R. Pipes, R. Rothschilds, B. Trethewey, and A. Smiley. Delamination growth in composite materials. *NASA Contractor Report 176416*, 5:161–250, 1985.
- A. L. Gol'denveizer. *Theory of thin elastic shells*. International Series of Monograph in Aeronautics and Astronautics, Pergamon Press, New York, 1961.
- A. L. Gol'denveizer. Derivation of an approximate theory of bending of a plate by the method of asymptotic integration of the equations of the theory of elasticity. *Journal of Applied Mathematics and Mechanics*, 26:1000–1025, 1962.
- A. L. Gol'denveizer and A. V. Kolos. On the derivation of two dimensional equation in the theory of thin elastic plate. *Journal of Applied Mathematics and Mechanics*, 29:151–166, 1965.
- F. Greco, P. Lonetti, and R. Zinno. An analytical delamination model for laminated plates including bridging effects. *International Journal of Solids and Structures*, 39:2435–2463, 2002.
- E. A. Green and P. M. Naghdi. A theory of laminated composite plates. *Journal of Applied Mathematics*, 29:1–23, 1982.
- A. A. Griffith. The phenomena of rupture and flow in solids. *Philosophical Transactions of the Royal Society (London), Series A*, 221:163–198, 1921.
- A. Grimaldi and J. N. Reddy. On delamination in plates: a unilateral contact approach. *In Unilateral Problems in Structural Analysis, CISM Courses and Lectures No. 288, Springer-Verlag, NY*, pages 299–314, 1985.
- R. Gutkin, M. L. Laffan, S. T. Pinho, P. Robinson, and P. T. Curtis. Modelling the r-curve effect and its specimen-dependence. *International Journal of Solids and Structures*, 48:1767–1777, 2011.
- G. Hadj-Ahmed, R. Foret and A. Ehrlacher. Stress analysis in adhesive joints with a multiparticle model of multilayered materials (M4). *International Journal of Adhesion and Adhesives*, 21:297–307, 2001.
- P. W. Harper and S. R. Hallett. Cohesive zone length in numerical simulations of composite delamination. *Engineering Fracture Mechanics*, 75:4774–4792, 2008.

RÉFÉRENCES BIBLIOGRAPHIQUES

- S. Hashemi, A. J. Kinloch, and J. G. Williams. Mechanics and mechanisms of delamination in a poly(ethersulphone)-fibre composite. *Composites Science and Technology*, 37:429–462, 1990.
- S. Hashemi, A. J. Kinloch, and J. G. Williams. Mixed-mode fracture in fiber-polymer composite laminates. *Composite Materials: Fatigue and Fracture, Philadelphia, PA, American Society for Testing and Materials*, 3:143–168, 1991.
- T. Hayashi. Analytical study of interlaminar shear stresses in a laminated composite plate. *Transaction of Japan Society for Aeronautical Engineering and Space Science*, 10:43–48, 1967.
- F. B. Hildebrand, E. Reissner, and G. B. Thomas. Notes on the foundations of the theory of small displacements of orthotropic shells. *NACA TN-1833*, 1949.
- T. M. Hsu and J. T. S. Wang. A theory of laminated cylindrical shells consisting of layers of orthotropic laminae. *American Institute of Aeronautics and Astronautics Journal*, 8:2141–2146, 1970.
- E. V. Iarve and N. J. Pagano. Singular full-field stresses in composite laminates with open holes. *International Journal of Solids and Structures*, 38:1–28, 2001.
- G. R. Irwin. Fracture. *Handbuch Der Physik (Berlin, Springer-Verlag)*, 6:551–590, 1958.
- T. K. Jacobsen and B. F. Sørensen. Mode I intra-laminar crack growth in composites - modelling of r-curves from measured bridging laws. *Composites Part A: Applied Science and Manufacturing*, 32:1–11, 2001.
- M. W. Johnson and O. E. Widera. An asymptotic theory for the vibration of non-homogeneous plates. *Acta Mechanica*, 12:131–142, 1971.
- F. Ju, H. P. Lee, and K. H. Lee. Finite element analysis of free vibration of delaminated composite plates. *Composites Engineering*, 5:195–209, 1995.
- R. A. Jurf and R. B. Pipes. Interlaminar fracture of composite materials. *Journal of Composite Materials*, 16:386–394, 1982.
- L. M. Kachanov. Rupture time under creep conditions (in russian). *Izvestia Akademii Nauk SSSR, Otdelenie tekhnicheskich nauk*, 8:26–31, 1958.
- Z. Kaczowski. Plates-statistical calculations. *Warsaw: Arkady*, 1968.
- M. F. Kanninen. Augmented double cantilever beam model for studying crack propagation and arrest. *International Journal of Fracture*, 9:83–92, 1973.
- K. Kant. Numerical analysis of thick plates. *Computer Methods in Applied Mechanics and Engineering*, 31:1–18, 1982.

RÉFÉRENCES BIBLIOGRAPHIQUES

- K. Kant, D. R. J. Owen, and O. C. Zienkiewicz. A refined higher order c^0 plate bending element. *Computers and Structures*, 15:177–183, 1982.
- T. Kant and R. K. Khare. A higher-order facet quadrilateral composite shell element. *International Journal for Numerical Methods in Engineering*, 40:4477–4499, 1997.
- T. Kant and Mallikarjuna. A higher-order theory for free vibration of unsymmetrically laminated composite and sandwich plates-finite element evaluations. *Composite Structures*, 32:1125–1132, 1989.
- T. Kant and B. S. Manjunatha. An unsymmetric frc laminate c^0 finite element model with 12 degrees of freedom per node. *Engineering Computations*, 5:300–308, 1988.
- T. Kant and K. Swaminathan. Analytical solutions for free vibration of laminated composite and sandwich plates based on a higher-order refined theory. *Composite Structures*, 53:73–85, 2001.
- T. Kant and K. Swaminathan. Analytical solutions for the static analysis of laminated composite and sandwich plates based on a higher order refined theory. *Composite Structures*, 56:329–344, 2002.
- M. Karama, K. S. Afaq, and S. Mistou. Mechanical behaviour of laminated composite beam by new multi-layered laminated composite structures. model with transverse shear stress continuity. *International Journal of Solids and Structures*, 40:1525–1546, 2003.
- H. S. Kim, A. Chattopadhyay, and A. Ghoshal. Characterization of delamination effect on composite laminates using a new generalized layerwise approach. *Computers and Structures*, 81:1555–1566, 2003.
- J. S. Kim and M. Cho. Buckling analysis for delaminated composites using plate bending elements based on higher-order zig-zag theory. *International Journal for Numerical Methods in Engineering*, 55:1323–1343, 2002.
- R. Y. Kim and S. R. Soni. Experimental and analytical studies on the onset of delamination in laminated composites. *Journal of Composite Materials*, 18:70–80, 1984.
- R. Y. Kim and S. R. Soni. Failure of composite laminates due to combined interlaminar normal and shear stresses. *Composites 86: Recent Advances in Japan and the United States*, 86:341–350, 1986.
- G. Kirchhoff. Über das gleichwicht und die bewegung eine elastischen schiebe. *Z Angew Math*, 40:51–88, 1850.
- R. Krueger and T. K. O'Brien. A shell/3d modeling technique for the analysis of delaminated composite laminates. *Composites Part A: Applied Science and Manufacturing*, 32:24–44, 2001.

RÉFÉRENCES BIBLIOGRAPHIQUES

- M. C. Lafarie-Frenot. Damage mechanisms induced by cyclic ply-stresses in carbon-epoxy laminates: Environmental effects. *International Journal of Fatigue*, 28:1202–1216, 2006.
- M. C. Lafarie-Frenot and N. Q. Ho. Influence of free edge intralaminar stresses on damage process in CFRP laminates under thermal cycling conditions. *Composites Science and Technology*, 66:1354–1365, 2006.
- M. C. Lafarie-Frenot, C. Hénaff-Gardin, and D. Gamby. Matrix cracking induced by cyclic ply stresses in composite laminates. *Composites Science and Technology*, 61:2327–2336, 2001.
- L. Lagunegrand, T. Lorriot, R. Harry, H. Wargnier, and J. M. Quenisset. Initiation of free-edge delamination in composite laminates. *Composites Science and Technology*, 66:1315–1327, 2006.
- P. L. Larsson. On multiple delamination buckling and growth in composite plates. *International Journal of Solids and Structures*, 27:1623–1637, 1991.
- F. Lécuyer. *Etude des effets de bord dans les structures minces multicouches*. PhD thesis, Université Paris VI, France, 1991.
- F. Lécuyer and D. Engrand. A methodology for the identification of a criterion for delamination intitution. *Journées Nationales sur les Composites*, 1992.
- A. Lebée. *Homogénéisation de plaques périodiques épaisses : application aux panneaux sandwichs à âme pliable en chevrons*. PhD thesis, Ecole Nationale des Ponts et Chaussées - Université Paris-Est, France, 2010.
- A. Lebée and K. Sab. A bending-gradient model for thick plates. part I: Theory. *International Journal of Solids and Structures*, 48:2878–2888, 2011a.
- A. Lebée and K. Sab. A bending-gradient model for thick plates. part II: Closed-form solutions for cylindrical bending of laminates. *International Journal of Solids and Structures*, 48:2889–2901, 2011b.
- A. Lebée and K. Sab. Homogenization of thick periodic plates: Application of the bending-gradient plate theory to a folded core sandwich panel. *International Journal of Solids and Structures*, 49:2778–2792, 2012.
- J. Lee. Free vibration analysis of delaminated composite beams. *Composite Structures*, 74:121–129, 2000.
- K. H. Lee, N. R. Senthilnathan, S. P. Lim, and S. T. Chow. An improved zig-zag model for the bending analysis of laminated composite plates. *Composite Structures*, 15:137–148, 1990.
- D. Leguillon. A method based on singularity theory to predict edge delamination of laminates. *International Journal of Fracture*, 100:105–120, 1999.

RÉFÉRENCES BIBLIOGRAPHIQUES

- D. Leguillon. Strength or toughness? A criterion for crack onset at a notch. *European Journal of Mechanics-A/Solids*, 21:61–72, 2002.
- D. Leguillon and E. Sanchez-Palencia. Computation of singular solutions in elliptic problems and elasticity. *Journal of Applied Mathematics and Mechanics*, 68, 1987.
- D. Leguillon, G. Marion, R. Harry, and D. Lécuyer. The onset of delamination at stress-free edges in angle-ply laminates - analysis of two criteria. *Composites Science and Technology*, 61:377–382, 2001.
- S. G. Lekhnitskii. Strength calculation of composite beams. *Vestnik Inzhen. i Tekhnikov*, No.9, 1935.
- S. G. Lekhnitskii. *Theory of elasticity of an anisotropic body*. Mir Publishers, Moscow, 1981.
- M. Levinson. An accurate, simple theory of the statics and dynamics of elastic plates. *Mechanics Research Communications*, 7:343–350, 1980.
- L. Librescu. *Elastostatics and kinematics of anisotropic and heterogeneous shell type structures*. Noordhoff International Publishing, 1975.
- G. Limam, O. Foret and A. Ehrlacher. Rc beam strengthened with composite material : a limit analysis approach and experimental study. *Composite Structures*, 59:467–472, 2003.
- J. Lindemann and W. Becker. The tendency for free-edge delamination in laminates and its minimization. *Composites Science and Technology*, 62:233–242, 2002.
- K. H. Lo, R. M. Christensen, and E. M. Wu. A higher-order theory of plate deformation. part I: Homogeneous plates. *Journal of Applied Mechanics*, 44:663–668, 1977a.
- K. H. Lo, R. M. Christensen, and E. M. Wu. A higher-order theory of plate deformation. part II: Laminated plates. *Journal of Applied Mechanics*, 44:669–676, 1977b.
- Th. Lorriot, G. Marion, R. Harry, and H. Wargnier. Onset of free-edge delamination in composite laminates under tensile loading. *Composites Part B: Engineering*, 34: 459–471, 2003.
- A. E. H. Love. *A treatise on the mathematical theory of elasticity*. Cambridge University Press, Cambridge, 4th edition edition, 1927.
- P. Malekzadeh, M. Farid, and P. Zahedinejad. A three-dimensional layerwise-differential quadrature free vibration analysis of laminated cylindrical shells. *International Journal of Pressure Vessels and Piping*, 85:450–458, 2008a.
- P. Malekzadeh, A. R. Setoodeh, and E. Barmshouri. A hybrid layerwise and differential quadrature method for in-plane free vibration of laminated thick circular arches. *Journal of Sound and Vibration*, 315:212–225, 2008b.

RÉFÉRENCES BIBLIOGRAPHIQUES

- S. Mall and N. K. Kochhar. Criterion for mixed-mode fracture in composite bonded joints. *NASA Contractor Report 178112*, 1986.
- J. L. Mantari, A. S. Oktem, and C. Guedes Soares. Static and dynamic analysis of laminated composite and sandwich plates and shells by using a new higher-order shear deformation theory. *Composite Structures*, 94:37–49, 2011.
- J. L. Mantari, A. S. Oktem, and C. Guedes Soares. A new higher order shear deformation theory for sandwich and composite laminated plates. *Composites Part B: Engineering*, 43:1489–1499, 2012a.
- J. L. Mantari, A. S. Oktem, and C. Guedes Soares. A new higher order shear deformation theory for sandwich and composite laminated plates. *Composites Part B: Engineering*, 43:1489–1499, 2012b.
- G. Marion. *Étude expérimentale et théorique de l'amorçage du délaminage au bord de matériaux composites stratifiés*. PhD thesis, Université de Bordeaux I, France, 2000.
- E. Martin and D. Leguillon. Energetic conditions for interfacial failure in the vicinity of a matrix crack in brittle matrix composites. *International Journal of Solids and Structures*, 41:6937–6948, 2004.
- E. Martin, B. Poitou, D. Leguillon, and J. M. Gatt. Competition between deflection and penetration at an interface in the vicinity of a main crack. *International Journal of Fracture*, 151:247–268, 2008.
- E. Martin, D. Leguillon, and N. Carrère. A twofold strength and toughness criterion for the onset of free-edge shear delamination in angle-ply laminates. *International Journal of Solids and Structures*, 47:1297–1305, 2010.
- E. Martin, D. Leguillon, and N. Carrère. A coupled strength and toughness criterion for the prediction of the open hole tensile strength of a composite plate. *International Journal of Solids and Structures*, 49:3915–3922, 2012.
- S. T. Mau. A refined laminated plate theory. *Journal of Applied Mechanics*, 40:606–607, 1973.
- R. D. Mindlin. Influence of rotatory inertia and shear in flexural motions of isotropic elastic plates. *Journal of Applied Mechanics*, 18:1031–1036, 1951.
- C. Mittelstedt and W. Becker. A single-layer theory approach to stress concentration phenomena in layered plates. *Composites Science and Technology*, 64:1737–1748, 2004).
- C. Mittelstedt and W. Becker. Asymptotic analysis of stress singularities in composite laminates by the boundary finite element method. *Composite Structures*, 71:210–219, 2005.

RÉFÉRENCES BIBLIOGRAPHIQUES

- C. Mittelstedt and W. Becker. Reddy's layerwise laminate plate theory for the computation of elastic fields in the vicinity of straight free laminate edges. *Materials Science and Engineering*, 498:76–80, 2008.
- H. Murakami. Laminated composite plate theory with improved in-plane responses. *Journal of Applied Mechanics*, 53:661–666, 1986.
- M. V. V. Murthy. An improved transverse shear deformation theory for laminated anisotropic plates. *NASA Technical Paper 1903*, pages 1–37, 1981.
- M. V. V. S. Murthy, D. Roy Mahapatra, K. Badarinarayana, and S. Gopalakrishnan. A refined higher order finite element for asymmetric composite beams. *Composite Structures*, 67:27–35, 2005.
- T. Naciri, A. Ehrlacher, and A. Chabot. Interlaminar stress analysis with a new multi-particle modelization of multilayered materials (M4). *Composites Science and Technology*, 58:337–343, 1998.
- R. B. Nelson and D. R. Lorch. A refined theory for laminated orthotropic plates. *Journal of Applied Mechanics*, 41:177–183, 1974.
- D. T. Nguyen. *Benchmark d'un modèle layer wise de multicouches et implémentation du modèle dans Abaqus*. PhD thesis, Ecole Nationale des Ponts et Chaussées - Université Paris-Est, France, 2012.
- T. K. Nguyen, K. Sab, and G. Bonnet. First-order shear deformation plate models for functionally graded materials. *Composite Structures*, 83:25–36, 2008.
- V. T. Nguyen. *Modélisation globale et locale des structures multicouches par éléments finis de plaque*. PhD thesis, Ecole Nationale des Ponts et Chaussées, France, 2004.
- V. T. Nguyen and J. F. Caron. A new finite element for free edge effect analysis in laminated composites. *Computers and Structures*, 84:1538–1546, 2006.
- V. T. Nguyen and J. F. Caron. Finite element analysis of free-edge stresses in composite laminates under mechanical and thermal loading. *Composites Science and Technology*, 69:40–49, 2009.
- K. F. Nilsson. On growth of crack front in D.C.B.-test. *Composites Engineering*, 3: 527–546, 1993.
- A. K. Noor. Mixed finite-difference scheme for analysis of simply supported thick plates. *Computers and Structures*, 3:967–982, 1973a.
- A. K. Noor. Free vibrations of multilayered composite plates. *American Institute of Aeronautics and Astronautics Journal*, 11:1038–1039, 1973b.
- A. Nosier and A. Bahrami. Free-edge stresses in antisymmetric angle-ply laminates in extension and torsion. *International Journal of Solids and Structures*, 43:6800–6816, 2006.

RÉFÉRENCES BIBLIOGRAPHIQUES

- A. Nosier and A. Bahrami. Interlaminar stresses in antisymmetric angle-ply laminates. *Composite Structures*, 78:18–33, 2007.
- A. Nosier and M. Maleki. Free-edge stresses in general composite laminates. *International Journal of Mechanical Sciences*, 50:1435–1447, 2008.
- J. Oh, M. Cho, and J. S. Kim. Buckling analysis of a composite shell with multiple delaminations based on a higher order zig-zag theory. *Finite Elements in Analysis and Design*, 44:675–685, 2008.
- C. Ossadzow, P. Muller, and M. Touratier. Wave dispersion in deep multilayered doubly curved viscoelastic shells. *Journal of Sound and Vibration*, 214:531–552, 1998.
- Y. Ousset. Numerical simulation of delamination growth in layered composite plates. *European Journal of Mechanics-A/Solids*, 18:291–312, 1999.
- D. R. J. Owen and Z. H. Li. A refined analysis of laminated plates by finite element displacement methods -I. fundamentals and static analysis. *Computers and Structures*, 26:907–914, 1987a.
- D. R. J. Owen and Z. H. Li. A refined analysis of laminated plates by finite element displacement methods -II. vibration and stability. *Computers and Structures*, 26:915–923, 1987b.
- N. J. Pagano. Exact solutions for composite laminates in cylindrical bending. *Journal of Composite Materials*, 3:398–411, 1969.
- N. J. Pagano. Influence of shear coupling in cylindrical bending of anisotropic laminates. *Journal of Composite Materials*, 4:330–343, 1970a.
- N. J. Pagano. Exact solutions for rectangular bidirectional composites and sandwich plates. *Journal of Composite Materials*, 4:20–34, 1970b.
- N. J. Pagano. On the calculation of interlaminar normal stress in composite laminate. *Journal of Composite Materials*, 8:65–81, 1974.
- N. J. Pagano. Stress fields in composite laminates. *International Journal of Solids and Structures*, 14:385–400, 1978a.
- N. J. Pagano. Free edge stress fields in composite laminates. *International Journal of Solids and Structures*, 14:401–406, 1978b.
- N. J. Pagano and S. R. Soni. Global-local laminate variational model. *International Journal of Solids and Structures*, 19:207–228, 1983.
- V. Panc. Theories of elastic plates. *Prague: Academia*, 1975.
- S. K. Panda and B. N. Singh. Nonlinear free vibration of spherical shell panel using higher order shear deformation theory - A finite element approach. *International Journal of Pressure Vessels and Piping*, 86:373–383, 2009.

RÉFÉRENCES BIBLIOGRAPHIQUES

- B. N. Pandya and T. Kant. Flexural analysis of laminated composites using a refined higher-order c^0 plate bending elements. *Computer Methods in Applied Mechanics and Engineering*, 66:173–198, 1988a.
- B. N. Pandya and T. Kant. Higher-order shear deformable theories for flexure of sandwich plates - finite element evaluations. *International Journal of Solids and Structures*, 24:1267–1286, 1988b.
- B. N. Pandya and T. Kant. A refined higher-order generally orthotropic c^0 plate bending element. *Computers and Structures*, 28:119–133, 1988c.
- B. N. Pandya and T. Kant. Finite element stress analysis of laminated composites using a higher-order displacement model. *Composites Science and Technology*, 32:137–155, 1988d.
- O. Park and B. V. Sankar. Crack-tip force method for computing energy release rate in delaminated plates. *Composite Structures*, 55:429–434, 2002.
- R. B. Pipes and N. J. Pagano. Interlaminar stresses in composite laminates under uniform axial extension. *Journal of Composite Materials*, 4:538–548, 1970.
- R. B. Pipes and N. J. Pagano. Interlaminar stresses in composite laminates - an approximate elasticity solution. *Journal of Applied Mechanics*, 41:668–672, 1974.
- O. Polita and M. Touratier. A new laminated triangular finite element assuring interface continuity for displacements and stresses. *Composite Structures*, 38:37–44, 1997.
- S. Pradyumna and J. Y. Bandyopadhyay. Free vibration analysis of functionally graded curved panels using a higher-order finite element formulation. *Journal of Sound and Vibration*, 318:176–192, 2008.
- A. H. Puppo and H. A. Evensen. Interlaminar shear in laminated composites under generalized plane stress. *Journal of Composite Materials*, 4:204–220, 1970.
- P. Qiao and J. Wang. On the energy release rate and mode mix of delaminated shear deformable composite plates. *International Journal of Solids and Structures*, 41:2757–2779, 2004.
- Y. Qiu, M. A. Crisfield, and G. Alfano. An interface element formulation for the simulation of delamination with buckling. *Engineering Fracture Mechanics*, 68:1755–1776, 2001.
- B. K. Raghu Prasada and D. V. T. G. Pavan Kumar. Analysis of composite enf specimen using higher order beam theories. *Thin-Walled Structures*, 46:676–688, 2008.
- B. K. Rath. and Y. C. Das. Vibration of layered shells. *Journal of Sound and Vibration*, 28:737–757, 1973.

RÉFÉRENCES BIBLIOGRAPHIQUES

- J. N. Reddy. A simple higher-order theory for laminated composite plates. *Journal of Applied Mechanics*, 51:745–752, 1984a.
- J. N. Reddy. A refined nonlinear theory of plates with transverse shear deformation. *International Journal of Solids and Structures*, 20:881–896, 1984b.
- J. N. Reddy. A generalization of two-dimensional theories of laminated composite plates. *Communications in Applied Numerical Method*, 3:173–180, 1987.
- J. N. Reddy. *Mechanics of Laminated Composite Plates, Theory and Analysis*. CRC Press, 1997.
- J. N. Reddy and C. F. Liu. A higher-order shear deformation theory of laminated elastic shells. *International Journal of Engineering Science*, 23:319–330, 1985.
- J. R. Reeder. An evaluation of mixed-mode delamination failure criteria. *NASA Technical Memorandum 104210*, 2002.
- J. R. Reeder, S. Kyongchan, P. B. Chunchu, and D. R. Ambur. Postbuckling and growth of delaminations in composite plates subjected to axial compression. *AIAA/ASME/ASCE/AHS/ASC Structures, Structural Dynamics, and Materials Conference, Denver, Colorado*, 1746:10, 2002.
- E. Reissner. The effects of transverse shear deformation on the bending of elastic plates. *Journal of Applied Mechanics*, 12:69–76, 1945.
- E. Reissner. On a variational theorem in elasticity. *Journal of Mathematical Physics*, 29:90–95, 1950.
- E. Reissner. On transverse bending of plates including the effects of transverse shear deformation. *International Journal of Solids and Structures*, 25:495–502, 1975.
- E. Reissner. On a certain mixed variational theory and a proposed application. *International Journal for Numerical Methods in Engineering*, 20:1366–1368, 1984.
- E. Reissner. On a mixed variational theorem and on a shear deformable plate theory. *International Journal for Numerical Methods in Engineering*, 23:193–198, 1986.
- J. G. Ren. A new theory of laminated plate. *Composites Science and Technology*, 26:225–239, 1986a.
- J. G. Ren. Bending theory of laminated plates. *Composites Science and Technology*, 27:225–248, 1986b.
- J. G. Ren. Exact solutions for laminated cylindrical shells in cylindrical bending. *Composites Science and Technology*, 29:169–187, 1987.
- J. R. Rice. A path independent integral and the approximate analysis of strain concentration by notches and cracks. *Journal of Applied Mechanics*, 35:379–386, 1968.

RÉFÉRENCES BIBLIOGRAPHIQUES

- D. H. Robbins and J. N. Reddy. Modeling of thick composites using a layerwise laminate theory. *International Journal for Numerical Methods in Engineering*, 36:655–677, 1993.
- N. Saeedi, K. Sab, and J. F. Caron. Delaminated multilayered plates under uniaxial extension. part I: Analytical analysis using a layerwise stress approach. *International Journal of Solids and Structures*, 49:3711–3726, 2012a.
- N. Saeedi, K. Sab, and J. F. Caron. Delaminated multilayered plates under uniaxial extension. part II: Very efficient layerwise mesh strategy for the prediction of delamination onset. *International Journal of Solids and Structures*, 49:3727–3740, 2012b.
- N. Saeedi, K. Sab, and J. F. Caron. Cylindrical bending of multilayered plates with multi-delamination via a layerwise stress approach. *Composite Structures*, 95:728–739, 2012c.
- N. Saeedi, K. Sab, and J. F. Caron. Stress analysis of long multilayered plates subjected to invariant loading: Analytical solutions by a layerwise stress model. *Composite Structures*, 100:307–322, 2013.
- M. R. Salari, E. Spacone, P. B. Shing, and D. M. Frangopol. Nonlinear analysis of composite beams with deformable shear connectors. *Journal of Structural Engineering-ASCE*, 124:1148–1158, 1998.
- M. Savoia and J. N. Reddy. A variational approach to three-dimensional elasticity solutions of laminated composite plates. *Journal of Applied Mechanics*, 59:S166–S175, 1992.
- S. Schnabl, I. Planinc, M. Saje, B. Cas, and G. Turk. An analytical model of layered continuous beams with partial interaction. *Structural Engineering and Mechanics*, 22:263–278, 2006.
- P. Seide. An improved approximate theory for the bending of laminated plates. *American Institute of Aeronautics and Astronautics Journal*, 5:451–466, 1980.
- P. Seide and R. A. Chaudhuri. Triangular finite element for analysis of thick laminated shells. *International Journal for Numerical Methods in Engineering*, 24:1563–1579, 1987.
- Ch. She, Y. W. Zhang, and K. Y. Zeng. A three-dimensional finite element analysis of interface delamination in a ductile film/hard substrate system induced by wedge indentation. *Engineering Fracture Mechanics*, 76:2272–2280, 2009.
- A. H. Sheikh and A. Chakrabarti. A new plate bending element based on higher-order shear deformation theory for the analysis of composite plates. *Finite Elements in Analysis and Design*, 39:883–903, 2003.
- M. H. Shen and J. E. Grady. Free vibrations of delaminated beams. *American Institute of Aeronautics and Astronautics Journal*, 30:1361–1370, 1992.

RÉFÉRENCES BIBLIOGRAPHIQUES

- A. Sinan Oktem and C. Guedes Soares. Boundary discontinuous fourier solution for plates and doubly curved panels using a higher order theory. *Composites Part B: Engineering*, 42:842–850, 2011.
- K. P. Soldatos and T. Timarci. A unified formulation of laminated composite, shear deformable, five-degrees-of-freedom cylindrical shell theories. *Composite Structures*, 25:165–171, 1993.
- J. B. M. Sousa and A. R. da Silva. Analytical and numerical analysis of multilayered beams with interlayer slip. *Engineering Structures*, 32:1671–1680, 2010.
- B. Spencer and J. T. Barnby. The effects of notch and fibre angles on crack propagation in fibre-reinforced polymers. *Journal of Material Science*, 11:83–88, 1976.
- N. Sridhar, R. Massabò, B. N. Cox, and I. Beyerlein. Delamination dynamics in through-thickness reinforced laminates with application to dcb specimen. *International Journal of Fracture*, 118:119–144, 2002.
- S. Srinivas. A refined analysis of laminated composites. *Journal of Sound and Vibration*, 30:495–507, 1973.
- S. Srinivas and A. K. Rao. Bending, vibration and buckling of simply supported thick orthotropic rectangular plates and laminates. *International Journal of Solids and Structures*, 6:1463–1481, 1970.
- S. Srinivas, C. V. Joga Rao, and A. K. Rao. An exact analysis for vibration of simply-supported homogeneous and laminated thick rectangular plates. *Journal of Sound and Vibration*, 12:187–199, 1970.
- Y. Stavsky and R. Loewy. On vibrations of heterogeneous orthotropic shells. *Journal of Sound and Vibration*, 15:235–236, 1971.
- S. Sudha Ramesh, C. M. Wang, J. N. Reddy, and K. K. Ang. A higher-order plate element for accurate prediction of interlaminar stresses in laminated composite plates. *Composite Structures*, 91:337–357, 2009.
- C. T. Sun and S. G. Zhou. Failure of quasi-isotropic composite laminates with free-edges. *Journal of Composites Technology and Research*, 7:515–557, 1988.
- M. A. Sutton, X. Deng, F. Ma, and J. C. Newman Jr. Development and application of a crack tip opening displacement-based mixed mode fracture criterion. *International Journal of Solids and Structures*, 37:3591–3618, 2000.
- K. Swaminathan and D. Ragounadin. Analytical solutions using a higher-order refined theory for the static analysis of antisymmetric angle-ply composite and sandwich plates. *Composite Structures*, 64:405–417, 2004.
- G. W. Swift and R. A. Heller. Layered beam analysis. *Journal of the Engineering Mechanics Division*, 100:267–282, 1974.

RÉFÉRENCES BIBLIOGRAPHIQUES

- S. Tang and A. Levy. A boundary layer theory. part II: Extension of laminated finite strip. *Journal of Composite Materials*, 9:42–52, 1975a.
- S. Tang and A. Levy. A boundary layer theory. part I: Laminated composites in plane stress. *Journal of Composite Materials*, 9:33–41, 1975b.
- Z. Tian, F. Zhao, and Q. Yang. Straight free-edge effects in laminated composites. *Finite Elements in Analysis and Design*, 41:1–14, 2004.
- T. C. T. Ting and S. C. Chou. Edge singularities in anisotropic composites. *International Journal of Solids and Structures*, 17:1057–1068, 1981.
- A. Toledano and H. Murakami. A composite plate theory for arbitrary laminate configurations. *Journal of Applied Mechanics*, 54:181–189, 1987a.
- A. Toledano and H. Murakami. A high-order laminated plate theory with improved in-plane responses. *International Journal of Solids and Structures*, 23:111–131, 1987b.
- D. A. F. Torres, P. de Tarso R. Mendonça, and C. S. de Barcellos. Evaluation and verification of an HSDT-layerwise generalized finite element formulation for adaptive piezoelectric laminated plates. *Computer Methods in Applied Mechanics and Engineering*, 200:675–691, 2011.
- M. Touratier. An efficient standard plate theory. *International Journal of Engineering Science*, 29:901–916, 1991.
- M. Touratier. A generalization of shear deformation theories for axisymmetric multi-layered shells. *International Journal of Solids and Structures*, 29:1379–1399, 1992a.
- M. Touratier. A refined theories for laminated shallow shells. *International Journal of Solids and Structures*, 29:1401–1415, 1992b.
- Q. D. Tran. *Modèle simplifié pour les chaussées fissurées multicouches*. PhD thesis, Ecole Nationale des Ponts et Chaussées, France, 2004.
- T. K. Varadan and K. Bhaskar. Bending of laminated orthotropic cylindrical shells - an elasticity approach. *Composite Structures*, 17:141–156, 1991.
- B. F. Vlasov. Ob uravneniakh izgiba plastinok (on the equations of bending of plates). *Doklady Akademii Nauk Azerbejanskoi SSR*, 3:955–979, 1957.
- A. S. D. Wang. Fracture analysis of interlaminar cracking. interlaminar response of composite materials. *Composite Material Series (Edited by N.J. Pagano)*, 5:69–109, 1989.
- A. S. D. Wang and F. W. Crossman. Some new results on edge effect in symmetric composite laminates. *Journal of Composite Materials*, 11:92–106, 1977a.
- A. S. D. Wang and F. W. Crossman. Edge-effect on thermally induced stresses in composite laminates. *Journal of Composite Materials*, 11:300–312, 1977b.

RÉFÉRENCES BIBLIOGRAPHIQUES

- A. S. D. Wang and F. W. Crossman. Initiation and growth of transverse cracks and edge delamination in composite laminates: part I. an energy method. *Journal of Composite Materials*, 14:71–87, 1980.
- S. S. Wang. Fracture mechanics for delamination problems in composite materials. *Journal of Composite Materials*, 17:210–223, 1983.
- S. S. Wang and I. Choi. Boundary-layer effects in composite laminates. part I: Free-edge stress singularities. *Journal of Applied Mechanics*, 49:541–548, 1982a.
- S. S. Wang and I. Choi. Boundary layer effects in composite laminates. part II: Free-edge stress solutions and basic characteristic. *Journal of Applied Mechanics*, 49:549–560, 1982b.
- A. A. Wells. Unstable crack propagation in metals: cleavage and fracture. *Proceedings of the crack propagation symposium, college of aeronautics, Cranfield*, 1:210–230, 1961.
- K. Werner. The fatigue crack growth rate and crack opening displacement in 18g2a-steel under tension. *International Journal of Fatigue*, 39:25–31, 2012.
- J. D. Whitcomb. Analysis of instability-related growth of a through-width delamination. *NASA Technical Memorandum 86301*, 1984.
- J. M. Whitney. The effects of transverse shear deformation on the bending of laminated plates. *Journal of Composite Materials*, 3:534–547, 1969.
- J. M. Whitney. Shear correction factors for orthotropic laminates under static load. *Journal of Applied Mechanics*, 40:302–304, 1973.
- J. M. Whitney. Experimental characterization of delamination fracture. *Composite Material Series - Interlaminar Response of Composite Materials*, 5:161–250, 1989.
- J. M. Whitney. On the use of higher-order plate theories for determining free-edge stresses. *Journal of Reinforced Plastics and Composites*, 16:731–743, 1997.
- J. M. Whitney and R. J. Nuismer. Stress fracture criteria for laminated composites containing stress concentrations. *Composites Science and Technology*, 8:253–265, 1974.
- J. M. Whitney and C. T. Sun. A higher-order theory for extensional motion of laminated composites. *Journal of Sound and Vibration*, 30:85–97, 1973.
- O. E. Widera. An asymptotic theory for the motion of elastic plates. *Acta Mechanica*, 9:54–66, 1970.
- J. G. Williams. The fracture mechanics of delamination tests. *Journal of Strain Analysis for Engineering*, 24:207–214,, 1989.
- T. O. Williams. Efficiency and accuracy considerations in a unified plate theory with delamination. *Composite Structures*, 52:27–40, 2001.

RÉFÉRENCES BIBLIOGRAPHIQUES

- T. O. Williams and F. L. Addressio. A general theory for laminated plates with delaminations. *International Journal of Solids and Structures*, 34:2003–2024, 1997.
- G. Wimmer, C. Schuecker, and H. E. Pettermann. Numerical simulation of delamination in laminated composite components - a combination of a strength criterion and fracture mechanics. *Composites Part B: Engineering*, 40:158–165, 2009.
- C. P. Wu and C. S. Hsu. A new local high-order laminate theory. *Composite Structures*, 25:439–448, 1993.
- E. M. Wu and R. C. Reuter Jr. Crack extension in fiberglass reinforced plastics. *T. & A.M Report No. 275*, 1965.
- L. Xia, T. H. Hyde, and A. A. Becker. An assessment of the crack tip opening displacement criterion for predicting creep crack growth. *International Journal of Fracture*, 77:29–40, 1996.
- A. M. Yan, E. Marechal, and H. Nguyen-Dang. A finite-element model of mixed-mode delamination in laminated composites with an r-curve effect. *Composites Science and Technology*, 61:1413–1427, 2001.
- X. Q. Yan, S. Y. Du, and D. Wang. An engineering method of determining the delamination fracture toughness of composite laminates. *Engineering Fracture Mechanics*, 39:623–627, 1991.
- W. L. Yin and J. T. S. Wang. The energy-release rate in the growth of a one-dimensional delamination. *Journal of Applied Mechanics*, 51:939–941, 1984.
- W. L. Yin, S. N. Sallam, and G. J. Simtses. Ultimate axial load capacity of a delaminated beam-plate. *American Institute of Aeronautics and Astronautics Journal*, 46:123–128, 1986.
- R. Yuuki, J. Q. Liu, J. Q. Xu, T. Ohira, and T. Ono. Mixed mode fracture criteria for an interface crack. *Engineering Fracture Mechanics*, 47:367–377, 1994.
- A. M. Zenkour and M. E. Fares. Non-homogeneous response of cross-ply laminated elastic plates using a high-order theory. *Composite Structures*, 44:297–305, 1999.
- Y. X. Zhang and C. H. Yang. Recent developments in finite element analysis for laminated composite plates. *Composite Structures*, 88:147–157, 2009.
- Z. Zou, S. R. Reid, S. Li, and P. D. Soden. Application of a delamination model to laminated composite structures. *Composite Structures*, 56:375–389, 2002.
- J. Zuo, X. Deng, M. A. Sutton, and C. S. Cheng. Three-dimensional crack growth in ductile materials: Effect of stress constraint on crack tunneling. *Journal of Pressure Vessel Technology*, 130:314011–314018, 2008.

RÉFÉRENCES BIBLIOGRAPHIQUES

- R. I. Zwiers, T. C. T. Ting, and R. L. Spilker. On the logarithmic singularity of free-edge stress in laminated composites under uniform extension. *Journal of Applied Mechanics*, 49:561–569, 1982.